Design and Development of Influenza Neuraminidase Nanoparticle Vaccine

Leiyan Wei
St Catherine's College
And
Chinese Academy of Medical Science Oxford Institute; MRC Weatherall Institute of Molecular Medicine
University of Oxford

A thesis submitted for the degree of
Doctor of Philosophy
Michaelmas 2025

Abstract

Lay abstract

Influenza continues to cause significant illness and death worldwide, with existing vaccines offering only limited protection. While these vaccines focus on a surface protein called haemagglutinin (HA), another key protein, neuraminidase (NA), has been less extensively studied as a vaccine target. NA facilitates viral spread by releasing the virus from infected cells, and NA monoclonal antibodies have been found to be protective and broadly reactive. In this thesis, we explore NA as a vaccine target.

Our research developed a NA-based vaccine platform using nanoparticles to enhance the immune response. This NA vaccine, combined with an adjuvant, protected mice against deadly doses of three different influenza strains, even at very low vaccine doses. We also explored a multivalent version of this vaccine to prepare for potential future pandemics. Additionally, we addressed challenges in producing a soluble NA vaccine at high yield by engineering the NA sequence based on its structure. The engineered vaccine NA generated a strong antibody response in mice and showed protection against severe influenza infections. Our findings highlight that NA-based vaccines hold great promise for improving flu prevention and preparing for future outbreaks.

Scientific abstract

Influenza remains a major cause of morbidity and mortality worldwide. Current vaccines are based on haemagglutinin (HA), and the vaccine effectiveness remains sub-optimal. Neuraminidase (NA), another surface glycoprotein, has been underexplored as a vaccine target. The NA tetramer catalyses the sialic acid, facilitating the release of virions from infected cells. NA protein vaccines have been reported to generate protective antibodies in several animal models, as well as in humans.

We previously established a nanoparticle-based NA vaccine platform, achieved through covalent linkage between SpyTag and SpyCatcher tags on the NA and mi3 virus-like particle (VLP) respectively. NA-VLP, adjuvanted with AddaVax, generated a better antibody response in mice compared to NA protein alone, demonstrating a dose sparing effect when challenged with three different influenza strains from H1N1 and H3N2 subtypes (X-179A, X-31, and PR8). Animals were protected against a lethal virus challenge with as low as 0.1 μg NA-VLP protein conjugate. Additionally, we tested a multivalent NA-VLP mix vaccine in mice to evaluate its potential for future pandemic preparedness.

Production of soluble NA as stable tetramers and at high yield has been a significant hurdle in NA vaccine development. We overcame this challenge by creating a hybrid NA, in which the surface antigenic loops from the vaccine NA were transplanted onto the scaffold of a stable, high-yielding NA. The hybrid NA was produced as stable tetramers at yields up to ~5 - 50-fold higher than the original NA. Immunization of mice with the hybrid NA induced protective antibodies.

These findings highlight NA as a promising target for influenza vaccines and provide valuable insights into future vaccine design and manufacturing.

Declaration

The intellectual content, ideas, analyses, and conclusions presented in this thesis represents my own work, except where stated below:

Chapter 2: The thermal stability and unfolding of NA proteins were analyzed using the nanoDSF (differential scanning fluorimetry) technique on a Prometheus Panta instrument (Nanotemper), with measurements performed by Pramila.

Chapter 4: Constructs designs were made my Dr Rijal. Protein production and animal studies were conducted in collaboration with Pramila Rijal.

Chapter 5: The concept of "loop-grafting" were developed by Prof Alain Townsend and Dr Pramila Rijal, and the animal studies and sample analysis were carried out in collaboration with Pramila Rijal.

Chapter 6: The chicken experiments described in section 6.2 were conducted in collaboration with Prof Munir Iqbal from the Pirbright Institute.

This thesis incorporates the use of artificial intelligence (AI) tools to support various aspects of its preparation. Specifically, OpenAI's ChatGPT was used for language and grammar assistance, formatting and polishing. I affirm that the use of ChatGPT complies with institutional guidelines for ethical and academic integrity.

Acknowledgements

I would like to express my sincere gratitude to everyone who provided me with support and guidance throughout the completion of this thesis. First and foremost, I extend my deepest appreciation to my advisor, Professor Alain Townsend and Dr. Pramila Rijal for their invaluable mentorship, constructive feedback, and unwavering patience. Their expertise and guidance were instrumental in shaping my research and helping me navigate the challenges that arose along the way.

I owe special thanks to my colleagues and fellow graduate students in the Townsend lab and MRC WIMM. Our lively discussions, brainstorming sessions, and mutual support made this journey truly enjoyable. I am also thankful for the administrative staff who assisted me in overcoming countless procedural and logistical hurdles.

A heartfelt thank you goes out to my family and friends who never ceased to believe in me. Your moral support, understanding, and patience provided me with the strength and motivation to keep going. Without their unwavering faith in my abilities, this thesis would not have been possible.

Finally, I appreciate the funding and resources provided by COI/CAMS, which allowed me to carry out my research effectively. The assistance and support received from all these individuals and institutions have been pivotal in the successful completion of my thesis.

Thank you all for being part of this journey.

Table of Contents

List of Tables

List of Figures

List of Appendices

Chapter 1 Introduction to Influenza

1.1 Influenza virus

1.1.1 Influenza as a globally health concern

Influenza, commonly known as the flu, is a highly contagious respiratory illness caused by the influenza virus, a member of the Orthomyxoviridae family. It remains a significant global health threat in its zoonotic, seasonal, and pandemic forms. These forms result in substantial mortality and morbidity, particularly among vulnerable populations and in developing countries (Bresee et al., 2018; Fischer et al., 2014). Seasonal influenza viruses evolve continuously, causing severe illness annually, especially among the elderly, children, pregnant women, and those with underlying chronic conditions. Globally, it is estimated that influenza affects 1 billion people each year, with 3 to 5 million cases being severe and 290,000 to 650,000 resulting in influenza-related respiratory deaths (*Global Influenza Strategy 2019–2030*; Iuliano et al., 2018).

Influenza viruses circulating among domestic poultry, wild birds, and swine represent a persistent threat to human health as they can occasionally cross species barriers and infect humans, potentially leading to pandemics. The first human case of avian influenza A (H5N1) was detected in 1997 (Chan, 2002), with its re-emergence in 2003, signalling the potential for a pandemic. Since then, other avian influenza strains, including A(H5N6) and A(H9N2), have sporadically infected humans, often with severe outcomes. Notably, the avian influenza A(H7N9) subtype (Butler, 2013), which emerged in China in 2013, has caused unusually severe human infections, further emphasizing the threat these viruses pose. Although these viruses have not yet acquired the ability to spread efficiently between humans, they are only a few mutations away from becoming a pandemic threat (Cao et al., 2023).

This ongoing risk underscores the importance of continuous and collaborative efforts. Integrating human, animal, and environmental health is essential to improve surveillance, vaccination, and response strategies against emerging infectious diseases.

1.1.2 Influenza discovery history

The history of the discovery and isolation of the influenza virus is a fascinating narrative spanning over a century, showcasing remarkable advancements in virology. A brief overview of this discovery is depicted in Figure 1.1, with the detailed timeline summarised as follows (*History of Flu (Influenza): Outbreaks and Vaccine Timeline*; *History of Influenza Vaccination*; Threats et al., 2005):

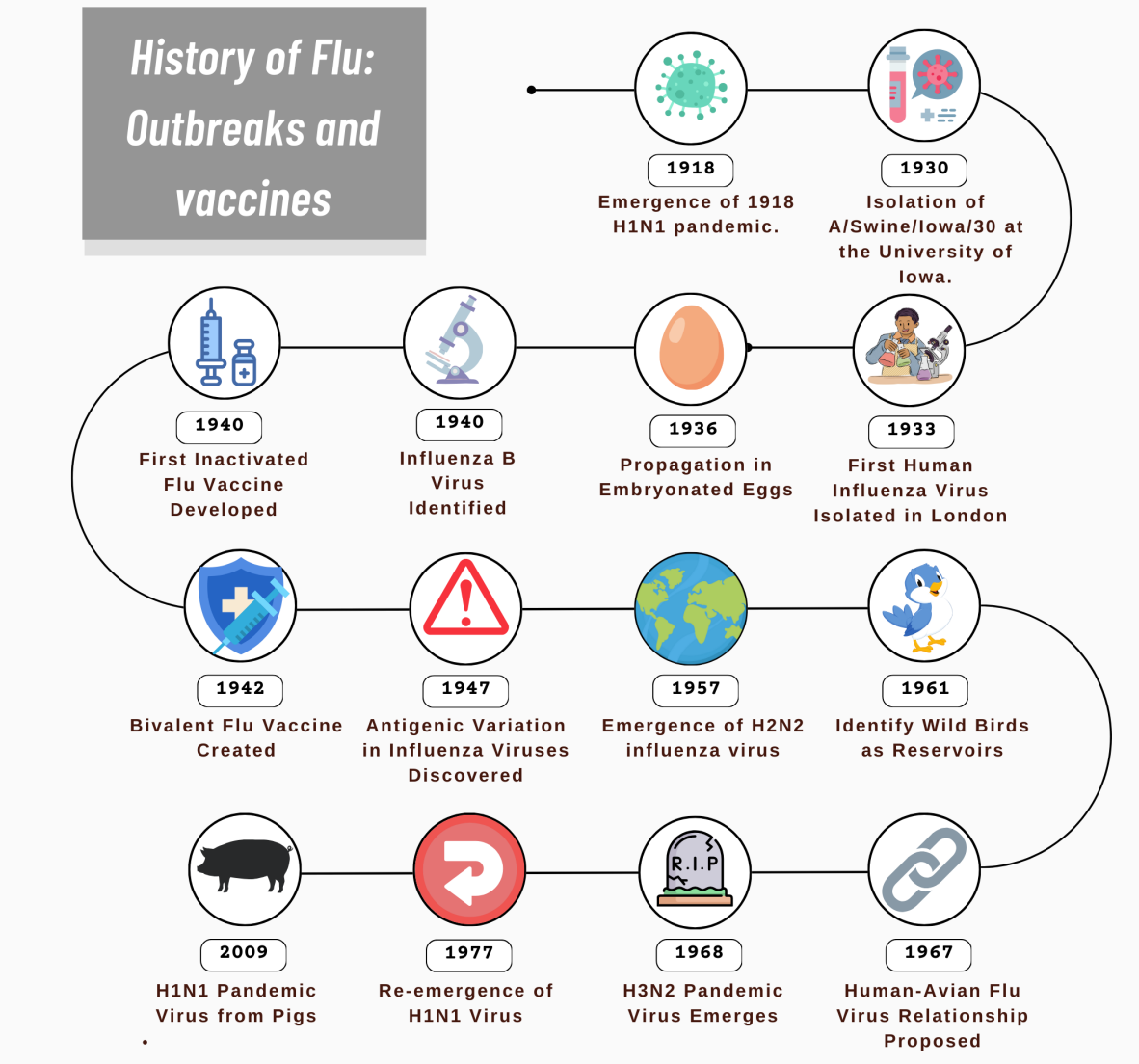

Figure 1.1 **Influenza Discovery and Vaccine Timeline**

Key milestones in influenza discovery:

1918: The first significant breakthrough in the identification of influenza viruses came with the recognition of the H1N1 subtype during the 1918–1919 pandemic, which demonstrated the virus's capacity for rapid global spread and severe consequences.

1930: The first swine influenza virus A/Swine/Iowa/30 was isolated at the University of Iowa.

1933: Wilson Smith, Sir Christopher Andrews, and Sir Patrick Laidlaw isolated the first human influenza virus in London by intranasally inoculating ferrets with human nasopharyngeal washes from an influenza patient (Smith et al., 1933).
1936: Frank Macfarlane Burnet discovered that influenza viruses could be propagated in embryonated hens' eggs, a technique still used in vaccine production today.
1940: An antigenically distinct influenza virus, type B (B/Lee/40), was isolated by Dr. Francis and Dr. Schaefer.
1940: Thomas Francis Jr. and Jonas Salk developed the first inactivated influenza vaccine at the University of Michigan, using fertilized chicken eggs-a method still in use today (Francis et al., 1947).
1942: After the discovery of influenza B viruses, a bivalent vaccine offering protection against both influenza A and B viruses was produced.
1947: A seasonal flu epidemic revealed antigenic changes in circulating influenza viruses, rendering existing vaccines ineffective and underscoring the importance of continuous virus surveillance.
1957: The H2N2 influenza virus emerged, marking another pandemic.
1961: An outbreak in South Africa suggested that wild birds might serve as reservoirs for influenza A viruses.
1967: Dr. H.G. Pereira and colleagues found an antigenic link between the 1957 human pandemic virus and an influenza A virus from a turkey, suggesting an avian origin for human influenza viruses.
1968: The H3N2 influenza virus caused a pandemic, leading to approximately 100,000 deaths in the U.S. and 1 million globally, primarily affecting individuals aged 65 and older. The H3N2 viruses circulating today are descendants of this strain.
1977: The H1N1 influenza virus re-emerged, further complicating influenza surveillance and vaccination efforts.
2003: Nasal spray LAIV licensed in 2003.
2009: A novel H1N1 pandemic virus, originating from pigs, emerged, causing a global health crisis.
2013: Vaccine using recombinant DNA technology approved.

Influenza viruses have caused numerous pandemics throughout history, profoundly affecting global health and society (Table 1.1). The 20th century saw three major pandemics: the 1918 H1N1 pandemic, the 1957 H2N2 pandemic, and the 1968 H3N2 pandemic (Kilbourne, 2006). In the 21st century, an unexpected H1N1 pandemic originating from swine emerged in 2009. The dynamics of circulating influenza strains in humans are depicted in Figure 1.2.

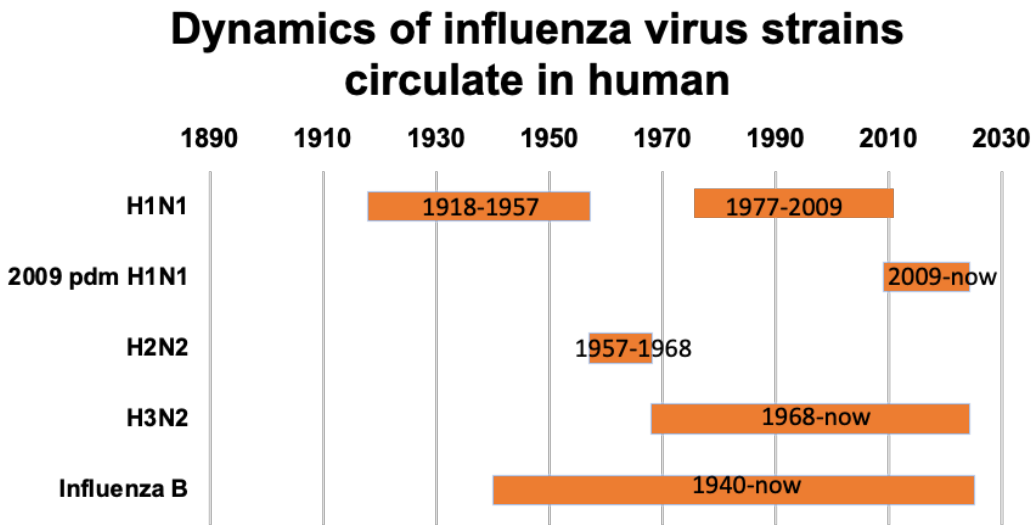

Figure 1.2 **Dynamics of Influenza Virus Strains Circulating in Human**

Table 1.1 Influenza Pandemic Timeline

Pandemic	Strain	Period	Approximate Number of Death	Notes
Spanish Flu	H1N1	1918-1929	40-50 million	One of the deadliest pandemics in history
Asian Flu	H2N2	1957-1958	1-2 million	Originated in East Asia
Hong Kong Flu	H3N2	1968-1979	500,000-2million	Originated in Hong Kong
Russian Flu	H1N1	1977-1978	700,000	Re-emergence of H1N1, mostly infect young population
Pandemic 2009 (pdm)	H1N1	2009-2010	Up to 575,000	Originated from pigs

1.1.3 Influenza Classification and Reassortment

The name “influenza” is derived from the Latin word for “influence,” referring to the cold influence associated with the seasonal appearance of the virus (Field’s Virology; Volume 1: Emerging Viruses, 7th Edition). Influenza virus belongs to the Orthomyxoviridae family (Genetics of the Influenza Virus | Learn Science at Scitable). Influenza names are designated according to their genus, the isolated species (omitted if human), the location of isolation, the isolate number, the year of isolation, and the haemagglutinin (HA) and neuraminidase (NA) subtypes. For example, the seventh isolation of a human H1N1 influenza A virus in California in 2009 is written as A/California/7/2009 (H1N1) (Field’s Virology; Volume 1: Emerging Viruses, 7th Edition). There are 19 different HA subtypes (H19 recently reported by(Fereidouni et al., 2023), not shown in Fig. 1.3) and 11 NA subtypes, as shown in Fig. 1.3.

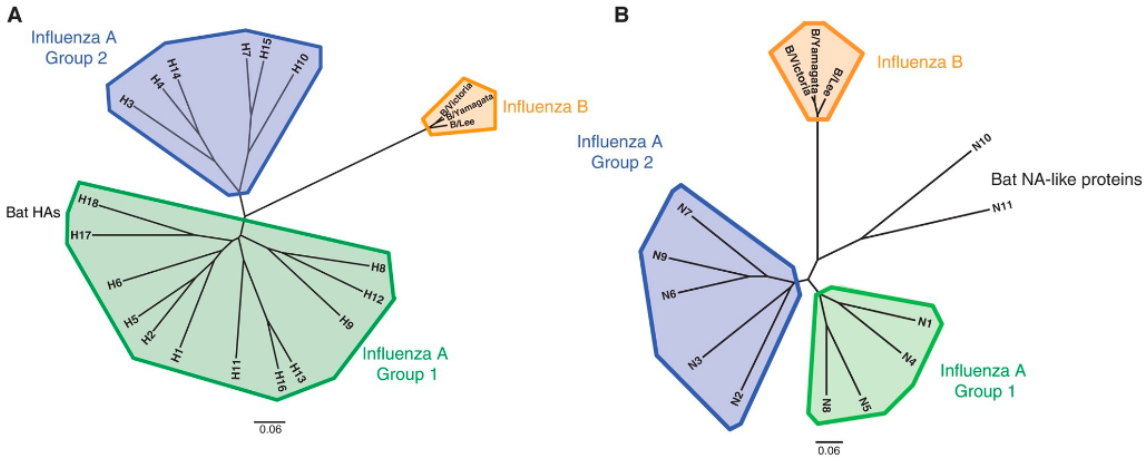

Figure 1.3 **Phylogeny of Influenza A and B viruses hemagglutinins (HAs) and neuraminidases (NAs) (Cited from (Field’s Virology; Volume 1: Emerging Viruses, 7th Edition)).**
Unrooted, radial phylogenic trees based on amino acid sequences of the HA (A) and NA (B) proteins from representative influenza A and B viruses.

Within one genus, taking influenza A viruses as an example, influenza viruses undergo reassortment—a process in which gene segments are exchanged between different strains during co-infection (Steel & Lowen, 2014). This mechanism generates viral diversity and plays a crucial role in influenza evolution.

Reassortment can lead to **antigenic shifts**, potentially modifying host range, pathology, and transmission of the virus (Urbaniak & Markowska-Daniel, 2014). Notable examples include the 1957 Asian flu, 1968 Hong Kong flu, and the 2009 H1N1 pandemic.

The likelihood of reassortment depends on various factors, including coinfection probability, mixing of gene segments, and fitness of reassortant genotypes (Lowen, 2017). Along with mutations, reassortment contributes to the virus's ability to cause annual epidemics and occasional pandemics (Shao et al., 2017).

This continual genetic evolution leads to the unpredictable nature of influenza virus, as seen with various avian influenza strains that have crossed species barriers and infected humans in recent years (Khanna et al., 2009).

1.1.4 Influenza virion structure and subtypes

The structure of the influenza A virus is complex, as shown in Fig. 1.4. The genome of the virus is encased in a capsid consisting of HA, NA, and M2 (Fig 1.4A, (*Field's Virology; Volume 1: Emerging Viruses, 7th Edition*)).

The morphology of the influenza A virus is characterised by distinctive spikes observed in negatively stained electron micrographs, as shown in Fig. 1.4B. These spikes, composed of HA and NA, are 10–14 nm in length, while the spherical particle has an estimated diameter of approximately 100 nm (Laver & Valentine, 1969).

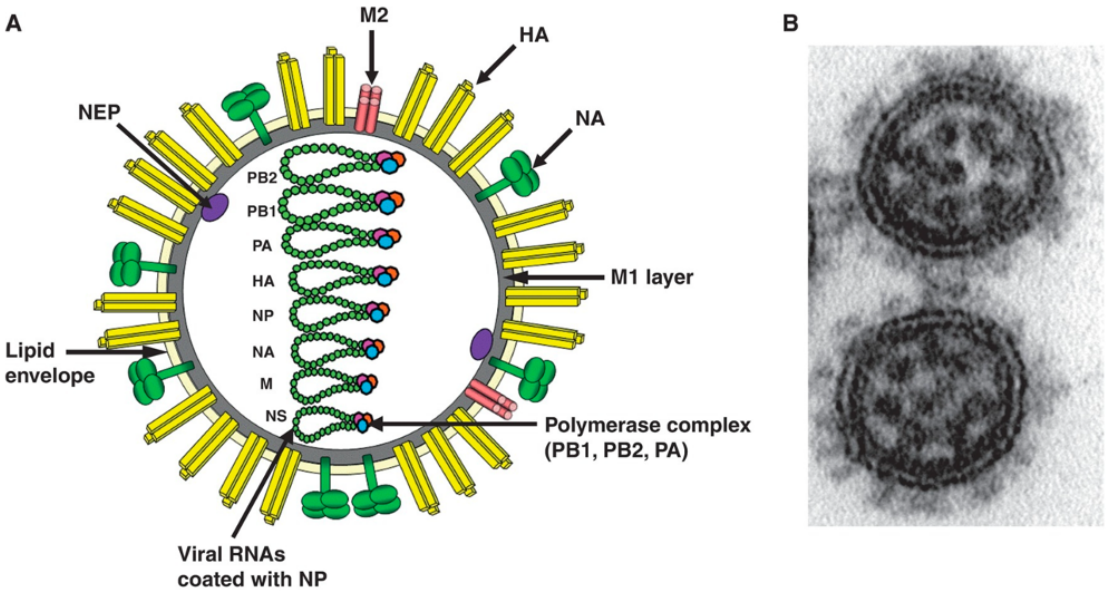

Figure 1.4 **Schematic diagram and electron micrograph of influenza virus particle（Cited from (Field's Virology; Volume 1: Emerging Viruses, 7th Edition)**
A: The HA, NA and M2 proteins are inserted into the host-derived lipid envelope. HA is found as trimer and NA and M2 as tetramer. B: Electron micrograph thin-section image of influenza virus particle (diameter ~100nm), with HA and NA visible on the surface.

Hemagglutinin (HA) is responsible for the virus's ability to bind to sialic acid receptors on the host cell surface, initiating the infection process (Gamblin & Skehel, 2010). After the virus enters the host cell, the HA protein undergoes a conformational change, exposing a fusion peptide that facilitates the merger of the viral and cellular membranes (Boonstra et al., 2018). This entry mechanism is a critical aspect of the influenza virus's life cycle, allowing the viral genetic material to be delivered into the host cell's cytoplasm.

In contrast, the neuraminidase protein (NA) plays a crucial role in viral egress, or release, from the host cell (Gamblin & Skehel, 2010). NA cleaves the sialic acid bonds that tether newly formed virions to the host cell surface, enabling the virus to detach and infect neighbouring cells(Sakai et al., 2017).

The genome of the influenza A virus consists of eight negative-sense discrete RNA segments, each encoding a specific core viral protein, as shown in Table 1.2. In addition to the core proteins, some genes, such as PA and PB1, also encode additional proteins. The viral RNA is

closely associated with nucleoprotein and the components of the viral polymerase complex, forming the viral ribonucleoprotein (vRNP) complexes (Akkina et al., 1991; Richardson & Akkina, 1991), reviewed in *Field's Virology; Volume 1: Emerging Viruses, 7th Edition*).

Table 1.2 Influenza genome segments and functions

Segment	Proteins Expressed	Function
1	PB2 (Polymerase Basic 2)	Part of the RNA-dependent RNA polymerase complex; involved in cap-snatching
2	PB1 (Polymerase Basic 1)	Core component of the RNA-dependent RNA polymerase complex
	PB1-F2 (in some strains)	Pro-apoptotic activity; modulates host immune response
	PB1-N40	N-terminally truncated version of PB1; exact function not fully understood
3	PA (Polymerase Acidic)	Part of the RNA-dependent RNA polymerase complex; endonuclease activity
	PA-X	Modulates host gene expression; involved in host shutoff
4	HA (Hemagglutinin)	Viral attachment to host cells; fusion of viral and cellular membranes
5	NP (Nucleoprotein)	Encapsidates viral RNA; essential for transcription and replication
6	NA (Neuraminidase)	Cleaves sialic acid; facilitates virus release and spread
7	M1 (Matrix protein 1)	Forms the viral matrix; involved in virion assembly and budding
	M2 (Matrix protein 2)	Ion channel; important for viral uncoating and assembly
	M42 (in some strains)	Alternative form of M2 ion channel
8	NS1 (Non-structural protein 1)	Interferon antagonist; modulates host immune response
	NEP/NS2 (Nuclear Export Protein)	Mediates export of viral RNPs from the nucleus; involved in virion assembly

The intricate structure of the influenza virion, with its surface glycoproteins and segmented genome, endows the virus with a remarkable capacity for adaptation and evolution. The phenomenon of **antigenic drift**, driven by the high mutation rate of the viral polymerase due to the absence of a proofreading mechanism (3' to 5' exonuclease activity), enables the influenza virus to gradually accumulate changes in its surface proteins, thereby evading the host's long-term adaptive immune responses.

1.2 Historical influenza vaccine study

1.2.1 Historical development of influenza vaccines and focus on HA as primary antigen

The development of influenza vaccines is challenged by the substantial antigenic shift and drift of the influenza virus, leading to widely varying vaccine efficacy (Ortiz de Lejarazu & Tamames, 2015). Consequently, current seasonal influenza vaccines are updated annually, relying on the global surveillance system to predict the future circulating strains. While these vaccines target predicted seasonal strains, their efficacy can vary significantly, ranging from 10% to 60%, due to mismatches and population vulnerabilities (CDC, 2024).

Historically, influenza vaccine development has focused on hemagglutinin (HA) as the primary antigen, owing to its abundance and immune dominance (Johansson et al., 1987; Wohlbold & Krammer, 2014). HA plays a crucial role in viral entry through receptor binding and membrane fusion and exhibits the highest rates of adaptive evolution among influenza proteins (Bhatt et al., 2011).

To address these challenges, researchers have explored various strategies to create a universal influenza vaccine, including stalk-directed, consensus-based, and computationally derived HA immunogens (Bullard & Weaver, 2021). The role of adjuvants in enhancing humoral responses and their impact on vaccine-elicited antibody repertoires are also being investigated to broaden protection against influenza A viruses (Nagashima & Mousa, 2021).

As a result of this historical emphasis on HA, licensed influenza vaccines are quantified based on HA content (Myers et al., 2023). The current licensed seasonal vaccines in the UK are primarily quadrivalent, comprising four strains of the influenza virus. These vaccines are tailored to different age groups and employ various manufacturing methods, as outlined in Table 1.3 (*Flu Vaccines for the 2024 to 2025 Season*).

Table 1.3 List of current licensed vaccines

Vaccine Name	Manufacturer	Production Method	Vaccine Type	Adjuvant	Age Group	Route of Administration	HA Content
Cell-based Quadrivalent Influenza Vaccine (QIVc/Flucelvax)	CSL Seqirus	MDCK cells	Inactivated Subunit	None	From 6 months	Intramuscular (IM)	15 µg HA per strain
Fluenz/FluMist (LAIV)	AstraZeneca	Egg-based	Live attenuated	None	2 to 18 years	Intranasal	10^6.5-7.5 FFU of live attenuated virus per strain
Quadrivalent Influenza Vaccine (QIVe)	Sanofi	Egg-based	Inactivated Split virion	None	From 6 months	IM	15 µg HA per strain
Influenza Tetra MYL (QIVe)	Viatris	Egg-based	Inactivated Split virion	None	From 6 months	IM	15 µg HA per strain
Quadrivalent Influenza Vaccine – High Dose (QIV-HD)	Sanofi	Egg-based	Inactivated Split virion	None	From 60 years	IM	60 µg HA per strain
Adjuvanted Quadrivalent Influenza Vaccine (aQIV/Fluad)	CSL Seqirus	Egg-based	Inactivated Subunit	MF59	From 60 years	IM	15 µg HA per strain
Flublok Recombinant Influenza Vaccine	Sanofi (Protein Sciences)	Baculovirus expression system	Recombinant protein	None	From 65 years	IM	45 µg HA per strain

FFU: fluorescent focus unit

Note that, Split virion vaccines contain inactivated influenza virus that has been split or disrupted, including surface antigens and internal proteins of the virus, whereas subunit vaccines contain only highly purified surface antigens (HA and NA) of the influenza virus, without internal proteins.

1.2.2 Evolution of research on NA as vaccine candidate

A list of milestones in the discovery of NA are listed in Table 1.4.
In early studies, hemagglutinin's ability to agglutinate red blood cells was discovered in 1941. Shortly afterwards, Hirst observed the "receptor-destroying enzyme," which released the virus from attached red blood cells (Hirst, 1942). This enzyme was later characterised and named neuraminidase (NA) for its ability to cleave N-acetyl neuraminic acid (Burnet, 1951; Gottschalk, 1957).

The application of negative staining in electron microscopy to study virus structures (Brenner & Horne, 1959), marked significant progress. By 1960, electron micrographs of influenza revealed well-defined surface projections with pleomorphism (Horne et al., 1960). Subsequent morphological studies detailed the neuraminidase structure, showing its subunits aggregated by the tips of their tails, forming a "dandelion-like" homotetramer structure (Laver & Kilbourne, 1966; Laver & Valentine, 1969). Alongside these structural insights, Laver and Kilbourne developed the first neuraminidase assay, using heavily glycosylated fetuin to estimate enzymatic activity (Laver & Kilbourne, 1966).

Using this fetuin-based assay, researchers demonstrated that NA evolves independently of HA. This was evidenced by the 1968 Hong Kong pandemic, during which HA exhibited a clear antigenic shift while NA remained consistent with the H2N2 strain circulating since 1957 (Schulman & Kilbourne, 1969).

Later, the isolation of NA using pronase enabled crystallisation with purified NA, advancing structural analysis and facilitating the measurement of serum responses to NA as a standalone vaccine antigen (Laver, 1978). Building on this, Colman and Varghese revealed the first three-dimensional structures of various N2 strains in 1983 (Colman et al., 1983). Although vaccine development efforts during this period predominantly focused on HA, Kilbourne and collaborators made significant progress in investigating NA as a potential vaccine candidate (Johansson et al., 1998; Kilbourne, 1976; Kilbourne et al., 1995).

Kilbourne and colleagues also introduced the concept of "permissive" vaccination, suggesting that while NA-based vaccines might not prevent infection, they could allow asymptomatic infection and enhance immune responses. This approach could promote stronger and faster responses to subsequent infections by new influenza strains, aided by pre-existing NA immunity (Couch et al., 1974; Johansson et al., 1993).

The discovery of NC41, the first antibody shown to bind neuraminidase, reignited interest in the broad immunity provided by NA (Malby et al., 1994; Tulip, Varghese, Laver, et al., 1992).

Table 1.4 Milestones in understanding NA's role in influenza infection and immunity

Year	Milestone	Description	References
1941	Discovery of Hemagglutination	Hirst discovered that influenza virus particles cause red blood cells to agglutinate, forming a lattice (hemagglutination).	(Hirst, 1941)
1942	Development of Hemagglutination Assay	Hirst developed the hemagglutination assay, an important method for studying viruses.	(Hirst, 1942)
1942	Discovery of Receptor-Destroying Enzyme	Hirst observed that hemagglutination wears off over time and identified an intrinsic enzymatic activity (later known as neuraminidase) that releases the virus from red blood cells, describing it as a "receptor-destroying enzyme."	(Hirst, 1942)
1947	Characterization of Receptor-Destroying Enzyme	Burnet and colleagues characterized the "receptor-destroying enzyme," linking it more closely to influenza's biology.	(Burnet, 1951)
1960	Electron Micrographs of Influenza Virus	Electron microscopy provided the first detailed images of the influenza virus, contributing to the understanding of its structure.	(Horne et al., 1960)
1966	First Neuraminidase Assay	Laver and Kilbourne described the first neuraminidase assay, marking a significant step in the study of influenza enzymes.	(Laver & Kilbourne, 1966)
1966	Isolation of Hemagglutinin and Neuraminidase Subunits	Laver and Valentine studied the morphology of the isolated hemagglutinin and neuraminidase subunits of the influenza virus.	(Laver & Valentine, 1969; Laver & Webster, 1966)
1978	Isolation and Crystallization of Neuraminidase	Laver isolated neuraminidase using Pronase and later performed crystallization on H3N2 and H2N2 strains, advancing structural studies of the enzyme.	(Laver, 1978)
1983	Crystal Structure of Neuraminidase	Colman and Varghese solved the 3-dimensional structure of influenza neuraminidase, providing critical insights into its function and potential as a drug target.	(Colman et al., 1983; Varghese et al., 1983)
1991	Discovery of N9 Antibody Structure	Research led to the discovery of the structure of antibodies against the N9 subtype of neuraminidase, using mouse monoclonal antibodies.	(Malby et al., 1994; Tulip, Varghese, Laver, et al., 1992; Tulip, Varghese, Webster, et al., 1992)
1991	Development of ELLA Assay	The Enzyme-Linked Lectin Assay (ELLA) was developed, allowing for more detailed studies of neuraminidase activity and inhibition.	(Lambré et al., 1990, 1991)
1995	First Vaccine Using Purified Neuraminidase	The first and only human trial of a vaccine containing purified neuraminidase was conducted, highlighting NA as a potential vaccine target.	(Kilbourne et al., 1995)

1.3 Dissecting NA as a promising vaccine target

1.3.1 NA structure and activity as a sialidase

The structure of neuraminidase (NA) has been extensively studied. When embedded in the viral envelope, NA constitutes approximately 10–20% of the total glycoproteins on the surface. For an average-sized virion, this translates to roughly 300–400 HA spikes and 40–50 NA spikes (Moulès et al., 2011).

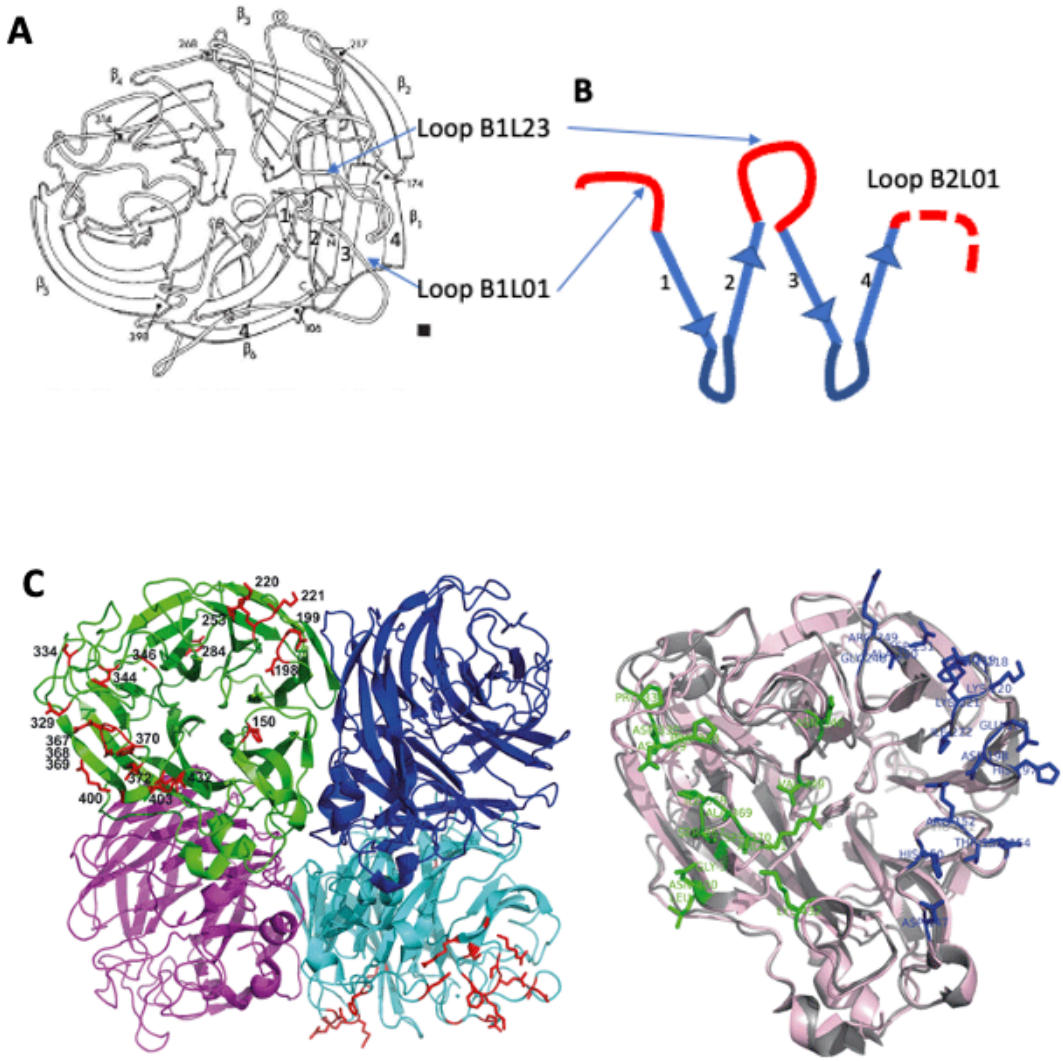

Figure 1.5 **Structure analysis of NA**
A)Structure revealed by Colman and Varghese in 1983(Colman et al., 1983; Varghese et al., 1983). B) Topology of each beta sheet in NA. C) Escape mutations in NAs surrounded the active site are shown as red rods on the green and cyan subunits. The NA is oriented such that the catalytic site of the green subunit is facing directly upward (Air, 2012). D) Epitope mapping of mAbs NC41 (green) and Mem5 (blue) with therapeutic potential targeting the N9 NA (pink) of influenza A(H7N9) virus (Air, 2012).

Early exploration using electron microscopy revealed details of the neuraminidase structure, including its subunits aggregated by the tips of their tails, forming a dandelion-like arrangement (Laver & Kilbourne, 1966; Laver & Valentine, 1969; Laver & Webster, 1966). Shortly thereafter, the first crystal structure of NA was published by Colman and Varghese in 1983 (Colman et al., 1983; Varghese et al., 1983).

NA is a homotetramer composed of four identical polypeptide chains. These chains form a box-shaped "head" connected to the viral membrane via a stalk and transmembrane domain. Each monomer of the tetramer consists of approximately 470 amino acid residues, while the stalk is around 15 Å wide and ranges from 60 to 100 Å in length. The entire tetramer has a molecular mass of approximately 240 kDa. The head domain of the tetramer measures about 80 x 80 x 40 Å and features a six-bladed propeller structure that houses the catalytic site (Shtyrya et al., 2009). ach monomer contains six β-sheets, each comprising four strands with a "W"-shaped topology (Fig. 1.5 A & B).

The upper surface of the head domain, which contains the catalytic pocket, is formed by 12 loops of the polypeptide chain. Six loops connect strand 4 of one sheet to strand 1 of the next (designated as L01), while the other six loops connect strand 2 to strand 2 (designated as L23) (Fig. 1.5). Together, these 12 loops outline the catalytic pocket, giving it a flower-like shape.

Eighteen highly conserved charged amino acids have been identified in all influenza A and B neuraminidase strains (Colman et al., 1983, 1987):
Negatively charged residues: Glu 119, Asp 151, Asp 198, Glu 227, Asp 243, Glu 276, Glu 277, Asp 330, Glu 425.
Positively charged residues: Arg 118, Arg 152, Arg 224, His 274, Arg 292, Lys 350.
Hydrophobic residues: Tyr 121, Leu 134, Trp 178 (N2 numbering).

The active site of neuraminidase comprises eight catalytic and eleven framework residues, as shown in Fig. 1.6 (Baek et al., 2014). The catalytic residues, conserved across all influenza A neuraminidases, directly interact with the sialic acid receptor. Meanwhile, the framework residues are essential for maintaining the enzyme's overall structure and functionality.

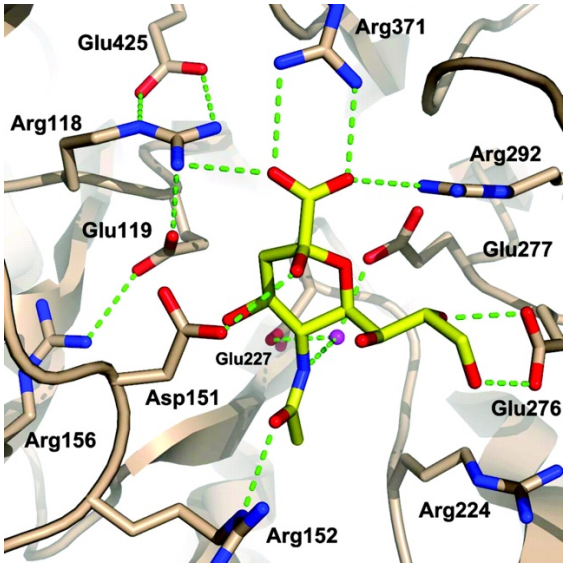

Figure 1.6 **Structure of complex between NA and sialic acid, showing NA catalytic and framework residues (cited from (Baek et al., 2014))**
Sialic acid is depicted as yellow bars. Positively charged residues are shown in blue, while negatively charged residues are shown in red.

Some avian neuraminidases (N1, N2, N5, N6, and N9) possess a second sialic acid-binding site (2SBS) formed by six residues, as outlined in Table 1.5 (revised from (McAuley et al., 2019)). The 2SBS is known to enhance catalytic activity, influence host tropism and adaptation, and affect the HA-NA balance.

Table 1.5 List of catalytic, framework and second sialic acid biding site (2SBS)

Residue Type	Amino Acid (Position)	Charge	Interaction with Sialic Acid / Structural Role
Catalytic	Arg (118)	Positive (Polar)	Ionic interaction with carboxylate of sialic acid
Catalytic	Asp (151)	Negative (Polar)	Polar contact with sialic acid
Catalytic	Arg (152)	Positive (Polar)	Binds to acetamido group on sugar ring
Catalytic	Arg (224)	Positive (Polar)	Non-polar contact with glycerol fragment of sialic acid
Catalytic	Glu (276)	Negative (Polar)	Interacts with 8- and 9-hydroxyl groups on glycerol side chain
Catalytic	Arg (292)	Positive (Polar)	Ionic interaction with carboxylate of sialic acid
Catalytic	Arg (371)	Positive (Polar)	Ionic interaction with carboxylate of sialic acid

Residue Type	Amino Acid (Position)	Charge	Interaction with Sialic Acid / Structural Role
Catalytic	Tyr (406)	Neutral (Polar)	Polar contact, forms covalent bond during reaction (catalytic nucleophile)
Framework	Glu (119)	Negative (Polar)	Structural role: maintains active site shape
Framework	Arg (156)	Positive (Polar)	Structural role: stabilizes enzyme structure
Framework	Trp (178)	Neutral (Hydrophobic)	Structural role: maintains active site pocket
Framework	Ser (179)	Neutral (Polar)	Structural role: contributes to enzyme stability
Framework	Asp/Asn (198)	Negative (Polar/Neutral)	Structural role: maintains active site shape
Framework	Ile (222)	Neutral (Hydrophobic)	Structural role: contributes to enzyme stability
Framework	Glu (227)	Negative (Polar)	Structural role: maintains active site shape
Framework	His (274)	Positive (Polar)	Structural role: important for drug binding and resistance
Framework	Glu (277)	Negative (Polar)	Structural role: stabilizes enzyme structure
Framework	Asn (294)	Neutral (Polar)	Structural role: maintains active site pocket
Framework	Glu (425)	Negative (Polar)	Structural role: contributes to enzyme stability
2SBS	Ser (367)	Neutral (Polar)	Hydrogen bond with sialic acid in second binding site
2SBS	Ser (370)	Neutral (Polar)	Hydrogen bond with sialic acid in second binding site

Residue Type	Amino Acid (Position)	Charge	Interaction with Sialic Acid / Structural Role
2SBS	Ser (372)	Neutral (Polar)	Hydrogen bond with sialic acid in second binding site
2SBS	Asn (400)	Neutral (Polar)	Hydrogen bond with sialic acid in second binding site
2SBS	Trp (403)	Neutral (Hydrophobic)	Hydrophobic interaction with sialic acid in second binding site
2SBS	Lys (432)	Positive (Polar)	Hydrogen bond with sialic acid (direct in N9, via water in N2 and N5)

N2 numbering (as in PDB 1nn2) is used here.

Despite the highly conserved epitopes surrounding the catalytic site, numerous neuraminidase (NA) epitopes identified using escape mutants are located on the upper surface near the concave catalytic site of a monomer, as illustrated in Fig. 1.5C ((Webster et al., 1987)reviewed in (Air, 2012)). In addition to the classical method of epitope mapping via escape mutations, computational approaches—including sequence alignment, 3D modelling, and epitope prediction algorithms—have been employed to identify potential epitopes in the H1N1 strain (Loyola et al., 2013).

Immunoinformatics-based methods have successfully predicted and experimentally validated linear B-cell epitopes on the NA of 2009 A/H1N1 viruses. Among these, five peptides demonstrated potential as synthetic vaccine candidates (Huang et al., 2011).

1.3.2 NA antibodies as a correlate of protection in humans

Antibodies to NA is different from the neuralization antibodies against HA as they do not directly neutralise viral infectivity (Kilbourne et al., 1968). This aligns with the sialidase function of NA, which facilitates the release of virions from infected cells (Gilbert et al., 2019; Giurgea et al., 2020).

Although human sera possess a limited antibody repertoire to NA antigenic variants, as selected with monoclonal antibodies (Natali et al., 1984), NA immunity is usually broader compared to HA (reviewed in (Eichelberger & Monto, 2019). Studies in human populations with infection showed little correlation between haemagglutinin-inhibition (HAI) titres and neuraminidase-inhibiting (NAI) titres (Couch et al., 2013; Desheva et al., 2015; Monto et al., 2015; Rumfelt et al., 2023). However, studies in vaccinated populations demonstrated that NAI titres independently correlate with vaccine efficacy (Monto et al., 2015).

Analyses of serum and nasal secretions (NS) in healthy adults monitored for influenza infection revealed that increasing anti-HA and anti-NA titres in both serum and NS correlated with reduced infection and infection-associated illness, independently predicting immunity. Notably, only serum NAI titres independently predicted reduced illness (Couch et al., 2013).

In murine models, intranasal vaccination with adjuvanted NA conferred greater heterologous protection compared to adjuvanted HA in H1N1 challenge studies (Kawai et al., 2021). Similarly, studies examining the transfer of antisera in mice prior to influenza B virus infection found that NA antisera provided superior protection against heterologous IBV strains compared to HA antisera (Portela Catani et al., 2023). This corresponds to the "one-way" drift phenomenon, whereby antiserum generated against one virus shows reduced inhibition of the other, but the reciprocal antiserum continues to inhibit both viruses (reviewed in (Eichelberger & Monto, 2019); (Sandbulte et al., 2009)).

These findings suggest that NA contains more conserved epitopes, contributing to broad cross-protection. This is consistent with conserved epitope mapping results in H1N1 and H5N1 (Wan et al., 2013).

1.3.3 Monoclonal antibodies to NA

Take a deeper look at molecular level, more and more NA-specific antibodies bind to conserved epitopes and protect against heterologous viruses are reported recently (See Table 1.6 below). First monoclonal NA antibody HCA-2 binds to all influenza A subtypes was first reported in 2013, targeting the conserved linear epitope (aa222-230) was reported to bind all influenza A NA subtypes (Doyle et al., 2013). Another anti-NA antibody (1G01) binds right into the catalytic site and inhibition a wide range of both influenza A and B subtypes was reported in 2018 (Chen et al., 2018). More pan influenza cross-reactive antibodies have been reported, namely FNI9 (Momont et al., 2023), DA03E17 (Yasuhara et al., 2022), indicating the persisting antibody population targeting the conserved epitopes including the catalytic site residues.

Table 1.6 NA antibodies and binding characteristics

Antibody	Binding Characteristics	NA Inhibition	Origin	Other Information	Reference
FNI9	Broad reactivity against group 1 and 2 IAVs, IBVs	Potent inhibition of all group 1 and 2 IAVs, IBVs	Human	Synergizes with HA stem-directed mAbs; induces complement-dependent cytotoxicity	(Momont et al., 2023)
FNI17	Strong reactivity against IBV NAs	Strongest inhibition of IBV NAs; weakest against N2 antigens	Human	Affected by N245 glycosylation in N2 NAs	(Momont et al., 2023)
FNI19	Reactivity against N1, N2, and IBV NAs	Similar to FNI9; strong inhibition of N1, N2, and IBV NAs	Human	Broad neutralization against seasonal IAV and IBV strains	(Momont et al., 2023)
1G01	Reactivity against N1 and N2 NAs	Strong inhibition of N1 and N2 NAs; limited coverage of IBV strains	Human	Affected by the oseltamivir-resistant mutation H275Y (H3N2); Affected by N245 glycosylation in N2 NAs	(Momont et al., 2023; Stadlbauer et al., 2019)

AG7C	Broad reactivity against N1 NAs from 1918-2018	Inhibits N1 NAs from H1N1 (1918-2018) and H5N1 (2004-2015) viruses	Human (vaccinated)	Provides prophylactic protection in mice; does not require Fc engagement for protection	(Rijal et al., 2020)
AF9C	Broad reactivity against N1 NAs from 1918-2018	Inhibits N1 NAs from all H1N1 viruses tested (1918-2018); less reactive with H5N1 N1 NAs	Human (vaccinated)	Provides prophylactic protection in mice	(Rijal et al., 2020)
Z2B3	Cross-reactive with group 1 (N1) and group 2 (N9) NAs	Inhibits both N1 and N9 NAs; reduced activity against recent clade 6B.1 H1N1pdm09 viruses (post-2014)	Human (H7N9-infected child)	Isolated from mild H7N9 infection; likely selected from memory cells induced by previous N1 NA exposure	(Jiang et al., 2020; Rijal et al., 2020)Rijal et al., 2020 JVirol, Jiang et al mBio
DA03E17	Broad reactivity against IAV group 1 (N1, N4, N5, N8), group 2 (N2, N3, N6, N7, N9), and IBVs	Direct inhibition of NA activity across IAV and IBV strains	Human (H1N1pdm09-infected)	Targets highly conserved NA active site; uses long CDR H3 with DR motif for receptor mimicry; provides in vivo protection against multiple influenza subtypes	(Yasuhara et al., 2022)

1.3.4 Neuraminidase assays

Enzymatic activity and structural integrity are both key indicators for NA immunogenicity. For viruses and purified NA, two widely used assays are employed to semi-quantify NA activity: the enzyme-linked lectin assay (ELLA) and the MUNANA (2'-(4-methylumbelliferyl)-α-D-N-acetylneuraminic acid) assay (details in Chapter 2, Methods).

In the ELLA assay, NA catalytic activity is measured using fetuin, a heavily glycosylated plasma protein produced by the liver and adipose tissue (Lambré et al., 1990, 1991). When fetuin is digested by NA, sialic acid is removed from its N-linked glycosylation sites, exposing carbohydrates that can be quantified using Peanut Agglutinin Lectin-HRP (PNA-HRP) (Couzens et al., 2014). By applying a specific virus or NA concentration, ELLA is widely used to determine NA inhibition titres. This makes it the most suitable assay for serology studies due to its reported inter- and intra-laboratory reproducibility (Eichelberger et al., 2016).

The MUNANA assay measures NA activity using the fluorescent substrate 2'-(4-methylumbelliferyl)-α-D-N-acetylneuraminic acid (MUNANA). In the presence of inhibitors, this assay can determine the concentration of monoclonal antibodies (mAbs) or drugs required to inhibit enzymatic activity by 50% (IC50).

Based on personal communication with Pramila, we hypothesise that monoclonal antibodies targeting the catalytic site inhibit both fetuin and MUNANA substrates, whereas mAbs binding outside the catalytic residues selectively inhibit only the fetuin substrate.

Quantifying mixtures of different NA subtypes is more complex than confirming NA immunogenicity. While ELLA and MUNANA assays are effective indicators of enzymatic activity, they face challenges in distinguishing between various NA subtypes within a mixture.

Using a pre-characterised antibody panel, ELISA is a powerful tool to test epitopes formed with correct folding. Infecting MDCK cells with virus provides an ideal coating of NA in its native form. Alternatively, correctly folded recombinant NA is also considered a viable option for antibody and serology analysis (Wan et al., 2013).

Current inactivated influenza vaccines (IIVs) are quantified based on their hemagglutinin (HA) content, whereas live-attenuated influenza vaccines (LAIVs) are quantified by potency assays, with HA playing a supportive but not primary role. And current live-attenuated influenza vaccines are quantified by potency test with HA playing a major role.However, the amount and enzymatic activity of NA are largely overlooked due to the lack of robust measurement methods. This oversight results in inconsistent NA responses in populations vaccinated with seasonal influenza vaccines (Z. Gao et al., 2020).

Recent advancements include the development of a mass spectrometry (MS) method capable of accurately quantifying both HA and NA simultaneously, as well as distinguishing between different subtypes (Williams et al., 2012). This method determines the molar amount of HA or NA subtypes using subtype-specific isotopically-labelled peptides. However, while this technique provides precise measurements of each NA subtype in seasonal vaccines, it does not assess enzymatic activity or structural integrity, and therefore cannot determine immunogenicity.

The isotope dilution MS (IDMS) method employs isotopically-labelled peptide standards specific to each influenza type and subtype. It provides a reliable approach for measuring the absolute concentration of NA subtypes in seasonal and pandemic vaccines (Wan et al., 2017). While this method does not reflect NA immunogenicity, it offers significant utility in determining the exact composition of vaccines.

1.4 Rationale for NA-VLP vaccines

1.4.1 Virus like particles (VLPs) as novel vaccine platforms

Virus-like particles (VLPs) are self-assembled structures composed of viral or non-viral proteins. They mimic the form and size of a virus particle but lack the genetic genome and material required to infect host cells and produce new virions (Syomin & Ilyin, 2019).

Both prokaryotic and eukaryotic systems can be employed for producing VLP-based vaccines. Eukaryotic systems include the baculovirus/insect cell (B/IC) system, mammalian cell systems, plants, and yeasts. Prokaryotic expression systems primarily rely on *Escherichia coli* as the bacterial platform for recombinant protein production (reviewed by (Nooraei et al., 2021)).

VLP-based vaccine can effectively induce both humoral and cellular immunity (Guo et al., 2019; Serradell et al., 2019). After administration, VLP-based vaccines can be taken up by APC such as dendritic cells (DCs) and initiates the DC maturation process leading to the stimulation of production of pro-inflammatory factors (Fiebiger et al., 2001). The proper size and repetitive structure of VLP also guarantee its efficient transport to follicular DCs in vivo in the absence of prior immunity (Link et al., 2012; Manolova et al., 2008).

VLP-based vaccines are processed and presented by both MHC-I and MHC-II molecules, facilitating recognition by CD4+ T helper cells and CD8+ cytotoxic T cells, which drive humoral and cellular immune responses (Keene & Forman, 1982; Parker, 1993). Additionally, B cells can directly detect VLPs and activate humoral immunity independently of innate immunity or T helper cells in certain case (Bessa et al., 2012).

For influenza-specific VLP-based vaccines, broader immune responses have been observed compared to recombinant haemagglutinin (HA) or whole inactivated virion vaccines (Bright et al., 2007). Furthermore, the multimerisation of antigens using nanoparticles enhances B-cell receptor cross-linking, leading to stronger B-cell activation and a more robust antibody response (Veneziano et al., 2020).

In addition to their potential for broad-spectrum protection, VLP-based vaccines have other attractive features. Their production process is generally more scalable and less complex than traditional egg-based or cell-culture-based influenza vaccines, potentially allowing for faster and more flexible manufacturing capabilities (Sebastian & Lambe, 2018). Also, several virus-like particle-based influenza vaccine candidates have shown promising results in clinical trials, demonstrating their potential as more efficient and safer alternatives for current vaccine (Liu et al., 2023; Lopez et al., 2024; Pushko & Tretyakova, 2020; Ross, 2019).

1.4.2 SpyCatcher003-mi3 VLP platform

Glycoprotein-based VLP platforms have also demonstrated their advantages as potential vaccine platforms with improved immunogenicity in influenza virus (Rahikainen et al., 2021), coronavirus (Tan et al., 2021; Walls et al., 2020), RSV (Marcandalli et al., 2019), Lassa virus (Brouwer et al., 2022).

The glycoprotein-base VLP platform, named SpyCatcher-003 VLP (mi3 for short in later text), we employed in this project showed efficient production, quantitative amide bond formation, and extraordinary resilience (Rahikainen et al., 2021). The scaffold of mi3 is modified based on the structurally engineered trimeric aldolase from the thermophilic bacterium *Thermotoga maritima* (Hsia et al., 2016). SpyCatcher, the 12 kDa protein forming a spontaneous amine bond to its peptide partner SpyTag, was engineered to the scaffold to form the Mi3 particle (Bruun et al., 2018; Keeble & Howarth, 2020). The Mi3 particle used in this project is the updated SpyCathcher003-mi3 version with enhanced stability and decreased pre-existing sera-reactivity as described earlier (Rahikainen et al., 2021).

By adding the 16 amino-acid SpyTag developed by the Howarth group (Rahikainen et al., 2021), we are able to design recombinant NA that can spontaneously form the amine bond with the mi3 particle, as shown in Figure 1.7. The VLP-display of NA with a C4 symmetry has been disclosed by Howarth group earlier as well.

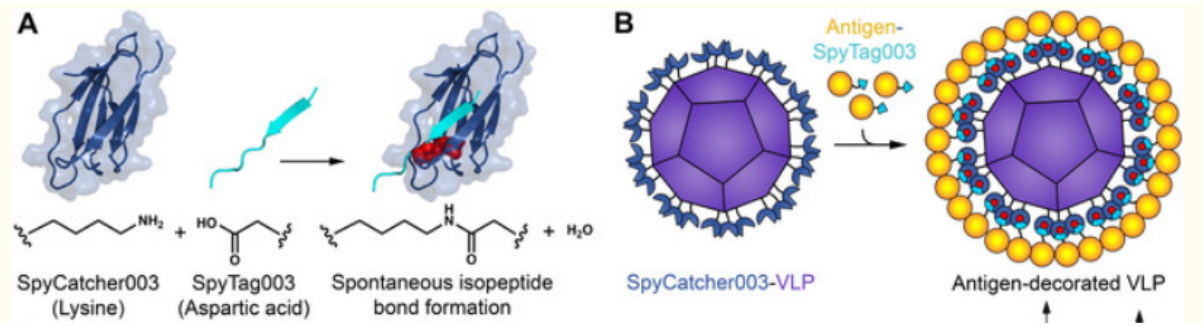

Figure 1.7 **Schematic diagram of SpyCatcher-SpyTag technology (cited from (Rahikainen et al., 2021))**
A)Schematic of reactive protein/peptide pair. Lysine on SpyCatcher003 (dark blue) forms a spontaneous amide bond with aspartic acid of SpyTag003 (cyan). B) Nano-vaccine assembly. Antigen with SpyTag003 (yellow) to SpyCatcher003-VLP (cyan) allows simple efficient assembly of the antigen-VLP particle.

1.5 Preclinical studies and clinical studies

1.5.1 Purified NA as a vaccine candidate

As we summarized in Table 1.2, the neuraminidase was isolated and crystalized in late 70s (Laver, 1978). It was only after this milestone that researchers were able to investigate NA-related immune responses using purified NA. Early experiments revealed that anti-NA serum generated from rabbits reduced plaque size, plaque numbers, and virus titres, but notably, it did not neutralize the virus (Kilbourne et al., 1968).

With advancements in NA-related assays, purified NA has been proven to be immunogenic and protective. It has demonstrated the ability to provide homologous and certain heterologous protection within the same subtype. These effects include reducing lung viral titres and pulmonary lesions in multiple animal models, as detailed in Table 1.7.

The table summarizes various studies on the immunogenicity and protective effects of neuraminidase (NA) in influenza vaccines across different subjects, including mice, chickens, ferrets, and guinea pigs. Several vaccine strains were tested, including A/Puerto Rico/8/34 H1N1, A/Hong Kong/1/68 H3N2, and A/Netherlands/602/2009 H1N1 (Similar to A/California/7/2009 H1N1 used in our lab), which are also involved in this project as mice challenge strains.

Different methods of NA antigen purification, as evolved with the technology advancement, including electrophoresis and recombinant expression systems. Vaccination was typically administered through subcutaneous (SC), intramuscular (IM), or intranasal (IN) routes, often with adjuvants like Freund's, SAS, or poly I: C. Outcomes are generally consistent, demonstrating increased neuraminidase inhibition (NAI) titres, decreased pulmonary and nasal virus titres, and reduced lung pathology in challenge models. Some studies highlighted that protection was enhanced when combining multiple vaccine doses or using recombinant NA. Additionally, mice and ferrets displayed improved survival rates and decreased viral loads after sequential homologous and heterologous influenza challenges.

The relative instability of NA has been addressed through various stabilization techniques, including tetramerizing zippers and inter-protomer mutations (Creytens et al., 2021; Ellis et al., 2022; Rahikainen et al., 2021). Computationally engineered NA antigens have shown broad within-subtype protection in animal models (Job et al., 2018). As NA-inhibiting antibodies correlate with protection against influenza in humans, there is growing interest in incorporating NA into current vaccine strategies to improve efficacy and broaden protection (Creytens et al., 2021).

Table 1.7 Summary of NA as vaccine candidate in animal models

Subject	Vaccine Strains	Vaccine Content	Neuraminidase Antigen Resource	Administration Method	Vaccine Dose	Adjuvant	Challenge Strain	Outcome	Reference
MF-1(Manor Farm) mice	X-7 (F1)	NA	Electrophoresis-purified N2 from viruses	SC	Single dose	Freund's adjuvant	X-3, X-7, X1L, X9	Increased NAI titers, decreased pulmonary virus titers, diminished lung lesions	Schulman et al. 1968
White leghorn chickens	A/NWS/33(HI)-RI/5+ (N2) [X-7FI]	NA	Electrophoresis-purified N2 from viruses	IN	Single dose, 10 μg	Freund's adjuvant	A/Chicken/Pennsylvania/1370/83 (H5N2), 10^5 EID50 or 100LD50	Increased NAI titers, decreased tracheal and cloacal viral titers, no disease signs after exposure.	Webster et al.1988 Virology
BALB/c mice	A/Hong Kong/1/68 H3N2	NA	Chromatography-purified N2 from viruses	Prime:Hind foorpads with FCA, IV without adjuvant, Boost: IP	Two doses, Prime: multi-dose group, Boost: 1 μg	not mention	A/Hong Kong/1/68, 100LD50	Increased NAI titers, increased ELISA antibody titers, decreased pulmonary virus titers with homotypic challenge	Johansson et al. 1989
BALB/c mice	A/Hong Kong/1/68 H3N2	NA, whole virus	Chromatography-purified influenza A N2	N/A	Two does, dose not mention	not mention	A/Hong Kong/1/68 H3N2; A/Philippines/2/82 H3N2; A/Leningrad/360/86 H3N2	Purified NA vaccine is ultimately superior compared to inactivated virus vaccine in both homologous and heterologous infection.	Johansson and Kilbourne, 1990 JID
BALB/c mice	A/Hong Kong/1/68 H3N2	NA, whole virus	Chromatography-purified influenza A N2	N/A	Two does, dose not mention	not mention	A/Hong Kong/1/68 H3N2 (X31)	NAI titers increased and reached a high level 7 days post boost vaccine. Maximal reduction in pulmonary virus replication durinh initial (postvaccination) infection was achieved with WV vaccine, but in second infection by NA vaccine.	Johansson and Kilbourne, 1991 Vaccine
BALB/c mice	A/Victoria/3/75 H3N2	NA	Yeast expression system influenza A N2	SC	Three doses, 2 μg	prime with Ribi adjuvant, 2 boost with Lipid A	A/Victoria/3/75, 10 LD50	Increased survival	Martinet et al. 1997
BALB/c mice	A/Hong Kong/1/68 H3N2; A/Puerto Rico/8/34 H1N1; B/Yamagata/16/88	NA	Recombinant NA expressed in baculovirus expression system	IM, IN	Two doses, 5 μg	poly I: C	A/Puerto Rico/8/34 H1N1; A/Vietnam/1203/04 H1N1; A/Netherlands/602/09; A/Hong Kong/1/68 H3N2; A/Philippines/2/82; B/Victoria/2/87; B/Yamagata/16/88; B/Malaysia/2506/04	Mice immunized with N1 and N2 showed protection within subtype; Mice immunized with B Yamagata were protected from mobidity and mortality from challenge of B victoria; Neither N1 or N2 could provide hetrosubtypic protection	Wohlbold et al. 2011
Ferrets (Mustela putorius furo)	A/Netherlands/602/2009	NA	Recombinant NA expressed in HEK293T cells	IM	Two doses, 3.75 μg	multi-adjuvant tested	A/Netherlands/602/2009, 10^6 TCID50	Increased NAI titers, decreased pulmonary virus titers, decreased lung pathology	Bosch et al. 2010
Guinea pigs	B/Malaysia/2506/2004	NA	Recombinant NA expressed in baculovirus expression system	IM, IN	Two doses, 10 μg	poly I: C	B/Malaysia/2506/2004 (IBV)	Increased NAI titers, increased ELISA antibody titers, decreased nasal wash virus titers, decreased transmission	MacMahon et al. 2019
BALB/c mice	Cluster-based consensus design of NA	NA	Recombinant NA expressed in HEK293T cells	SC	Two doses, 1 μg	SAS	A/Puerto Rico/8/34 H1N1; A/USSR/90/1977 (H1N1); A/New Caledonia/20/1999 (H1N1); A/Belarus/221/2009 (H1N1); A/swine/Belgium/1/1998 (H1N1); A/Vietnam/1194/2004 (H5N1) - NIBRG-14, 5LD50	The protection provided by the cluster-based consensus (CBC) designed NAs correlated to NAI titres. Sera raised to the consensus NAs displayed a broader pattern of reactivity and protection than naturally occurring NAs. potentially supporting a predictive approach to antigen design.	Job et al., 2018

1.5.2 Overview of preclinical studies evaluating NA-VLP platforms

In addition to studies focusing on NA-based vaccines, neuraminidase virus-like particle (NA-VLP) platforms have shown significant potential as vaccine platforms. These platforms have demonstrated enhanced immunogenicity against a variety of viruses, including coronaviruses (Tan et al., 2021; Walls et al., 2020), RSV (Marcandalli et al., 2019), and Lassa virus (Brouwer et al., 2022). Table 1.8 summarizes key preclinical studies evaluating the efficacy of NA-VLP platforms.

With advancements in material science, more nanoparticle-based VLP platforms are being developed, alongside the widely used insect cell systems. NA-based nanoparticle platforms are emerging as promising influenza vaccine candidates. Studies have shown that NA-displaying VLPs and self-assembling protein nanoparticles elicit stronger antibody responses and provide superior cross-protection against diverse influenza strains, even at much lower doses compared to traditional split-virus vaccines (Y.-J. Kim et al., 2017; Pascha et al., 2024). These platforms induce higher titers of NA-binding and -inhibiting antibodies, enhance cellular immunity, and offer protection against lethal viral challenges.

Table 1.8 Summary of NA-VLP as vaccine candidate in animal model

Vaccine Strain	Vaccine Content	Neuraminidase Antigen Resource	Administration Method	Vaccine Dose	Adjuvant	Challenge Strain	Outcome	Reference
A/Perth/16/2009 H3N2; A/California/04/2009 H1N1	NA-VLP, VLP	Tni cells, Trichoplusiani(Tni) insect cell	IM, IN	Two does, 5 μg NA-VLP solution	/	A/Perth/16/2009 H3N2; A/California/04/2009 H1N1; 5 LD50	For the reported N2 NA-VLP, IM gave higher sera IgG and NAI titre, reduced the lung virus titre and give better protection. As dose increase, Vaccination with NA2 VLPs has a dose dependent effect on serum IgG levels and morbidity after challenge; Vaccination with NA2 VLPs was not protective in a heterosubtypic H1N1 lethal challenge model. bivalent vaccination with NA1 and NA2 VLPs demonstrated no antigenic competition in anti-NA IgG responses and protected against lethal challenge with H1N1 and H3N2 viruses.	Menne et al. 2021 Virology
A/Indonesia/05/2005 H5N1; A/Brisbane/10/2007 H3N2 (control)	NA-VLP	NA-VLP harvested from baculovirus-infected Sf9 cells	IM	2300mU/mL, 0.5 mL (based on NA activity)	/	10^6 PFU of A/Indonesia/05/2005 (H5N1)	Ferrets vaccinated with influenza N1 NA VLPs elicited high-titer serum NAinhibition (NI) antibody titers and were protected from lethal challenge with A/Indonesia/05/2005 virus. Moreover, N1-immune ferrets shed less infectious virus than similarly challenged control animals. In contrast, ferrets administered control N2 NA VLPs were not protected against H5N1 virus challenge.	Smith et al. 2017
A/North Carolina/07/ 2013 H1N1; A/Hong Kong/1968 H3N2	NA-mi3	Freestyle 293-F cells	IM	0.1 μg NA, 0.1 μg NA-mi3; 1 μg NA, 1 μg NA-mi3	SAS	H1N1 Bel/09 4LD50; H3N2 X31 4LD50	Immunization of mice with NA-Mi3 nanoparticles induced higher titers of NA-binding and -inhibiting antibodies and improved protection against a lethal challenge compared to unconjugated NA. Mosaic nanoparticles elicited antibody titers that were similar or superior to the homotypic nanoparticles and effectively protected against H1N1 and H3N2 challenge viruses.	Pascha et al. 2024

1.6 Challenges and future directions

1.6.1 Remaining obstacles in the development and implementation of NA-based vaccines

Despite the potential advantages of incorporating NA as a vaccine component, its expression and assembly pose significant challenges. Research suggests that both the transmembrane domain (TMD) and the enzymatic head domain are crucial for NA tetramerization and activity (Da Silva et al., 2013). Replacing the natural NA stalk with artificial tetramerization domains has been shown to enhance the stability and solubility of recombinant NA (Schmidt et al., 2011).

Expression systems employing mammalian or insect cells have successfully produced tetrameric, enzymatically active, and immunogenic recombinant NA (Prevato et al., 2015; Schmidt et al., 2011; van der Woude et al., 2020). However, the yield of expressed recombinant NA can vary significantly depending on the viral strain, as summarised by Pramila in Table 1.9. This table is also included in the loop-grafting manuscript provided in Appendix 11 (Rijal et al., 2024).

Table 1.9 Literature review of recombinant NA expression yields in various expression system (Seen Appendix 11)

Literature	Subtype (NA)	Virus type	Expression System	Yield
Prevato 2015	N1	H1N1/09	Expi293F	**30 mg/L**
Ellis 2022	N1, N2, N8	H1N1/09, H1N1/15, H3N2/05, H10N8/13	Expi293F	**upto 30 mg/L**
Ecker 2020	N1, N2	H1N1/09 H1N1/18, H3N2/13, H3N2/14, H3N2/16	Expi293F	**upto 28 mg/L**
Prevato 2015	N1	H5N1	Expi293F	**6 mg/L**
Martinet 1997	N2	H3N2/1975	*P Pastoris*	**2.5–3 mg/L**
Woude 2020	N2	H3N2	293T	**2.5 mg/L**
Subathra 2014	N1	H1N1	*P Pastoris*	**2 mg/L**
Schmidt 2011	N1	H1N1	Sf21	**0.5-1.8 mg/L**
Nivitchanyong 2011	N1	H5N1	293-F	**0.3-0.7 mg/L**
Margine 2013	N9	H7N9/2013	Sf9	**0.2-0.7 mg/L**
Liu 2015	N1	H1N1/09, H5N1	Sf9	**0.25-0.5 mg/L**

Various approaches, such as codon optimisation, GFP fusion, consensus sequence design, and interface modification, have been employed to improve NA expression and stability(Ellis et al., 2022; van der Woude et al., 2020). Nonetheless, the outcomes have remained suboptimal.

1.6.2 Strategies to overcome immunological challenges and enhance vaccine efficacy

Current influenza virus vaccines rely on annually updated immune responses elicited by predicted circulating strains. However, their protective effect is often limited by antigenic mismatch, which occurs when the predicted vaccine strain differs from the actual circulating strain (Pica et al., 2011; Pica & Palese, 2013).

One proposed solution to this challenge is the development of Universal Influenza Vaccine Strategies, aimed at providing broad protection against multiple virus strains. These strategies focus on targeting conserved regions of viral proteins, such as the HA stalk domain and matrix 2 protein (reviewed in (Pica & Palese, 2013)). HA-focused strategies include the use of stalk-directed, consensus-based, and computationally derived immunogens to enhance cross-reactive immunity (Bullard & Weaver, 2021). Additional approaches aim to boost T-cell responses by selecting appropriate vectors, employing adjuvants, and utilising alternative routes of administration (He et al., 2018).

Innovative vaccine platforms are being developed to generate robust cross-protective immunity, with several candidates advancing to clinical trials (Hu et al., 2022). These platforms are designed to address challenges posed by antigenic drift, antigenic shift, and the emergence of pandemic viruses.

NA has also garnered attention due to the broad efficacy of anti-NA antibodies (Chen et al., 2018; Doyle et al., 2013; Momont et al., 2023; Yasuhara et al., 2022), its relatively slower antigenic drift compared to HA (Sandbulte et al., 2009; Westgeest et al., 2012), and the cross-protection observed within a single subtype (Wohlbold et al., 2015).

While current seasonal vaccines have limited efficacy due to strain mismatches and interference from pre-existing immunity, universal vaccine strategies have demonstrated promise in animal models and early clinical studies. Significant progress has been made in recent years, including the identification of new targets, the development of novel vaccination strategies, and the advancement of multiple candidates to human clinical trials. However, several challenges remain to be addressed (Nachbagauer & Palese, 2020).

1.6.3 Synopsis of this thesis

While current seasonal vaccines face limitations due to strain mismatches and interference from pre-existing immunity, recent advances in universal influenza vaccine strategies have shown promise in addressing these challenges.

Among these efforts, NA has emerged as a key target due to its slower antigenic drift compared to HA and the broad efficacy of anti-NA antibodies. Building on this foundation, this thesis explores the development of an influenza neuraminidase vaccine displayed on the surface of mi3 virus-like particles.

Key findings in each chapter are listed below:

Chapter 3: Comparison of various constructs and mammalian expression systems for producing soluble recombinant neuraminidase reveals significant heterogenecity in expression and enzymatic activity depending on the NA strain and subtype.

Chapter 4: Demonstrate that NA vaccines generate protective antibody responses capable of inhibiting NA activity and providing protection against lethal viral challenges.

Chapter 5: Improvement of NA expression using the loop-transfer technique, with findings currently available in preprint (Manuscript attached in Appendix 11): https://www.biorxiv.org/content/10.1101/2024.10.11.617814v2.

Chapter 6: Characterization of N8 neuraminidase from the potentially pandemic H5N8 virus, combined with immunization studies in chickens in collaboration with Prof. Munir Iqbal.

Chapter 2 Materials and Methods

2.1 Material and resource availability

2.1.1 Lead contact

Further information and requests for resources and reagents should be directed to and will be fulfilled by the lead contact, Leiyan Wei (leiyan.wei@rdm.ox.ac.uk).

2.1.2 Material and resource availability

Material and resource relating to more than one method is listed in Table 2.1, including medium, buffers and equipment. The source of specific antibodies, reagents and instruments used in this project are listed in the relevant KRT as needed. The detailed design of recombinant neuraminidases will be disclosed in Chapter 3 in detail.

Table 2.1

REAGENT or RESOURCE		SOURCE	IDENTIFIER
Chemicals and Buffers			
PBS(1x)		Made in-house	Auto-cleaved by WIMM facility
PBS/0.1% BSA	PBS	Made in-house	N/A
	0.1% BSA (Blocker BSA)	Thermo Fisher Scientific	37525
LB		Made in-house	Auto-cleaved by WIMM facility
LB-Agar		Made in-house	Auto-cleaved by WIMM facility
Amphicilin			
VGM buffer	DMEM	Gibco, Thermo Fisher Scientific	
	0.1% BSA (Blocker BSA)	Thermo Fisher Scientific	37525
	1:1000 Pen/Strep	Sigma-Aldrich	P4333
	2 mM L-Glutamine	Sigma-Aldrich	G7513
	HEPES buffer		
D10	DMEM	Gibco, Thermo Fisher Scientific	
	10% BSA	Sigma-Aldrich	F9665
Experimental models: Cell lines			
ExpiCHO		Thermo Fisher Scientific	N/A
Expi293		Thermo Fisher Scientific	N/A
MDCK-SIAT1		AT lab	In-house stock
Software and algorithms			
SnapGene		SnapGene	https://www.snapgene.com/
PRISM 10		GraphPad Software	https://www.graphpad.com
CLARIOstar microplate reader		BMG LABTECH	https://www.bmglabtech.com/
Other			
Floor-Standing Centrifuges		WIMM facility	Room 362
Benchtop&Micro Centrifuges		AT lab	N/A
Pipettes and Multichannel		AT lab	N/A
Nanodrop		Thermo Fisher Scientific	N/A

Multitron Cell incubator	INFORS-HT	N/A
Plastic consumables (Eppendorf, falcon, flask, PCR tube)	WIMM facility	N/A

2.2 Growing wild type virus and Pseudotype influenza virus

Virus was titrated by haemagglutination assay, TCID50 by limitation dilution.
Day -2: Seed around 6 - 8 M of MDCK-SIAT1 cells to 175cc flask with 40 mL D10 to form a monolayer 48h prior to the virus infection.
Day 0: Remove the D10 medium with pipette and rinse cells with PBS for twice. Infect monolayer MDCK-SIAT1 cells with 10 mL of VGM diluted wild type seed virus (final multiple rate <0.1) for 1 hour. Add 40 mL of VGM/TPCK-trypsin (final concentration 0.75 µg/mL, 37.5 µg of TPCK-trypsin per flask in total) and incubate for 48h before harvest.
Day 2: Harvest the wild type virus. Transfer the medium within the flask to 50 ml falcon, spin down at 1000rpm for 5 min to remove the cell debris, collect the supernatant, aliquot and store at -80 ℃.

Similar to wild type virus growing, Pseudotyped influenza viruses (S-FLU) were made with the same protocol but lenti virus transduced MDCK-SIAT1 cell lines with HA expressed on the cell surface as describe by Powell before (Powell et al. 2012). S-FLU is a single cycle influenza A/PR/8/1934 reassortant with the hemagglutinin disabled by inactivate of the signal sequence. In this project, some of the previous S-FLU made in Alain Townsend's lab were used for neuraminidase assay when wild type viruses werenot accessible.

2.3 Recombinant Neuraminidase expression

Table 2.2

REAGENT or RESOURCE	SOURCE	IDENTIFIER
Chemicals, peptides, and recombinant proteins		
Q5 High-Fidelity 2X Master Mix	New England Biolabs	M0492S
AgeI-HF	New England Biolabs	R3552S
EcoRI-HF	New England Biolabs	R3101S
NotI-HF	New England Biolabs	R3189S
BamHI-HF	New England Biolabs	R3136S
Quick Ligation Kit	New England Biolabs	M2200S
Gibson Assembly Cloning Kit	New England Biolabs	E5510S
QIAquick PCR purification Kit	QIAGEN	28104
QIAGEN Plasmid Mini Kit	QIAGEN	12123
QIAGEN Plasmid Maxi Kit	QIAGEN	12162
Oligonucleotides		
PCR primers	Integrated DNA Technologies	N/A
Recombinant DNA		
Designed DNA fragments with NA sequences	Thermo Fisher	N/A
Designed DNA fragments with NA sequences	Genscript	N/A
Whole plasmid with NA sequences	Genscript	N/A
Bacterial and virus strains		
NEB 5-alpha Competent *E. coli* cells	New England Biolabs	C2987

2.3.1 PCR

The designated recombinant neuraminidase sequences were ordered from Thermo Fisher or Genscript (NA fragment only or whole plasmid). Commonly used materials were listed in

Table 2.2. PCR steps are modified from the protocols posted on the New England Biolabs (NEB) website:

1. Assemble all reaction components in room temperature, prepare the template DNA, primers in advance. The reaction components should be mixed prior to the PCR according to the mix guidance below:

	25 µl RXN
Q5 High-Fidelity 2X Master Mix	12.5 µl
10 µM Forward Primer	1.25 µl
10 µM Reverse Primer	1.25 µl
Template DNA	1 µl (concentration 10-40 ng/)
Nuclease-Free Water	9 µl

Note: Gently mix the reaction. Collect all liquid at the bottom of the tube with a quick spin.

2. Transfer the PCR tubes to the thermocycler and begin the PCR program.
3. PCR program are usually set as the thermocycling program below:

Step	Temp	Time
Initial Denaturation	98 ℃	30 seconds
Amplification: 25 cycles	98 ℃	5-10 seconds
	50-72 ℃*	10-30 seconds
	72 ℃	20-30 seconds/kb
Final Extension	72 ℃	2 minutes
Hold	4 ℃	∞

Note: *Tm can be calculated by NEB Tm Calculator (https://tmcalculator.neb.com/)

2.3.2 Digestion

PCR products or ordered DNA fragments containing designated NA or plasmid sequences are digested with restriction enzyme kits ordered from NEB as listed in Table 2.2. The reaction components are mixed as the guidance below in room temperature (taking AgeI and EcoRI as example):

Component	For 50 µL reaction
DNA	1 µg
10X rCutSmart Buffer	5 µl (1X)
EcoRI-HF	1.0 µl (20 units)
AgeI-HF	1.0 µl (20 units)
Nuclease-free Water	to 50 µL

The digestion should be finished within 15 min with the HF restriction enzymes
The prepared inserts (PI) or prepared expression vectors (PV) are purified with QIAquick PCR purification kit and elute in 30 µL ddH_2O. The PIs and PVs are labelled as follows (taking PI as an example): PI restriction enzyme a/DNA fragment or plasmid/restriction enzyme b Date of preparation/concentration (ng/µL)

2.3.3 Ligation

The prepared inserts and prepare vectors with matched sticky ends are ligated by ligase kit (NEB). The reaction components are mixed as the guidance below in room temperature and the ligation reaction should last for more than 1 hour (ligation overnight should work as well).

2.3.4 Gibson cloning

The designated DNA fragments and prepared expression vectors can also be connected via Gibson cloning to escape the PCR, digestion and ligation process. However, this method showed lower success rate compare to the traditional routine.

2.3.5 Transformation and miniprep

The transformation and miniprep preparation process usually takes about 4 working days including the sequencing confirmation.

Day 1: transformation with the ligation product or ordered whole plasmids.

4. For C2987H: Thaw a tube of NEB 5-alpha Competent *E. coli* cells on ice for 10 minutes. Mix gently and carefully pipette 10 µl of cells into a transformation tube on ice.
5. Add 1 µl of plasmid DNA or 5 µl of ligation product to the cell mixture. Carefully flick the tube 4-5 times to mix cells and DNA.
6. Place the mixture on ice for 30 minutes. Do not mix.
7. Heat shock at exactly 42°C for exactly 30 seconds. Do not mix.
8. Place on ice for 5 minutes. Do not mix.
9. Pipette 950 µl of LB broth without amphicilin into the mixture.
10. Place at 37°C for 60 minutes. Shake vigorously (250 rpm).
11. Spread 50-100 µl of each dilution onto a selection plate and incubate overnight at 37°C. Alternatively, incubate at 30°C for 24-36 hours or 25°C for 48 hours.

Day 2: Pick 3-4 colonies from the transformation and seed into the LB broth with Ampicillin. For each target plasmid, 3-4 colonies were picked by 200 µL tips and grown separately in 14 mL LB culture medium with 1:1000 diluted Ampicillin for 18 hours at 37 ℃ CO_2 incubator at 225 rpm. Make sure each culture is marked properly.

Day 3: Extract DNA by Miniprep or Maxiprep according to the sample size. The manual for Miniprep and Maxiprep can be found on QIAGEN website (https://www.qiagen.com/us).

2.3.6 Expressing Neuraminidase in ExpiCHO/Expi293 cells

The ExpiCHO cell expression system manual can be found on (*ExpiCHO Expression System | Thermo Fisher Scientific - UK*).
The Expi293 cell expression system manual can be found on (*Expi293 Expression System - UK*)

2.4 Monoclonal antibody expression

The preparation of the monoclonal antibody and transfection in ExpiCHO cells is slightly different as the recombinant neuraminidase mentioned above. All the details are mentioned in the previous publications (Rijal et al., 2020).

The antibodies involved in this project are listed in Table 2.4

2.5 Protein purification (recombinant NA and Antibody)

Table 2.3 Key resources for protein purification

REAGENT or RESOURCE	SOURCE	IDENTIFIER
Chemicals, peptides, and recombinant proteins		
DPBS buffer	Thermo Fisher Scientific	14040133
Other		
HisTrap HP His tag protein purification columns	Cytiva	17524802
Zeba Spin Desalting Columns and Plates, 7K MWCO	Thermo Fisher Scientific	89889, 89891
ÄKTA start protein purification system	Cytiva	29022094

The protein supernatant can of ExpiCHO and Expi293 expression system should be ideally harvested on Day 8 and Day 6 to reach a balance of expression yield and extra impurity. The handbook of using HisTrap™HP 1ml and 5ml columns can be found on www.cytivalifesciences.com. This purification method is modified from the HisTrap HP, 1 ml and 5 ml instructions for use. The purification can be done with AKTA machine with set programs or by pumps semi-manually. Resources needed can be found in KRT table x.x. The column, buffers and AKTA machine should be prepared according to HisTrap HP 1ml and 5ml instructions for use before the first purification. Recharged columns are prepared before the purification.

2.5.1 His-Tag Purification

This method suits for purification of histidine-tagged recombinant proteins by immobilized metal ion affinity chromatography (IMAC) using HisTrap™ column, prepacked with precharged Ni Sepharose™ High Performance.

1. Fill the pumping tube or connecting tubes in the AKTA chromatography system with distilled water.
2. Remove the stopper and connect the column to the syringe (use the matched connector provided), connecting system tubing “drop-to- drop” to avoid introducing air into the system. Quickly remove the snap-off end at the column outlet to avoid over pressure.
3. Wash the column with 3 to 5 column volumes (CL) of distilled water.
4. Estimate the sample volume and add the 10x binding buffer to make the final concentration equal to 1x binding buffer.
5. Disconnect distilled water, connect sample to sample line, binding buffer to buffer A tube, elution buffer to B tube, respectively. Fill the collection tubes.
6. Start the AKTA set program for 5mL columns and type in the estimated volume of samples.
7. The program should be set as 5 column volumes (CV) binding buffer, sample loading, 10-15 CV binding buffer, 2 CV elution buffer.
8. Number the eppendorfs of elution and measure the protein concentration with the NanoDrop spectrophotometer with 2 µL of eluted protein using elution buffer as blanking to keep the tubes with target protein.

2.5.2 Desalting

9. Checking the desalting column to make sure the desalting size and sample size are suitable.
10. Follow the procedure for desalting according to the instruction provided by Thermo Scientific, Zeba Spin Desalting Columns and Plates, 7K MWCO Instructions (https://www.cytivalifesciences.com/). Using DPBS with Ca2+ and Mg2+ as storage buffer for the protein
11. Transfer the protein solution to the desalting column, spin at 1000 g for 2 min and collect the run through. Measure the concentration again, aliquot and label the protein as needed. Label format sample: protein name/transfection date/aliquot detail/made by.
12. Strep Tag II purification and Spy-Tag purification can also be used with similar procedure. Most recombinant neuraminidase mentioned in this study are purified through His-Tag purification.

2.5.3 Storage

The protein aliquot should be stored in -80 ℃ freezers for long-term storage with PBS or DPBS buffer with Ca^{2+} and Mg^{2+} as described by Giurgea et al(Giurgea et al., 2021). The DPBS buffer is ordered from Thermo Scientific directly, with a recipe of calcium chloride (100 mg/l, 0.9 mM), magnesium chloride (100 mg/l, 0.49 mM), potassium chloride (200 mg/l, 2.66 mM), potassium phosphate monobasic (200 mg/l, 1.47 mM), sodium chloride (8000 mg/l, 137.93 mM), and sodium phosphate dibasic (2160 mg/ l, 8.06 mM). For PBS buffer with Ca^{2+} and Mg^{2+}, the PBS buffer are made and insteriled within the institution, pre-concentrated and filtered calcium chloride and magnesium chloride solutions were added to match the final Ca^{2+} and Mg^{2+} with the ordered DBPS buffer.

2.6 Neuraminidase Characterisation

The standard characterisation process is illustrated in Fig 3.1.
As ELLA, ELISA and MUNANA assay share quite a lot of antibodies and viruses in common, the common materials and resources are listed here in KRT 2.6.
Table 2.4 Key resources NA characterisation

REAGENT or RESOURCE	SOURCE	IDENTIFIER
Antibodies		
1G01	Expressed in-house According to Chen et al. 2018	PDB: 6Q23
AG7C	Expressed in house, reported in Rijal et al.,2020	PDB:
AF9C	Expressed in house, reported in Rijal et al.,2020	N/A
Z2B3	Expressed in house, reported in Rijal et al.,2020	N/A
Z2C2	Expressed in house, reported in Rijal et al.,2020	N/A
P1-7C	Expressed in house, reported in Rijal et al.,2020	N/A
24-1C	Expressed in house	N/A
NmAb-1	Expressed in house, from adults post 2017-2018 TIV immunization, from Huang lab	N/A
NmAb-2	Expressed in house, from adults post 2017-2018 TIV immunization, from Huang lab	N/A
NmAb-4	Expressed in house, from adults post 2017-2018 TIV immunization, from Huang lab	N/A
NmAb-5	Expressed in house, from adults post 2017-2018 TIV immunization, from Huang lab	N/A
NmAb-6	Expressed in house, from adults post 2017-2018 TIV immunization, from Huang lab	N/A
NmAb-7	Expressed in house, from adults post 2017-2018 TIV immunization, from Huang lab	N/A

NmAb-13	Expressed in house, from adults post 2017-2018 TIV immunization, from Huang lab	N/A
NmAb-14	Expressed in house, from adults post 2017-2018 TIV immunization, from Huang lab	N/A
NmAb-15	Expressed in house, from adults post 2017-2018 TIV immunization, from Huang lab	N/A
NmAb-16	Expressed in house, from adults post 2017-2018 TIV immunization, from Huang lab	N/A
NmAb-18	Expressed in house, from adults post 2017-2018 TIV immunization, from Huang lab	N/A
NmAb-19	Expressed in house, from adults post 2017-2018 TIV immunization, from Huang lab	N/A
NmAb-20	Expressed in house, from adults post 2017-2018 TIV immunization, from Huang lab	N/A
NmAb-21	Expressed in house, from adults post 2017-2018 TIV immunization, from Huang lab	
NmAb-24	Expressed in house, from adults post 2017-2018 TIV immunization, from Huang lab	
NmAb-25	Expressed in house, from adults post 2017-2018 TIV immunization, from Huang lab	
NmAb-27	Expressed in house, from adults post 2017-2018 TIV immunization, from Huang lab	
NmAb-28	Expressed in house, from adults post 2017-2018 TIV immunization, from Huang lab	

Polyclonal Rabbit Anti-Human IgG HRP		Dako, Agilent	P0214
Polyclonal Goat Anti-Mouse IgG HRP		Dako, Agilent	P0447
Bacterial and virus strains			
X179A (reassorted from A/California/07/2009) (BSL-2)		Alain Townsend Lab stcok	Originally obtained from National Institute for Biological Standards and Control (NIBSC), UK
A/Sydney/5/2021 (BSL-2)		WIC	Worldwide Influenza Centre (WIC), Crick Insitute, London, UK
PR8 (A/Puerto Rico/8/1934) (BSL-2)		Alain Townsend Lab stock	
X31 (reassorted from A/Hongkong/1/1968) (BSL-2)		Alain Townsend Lab stock	
Biological samples			
Post boost vaccine sera from BALB/c mice		This project	N/A
Post boost vaccine dose sera from DBA/2 mice		For this project	N/A
Post boost vaccine dose sera from C57BL/6 mice		For this project	N/A
Chemicals, peptides, and recombinant proteins			
Recombinant NA (detailed in Chapter 3)		For this project	Details disclosed in Chapter 3
Fetuin		Sigma-Aldrich	F3385
Peanut Agglutinin-HRP		Sigma-Aldrich	L7759
KPL SureBlue (TMB substrate)		SeraCare	5120-0077
VGM buffer	DMEM	Gibco, Thermo Fisher Scientific	
	0.1% BSA (Blocker BSA)	Thermo Fisher Scientific	37525
	1:1000 Pen/Strep	Sigma-Aldrich	P4333
	2 mM L-Glutamine	Sigma-Aldrich	G7513
	HEPES buffer		
PBS/0.1% BSA	PBS	Made in-house	N/A
	0.1% BSA (Blocker BSA)	Thermo Fisher Scientific	37525
D10	DMEM	Gibco, Thermo Fisher Scientific	
	10% BSA	Sigma-Aldrich	F9665
Experimental models: Cell lines			
MDCK-SIAT1 cell		Alain Townsend Lab	(Matrosovich et al., 2003)
Software and algorithms			
PRISM 10		GraphPad Software	https://www.graphpad.com/features
Other			
Maxisorp Nunc-Immunoplate		Thermo Fisher Scientific	442404
96 well cell culture plate, round bottom with lid		Costar, Corning Inc.	3799
96 well cell culture plate, flat bottom with lid		Costar, Corning Inc.	3596

2.6.1 BS3 linking and SDS-PAGE

Table 2.5 Key resources BS-3 linking and SDS-PAGE

REAGENT or RESOURCE	SOURCE	IDENTIFIER
Chemicals, peptides, and recombinant proteins		
Pierce BS-3	Thermo Fisher Scientific	A39266
Critical commercial assays		
QC Coomassie Stain	Bio-Rad	161-0803
Bolt Bis-Tris Plus Kit	Invitrogen, Thermo Fisher Scientific	NW0412A-RS10, kit tools can be ordered seperately

This protocol is modified based on the Instructions of DSS and BS3 Crosslinkers (www. thermofisher.com).

1. Resolve 2mg BS3 in 576 µL PBS buffer, making the Crosslinker concentration as 6mM.
2. Resolve 2 µg protein in PBS buffer to make the final volume 20 µL.
3. Add 10 µL of the Crosslinker to the protein solution, the reaction concentration for BS-3 would be 2mM.
4. Incubate the reaction mixture at room temperature for 30 minutes.
5. Add the 6x protein loading dye to the mixture and heat inactivate the mixture at 95 ℃ for 5 minutes.
6. Run the crosslinked protein in SDS-PAGE and stain the protein gel in Coomassie Blue.

2.6.2 SEC

The oligomeric state of NA proteins was assessed via size-exclusion chromatography (SEC). Proteins were run on Superdex 200 Increase 10/300 GL column (Cytiva) equilibrated with PBS at a flow rate of 0.5 ml/min. Graphs were plotted using GraphPad Prism software.

Table 2.6 Key resources SEC

REAGENT or RESOURCE	SOURCE	IDENTIFIER
Software		
Unicorn 11.0	Cytiva	N/A
Other		
Superdex 200 Increase 10/300 GL column	Cytiva	N/A
Akta pure	Cytiva	WIMM facility

2.6.3 ELLA

Principle: The assay is based on the method developed by Lambre et al (Clinica Chimica Acta, 198, 183, 1991) from R Websters lab, and optimized by Couzens et al (J. Virol.Meth. 210, 7, 2014; also see the method detailed by them). The method relies on catalytic activity of NA on Fetuin. Fetuin is a heavily glycosylated plasma protein produced by the Liver and adipose tissue. When Fetuin is digested with Neuraminidase, sialic acid is removed from N-linked glycosylation site *which then exposes* carbohydrates, which can be bound by Peanut Agglutinin Lectin-HRP (PNA-HRP). This assay can be performed in a nunc microplate and develops with TMB or POD substrates.

Our method is based on the two papers above with some minor modifications. The reaction between NA and Fetuin is buffered in VGM. This allows the reactions to proceed in the 37℃ CO2 incubator for buffering. Washes are done with PBS without Tween 20. Sources of NA are wild type or S-FLU viruses or recombinant NA proteins. NA activity titration would be done before measuring NAI titers.

Material preparation:

1. Fetuin stock: Prepare stock solution of 1.25 mg/ml in PBS (=x50) and store in 1.2 ml aliquots at -20℃.
2. PNA-HRP stock: Prepare 10 ug/ml stock in PBS/0.1% BSA (=x10) and store in 1.2 ml aliquots at -20℃.
3. VGM: DMEM with 0.1% BSA, Pen/Strep, 2 mM Glutamine and HEPES buffer

Day 0

1. Coating Nunc plates with Fetuin solution. Prepare fetuin solution from stock for coating by diluting 50-fold. The coating concentration would be 25 mg/mL. Add azide to 0.02% and pipette 50 µl in each well of 96-well Nunc plates. Encapsulate the plates with plastic films and store them at 4 ℃ in cold room. Leave the plates o/n for fetuin to bind. The plates can be preserved for a maximum duration of two weeks, with azide to inhibit microbial proliferation. Alternatively, immediate use following a 2-hour room temperature coating has been successful.

Day 1

1. Prepare dilutions of sera/mAb (usually duplicates) in 60 µl in U-bottom 96 well plate, diluted in VGM. Leave one column for "NA/virus only" and "VGM only" for background measurement. A typical ELLA plate design is shown below.
2. Add source of NA (recombinant NA solution or diluted virus) in 60 µl to each well; add 60 µl VGM the "VGM only" column in the plate. There should be 120 µl in all wells. Leave the plates to mix on shaker (optional) for ~20 mins before transferring to Fetuin plates.
3. Retrieve Fetuin plates from cold room. Wash x3 with 150 µl sterile PBS (use sterile to avoid bugs growing during o/n incubation)
4. Transfer 100 µl of the Ab/NA mix to each well of Fetuin plate. Double check the control column for each plate.
5. Incubate 18 hours in 37℃ gassed CO2 incubator.

Day 2

Prepare PNA-HRP by diluting 0.6 ml stock into 6 ml PBS/0.1% BSA (avoid azide at this stage) for each plate (final concentration: 1 µg/ml).

1. Take off Ab/NA mix with multichannel, and add 150 µl PBS for first wash. When working with viruses, it is necessary to collect the mix solution and initial wash into a basin, redirecting it into a 1% Virkon solution within a sink. This procedure with wild-type viruses is recommended to be performed within a hood to avoid contamination.For recombinant NA proteins, standard flicking off procedures can be followed. Wash the sample 3x with PBS as previously outlined.
2. Add 50 µl PNA-HRP solution to all wells. Incubate on shaker for at least 1.5 hrs. (Longer incubation of 3-4 hrs can give a high background).
3. Flick off and wash x 3 PBS.
4. Develop 10 mins with TMB substrate.
5. Stop reaction with 50 µl 1M H2SO4 in each well.
6. Read absorbance at 450 nm.
7. Plot results with PRISM 10. Calculate results as needed.

2.6.4 MUNANA

This protocol is adapted from the methods provided by the Francis Crick Institution, WHO WIC. This SOP describes a fluorescent neuraminidase assay used to assess NA activity. Neuraminidase activity can be measured using the fluorescent substrate 2'-(4-methylumbelliferyl)-α-D-N-acetylneuraminic acid (MUNANA). This assay when performed in the presence of inhibitors allows the concentration of mAbs/drugs required to inhibit enzyme activity by 50% (IC50) to be determined as well.

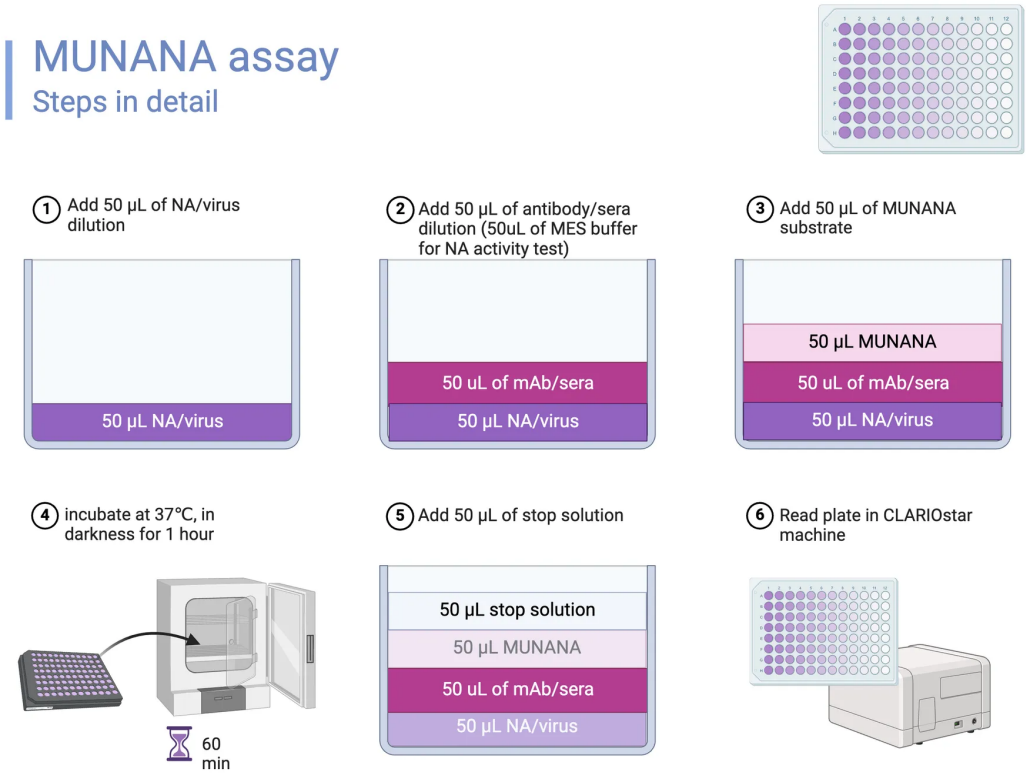

Figure 2.1 **MUNANA assay steps in detail**

For the neuraminidase activity assay, a total of four viruses or NA proteins may be assayed on a single 96 well plate as shown in Figure 2.1. This assay enables determination of the optimal virus or NA protein dilution in order to standardise virus neuraminidase activity when measuring IC50 values for the neuraminidase inhibitors/ mAbs.

Each virus sample is initially titrated by making serial two-fold dilutions in 96 well plate and then assayed in the presence of MUNANA. The optimal virus sample dilutions, which fall in the linear portion of the enzyme activity curve, are determined graphically.

Before beginning the assay book the CLARIOstar machine for one hour, in one hour's time.

1. 50µl MES assay buffer added to each well (use filter tips and add to the corner of the well)
2. Duplicate two-fold dilutions of each test virus/NA are prepared. 50µl of the first virus are placed in wells A1 giving a ½ dilution, mix virus and buffer for 3 times, continue adding samples till the first column is completed. Using multichannel to perform the serial dilution as designed. Use filter tips to dilute if virus handling is involved, check the level does not change in the tips and remains at 50µl.

3. Each virus in duplicate is serially diluted across the plate as far as column 11; discard 50µl from column 11. Column 12 contains 50µl of MES buffer only. This will be used to ascertain the average background reading to subtract from the raw data during the data analysis.
4. Add 50 ul MES assay buffer to all the well so that the total final volume will be 200 ul (same as the total assay volume).
5. Prepare the MUNANA substrate at a concentration of 100µM in MES assay buffer. Add 50µl of substrate to each well including the blank in column When adding the substrate start with the buffer in column 12 and work up the virus dilution. Add the substrate into the side of the well.
6. Ensure components of each well are mixed by gently tapping the plate. Cover/seal with aluminum foil and incubate at 37°C (do not use CO2 incubator to keep the pH) for 60 minutes. Make sure the lids are covered with foil to protect the florescent 4-MU from photobleaching.
7. Terminate the reaction by adding 50 µl of stop solution to each well. There is a 20-minute window to record the fluorescence, after that period the stop solution will degrade the 4-Methylumbelliferone sodium salt product.
8. Place plate(s) in a sealable box. Then take the plate(s) to Clariostar room for measurement. (An excitation wavelength of 355 nM and an emission wavelength of 460 nM at gain 2000 are used to detect fluorescence.)
9. Plot results with PRISM 10. Calculate results as needed.

2.6.5 ELISA

Day -2 (if using infected cells)

1. Resuspend MDCK-SIAT1 cells in VGM with a concentration of 0.3M/mL. Seed 100 µL of MDCK-SIAT cells in the flat bottom 96-well plate with lid.

Day -1

1. (If using infected cells), add 50 µL of virus dilution to each well and infect the cells overnight.
2. (If using stock antigen), dilute stock antigen to 2 µg/ml in PBS in a hood. Coat the ELISA NUNC plate with 50 µl of NA antigen per well and incubate for 2 hours at room temperature or overnight at 4 °C.

Day 0

1. Prepare 5% milk in PBS/0.02% azide.
2. Remove antigen with multichannel pipette, antigen can be re-stored at 4°C and reused once.
3. Wash plate with PBS, flick off the plate over the sink to remove the content. Repeat 2 times.
4. Block wells by adding 350 µl of 5% milk in PBS/0.02% azide, incubate for 2 hours at RT/ overnight at 4°C. Blocked plates can be stored at 4°C and used within a week.
5. If sample is sera, heat treat it at 56°C for 30 minutes.
6. Dilute serum samples in 1:20 with PBS (in hood).
7. Perform a 2-fold (or 5-fold if high titre sera) serial dilution of the antibodies/sera/supernatant with PBS in a round-bottomed 96-well plate starting from 60 µl of sample from col 1-11; well 12 should contain only PBS. Addition of samples has to be done in the hood, the rest can be done on bench. Perform each sample in duplicate.
8. Wash antigen-coated NUNC plates with PBS, flick over sink to remove. Repeat for 2 times.
9. Dry the plate by tapping it on dry towels.

10. Transfer 50 µl of diluted antibodies/sera/supernatant to respective well on the Nunc plates. Incubate for 1 hr (on a shaker: Optional).
11. Flick over sink to remove the content.
12. Wash plate with PBS, flick over sink to remove. Repeat for 2 times.
13. Dry the plate by tapping it on dry towels.
14. Add 50 µl of secondary antibody per well. Incubate for 1h.
15. Flick over sink to remove the content.
16. Wash plate with PBS, flick over sink to remove. Repeat for 3 times.
17. Optional: Dunk plates on a reservoir with tap water.
18. Dry the plate by tapping it on dry towels.
19. Add 50 µl of developer per well and incubate for 5 minutes.
20. Add 50 µl of 1M sulphuric acids immediately to stop the reaction.
21. Read the plate at 450 nm.
22. Use the template to determine EC50 concentration/titre.

2.7 NA-VLP conjugation

Several batches of SpyCatcher003 were used in this Study. SpyCather-mi3 VLPs were produced in *Escherichia coli* cytoplasm and purified with affinity resin-independent purification in Howarth lab (Rahikainen et al., 2021). Spycatcher003-mi3 virus-like particles (Lot No. 108-23-001-007) produced in *Bacillus subtilis*, were kindly provided by Ingenza Ltd. NA and VLP conjugations were done in DPBS with Calcium Magnesium at 4 ℃ overnight before later usage. 2 μg of NA-VLP (amount counted by NA content) was analysed using reduced SDS-PAGE. The conjugates were confirmed to have enzymatic activities and mAbs binding equivalent to the unconjugated proteins before all immunization test. Once conjugated NA-VLP were aliquoted and stored at -80 ℃ for longer storage and tests.

2.8 Mice immunization

6-7 weeks old Female mice (acclimatized for at least one week, so 7-8 weeks old at the start of the experiment) were obtained from Envigo and housed in individually vented cages in a specialised unit for infectious diseases. For the X-179A challenge model, DBA/2 OlaHsd (DBA/2 mice are more susceptible to human and avian isolates, compared to other mouse strains) were used for experiments, while for X31 and PR8 challenge, BALB/c OlaHsd mice were used. In experiments testing sera response only, C57BL/6 mice were used.

The mice were housed in accordance with the UK Home Office ethical and welfare guidelines, fed standard chow, and had access to water *ad libitum*. Mice were anesthetized with isoflurane (Abbott) and immunized via intramuscular injections with two doses of 0.5 µg (25 µL) of NA-VLP immunogens adjuvanted with AddaVax™ (Invivogen)1:1 vol/vol (50 µL in total), administered 3 weeks apart with BD Microfine (29G, U-100 Insulin 0.5 ml) needles.

Serum samples were collected 3 weeks after the booster dose: intermediate samples were obtained via tail vein and terminal samples via cardiac puncture of euthanised mice. Whole blood collected in tubes was allowed to clot at room temperature for 1-2 h before centrifugation at 10,000 *g* for 10 min. The clarified sera were transferred to fresh tubes and stored at -20 °C.

For virus challenge experiments, 50 uL virus was administered intranasally to anesthetized mice. The weight and clinical signs of mice were monitored regularly over a study period of 2-3 weeks until they either reached their endpoint (≤80% of their initial weight) or recovered to their initial weight. Mice reaching the endpoint were humanely euthanised. Kaplan-Meier survival analysis with the Logrank Mantel-Cox test was used for comparison.

2.9 Study Approval

Animal experiments were conducted in compliance with the UK Animals (Scientific Procedures) Act Project License (PP9362617, PPL holder: Tiong Ton), following the principles of the 3Rs (Replacement, Reduction and Refinement).

The study protocol and informed consent of human monoclonal antibody isolation were approved by the ethics committee at the National Taiwan University Hospital and Chang Gung Memorial Hospital and were carried out in accordance with the Declaration of Helsinki and Good Clinical Practice guidelines. Written informed consent was received from each adult prior to inclusion in the study.

Chapter 3 Neuraminidase expression, Characterisation and Conjugation

In this chapter, we developed a standardized methodology to design, express, and characterize recombinant neuraminidases (NAs).

A relatively extensive library of neuraminidase variants was established, encompassing a diverse range of neuraminidase sequences from different strains. This library enables comprehensive investigation of neuraminidase behaviour, providing insights into the tetramerization, protein yield, catalytic activity and structural integrity. By examining this broad spectrum of NAs, we aimed to identify common functional characteristics and underlying principles.

3.1 Recombinant NA: design, express and characterize

3.1.1 Recombinant NA expression and characterization

We established a standardised workflow for the design, expression, and characterisation of neuraminidase (NA). This methodology utilises standard molecular biology techniques to create recombinant DNA constructs encoding NAs, which are then introduced into suitable expression systems (ExpiCHO and Expi293) to produce NAs at scalable quantities. Following expression, the recombinant NAs are purified using chromatography techniques and characterised for their composition, enzymatic activity, and immunogenic epitopes.

Human codon-optimised cDNA sequences encoding recombinant NAs were cloned into the pCDNA3.1 or pCDNA3.4 expression vectors for transient transfection, as detailed in Chapter 2.

Our NA expression system was established in ExpiCHO and Expi293 cells. However, the expression and purification of large quantities of NA remain challenging. The first neuraminidase isolation was reported by Bucher in 1977 (Bucher, 1977). Since then, methods have been developed to amplify influenza viruses in eggs and cell culture systems to obtain NA from bulk virus production. Nevertheless, viral NA can become unstable post-cleavage by protease or treatment with detergents (Sahasrabudhe et al., 1998).

Alternative methods for expressing recombinant NA have been successfully developed in various systems, including yeast, insect cells, and mammalian cells. Comparative studies indicate that soluble recombinant NA expressed with a tetramerisation domain replacing the NA stalk typically maintains the native structural integrity of the NA head in tetrameric form. This supports the use of soluble recombinant NA in vaccine development (Streltsov et al., 2019).

The purification and characterisation process is summarised in Fig. 3.1. Purification of NA from suspension cell supernatants was conducted using a His-tag purification method, as detailed in Chapter 2. The characterisation of NA involved five distinct methods:

1. **Purity and Size Analysis:** Purified proteins were analysed for purity and size using three methods: reducing sodium dodecyl sulfate polyacrylamide gel electrophoresis (SDS-PAGE), non-reducing SDS-PAGE, and bis(sulfosuccinimidyl) suberate (BS-3) linked SDS-PAGE. BS-3, an amine-to-amine crosslinker, facilitated the interaction between protomers of dimeric or tetrameric NA, enabling accurate determination of NA size and oligomeric state.

2. **Size-Exclusion Chromatography (SEC):** SEC revealed distinct peaks corresponding to various NA forms, including aggregates, tetramers, dimers, and monomers.

3. **Enzyme-Linked Immunosorbent Assay (ELISA)**: ELISA was employed to evaluate the structural integrity of purified recombinant NA. Using our panel of selected monoclonal antibodies, ELISA detected conformation-specific epitopes, confirming structural fidelity.

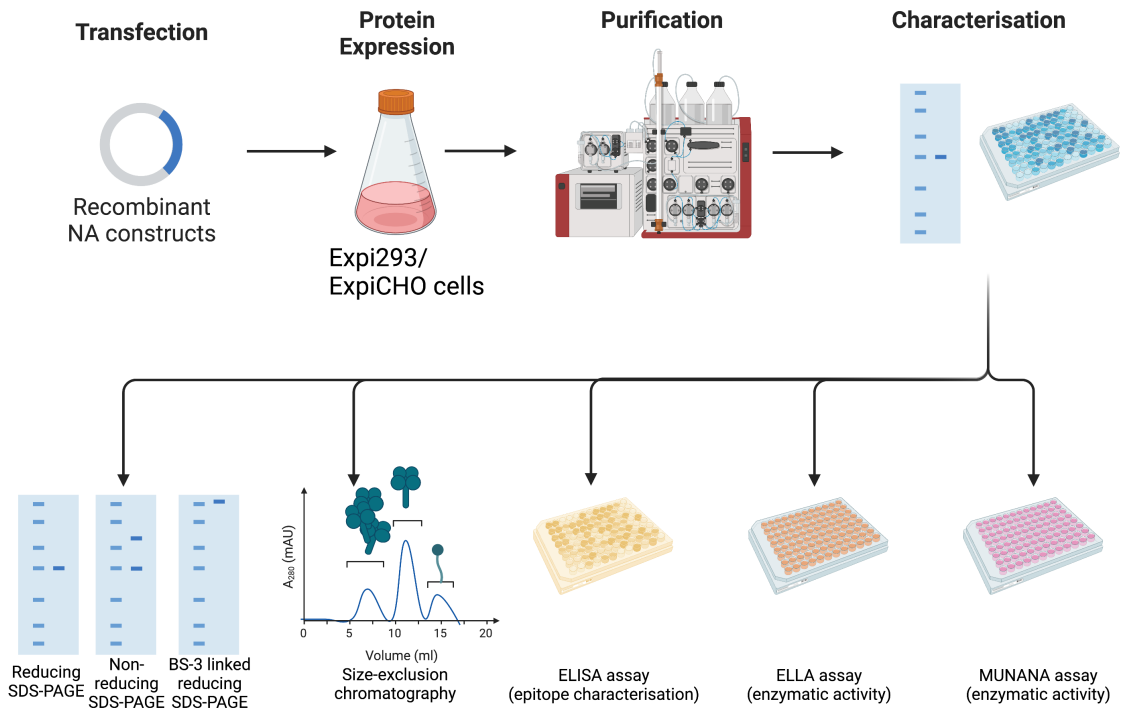

Figure 3.1 **Recombinant NA expression and characterization process**
Recombinant NA plasmids were transfected into either Expi293 or ExpiCHO cells, followed by purification and characterisation. Purified neuraminidases were run on SDS-PAGE with or without BS-3 linking. The size-exclusion chromatogram exhibited distinct peaks, including aggregates, tetramers, dimmers and monomers. Epitope characterisation was accomplished by Enzyme Linked Immunosorbent Assay (ELISA). Enzyme Linked Lectin Assay (ELLA), and 2′-(4-Methylumbelliferyl)-α-D-*N*-acetylneuraminic acid sodium salt hydrate (MUNANA) assay were used to assess enzymatic activity.

4. **Enzyme-linked le tin assay (ELLA):** ELLA is used to quantify the NA activity involved in removing sialic acid residues from a larger protein. Fetuin (48.4 kD), being heavily glycosylated with sialic acid on its N-linked glycosylation sites, serves as a substrate in this assay. Upon digestion by NA, the sialic acids are cleaved, exposing carbohydrate binding sites specific to the lectin peanut agglutinin (PNA). The amount of PNA bound correlates directly with the amount of sialic acid removed. In practical terms, peroxidase-conjugated PNA is used to detect and quantify the exposed carbohydrate binding sites on fetuin after NA treatment. This allowed the first lectin assay to be developed in 1990 (Lambré et al., 1990, 1991) and further modified in 2014 (Couzens et al., 2014). We are able to measure the NA activity from recombinant protein and virus via ELLA as well as the inhibition titres from monoclonal antibody and experimental sera.

5. **MUNANA assay:** the MUNANA assay is a fluorescence-based method used to measure NA activity and NA inhibition with small substrate similar in size to sialic acid. In this assay, the substrate 2'-(4-methylumbelliferyl)-α-D-N-acetylneuraminic acid (MUNANA, MW 489.4) is cleaved by NA, resulting in the release of the fluorescent product 4-methylumbelliferone (4-MU) and free N-acetylneuraminic acid. The amount of fluorescent 4-MU generated directly correlates with the NA activity, providing a quantitative measure of the

enzyme's ability to cleave the small molecule substrate. This assay is valuable for assessing NA activity in both purified NA and viral samples. Also, it is used to determine the inhibitory effects of antibodies, or experimental sera on NA function. However many antibodies capable of steric inhibition of NA acting on the large substrate fetuin do not inhibit the cleavage of MUNANA, which is thought to be limited to those antibodies that can bind directly to the active site of the enzyme.

3.1.2 Recombinant neuraminidase design

External tetramerization domains have been incorporated to produce recombinant soluble tetrameric neuraminidases (NAs), replacing the native tetrameric stalk. Three tetramerization domains have been used in recombinant NA constructs: human vasodilator-stimulated phosphoprotein (VASP) (Ellis et al., 2022) from humans, tetrabrachion (TB) from *Staphylothermus marinus* (Prevato et al., 2015; Schmidt et al., 2011; Streltsov et al., 2019), and GCN-4-pLI from yeast (Schmidt et al., 2011).

For the expression of pandemic N1 NA (A/California/7/2009, referred to as N1/09), DNA constructs were designed as depicted in Figure 3.1A with two different external tetrameric domains. Specifically, the N1/09 VASP construct included an H1 signal sequence at the N-terminus followed by a His6 tag for purification, SpyTag for particle conjugation, VASP domain for tetramerization, a thrombin site for cleavage, and the N1 NA head domain starting from residue 69. The NA head domain, defined by the pronase-release (Ward et al., 1982), spans residues 74 to 469 in N2 numbering. For the N1/09 sequence used in this study, the aligned head domain corresponds to residues 74 to 471. Alignment of the stalk region also revealed a region of sequence similarity from residues 70 to 73 (Schmidt et al., 2011), prompting the final selection of residue 69 as the starting point for the N1 NA head domain in this construct.

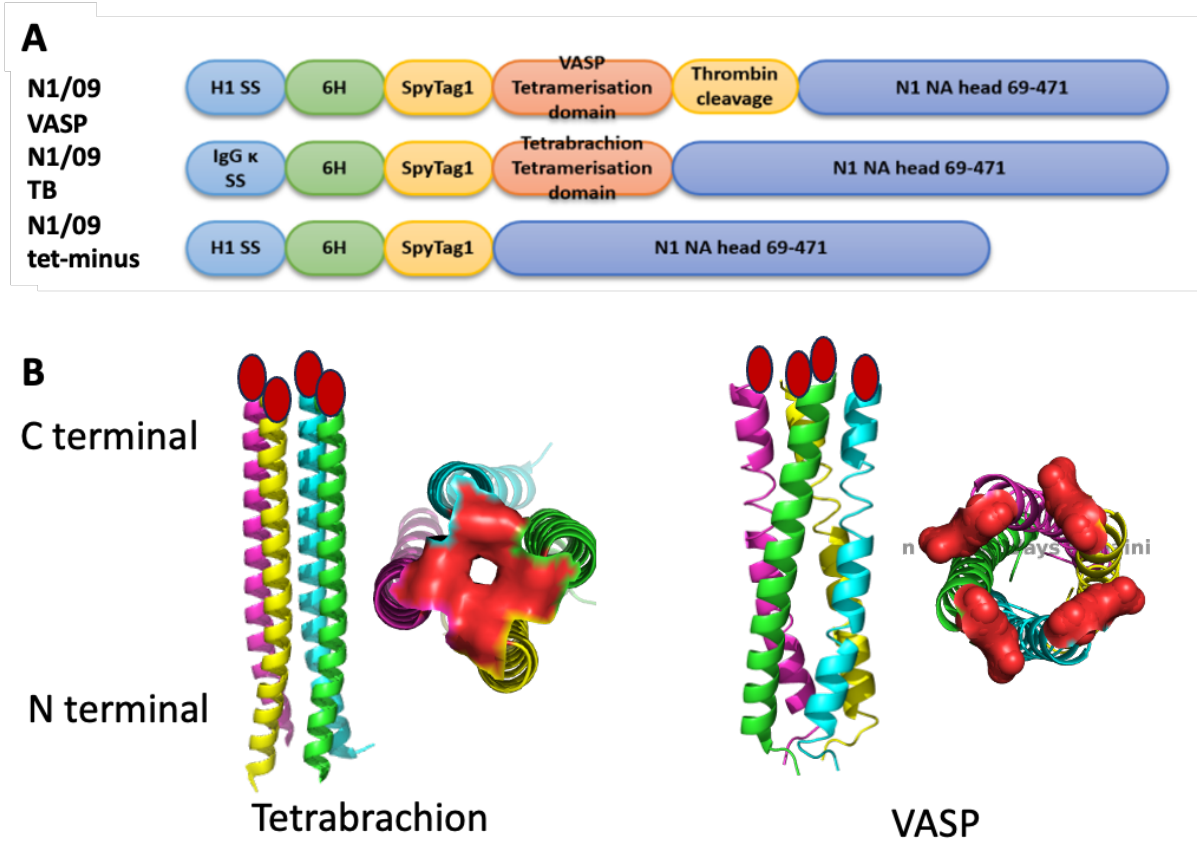

Figure 3.2 **Recombinant NA design**
A) Recombinant NA designs are presented taking N1/09 (A/California/7/2009 H1N1) as an example. Signal sequences, including H1,H1, H7 or IgG κ were incorporated. 6-His Tag and StrepII Tag were included as purification Tags. Options for tetramerization domain included VASP, Tetrabrachion, or no tetramerization. The Thrombin cleavage site, initially present in

N1/09 VASP, was removed in all subsequent recombinant NAs (design details can be found in Appendix 3.1).
B) Structure of Tetrabrachion (PDB: 1FE6, (Stetefeld et al., 2000)) and VASP (PDB: 1USE, (Kühnel et al., 2004)) tetramerization domains. The C terminal surfaces were outlined and highlighted in red for clarity.

The construct of N1/09 TB closely mirrored that of N1/09 VASP with some minor adjustments. Specifically, the signal sequence was changed to IgGκ (Schmidt et al., 2011), and the tetramerization domain was replaced with TB. Additionally, in consideration of further immunogenic applications, the thrombin cleavage site was omitted to minimize irrelevant immune responses.

Similarly, the construct of N1/09 TetDminus followed the same design principles but excluded any artificial stalk domain. For additional details on other recombinant protein designs, please refer to Appendix 1.

The structures of VASP and TB are illustrated in Figure 3.2B. Compared to VASP, TB exhibits a highly parallel right-handed coiled-coil structure (Kühnel et al., 2004; Stetefeld et al., 2000), which is anticipated to contribute to a more stable tetrameric NA configuration.
In our study, we expanded our selection of influenza virus strains to create a diverse library of neuraminidases (NAs), both with and without tetramerization domains, as outlined in Appendix 1.

For the N1 subtype, we focused on constructing recombinant NAs from three more strains: A/Puerto Rico/8/1934 (H1N1), isolated from a human patient in 1934;

A/mute swan/England/053054/2021 (H5N1), obtained from a mute swan infected with highly pathogenic avian influenza (HPAI) in 2021; and A/Victoria/2570/2019 (H1N1), a recent circulating seasonal strain.

For the N2 subtype, we selected two strains for recombinant NA construction: A/Hong Kong/1/1968 (H3N2), responsible for the 1968 Hong Kong flu pandemic; and A/Cambodia/E0826360/2020 (H3N2), a recent circulating seasonal strain.
Additionally, we explored various constructs for six different strains of N8, detailed in Chapter 6 of our study.

N6 was derived from A/Hubei/29578/2016 (H5N6), and N9 from A/Anhui/1/2013 (H7N9), both isolated from recent human infection cases. Furthermore, hybrid NAs were also constructed following similar principles, discussed further in Chapters 5 and 6.

These NA proteins have been abbreviated as follows for easier referring in Table 3.1:

Table 3.1 List of Influenza strain abbreviations

Abbreviated Name	**Influenza Strain**
N1/09	H1N1 A/California/7/2009
N1 MS	H5N1 A/mute swan/England/053054/2021
N1 PR8	H1N1 A/Puerto Rico/8/1934
N1/19	H1N1 NYMC X-379 (A/Victoria/2570/2019)

N2 X31	H3N2 A/Hong Kong/1/68
N2/20	H3N2 A/Cambodia/E0826360/2020
N6/16	H5N6 A/Hubei/29578/2016
N8/20	H5N8 A/chicken/England/030720/2020
N9/13	H7N9 A/Anhui/1/2013

This approach allowed us to study and compare a wide range of NAs from different influenza strains, leading to a comprehensive understanding of their common behaviour pattern as well as structural and functional diversity, benefiting future vaccine development and therapeutic strategies.

3.1.3 Recombinant neuraminidase expression

The expression of recombinant soluble neuraminidase (NA) varies significantly across published studies. As detailed in Table 1.8, the highest yield reported from mammalian systems is approximately 30 mg/L for the N1/2009 protein expressed in the Expi293 system (Prevato et al., 2015).

Several factors influence soluble NA expression, including the choice of tetramerization domain, fusion tags, plasmid selection, codon optimisation, and amino acid mutations. Even with similar constructs and expression conditions, expression levels can vary significantly due to differences in the NA head sequences (Dai et al., 2016; Ellis et al., 2022). These factors collectively impact the yield of recombinant NA, as documented in Appendix 2, which lists expression yields from highest to lowest.

Among the native NA head domain sequences tested, N1 MS TB achieved the highest yield at 380 mg/L, followed by three TetDminus recombinant NAs. This suggests that omitting the tetramerization domain may improve yield in certain cases.

Notably, these yields far exceed those listed in Table 1.8, with the highest strains achieving yields more than ten times greater than the highest reported yield in mammalian expression systems. However, despite these advancements, many strains still exhibited poor expression yields. For over half of the strains tested, yields were below 30 mg/L, highlighting the ongoing challenges in achieving satisfactory expression levels. To address these issues, Chapters 5 and 6 introduce a "loop-grafting" method aimed at improving the yield and stability of NA proteins.

When comparing different tetramerization domains, VASP-fused recombinant NAs generally yielded higher amounts compared to TB in both N1/09 and N8/20 cases (Appendix 2). Additionally, TetDminus versions of N1/19 and N8/20, which lack any tetramerization domains, exhibited improved expression, suggesting their potential as alternatives for overcoming expression challenges.

However, as detailed in Chapter 4, most NAs lacking a tetramerization domain, despite their high expression levels, were misfolded. This misfolding was evidenced by the loss of specific epitopes detected by monoclonal antibodies and the frequent absence of enzymatic activity.

3.2 Assembly of recombinant neuraminidase

3.2.1 Understanding main existing forms of rNA

We characterised 18 purified soluble recombinant neuraminidases (rNAs) using reducing SDS-PAGE, as shown in Figure 3.3. When BS-3 is added to a protein solution, its sulfo-NHS ester groups react with primary amines on the protein surfaces. This reaction forms covalent bonds between proteins in close proximity, effectively "cross-linking" them. Primary amines are found in lysine residues and the N-terminal amino acids of proteins.

In our analysis, the tetrameric, dimeric, or monomeric forms of the NA protein were distinguished based on cross-linking between the N-terminal free amines and amines from lysine residues. The presence of a top band around ~250 kDa in the BS-3 cross-linked reaction indicates that the protein is in a tetrameric form. The appearance of additional bands does not necessarily indicate heterogeneity in the protein. Conversely, if the protein does not form tetramers, no band will appear at ~250 kDa.

While the gel provides a straightforward method to determine whether the protein forms tetramers, it is not a definitive tool for assessing protein heterogeneity. To accurately evaluate protein heterogeneity, size-exclusion chromatography is essential.

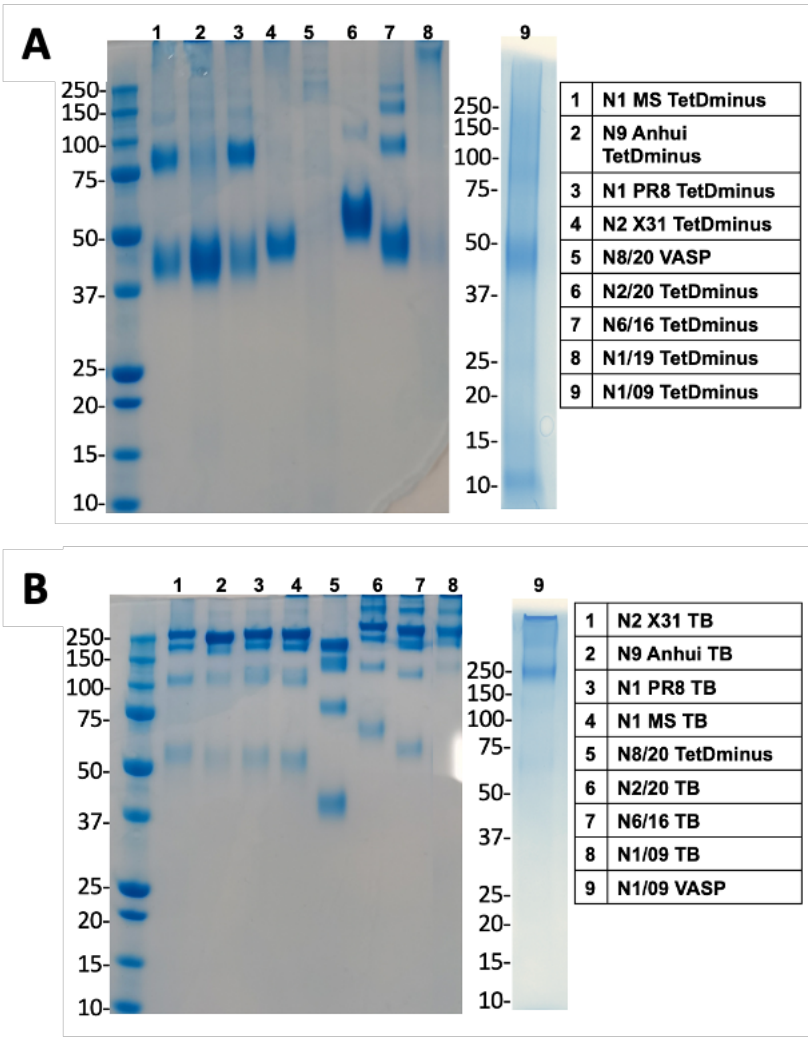

Figure 3.3 **BS-3 linked SDS-PAGE for neuraminidases expressed with TB, VASP, or without tetramerization domain**

BS-3 crosslinking helped to stabilize the structure of oligomers and can thus be used to reflect their native structure. A) Following a 30 min cross-linking with BS-3, 2 µg of the linked neuraminidase was loaded onto reducing SDS-PAGE. Each well contained neuraminidase as indicated. Most neuraminidases lacking tetramerization domain were included in the analysis, except for N8/20 VASP. B) All recombinant neuraminidases that formed tetramers were included. Expression yields were compiled and summarized in Appendix 2. Complete characterization with SDS-PAGE analysis is available in Appendix 4.

After a 30-minute crosslinking with BS-3, 2 µg of each neuraminidase (NA) sample was loaded onto reducing SDS-PAGE. As shown in Fig. 3.3A, eight TetDminus (lacking a tetramerisation domain) NAs predominantly existed as dimers or monomers. Specifically:

- **Dimers**: N1 MS TetDminus and N1 PR8 TetDminus appeared primarily as dimers.
- **Monomers**: N9 Anhui TetDminus, N2 X31 TetDminus, N2/20 TetDminus, and N1/09 TetDminus were mostly monomeric.
- **Mixed forms**: N6/16 TetDminus displayed four bands in Lane 7, with the monomeric band being the most prominent. This suggests a mixed form that may include some tetramers, requiring further size-exclusion chromatography (SEC) for clarification.
- **Aggregates**: N1/19 TetDminus showed protein bands concentrated in the upper region of SDS-PAGE, likely indicating aggregation.

In contrast, recombinant NAs expressed with **TB** and **VASP** domains consistently produced a prominent band at the tetramer size, confirming successful expression and tetramerisation when using an external tetramerisation domain (Fig. 3.3B).

N8/20 TetDminus was unique in forming a high-yield tetramer without any tetramerisation domain. Interestingly, this N8 protein failed to express when a TB domain was attached. A full investigation of this exceptional N8 NA and related N8 proteins is presented in Chapter 6.

Reducing SDS-PAGE and BS-3 SDS-PAGE results for all 28 recombinant NAs are detailed in Appendix 5, alongside SEC and NA activity data. This collective dataset highlights the critical role of tetramerisation domains—and selecting the appropriate one—in ensuring protein thermal stability and maintaining tetrameric conformation.

3.2.2 Understanding the compositions of rNA

Overall, BS-3 SDS-PAGE serves as a valuable tool in our research for quickly assessing the oligomeric states of recombinant proteins. SEC complements reducing SDS-PAGE and BS-3 cross-linked SDS-PAGE by providing a detailed analysis of the aggregation and oligomerization states of recombinant NAs. In our study, SEC analysis was conducted using a Superdex® 200 10/300 GL column, which separates proteins based on their size.

The SEC chromatogram revealed NAs in distinct forms: aggregates (A) eluting ~ 8 ml, tetramers (T) at ~ 12.5 ml, and dimers (D) at ~ 13.2 ml, monomers (M) at ~ 14.6 ml elution volume. These elution volumes correspond to the sizes of the various NA oligomeric states, allowing for precise determination of their compositions.

Size markers run in our own column ran as follows:

Protien size (MW, kDa)	Log MW (kDa)	SEC elution volume/ml	
		Marker batch 1	Marker batch 2
669	2.8	9.2	9.2
440	2.6	10.5	10.6
158	2.2	12.7	12.8
75	1.9	14.1	14.1
44	1.6	14.9	15.0

In our SEC analyses depicted in Figure 3.4 and detailed in Appendix 5, we observed distinct patterns for various recombinant neuraminidases (NAs), revealing their oligomeric states.

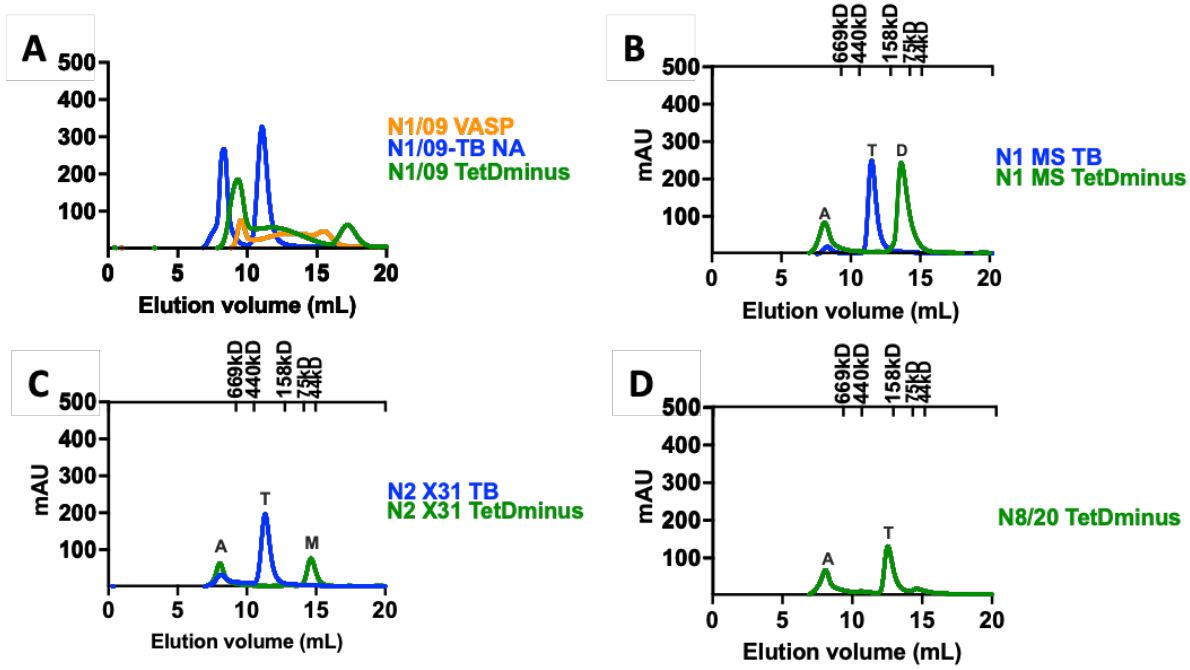

Figure 3.4 **Neuraminidase expressed as aggregates, tetramers, dimers, and monomers**

Size exclusion chromatography (SEC) analysis was conducted using a Superdex® 200 10/300 GL column. Neuraminidase(NA) was observed in various forms: aggregates(A), monomers (M), dimers (D), and tetramers (T).
A) NAs derived from A/California/7/2009 demonstrated different patterns in SEC. N1/09 TB exhibited aggregations and tetramers. The compositions of N1/09 VASP and N1/09 TetDminus were difficult to identify from SEC. (Note: The size reference for this chromatogram is not available as the column was borrowed from Davis' Lab, WIMM, Oxford.)
B) N1 MS TB from A/mute swan/England/053054/2021predominantly existed as tetramers with tiny aggregations. N1 MS TetDminus existed as aggregates and dimers.
C) The NA of A/Hong Kong/1/1968 existed mainly in its monomeric form in the absence of the tetramerization domain.
D) N8 NA from A/chicken/England/030720/2020 H5N8 was notable as the protein was capable of spontaneous tetramerization without TB or VASP.

In Fig. 3.4A, focusing on NAs derived from A/California/7/2009, distinct SEC patterns were identified: N1/09 TB exhibited peaks corresponding to aggregates and tetramers. In case of N1/09 VASP and N1/09 TetDminus, SEC analysis showed a complex pattern characterized by an initial aggregation peak followed by a flat peak (between elution volume 10-18 mL) corresponding to tetramers, dimers and monomers.

For N1 MS TB from A/mute swan/England/053054/2021 (Fig. 3.4B), this variant exhibited minimal aggregation and a prominent tetrameric peak. This pattern was consistent with another avian strain, A/turkey/Turkey/1/2005 (H5N1), which differed by 20 amino acids in the head region but showed a similar tetrameric structure (Prevato et al., 2015). N1 MS TetDminus showed a 4.7% of aggregates and was predominantly present as dimers.

Similar patterns were observed for N1 PR8 TB and N1 PR8 TetDminus (details in Appendix 5).

For N2 X31 (Fig. 3.4C), the TB-linked recombinant NA appeared mainly as a tetrameric protein with minimal aggregation. In contrast, NA expressed without any external tetramerization domain was monomeric with some degree of aggregation.
For N8/20 TetDminus (Fig. 3.4D), SEC analysis identified both an aggregation peak and a distinct tetrameric peak for this self-tetramerizing variant. Unfortunately, N8/20 VASP or TB did not yield sufficient protein for SEC analysis in our study.

Overall, our SEC data from various recombinant NAs (Appendix 5) provide insights into their structural forms and stability. Constructs with TB generally resulted in stable tetrameric NAs, with varying degrees of aggregation. NAs lacking external tetramerization domains exhibited diverse forms, ranging from monomers, dimers to tetramers.

Interestingly, N8/20 demonstrated unique self-tetramerization capability, despite initial challenges in expression when linked with TB or VASP.

3.3 Characterization of NA

3.3.1 Enzymatic activity of recombinant neuraminidases

In our enzymatic activity characterization using ELLA and MUNANA assays, we evaluated various strains of recombinant NAs with or without tetramerization domain to understand their catalytic activities (Fig. 3.5, Fig. 3.6). Area under curve (AUC) values of the NA activity titration curves are shown in Appendix 3. Higher value means higher activity. Individual curves for each NA are shown in Appendix 5.

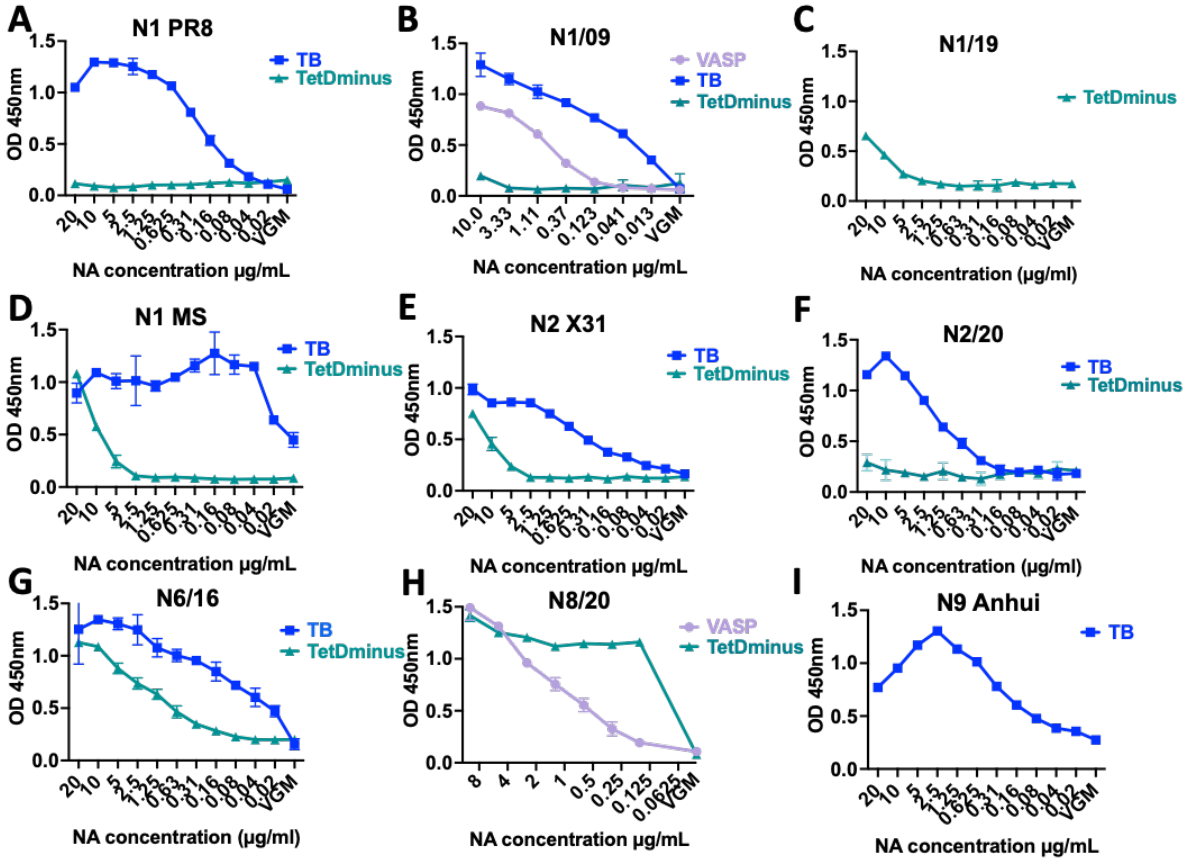

Figure 3.5 **Neuraminidases expressed without tetramerization domain had compromised catalytic activity (by ELLA) except N8/20**
A-I) Enzyme-linked lectin assay (ELLA) activity of recombinant neuraminidases from various strains. With the exception of N1/19(C) and N8/20(H), all other NAs were successfully expressed with tetramerization domain (TB or VASP) and exhibited significant activity. H) N8/20 TetDminus retained high enzymatic activity as a spontaneous tetramer, while other NAs expressed without the tetramerization domain demonstrated relatively lower activity. (The X-axis may vary due to different batches of results being plotted.)

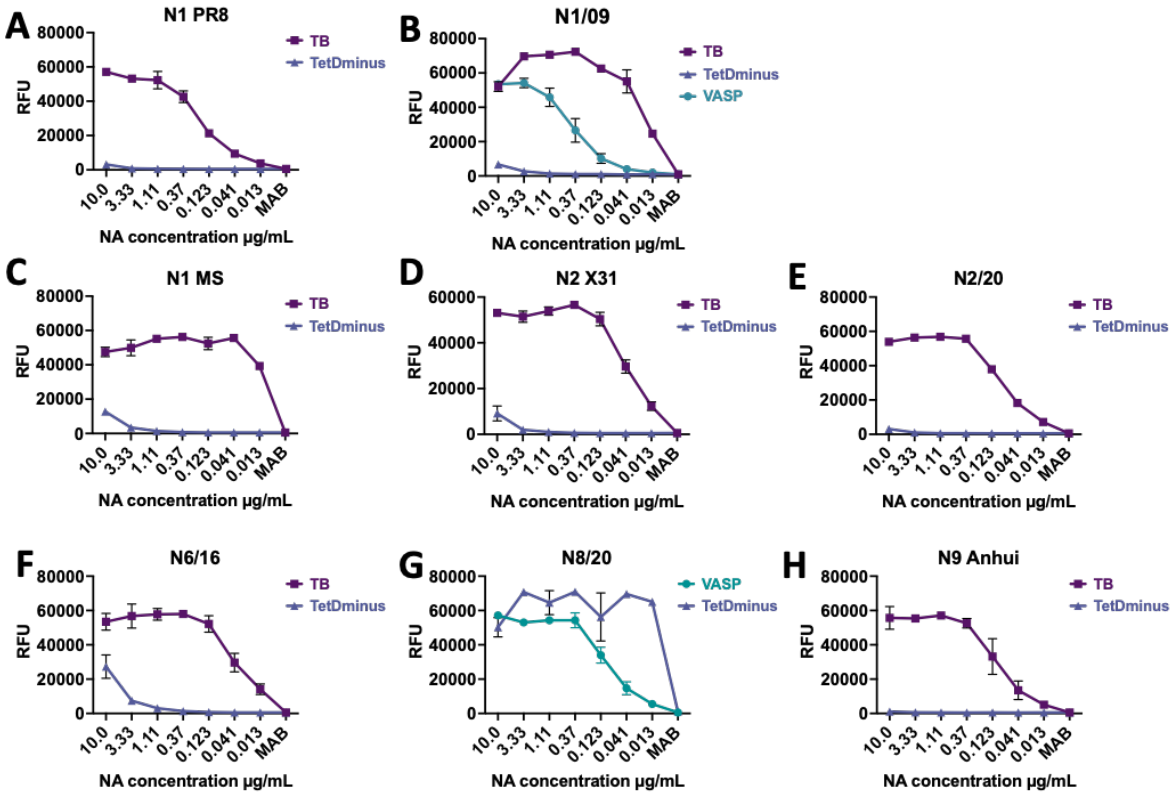

Figure 3.6 **Neuraminidases expressed without tetramerization domain had compromised catalytic activity (by MUNANA assay) except N8/20**
A-H) MUNANA activity of recombinant neuraminidases (NAs) from multiple strains. With the exception of N8/20(G), all other NAs can be successfully expressed with the tetramerization domain (TB) and exhibited significant activity. Also notably, N8/20 TetDminus retained high enzymatic activity as a spontaneous tetramer. While other NAs expressed without tetramerization domain demonstrated relatively low activity. RFU: Relative fluorescence units

N1 NAs:
N1 TB NAs (N1 PR8, N1/09, N1/19, N1 MS): These constructs, using TB as the tetramerization domain, consistently exhibited robust NA activity across both ELLA and MUNANA assays. Their enzymatic activity levels were comparable to those reported in similar studies (Dai et al., 2016; McMahon et al., 2020; Prevato et al., 2015; van der Woude et al., 2020).

N1 TetDminus NAs (N1 PR8 TetDminus, N1 MS TetDminus**)**: These variants, confirmed as dimeric forms through BS-3 cross-linked SDS-PAGE and SEC, showed reduced enzymatic activity compared to tetrameric forms expressed with TB domains. Notably, N1 MS TetDminus exhibited some enzymatic activity as a dimeric NA.

N2 NAs:
N2 TB NAs: The tetrameric versions of N2 X31 and N2/20 demonstrated high-level enzymatic activity similar to other TB-linked NAs.
N2 TetDminus NAs: Conversely, the monomeric forms exhibited minimal or no enzymatic activity, indicating the importance of tetramerization for NA function.

N6 NAs:
N6/16 TB and N6/16 TetDminus: The TB-linked N6/16 showed good enzymatic activity, while N6/16 TetDminus, which contained some tetramerized NA components, also displayed low level enzymatic activity.

N8/20 NAs:
N8/20 TetDminus: This variant formed a tetrameric structure without an external tetramerization domain and exhibited excellent catalytic activity, in contrast, N8/20 VASP, that expressed at very low level, although confirmed as a tetramer, showed relatively lower enzymatic activity.

N9 NAs:
N9 Anhui TetDminus: Similar to N1 PR8 TetDminus, N9 Anhui TetDminus showed minimal enzymatic activity in our assays. By contrast the N9 Anhui-TB tetramer showed strong enzymatic activity.

Overall, monomeric NAs generally exhibited none or minimal enzymatic activity, while dimeric NAs showed varied enzymatic activity depending on the specific strain. Tetramerized NAs, whether with external tetramerization domains or forming spontaneously like N8/20 TetDminus, consistently exhibited strong enzymatic activity. This agrees with the opinion that tetramerization and proper NA folding is crucial in maintaining NA functionality.

N1 MS TB and N8/20 TetDminus emerged as candidates with exceptional yield and catalytic activity. These insights contribute to the rational design of future NA constructs for improved enzymatic performance described in chapter 4.

3.3.2 Antibody binding to recombinant NAs

We selected an antibody panel of eight structurally well characterised monoclonal antibodies (seven isolated by our collaborative group) to detect NA epitopes and testify to the structural integrity of recombinant NA (Table 3.2). Seven of these have been co-crystallised with soluble NA to provide definitive binding information. AF9C, Z2B3, AG7C, and 1G01 have binding footprints that include the conserved catalytic site and they all bind within a single protomer. AS4C and M6B12 are N2 specific antibodies. AS4C binds close to, but not in, the catalytic site within a single protomer. M6B12 binds into the active site and spans two protomers.

Table 3.2 Specificities for selected mAbs

Antibody	MAb specificity	Binding site
AF9C[a]	Specific to N1 NA	To single protomer within catalytic site
Z2B3	Cross-reactive to N1, N6, and N9 NAs	To single protomer within catalytic site (PDB: 6LXJ)
AG7C[a]	Specific to N1 NA	To single protomer out of catalytic site
1G01	Cross-reactive to group 1 and group 2 NAs	To single protomer within catalytic site (PDB: 6Q23)
AS4C[a]	Specific to N2 NA	To single protomer
AQ2D	Specific to N2 NA	/
M6B12[a]	Specific to N2 NA	To two protomers and one protomer to catalytic site
CD6	Specific to N1 NA	Spanning over 2 protomers

[a]Structures of AF9C, AG7C,AS4C, M6B12 are not published yet. Binding site information clarified by Yan Wu's group, not published.

CD6 (Wan et al., 2015), which is specific to N1, spans two protomers, and binds on the side of the head region. The binding of CD6 has been characterised in detail by (Ellis et al., 2022) who showed that it bound only to tightly formed tetramers. Ellis et al were able to define two tetrameric forms of secreted NA, a loose form with head regions separated to a degree that prevented binding of CD6, and a tight form that bound CD6. This distinction has been applied in chapter 4.

A summary figure showing features of these key antibodies is shown in Table 1.6.
As shown in Fig. 3.7A, antibodies AF9C, Z2B3, AG7C, and 1G01 were chosen to recognize epitopes of group 1 rNAs. NA heads expressed without the tetramerization domain showed some epitope loss compared to the tetramerized ones, except for the self-tetramerized N8/20 TetDminus.

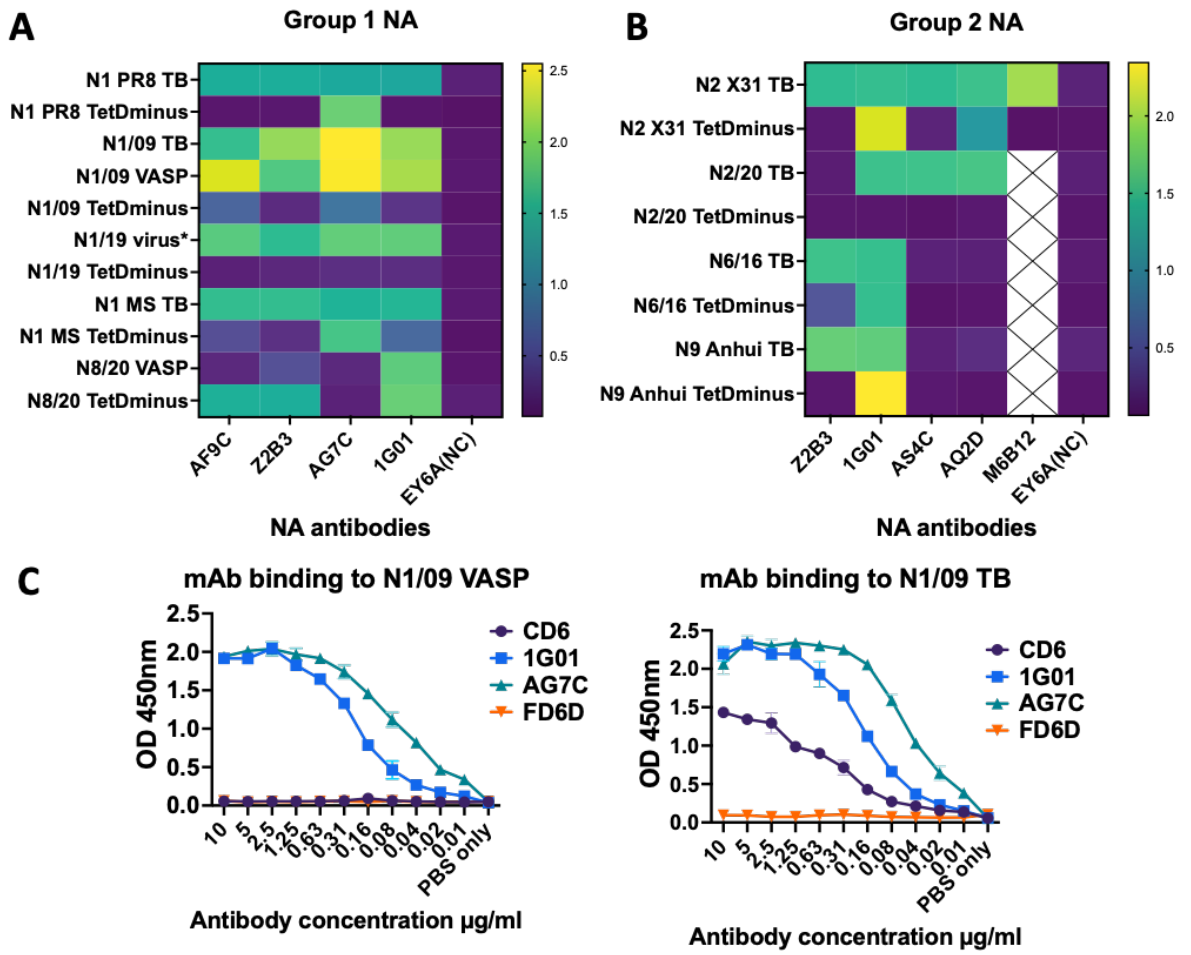

Figure 3.7 **Antibody binding to recombinant NAs showing efficient binding to tetrameric NAs not monomeric and dimeric NAs**
EY6A and FD6D are SARS-Cov2 mAbs used as a negative control. The color bar represents the optical density ($OD_{450}nm$) values from repeated single-point ELISA measurements. The cross symbol in panel B indicates missing data where the ELISA test with M6B12 was not performed.
A) Antibodies AF9C, Z2B3, AG7C, and 1G01 were chosen to recognize epitopes of group 1 rNAs. NA heads expressed without the tetramerization domain showed some epitope loss compared to the tetramerized ones, except for the self-tetramerized N8/20 TetDminus. B) Antibodies Z2B3, 1G01, AS4C, and AQ2D were selected to evaluate group 2 neuraminidases. Similarly, neuraminidases primarily existing as dimers and monomers experienced some loss of epitopes. C) Antibody CD6, binding to the neuraminidase head spanning over two protomers, lost its binding affinity to N1 VASP.

Similarly, antibodies Z2B3, 1G01, AS4C, and AQ2D were selected to evaluate group 2 neuraminidases (Fig. 3.7B). NAs primarily existing as dimers and monomers experienced some loss of epitopes compared to their tetramerized version.

For example, N1/19 TetDminus and N2/20 TetDminus did not bind to any of the related NA mAbs that recognised their tetrameric counterparts, either cell-expressed NA or soluble NA. However, soluble N8/20 TetDminus that formed spontaneous tetramers on its own, were bound

by mAbs. In the case of PR8 NA, TetDminus form only recognised one out of four mAbs (AG7C that has epitope outside the enzymatic cavity within a protomer).

These confirmed our hypothesis that tetramerization is required to maintain the structural integrity of NA (McMahon et al., 2020).

Antibodies CD6, 1G01, and AG7C were further titrated on N1/09 VASP and N1/09 TB-coated plates for detailed comparison of N1 tetramers held together by these contrasting tetramerisation domains (Fig. 3,7C). CD6, spanning across two protomers, demonstrated complete loss of binding to N1/09 VASP, indicating an "open confirmation" in the head region that affects its epitope (Ellis et al., 2022). In contrast, antibodies 1G01 and AG7C showed comparable binding between N1/09 VASP and N1/09 TB.

These findings emphasize that tetramerization plays a crucial role in preserving the native structural conformation and epitope accessibility of recombinant NAs.

3.3.3 Comparison between Expi293 and ExpiCHO expression system

The ExpiCHO and Expi293 expression systems are both high-yield, transient mammalian expression systems used for producing recombinant proteins, but they have some differences in terms of the cell lines used, yield, scalability, and applications (Durocher & Butler, 2009; Kunert & Reinhart, 2016). A comparison between ExpiCHO and Expi293 is listed below in Table 3.3.

Table 3.3 Comparison between ExpiCHO and Expi293

Feature	**ExpiCHO**	**Expi293**
Cell Line	Chinese Hamster Ovary (CHO) cells	Human Embryonic Kidney 293 (HEK293) cells
Expression Yield	Higher yields, often grams per litre	High yields, but typically lower than ExpiCHO
Scalability	Highly scalable for industrial production	Scalable, but less so than ExpiCHO
Common Applications	Therapeutic proteins, monoclonal antibodies	Structural biology, functional studies, proteins requiring human-like modifications
Post-translational Modifications	Similar to human but not identical	Human-like post-translational modifications

Note: this table is modified from (*ExpiCHO Expression System | Thermo Fisher Scientific - UK*)

In our experiments with neuraminidase (NA) expression, both the ExpiCHO and Expi293 systems proved to be versatile platforms for recombinant protein production. The expression yield varied depending on the strain of NA and the specific constructs used. Generally, ExpiCHO demonstrated a tendency to provide higher yields compared to Expi293 for the given constructs. Proteins purified from the ExpiCHO system typically showed less background bands in reducing SDS-PAGE compared to those from Expi293. This suggests that ExpiCHO may offer advantages in terms of purity and ease of protein purification.

Except the difference we noticed in yield and purification, the enzymatic activity remained consistent between ExpiCHO expressed NA and Expi293 expressed NA (Appendix 5).

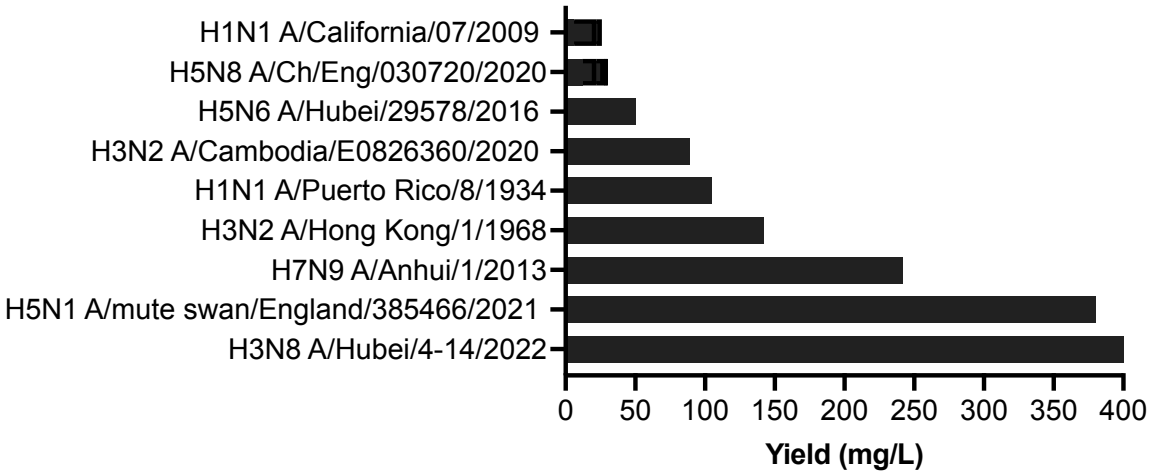

Figure 3.8 **Variation in production yield of NA proteins**
These are yields in ExpiCHO system for various NAs. All NAs were expressed with tetrabrachion domain, except for H3N8 A/Hubei/4-14/2022 which is a hybrid protein expressed as tetramers albeit without any tetramerisation domain (discussed in Chapter 6).

3.4 Discussion

In this chapter we tried to build a relatively extensive NA library and confirm some general rules regarding NA function and behaviour, such as the importance of external tetramerization to maintain the structure and catalytic activity. One prominent finding was the critical role of external tetramerization domains in maintaining the structural integrity and catalytic activity of most NAs. However, for all the general rules for NA, there's always an exception.

Importance of External Tetramerization:

- External tetramerization domains, such as TB (Tetrabrachion), generally facilitated the expression of properly folded and stable tetrameric NAs across various strains.
- This external structural support was crucial for preserving enzymatic activity and immunogenic epitopes, via proper NA folding. But there are some exceptions: despite the benefits of TB as an external tetramerization domain, certain strains within our library failed to express properly when paired with TB. N8/20 is the only protein which had undetectable expression with TB linked in our current test library.
- NAs expressed without external tetramerization domains often exhibited compromised enzymatic activity and immunogenic epitopes, highlighting the general importance of tetramerization.
- The differential protection between VASP and TB constructs underscores how tetramerization domains influence NA immunogenicity. Although both variants elicited neutralizing antibodies (NAI), the TB construct's enhanced structural rigidity (RMSD = 1.2Å vs. 2.8Å for VASP) likely confers greater protein stability—a feature that may explain its superior protective profile and improved vaccine performance.

Highly Polymorphic Nature:

- The extensive polymorphism observed in NAs led to a wide range of behaviours, including variability in protein yields, tetramerization capability, enzymatic activity, and immunogenicity.

Each NA protein shows an individual behaviour, particularly in tetramerisation and yield. Thorough knowledge of these variations led to the optimisation of expression described in later chapters.

Chapter 4 NA VLP as an experimental vaccine in mice

In this chapter, we developed a nano NA-VLP platform, where the coupling of neuraminidase (NA) and virus-like particles (VLPs) was achieved via covalent linkage between SpyTag and SpyCatcher. The NA-VLP, formulated with the adjuvant AddaVax, elicited a stronger antibody response in mice and protected mice from lethal challenge, demonstrating a dose-sparing effect. Furthermore, tetrameric NA-VLP provided superior protection compared to TetD-minus NA-VLP. Even at low doses, NA-VLP exhibited significant protective effects in a murine model. Collectively, our findings highlight the advantages of utilizing tetrameric NA-VLP in various challenge models.

4.1 Validation of NA-VLP assembly

As described in Chapter 3, N1/09 TB, N1/09 VASP, and N1/09 TetDminus were successfully expressed in ExpiCHO cells, purified, and characterized for subsequent immunization purposes. The production of tetrameric antigen-decorated virus-like particles (VLPs) using SpyTag/SpyCatcher technology has been successfully demonstrated (Rahikainen et al., 2021). We wanted to build on this work and investigate whether NA-VLP would be a promising vaccine approach for influenza.

The characterization of monomeric N1/09 TetDminus and tetrameric N1/09 TB and N1/09 VASP is described in previous chapter. The coupling of these three Spy tagged N1 NAs and SpyCatcher003-mi3 (referred to as mi3 hereafter) at different molar ratios is detailed in Appendix 6. The final antigen ratios (mi3: NA) chosen for N1/09 TB, N1/09 VASP, and N1/09 TetDminus were 1: 0.1, 1: 0.1, and 1: 0.5, respectively (Fig. 4.1A). These ratios were chosen to minimize the presence of free antigen and to achieve a strong and clear NA-VLP band on the SDS-PAGE. Compared to previous conjugations with monomeric, dimeric, and trimeric antigens, we consistently observed some free antigen even at low NA: VLP ratios. This could be attributed to some NA conjugating as a tetramer with three SpyCatcher units at one vertex of the icosahedron, leaving one free protomer with an unbound SpyTag. In later experiments, the ratio 1:0.3 to 1:0.4 is used to ensure optimal conjugation of NA on the mi3 nanoparticles leaving some unconjugated NA. Clear and strong NA-VLP bands can be observed in both cases.

The enzymatic activity of coupled NA and soluble free NA remained at the same level after conjugation (Fig. 4.1B). Consistent with previous NA activity data, the enzymatic activity of tetrameric NA-VLP was superior to that of monomeric NA-VLP.

Similarly, the selected antibody binding to NA and NA-VLP remained unchanged after conjugation (Fig. 4.1C). This indicates that coupling with mi3 did not alter any recognized epitopes of NA within single protomer. However, despite multimerization with mi3, the N1/09 TetDminus NA-VLP did not regain the epitopes recognized by AF9C and Z2B3. This suggested that multimerization with SpyTag/SpyCatcher did not alter the conformation of the incorrectly folded monomeric NA. This finding further confirms that NA expressed without the tetramerization domain undergoes a conformational change, as observed in most of our recombinant NA. The consistency of enzymatic activity and antibody binding both indicated that the structural integrity didn't alter with NA-VLP conjugation.

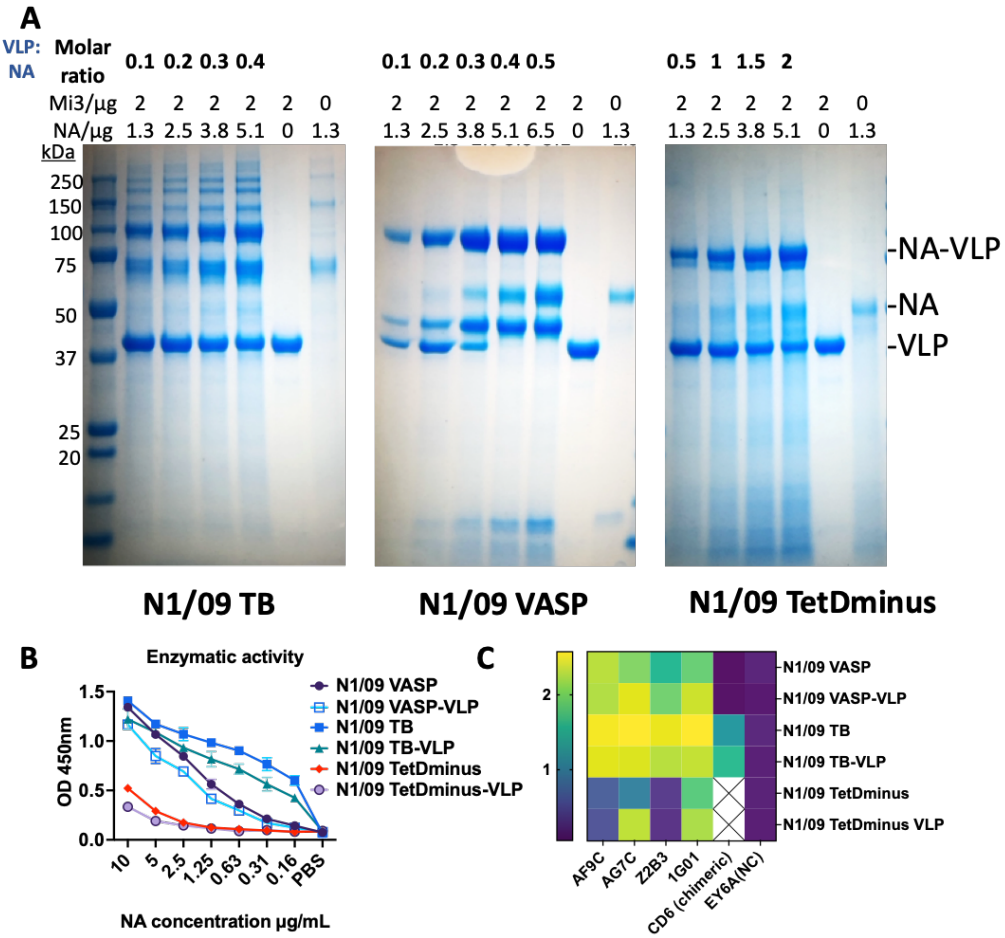

Figure 4.1 **SpyCatcher003-mi3 particles efficiently displayed tetrameric or monomeric N1/09 NA preserving its enzymatic activity and antigenicity.**

A) Coupling of N1/09 TB, N1/09 VASP and N1/09 TetDminus and mi3 at different molar NA:VLP ratio to make sure minimum free NA was left. The molar ratios of VLP: NA at 1: 0.1 to 1:2 are tested. A weak degradation band was seen in N1/09 VASP-VLP.

B) Assembly of NA-VLP did not prevent enzymatic activity of N1/09 and N1 MS.

C) Antibody epitopes on tetrameric NA were retained after formation of NA-VLP. Mabs AF9C, AG7C, Z2B3 and 1G01 are broadly reactive but depend on tetramer formation for full binding, so are weak on the N1/09 TetDminus monomer. CD6 (that binds across two monomers within the tetramer) is retained on N1/09 TB tetramer but is lost on the N1/09 VASP tetramer and monomeric NA (see text for further explanation).

4.2 NA-VLP protection in 2009 H1N1 (X-179A) challenge model

Previous work with VLP-conjugated N1/09 VASP demonstrated potent NA inhibition from mice sera vaccinated with 0.1 µg NA-decorated VLP, whereas none of the sera samples from the 0.1 µg free NA vaccinated group showed detectable inhibition levels (Rahikainen et al., 2021). In comparison to other studies using a mouse model for NA vaccination, the dose of free NA typically ranged between 1 to 5 µg (Table 1.7). Based on these findings, we selected 0.5 µg as our test dose to investigate whether our recombinant NA and NA-VLP can provide protection in a mouse model.

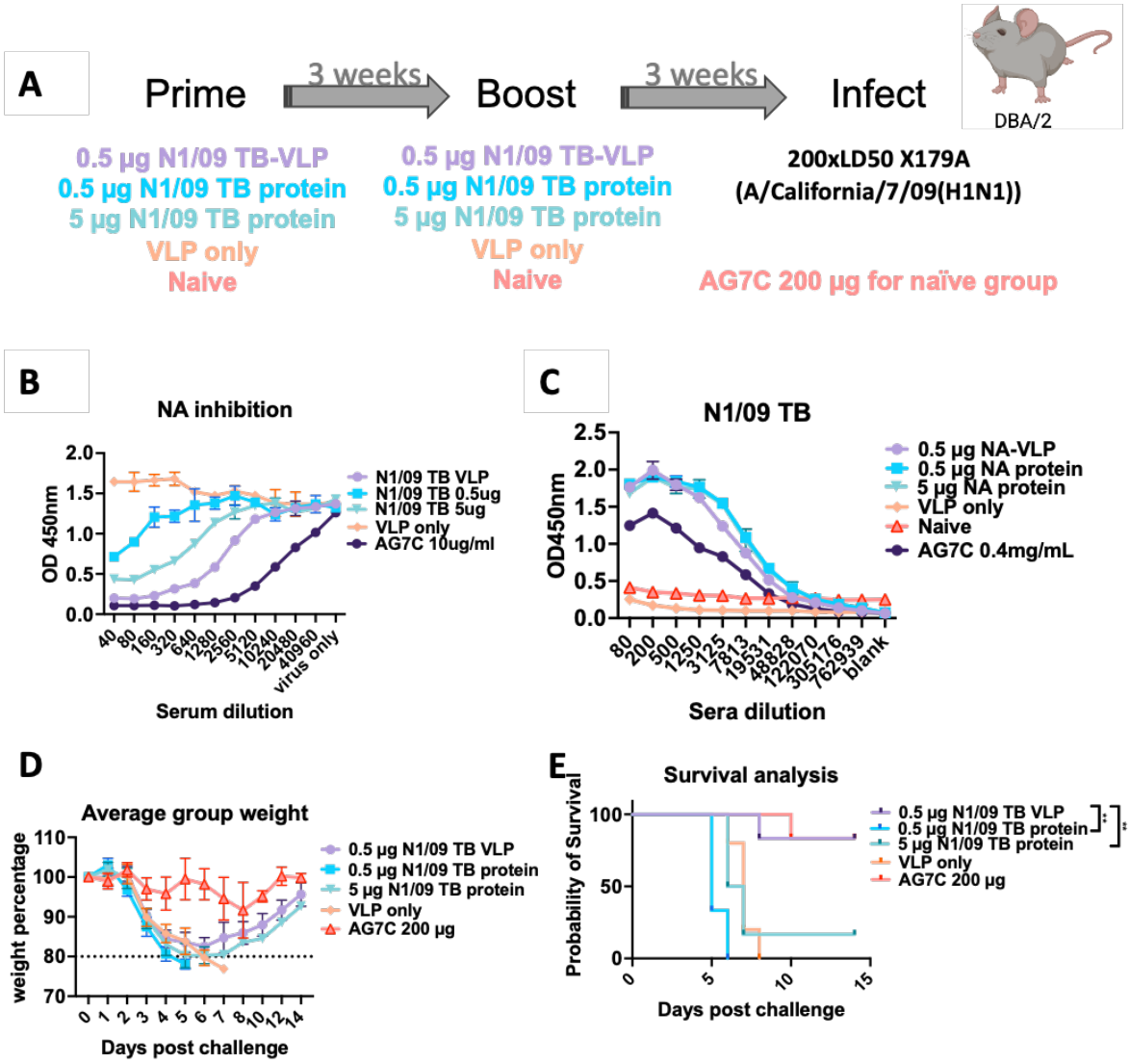

Figure 4.2 **Vaccination with NA-VLP protected mice from high-dose homologous viral challenge (X179A)**
A) Mice were vaccinated in a prime-boost regimen (IM, adjuvanted with AddaVax) with NA-VLP, NA protein from A/California/7/2009 (H1N1) , and challenged with 200xLD$_{50}$ X179A.
B) Three weeks post the boost, sera were collected and antibody inhibition against X179A virus was assessed via ELLA. Pooled sera were used for this result. Sera from the mice immunised with 0.5ug N1/09-TB-VLP titrate ~16x further than mice immunised with 0.5ug of N1/09-TB.
C) Antibody binding to recombinant N1/09 TB pre-challenge sera was assessed using ELISA. All three groups immunised with NA titrate similarly.

D,E) Three weeks post the boost, mice were challenged intranasally with X179A weight change (D) and mortality (E) were assessed over a 14-day time course. $n = 6$ mice/group and the experiment was repeated twice. The group immunised with 0.5ug N1/09-TB-VLP are protected compared to other groupPairwise comparisons were calculated by Gehan-Breslow-Wilcoxon test. Statistical significance is indicated by *($p < 0.05$), **($p < 0.01$), ***($p < 0.001$), ****($p < 0.0001$).

After characterising N1 NA and N1 NA-VLP, our next objective was to evaluate their ability to induce protective antibody responses and provide protection against a lethal viral challenge in a mouse model. To this end, DBA/2 mice were vaccinated with 0.5 µg of N1/09 TB VLP, 0.5 µg of N1/09 TB, or 5 µg of N1/09 TB, all formulated with AddaVax as an adjuvant, using a prime-boost regimen (Fig. 4.2A). Following vaccination, all mice were challenged with 200 LD50 of X-179A (A/California/7/2009 H1N1), a lethal dose significantly higher than those commonly reported in challenge studies to date (Table 1.7). A positive control group received 200 µg of AG7C 24 hours prior to the challenge.

Three weeks post-boost, sera were collected from mice via tail bleeding, and antibody responses were assessed using ELLA and ELISA (Fig. 4.2B, C). Neuraminidase inhibition (NAI) antibody titres against the matched X-179A virus were evaluated via ELLA with pooled sera. Both free NA and NA-VLP conjugates elicited robust antibody responses. A dose-sparing effect was observed between the 0.5 µg and 5 µg doses of free N1/09 TB, while mice vaccinated with 0.5 µg of NA-VLP exhibited the highest levels of antibody inhibition among all groups (Fig. 4.2B).

Specific binding antibodies were measured using ELISA with N1/09 TB-coated plates. All experimental groups showed comparable levels of binding to recombinant N1/09 TB (Fig. 4.2C). Among the groups, the 0.5 µg NA-VLP formulation elicited the strongest NAI antibody response, despite similar overall levels of NA-specific binding antibodies across all vaccinated groups.

After evaluating NA-specific and inhibiting antibody levels, we assessed protective efficacy. Remarkably, only the 0.5 µg NA-VLP group and the AG7C (positive monoclonal antibody control) group survived the high-lethal-dose viral challenge. All other experimental groups experienced significant weight loss (Fig. 4.2D, E). Even the higher dose of 5 µg of NA failed to protect mice from the lethal challenge.

To further investigate the impact of antigen conformation on antibody response and protective efficacy, we tested three versions of recombinant N1/09: N1/09 TB, N1/09 VASP, and N1/09 TetDminus, as detailed in Fig. 3.2. N1/09 TetDminus exhibited reduced antibody binding, suggesting incomplete folding or impaired tetrameric conformation due to the absence of a tetramerisation domain. To confirm these findings, we performed ELISA binding assays with a panel of monoclonal antibodies (Fig. 4.1). Previously published mAbs AG7C, AF9C, and Z2B3 (Rijal et al., 2020) specifically recognised N1 neuraminidases and bound to N1/09 VASP and TB forms but exhibited low or no binding to N1/09 TetDminus. These mAbs have been identified to bind to single NA protomers (personal communication with Yan Wu).

Additionally, we compared the binding of N1/09 VASP and TB forms to mAb CD6, which targets the lateral surface spanning two protomers (Wan et al., 2015). CD6 binding analysis revealed epitope differences between N1/09 TB and N1/09 VASP. This indicates that N1/09 VASP adopts an "open conformation," which could potentially be altered to a "closed

conformation" by modifying the tetramerisation domain or specific interface amino acids (Ellis et al., 2022).

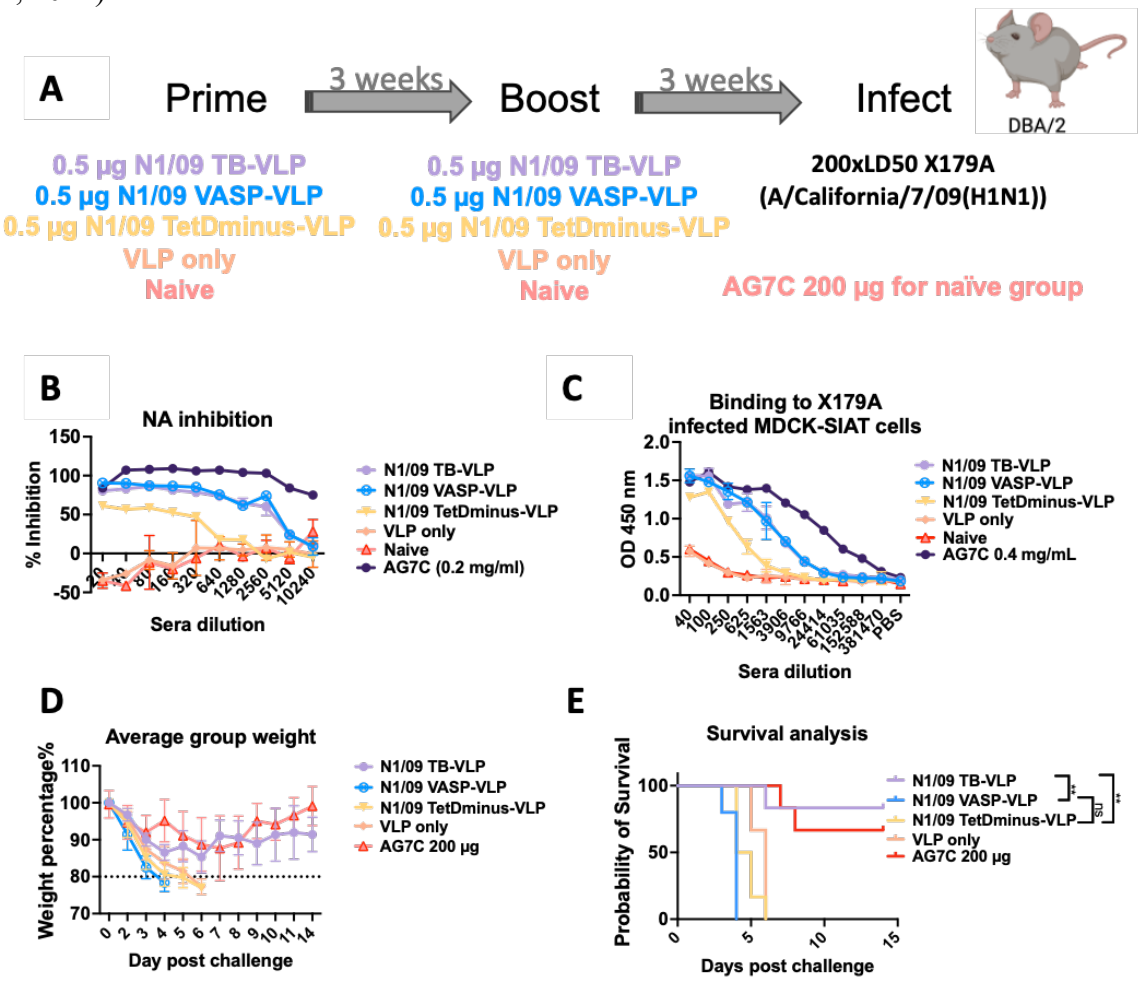

Figure 4.3 **Vaccination with a tetramer formed with TB was more effective than tetramers formed with VASP tetramerisation domain (X179A).**
A) Mice were vaccinated in a prime-boost regimen (IM, adjuvanted with AddaVax) with VASP NA-VLP, TB NA-VLP, and NA TetDminus-VLP from A/California/7/2009 (H1N1) , and challenged with 200 LD_{50} X179A.
B) Three weeks post the boost, sera were collected and antibody inhibition against X179A virus were assessed via ELLA. N1/09-TB-VLP and N1/09-VASP-VLP induced similar titres of NA inhibiting antibody.
C) Antibody binding to X179A infected MDCK-SIAT cells pre-challenge sera was assessed using ELISA. N1/09-TB-VLP and N1/09-VASP-VLP induced similar titres of NA binding antibody.
D,E) Three weeks post the boost, mice were challenged intranasally with X179A weight change (D) and mortality (E) were assessed over a 14-day time course. Vaccination N1/09-TB-VLP vaccination provided protection whereas vaccination with N1/09-VASP-VLP did not protect. $n = 6$ mice/group. Pairwise comparisons were calculated by Gehan-Breslow-Wilcoxon test. Statistical significance is indicated by *($p < 0.05$), **($p < 0.01$), ***($p < 0.001$), ****($p < 0.0001$).

The N1/09 TetDminus VLP group showed reduced levels of NA-specific and NA inhibition antibodies, possibly due to the loss of conformational epitopes. Conversely, mice immunized with tetrameric N1/09 TB and N1/09 VASP showed comparable levels of NA-related antibodies (Fig. 4.3 B, C). After challenge with a high lethal dose of X179A virus (200 LD_{50}),

survival was observed only in the N1/09 TB VLP group and AG7C group. In survivied groups, around 10-15% weight loss was noted as well(Fig. 4.3 D, E). To our surprise, the N1/09 VASP group demonstrated the same level of NAI antibodies as the protected group; however, none of the mice survived. Gao et al. reported a similar phenomenon where recombinant NA, employing VASP as the tetramerization domain, failed to protect mice compared to TB NA (J. Gao et al., 2021). Interestingly, extending the stem length restored the protective efficacy to the same level. We hypothesize that the shorter stem may result in an "open conformation" of NA (Ellis et al., 2022), exposing internal interfaces and potentially leading to ineffective antibody responses. In the H1N1 model, no direct correlation was observed between protection and NA inhibition titers. This suggests that evaluating multiple factors beyond NAI titers is essential to accurately assess the potential of an antigen to provide adequate vaccine protection.

These findings highlight the significance of structural integrity and closed conformation in recombinant NA as an advantageous vaccine antigen for pandemic N1 strains. Research has demonstrated that monomeric NA failed to confer protection in mice, underscoring the essential role of correct folding in generating adequate immune protection as an antigen (McMahon et al., 2020).

4.3 NA protection in 1968 H3N2 (X31) challenge model

H1N1 and H3N2 viruses are predominant in seasonal influenza infections. H3N2 first emerged in humans during the 1968 Hong Kong flu pandemic and has continued to circulate since then. Research into N2-based vaccinations could significantly enhance influenza pandemic preparedness and control efforts.

N2 X31 TB and N2 X31 TetDminus gene constructs were expressed as stable tetrameric and monomeric NA (Fig. 3.3). Similar to observations with N1/09, both N2 NAs efficiently assembled into mi3 particles while maintaining their enzymatic activity (Fig. 4.4A). The antibody binding capacity of the decorated nanoparticles remained unchanged, although the monomeric N2 X31 TetDminus showed a reduction in binding to Z2B3 and AQ2D (Fig. 4.4B). Detailed titration of N2 NA to VLP at various ratios is provided in Appendix 6.

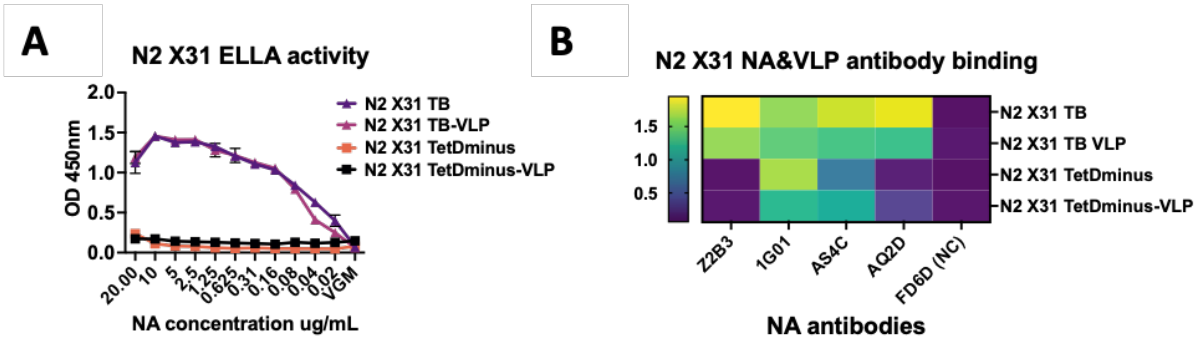

Figure 4.4 **SpyCatcher003-mi3 particles efficiently displayed tetrameric or monomeric N2 X31 NA preserving its enzymatic activity and antigenicity**
A) The formation of NA-VLP didn't affect the enzymatic activity of N2 X31 TB and N2 X31 TetDminus.
B) Antibody binding affinity to NA and NA-VLP in N2 X31 NA was consistent. N2 X31 TB bound to all 4 antibodies whereas Z2B3 and AQ2D lost most of binding to N2 X31 TetDminus.

To investigate the immune response and protective efficacy of N2 NA and N2 NA-VLP conjugates, BALB/c mice were immunized in a prime-boost regimen. Each mouse received either 0.5 µg of free N2 X31 TB or 0.5 µg of N2 X31 TB VLP via intramuscular injection with AddaVax as the adjuvant. Three weeks following the boost dose, sera were collected from the mice via tail-bleeding. 24 hours after sera collection, mice were intranasally infected with 10 LD_{50} of X31 virus, and their survival was monitored thereafter (Fig. 4.5A).
Similar to the previous 2009 H1N1 model, serological tests were conducted using ELLA and ELISA to assess the NAI titre and NA specific antibody levels. Both the free NA and NA-VLP groups showed robust antibody responses against the A/Hong Kong/1/1968 H3N2 (X31) virus. There was no significant difference observed between the two groups (Fig. 4.5 B, C).

Weight change (Fig. 4.5D) and mortality (Fig. 4.5E) were monitored over a 14-day period. Surprisingly, both free NA and NA-VLP immunized mice survived the lethal virus challenge despite experiencing significant weight loss. Notably, N2 X31 TB as a free antigen elicited a robust antibody response comparable to N2 X31 TB VLP, and both formulations provided protection against the lethal virus challenge.

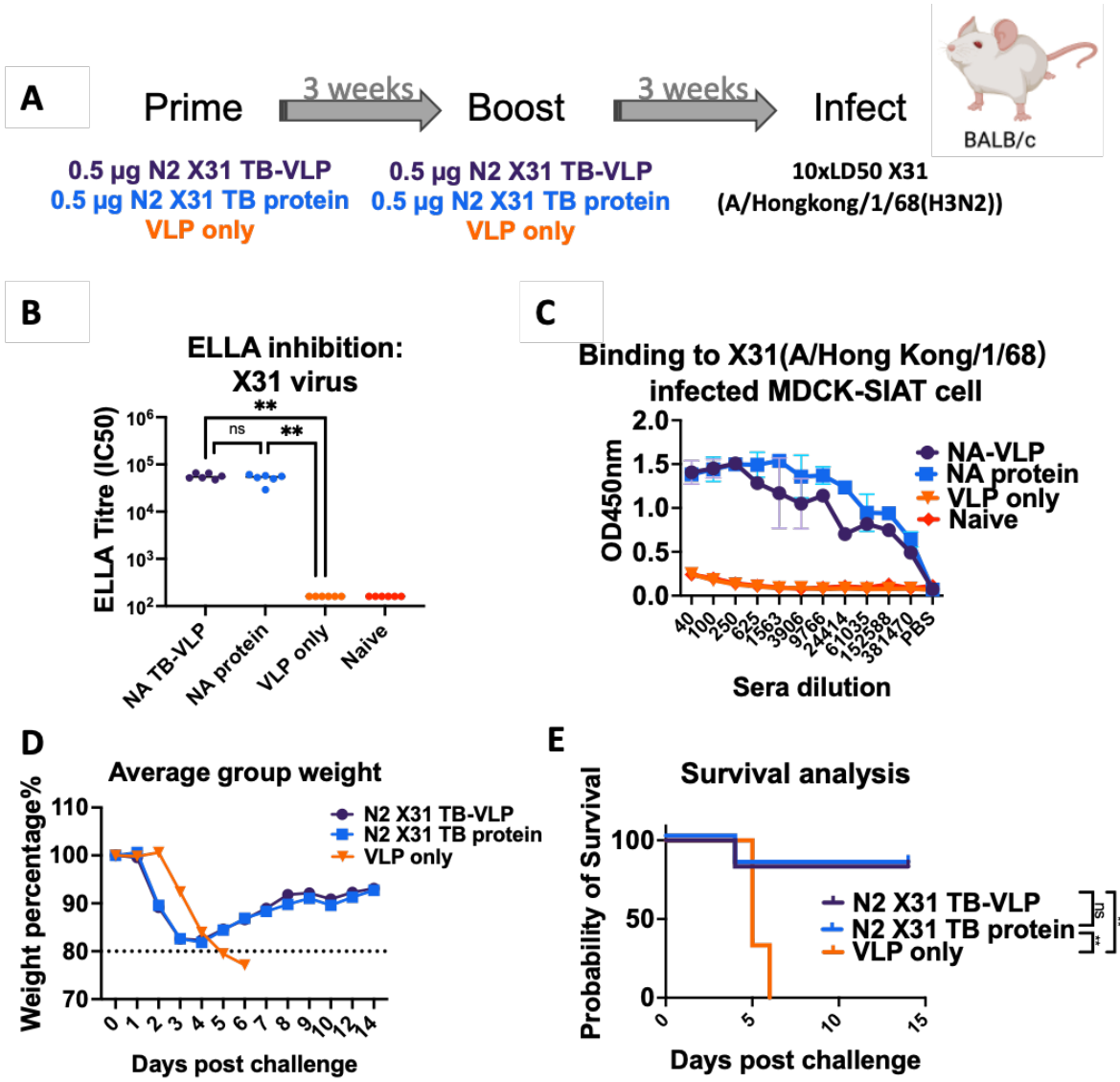

Figure 4.5 **Low dose of N2 X31 TB NA-VLP and NA alone both protected mice from lethal dose homologous challenge (X31)**

A) Mice were vaccinated in a prime-boost regimen (IM, adjuvanted with AddaVax) with NA-VLP, NA protein from A/Hong Kong/1/1968 (H3N2) , and challenged with 10 LD_{50} X31 virus.

B) Three weeks post the boost, sera were collected and antibody inhibition against X31 virus were assessed via ELLA. The N2 X31 TB tetramer and NA-VLP induced similar titres of N2 inhibiting antibody. Pairwise comparisons were analyzed with the Mann-Whitney U test.

C) Binding to X31 infected MDCK-SIAT cells pre-challenge sera was assessed using ELISA. The N2 X31 TB and NA-VLP group induced similar titres of N2 binding antibody.

D,E) Three weeks post the boost, mice were challenged intranasally with X31, weight change (D) and mortality (E) were assessed over a 14-day time course. Both vaccines containing tetramerised N2 protected mice from challeng $n = 6$ mice/group. Pairwise comparisons were calculated by Gehan-Breslow-Wilcoxon test. Statistical significance is indicated by *($p < 0.05$), **($p < 0.01$), ***($p < 0.001$), ****($p < 0.0001$).

In a similar experimental setup, we compared the immune response and protective efficacy of 0.5 µg of N2 X31 TB-VLP and 0.5 µg of N2 X31 TetDminus-VLP (Fig. 4.6A). Both

experimental groups immunized with N2 X31 TB-VLP and N2 X31 TetDminus-VLP developed high titres of NAI antibodies and NA-specific antibodies (Fig. 4.6 B, C). Compared to the N1/09 model (Fig. 4.3 B, C), the recombinant N2 X31 NA appeared to induce higher NA inhibition titres in both the monomeric NA-VLP and antigen-only groups. This sera observation correlated with enhanced protective efficacy in these groups.

Following challenge with 10 LD_{50} of X31 virus, mice vaccinated with 0.5 μg of N2 X31 TB VLP and N2 X31 TetDminus VLP both survived, albeit with significant weight loss (Fig. 4.6 D, E). This marked the first instance where mice survived a lethal virus challenge following vaccination with a partially folded antigen-decorated VLP. While this observation confirmed the potential of vaccine design with monomeric NA, the optimal approach remains pursuing correctly folded tetrameric NA. High neuraminidase inhibition (NAI) titres, elicited by both monomeric and tetrameric N2 NA-VLPs, were associated with protection in BALB/c mice, demonstrating the predictive value of NAI titres in the N2 X31 model.

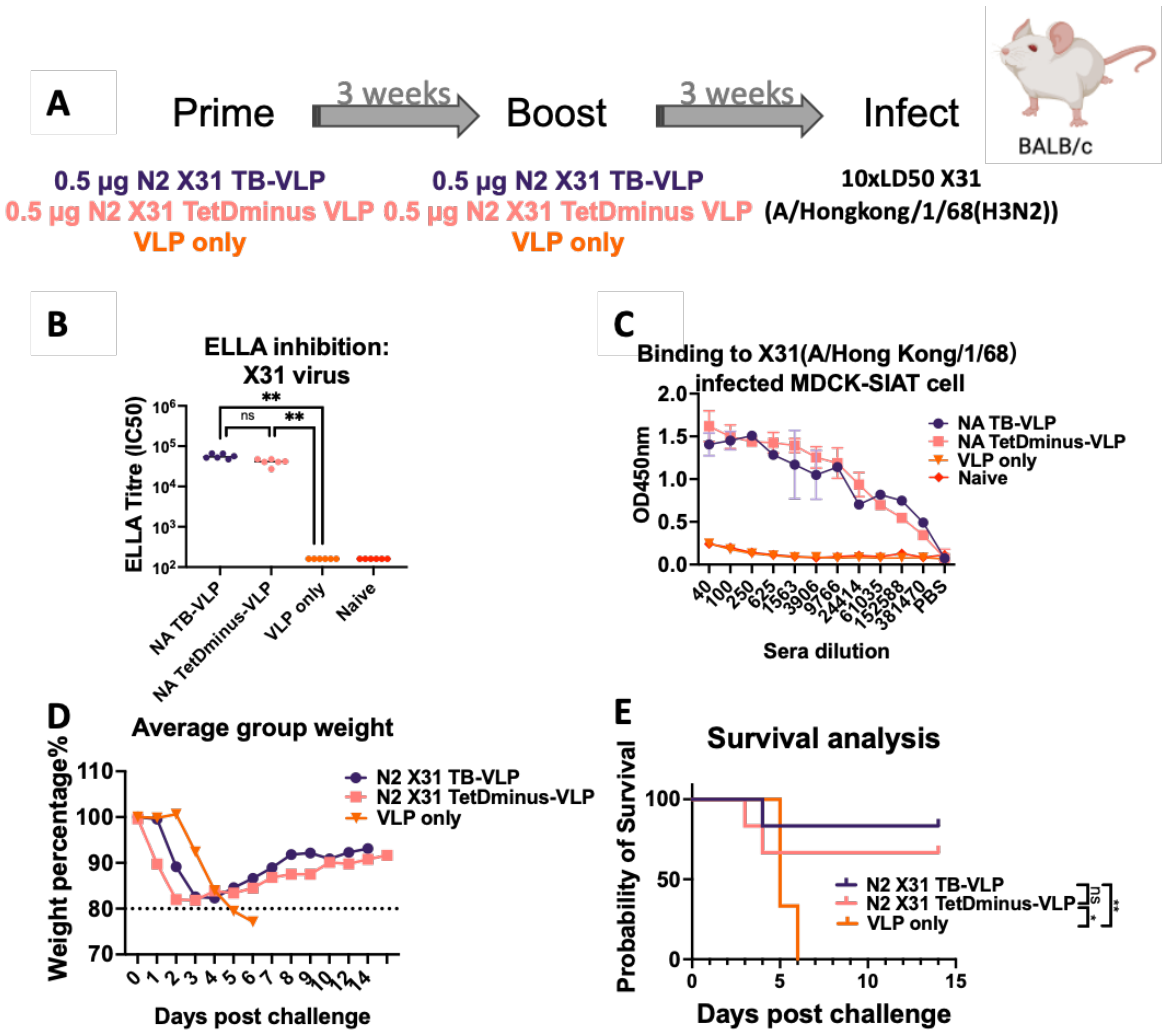

Figure 4.6 **Low dose of N2 X31 TB and TetDminus NA-VLP both protected mice from lethal dose X31 challenge (X31)**

Data partially overlaps with Fig. 4.5; both figures represent different subsets from the same experiment.

A) Mice were vaccinated in a prime-boost regimen (IM, adjuvanted with AddaVax) with N2 X31 TB and TetDminus NA-VLPs A/Hong Kong/1/1968 (H3N2) , and challenged with 10 LD_{50} X31 .

B) Three weeks post the boost, serum was collected and antibody inhibition against X31 virus were assessed via ELLA. Pairwise comparisons were analyzed with the Mann-Whitney U test.

C) Antibody binding to X31 infected MDCK-SIAT cells pre-challenge sera was assessed using ELISA.

D,E) Three weeks post the boost, mice were challenged intranasally with a lethal dose of X31, weight change (D) and mortality (E) were assessed over a 14-day time course. $n = 6$ mice/group. Pairwise comparisons were calculated by Gehan-Breslow-Wilcoxon test. Statistical significance is indicated by *($p < 0.05$), **($p < 0.01$), ***($p < 0.001$), ****($p < 0.0001$).

4.4 NA protection in 1934 H1N1 (PR8) challenge model

We also evaluated the NA-VLP in 1934 H1N1 model using N1 PR8 TB and N1 PR8 TetDminus, expressed as tetramers and dimers respectively (Fig. 3.3). Both recombinant N1 PR8 NAs were conjugated to mi3 particles and retained comparable activity in cleaving terminal sialic acid from fetuin (Fig. 4.7A). However, compared to N1 PR8 TB, N1 PR8 TetDminus lost binding epitopes for AF9C, Z2B3, and 1G01, suggesting compromised structural integrity due to incomplete tetramerization (Fig. 4.7B).

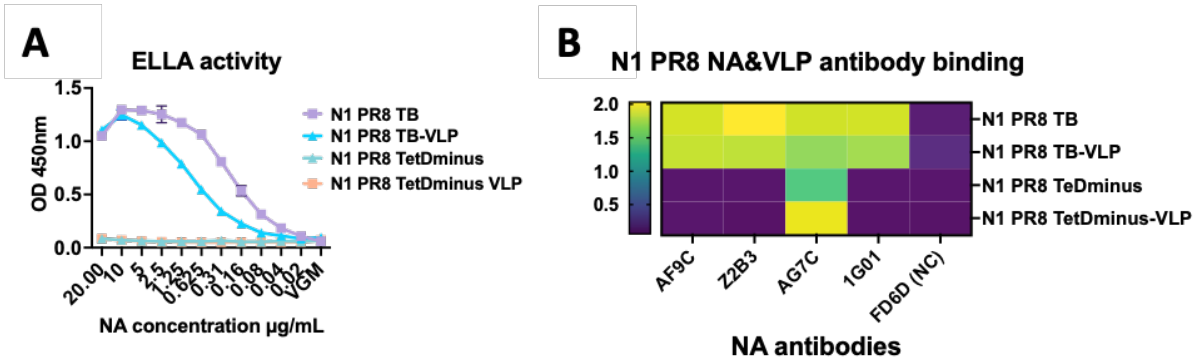

Figure 4.7 **SpyCatcher003-mi3 particles efficiently displayed tetrameric or monomeric N1 PR8 NA preserving its enzymatic activity and antigenicity**
A) ELLA activity of N1 PR8 vaccine preparations. ELLA activity of N1 PR8 TB is retained when the NA is assembled onto the mi3 particle. The N1 PR8 TetDminus and assembled VLP showed no ELLA activity.
B) Antibody binding to PR8 vaccine preparations. The epitopes for AF9C, Z2B3 and 1G01 were lost on N1 PR8 TetDminus.

BALB/c mice were vaccinated with 0.5 µg of N1 PR8 TB-VLP, 0.5 µg of N1 PR8 TB, or VLP alone in a prime-boost regimen with a 3-week interval. All vaccinations were administered via intramuscular injection with AddaVax as the adjuvant. Three weeks post the boost dose, mice were intranasally challenged with 1000 LD_{50} of PR8 virus. A positive control group received 200 µg of AG7C 24 hours prior to the challenge (Fig. 4.8A).

The NA inhibition antibody responses against PR8 virus, measured by ELLA, are presented in Fig. 4.8B. N1 PR8 TB-VLP exhibited a significantly higher NAI titre compared to the NA alone group. Additionally, the antibody binding levels to PR8-infected MDCK-SIAT cells were similar between the NA and NA-VLP groups (Fig. 4.8C). Consistent with our observations in the 2009 H1N1 model, NA-VLP tended to induce higher NAI titres while maintaining a similar level of total NA-specific antibodies.

After challenge with 1000 LD_{50} of PR8 virus, all mice in the N1 PR8 TB group and AG7C group survived without weight loss (Fig. 4.8D, E). However, only 2 out of 6 mice in the NA TB group survived the virus challenge, and these surviving mice experienced approximately 15-20% weight loss during the infection (Fig. 4.8D, E). Interestingly, when correlating individual NA inhibition (NAI) titres with survival data, it was observed that the highest NAI titre in the N1 PR8 TB group did not protect mice from death or weight loss, despite being comparable to the NAI titres in the NA-VLP group (Appendix 7).

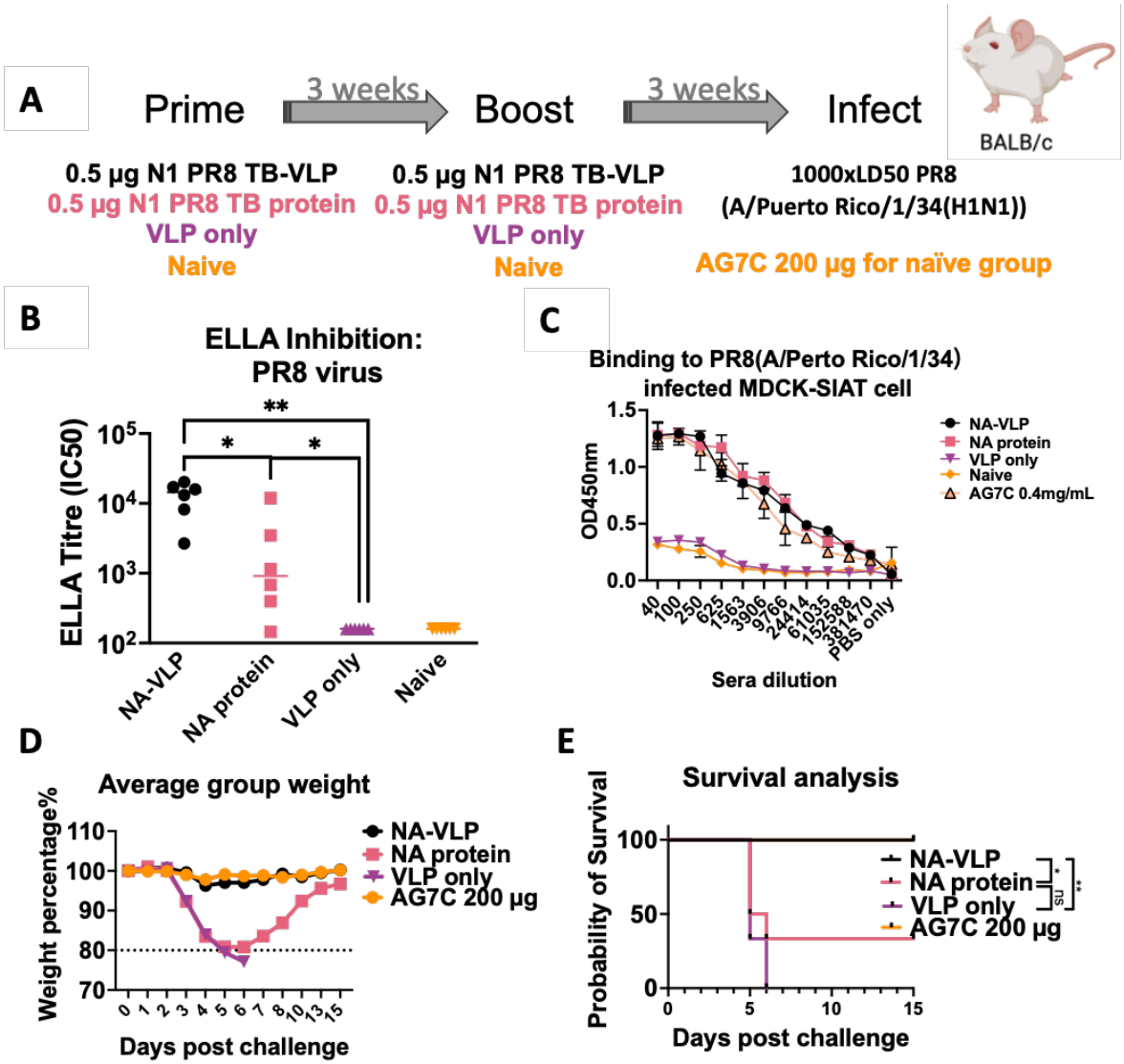

Figure 4.8 **Vaccination with N1 PR8 TB NA-VLP protected mice from high-dose homologous viral challenge (PR8)**

A) Mice were vaccinated in a prime-boost regimen (IM, adjuvanted with AddaVax) with NA-VLP, NA protein from A/Puerto Rico/8/1934 (H1N1) , and challenged with 1000 LD_{50} PR8 virus.

B) Three weeks post the boost, sera were collected and antibody inhibition against PR8 virus was assessed via ELLA. The N1 PR8 TB vaccination generated consistently higher titres in ELLA compared to vaccination with the same dose of protein not mounted on the VLP. Pairwise comparisons were analyzed with the Mann-Whitney U test.

C) Antibody binding to PR8 infected MDCK-SIAT1 cells. Pre-challenge sera were assessed using ELISA. Titres of binding antibody were similar after vaccination with tetramerised NA regardless of association with the VLP.

D,E) Three weeks post the boost, mice were challenged intranasally with a lethal dose of PR8, weight change (D) and mortality (E) were assessed over a 14-day time course. Full protection was seen only after vaccination with the N1 PR8 TB NA-VLP. $n = 6$ mice/group. Pairwise comparisons were calculated by Gehan-Breslow-Wilcoxon test. Statistical significance is indicated by *($p < 0.05$), **($p < 0.01$), ***($p < 0.001$), ****($p < 0.0001$).

A comparative study was conducted between 0.5 µg of N1 PR8 TB-VLP and 0.5 µg of N1 PR8 TetDminus-VLP at the same time. Both monomeric/dimeric N1 PR8 TetDminus-VLP and tetrameric N1 PR8 TB -VLP induced high NA inhibition (NAI) titres in BALB/c mice (Fig. 4.9B). Additionally, the levels of NA-specific binding antibodies were comparable between these two groups (Fig. 4.9C).

Upon challenge with a high lethal dose of 1000 LD_{50} of PR8 virus, 0.5 µg N1 PR8 TB-VLP provided complete protection to mice against death and weight loss (Fig. 4.9 D, E). In contrast, in the N1 PR8 TetDminus-VLP group, only two mice narrowly escaped exceeding 20% weight loss threshold and ultimately survived (Fig. 4.9 D, E). However, when analysing individual data, no correlation was found between NA inhibition (NAI) titres and protection among the mice (see Appendix 7).

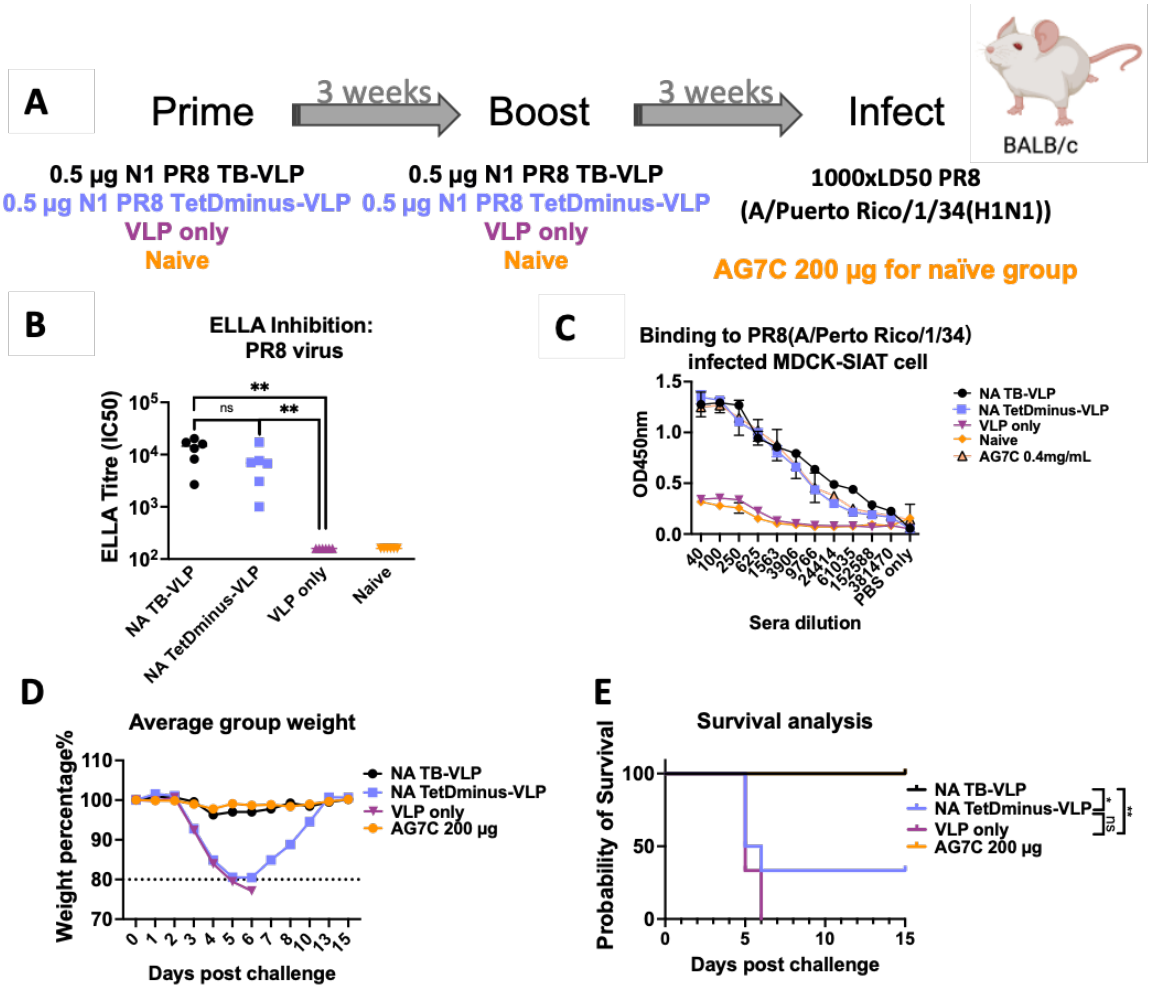

Figure 4.9 **Vaccination with tetrameric N1 PR8 NA decorated VLP protected mice from homologous viral challenge (PR8)**
Data partially overlaps with Fig. 4.8; both figures represent different subsets from the same experiment.

A) Mice were vaccinated in a prime-boost regimen (IM, adjuvanted with AddaVax) with NA-VLP, NA TetDminus-VLP from A/Puerto Rico/8/1934 (H1N1) , and challenged with 1000 LD_{50} PR8 virus.
B) Three weeks post the boost, sera were collected and antibody inhibition against PR8 virus was assessed via ELLA. The N1 PR8 TB vaccination and the N1 PR8 TetDminus generated comparable titres in ELLA. Pairwise comparisons were analyzed with the Mann-Whitney U test.
C) Antibody binding to PR8 infected MDCK-SIAT1 cells pre-challenge was assessed using ELISA. Titres of binding antibody were similar after vaccination with both tetramerised NA-VLP and NA-VLP without tetramerisation domain.
D,E) Three weeks post the boost, mice were challenged intranasally with a lethal dose of PR8, weight change (D) and mortality (E) were assessed over a 14-day time course. Full protection was seen only after vaccination with the N1 PR8 TB NA-VLP. $n = 6$ mice/group. Pairwise comparisons were calculated by Gehan-Breslow-Wilcoxon test. Statistical significance is indicated by *($p < 0.05$), **($p < 0.01$), ***($p < 0.001$), ****($p < 0.0001$).

Expanding on our current findings, we conducted an experiment using an extremely low dose of NA-VLP in the PR8 model (Fig. 4.10A). Surprisingly, 0.1 µg of N1 PR8 TB-VLP induced a comparable NA inhibition (NAI) titre to the 0.5 µg group (Fig. 4.10B) and resulted in similar protection outcomes, with a maximum weight loss of 10% (Fig. 4.10 C, D).

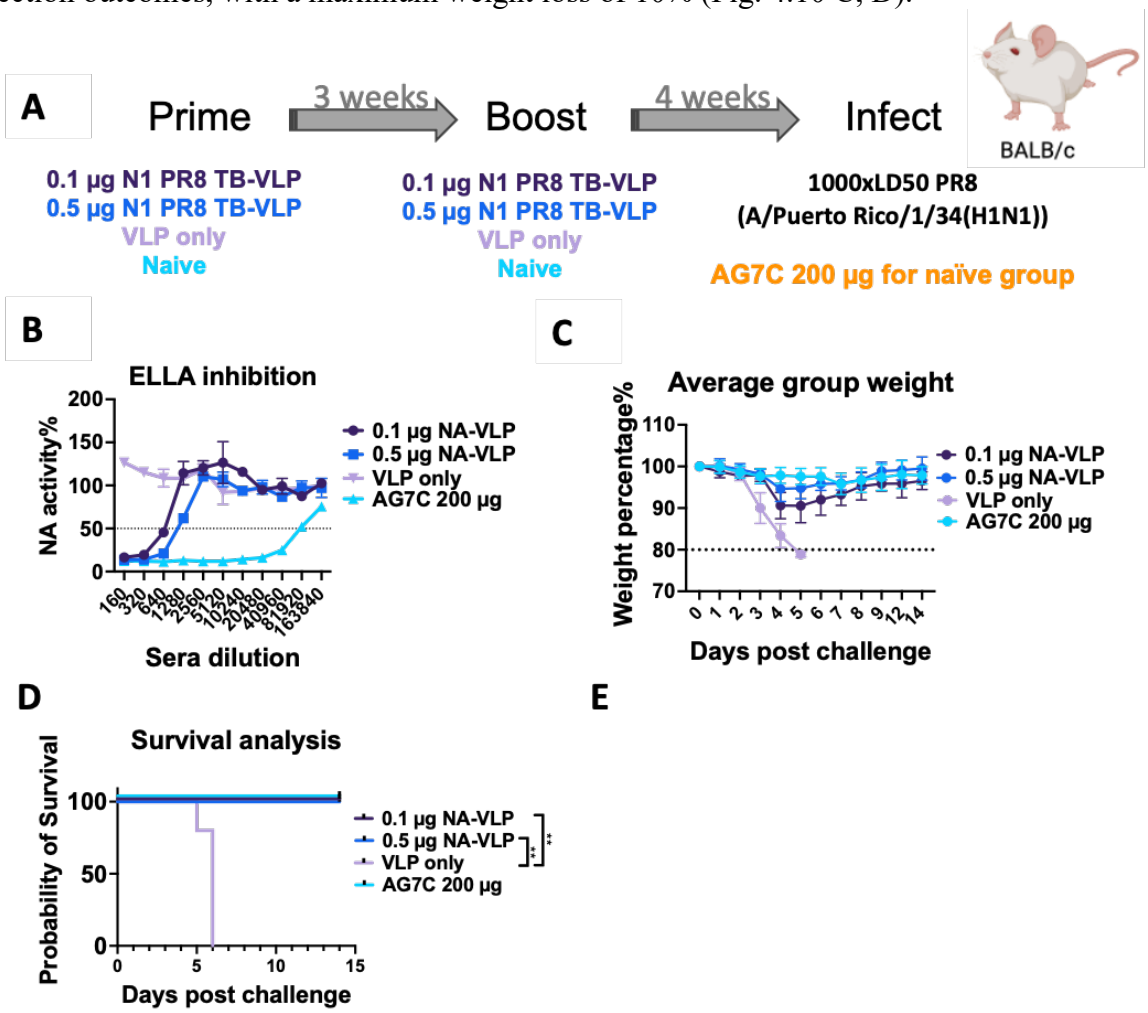

Figure 4.10 **Low dose of NA-VLP vaccination protect mice from homologous PR8 challenge**

A) Mice were vaccinated in a prime-boost regimen (IM, adjuvanted with AddaVax) with 0.1 µg NA-VLP, 0.5 µg NA-VLP from A/Puerto Rico/8/1934 (H1N1) , and challenged with 1000 LD_{50} PR8 virus. Pooled sera used for the ELLA result.

B) Four weeks post the boost, sera were collected and antibody inhibition against PR8 virus were assessed via ELLA. Lower dose NA-VLP generated similar ELLA titres to 0.5 µg NA-VLP group.

C,D) Four weeks post the boost, mice were challenged intranasally with a lethal dose of PR8, weight change (C) and mortality (D) were assessed over a 14-day time course. $n = 6$ mice/group. One of the mice in empty VLP group died 2 weeks after the boost dose for unknown reason. Pairwise comparisons were calculated by Gehan-Breslow-Wilcoxon test. Statistical significance is indicated by *($p < 0.05$), **($p < 0.01$), ***($p < 0.001$), ****($p < 0.0001$).

Based on our N1 PR8 vaccination results, we were able to infer several key findings regarding vaccine efficacy:

- The mi3 platform effectively enhanced NA inhibition (NAI) titres even at low vaccine doses, thereby enhancing protective efficacy.

- Structural integrity and proper NA head conformation would be crucial factors influencing protection.

- Combining points 1 and 2, an extremely low dose of NA-VLP could be sufficient to elicit significant protection against high lethal dose virus challenges. This potential efficacy could lead to a reduction in vaccine costs by 5-10 fold.

- These insights highlighted the importance of the mi3 platform in boosting immune responses and highlight the critical role of NA structure in vaccine effectiveness, suggesting promising avenues for optimizing influenza vaccine design.

4.5 N1 MS NA-VLP as potential vaccine for H5N1

H5N1 is among the influenza viruses that contribute to avian influenza, often associated with cases of Highly Pathogenic Avian Influenza (HPAI) annually. Since 2022, there has been a growing number of reports documenting fatalities in mammals caused by H5N1 viruses, affecting both terrestrial and aquatic mammals (*Influenza: A(H5N1)*, updated on 16 May 2024).

H5N1 poses a significant potential pandemic threat; however, comprehensive studies on the neuraminidase of H5N1 have been lacking. To address this gap, we selected the neuraminidase from the influenza strain A/mute swan/England/053054/2021, isolated from infected mute swans, for characterization and immunization studies.

The tetrameric N1 MS TB was successfully expressed in ExpiCHO cells with exceptional enzymatic activity (Fig. 3.5D).The vaccine was tested for protection against pdmH1N1/2009 in DBA/2 mice. For human and avian strains, DBA/2 mice are more susceptible and exhibit more severe symptoms. DBA/2 mice were immunized in a prime-boost regimen with a 3-week interval. The experimental groups were structured as follows: Group 1 received prime and boost doses of 0.5 µg of N1/09 TB-VLP; Group 2 received prime and boost doses of 0.5 µg of N1 MS TB-VLP; Group 3 received a prime dose of 0.5 µg of N1/09 TB-VLP followed by a boost dose of 0.5 µg of N1 MS TB-VLP, simulating human populations with immunity from the 2009 pandemic. All immunizations were administered via intramuscular injection using AddaVax as the adjuvant. Three weeks post-boost, mice were challenged with 200 LD_{50} of X-179A virus and monitored over a 14-day period (Fig. 4.11A).

The NAI titres against N1/2009 (X-179A virus) were relatively lower in the N1 MS TB VLP group compared to the N1/09 vaccine group (Fig. 4.11 B, C). While negative control sera generated high background signals in the ELLA assay (as previously reported), these nonspecific reactions diminished with serial dilution.

Despite a notable antigenic difference of 33 amino acids in the head region between N1/09 and N1 MS TB, two doses of N1 MS TB vaccination successfully protected mice from a high lethal dose challenge with X179A virus, albeit with relatively low cross-inhibition levels (Fig. 4.11 D, E). The observed weight loss effects were unexpected; both N1 MS TB-VLP and the mixed dose group exhibited moderate weight loss effects, yet all groups survived the virus challenge (Fig. 4.11 D, E). However, based on the protective efficacy of N1 MS TB against X179A virus challenge, we can infer some epitope similarity between these two antigens. Therefore, vaccination with one antigen could contribute to immunity against the other, suggesting potential cross-protection benefits.

In a similar comparison to N1 PR8 TB-VLP, vaccination with two doses of N1 MS TB-VLP was evaluated against a challenge with 1000 LD_{50} of PR8 virus (Fig. 4.11A). Despite a notable difference of 44 amino acids between the NA head sequences, the NA inhibition titres against PR8 virus in the N1 MS TB-VLP group were undetectable at a 1:160 dilution (Fig. 4.11B). Following the PR8 virus challenge, only 2 out of 6 mice in the N1 MS TB-VLP group survived, and these survivors experienced significant weight loss during the observation period (Fig. 4.12C, D).

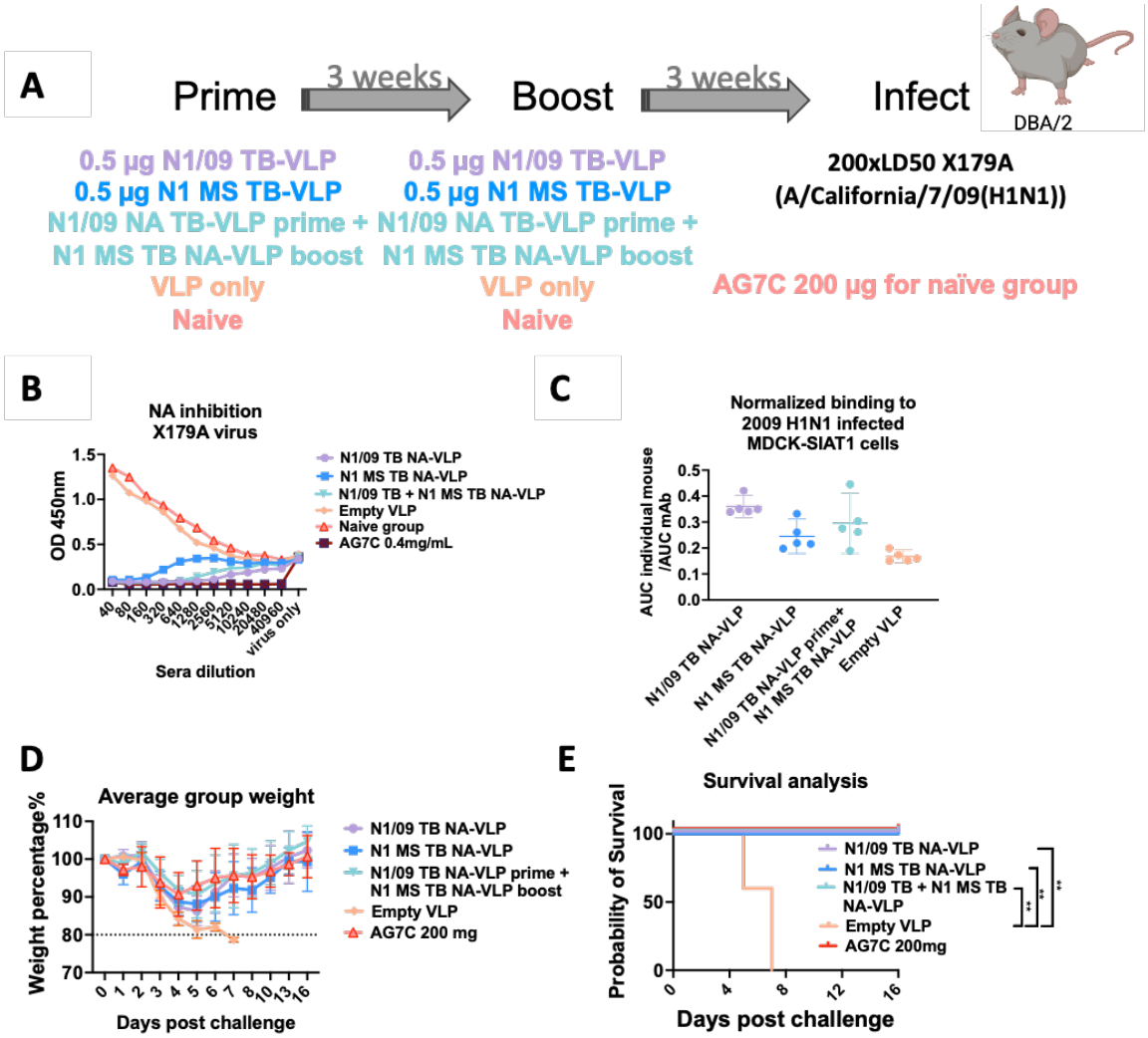

Figure 4.11 **Vaccination with N1/09 TB-VLP and N1 Ms TB -VLP protected mice from high-dose viral challenge with H1N1 2009 virus (X179A)**

A) Mice were vaccinated in a prime-boost regimen (IM, adjuvanted with AddaVax) with NA-VLP as presented, and challenged with 200 LD_{50} X179A. Pooled sera used for the ELLA assay.

B) Three weeks after the boost, serum was collected and antibody inhibition against X179A virus was assessed via ELLA assay. Vaccination twice with the N1 MS TB (from H5N1 2021) induced antibody that cross inhibited the N1/09 NA, although at lower titre than homologous vaccination.

C) Sera binding to X179A infected MDCK-SIAT1 cells pre-challenge was assessed using ELISA.

D,E) Three weeks post the boost, mice were challenged intranasally with X179A, weight change (D) and mortality (E) were assessed over a 16-day time course. $n = 6$ mice/group. Vaccination with N1 MS TB from the avian H5N1 2021 protected mice from challenge with 2009 H1N1 seasonal influenza. Pairwise comparisons were calculated by Gehan-Breslow-Wilcoxon test. Statistical significance is indicated by *($p < 0.05$), **($p < 0.01$), ***($p < 0.001$), ****($p < 0.0001$).

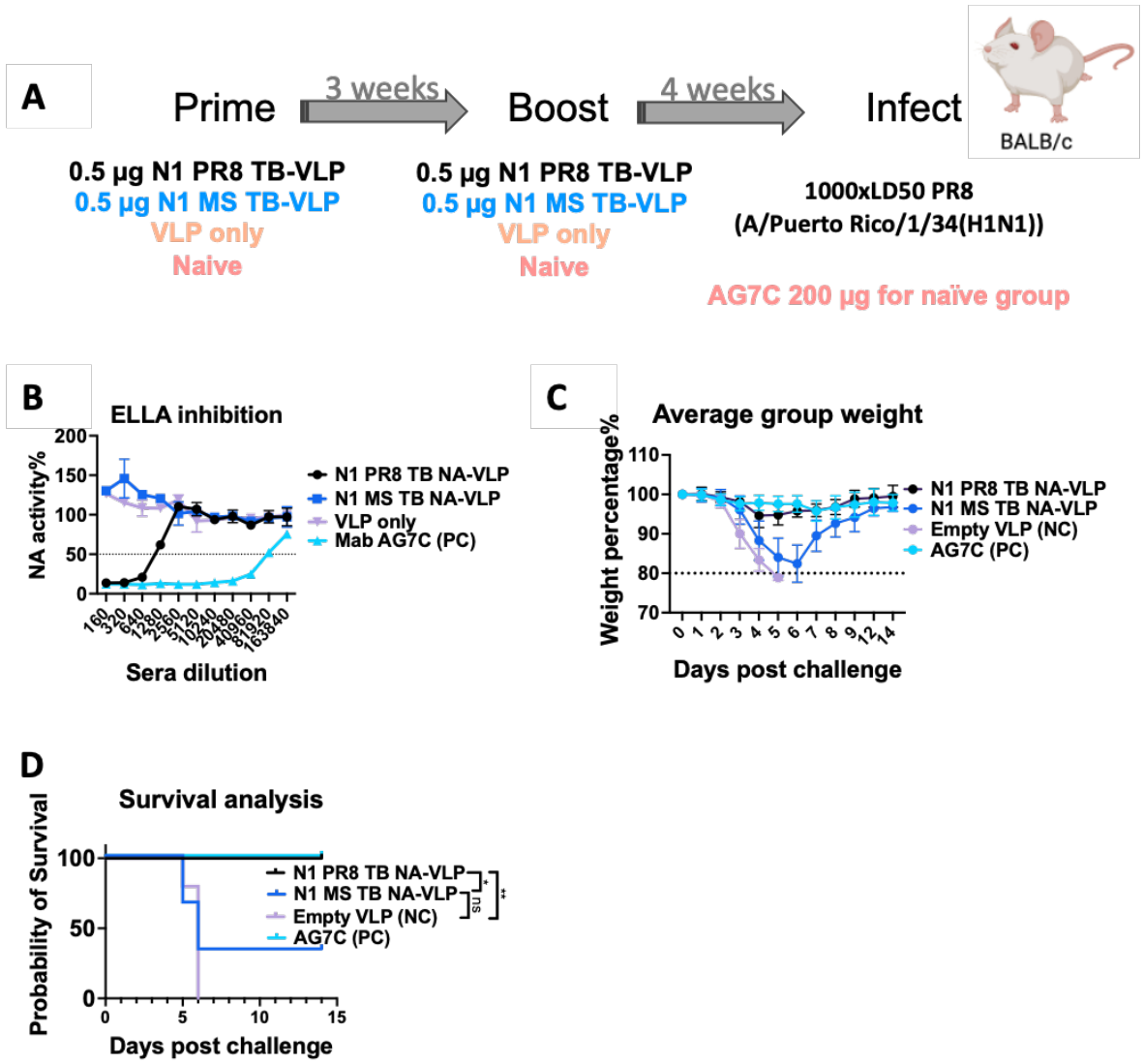

Figure 4.12 **N1 MS TB NA-VLP vaccination (derived from avian H5N1 2021) partially protected mice from A/PR/8/1934 H1N1 challenge (PR8)**

A) Mice were vaccinated in a prime-boost regimen (IM, adjuvanted with AddaVax) with 0.5 µg N1 PR8 TB NA-VLP, 0.5 µg N1 MS TB NA-VLP, and challenged with 1000 LD_{50} PR8 virus.

B) Four weeks post the boost, sera were collected and antibody inhibition against PR8 virus was assessed via ELLA.

C,D) Four weeks post the boost, mice were challenged intranasally with a lethal dose of PR8, weight change (C) and mortality (D) were assessed over a 14-day time course. $n = 6$ mice/group. One of the mice in empty VLP group died 2 weeks after the boost dose for unknown reason. Partial protection by the H5N1 N1 vaccine was seen despite the lack of induction NA inhibiting serum antibody in the ELLA assay. Pairwise comparisons were calculated by Gehan-Breslow-Wilcoxon test. Statistical significance is indicated by *($p < 0.05$), **($p < 0.01$), ***($p < 0.001$), ****($p < 0.0001$).

As a potential pandemic threat, we conducted further investigations into the dose-sparing effect of N1 MS TB and its matched VLP in BALB/c mice to better understand subsequent immune responses (Fig. 4.13A). Mice were vaccinated with three different doses of N1 MS TB or N1

MS TB VLP (0.1 μg NA-VLP, 0.5 μg NA-VLP, 0.1 μg N1 MS NA, 0.5 μg N1 MS NA, and 5 μg N1 MS NA).

All groups receiving N1 MS TB-related vaccines developed similar binding titres against N1 MS TB, encompassing antibodies targeting both the N1 MS TB head and our engineered stem region (including SpyTag and TB domain) (Fig. 4.13C).

In terms of NA inhibition (NAI) titres measured by ELLA, 5 μg of N1 MS TB exhibited the highest NAI titre, while the groups receiving 0.1 μg of N1 MS TB-VLP, 0.5 μg of N1 MS TB-VLP, and 0.5 μg of N1 MS TB developed similar NAI titres comparable to 0.4 mg/mL of AG7C. Notably, 0.1 μg of N1 MS TB-VLP showed a significantly higher ELLA titre compared to the same dose of N1 MS TB antigen alone, highlighting the ability of VLPs to enhance NA inhibition antibody responses even at extremely low doses (Fig. 4.13C). This underscores the dose-sparing potential of VLPs in vaccination strategies.

Next, we compared the cross-reactive NA inhibiting antibodies in these vaccine groups. When assessing the cross-inhibition effect with PR8 virus, 0.5 μg N1 MS TB-VLP induced more inhibition antibodies compared to the same amount of free antigen. 5 μg N1 MS TB group elicited slightly higher level of PR8 inhibiting antibodies compared to 0.5 μg N1 MS TB-VLP (Fig. 4.13D).

Although the homologous antibody response was similar between the NA-free protein and NA-VLP vaccines at the tested dose of 0.5 μg, the NA-VLP vaccine demonstrated a higher level of subtype cross-reactiveantibodies (Fig. 4.13E) suggesting the VLP coupling generated more robust cross-reactive antibodies. Furthermore, the dose-sparing effect of the NA-VLP vaccine was particularly evident at the lower dose of 0.1 μg.

Overall, coupling with VLPs facilitated the generation of NA inhibition antibodies, as demonstrated by comparable inhibition antibody levels observed against X179A virus as well (Fig. 4.13F). These findings highlight the potential of VLPs in enhancing immune responses and optimizing vaccine doses against influenza viruses like N1 MS TB.

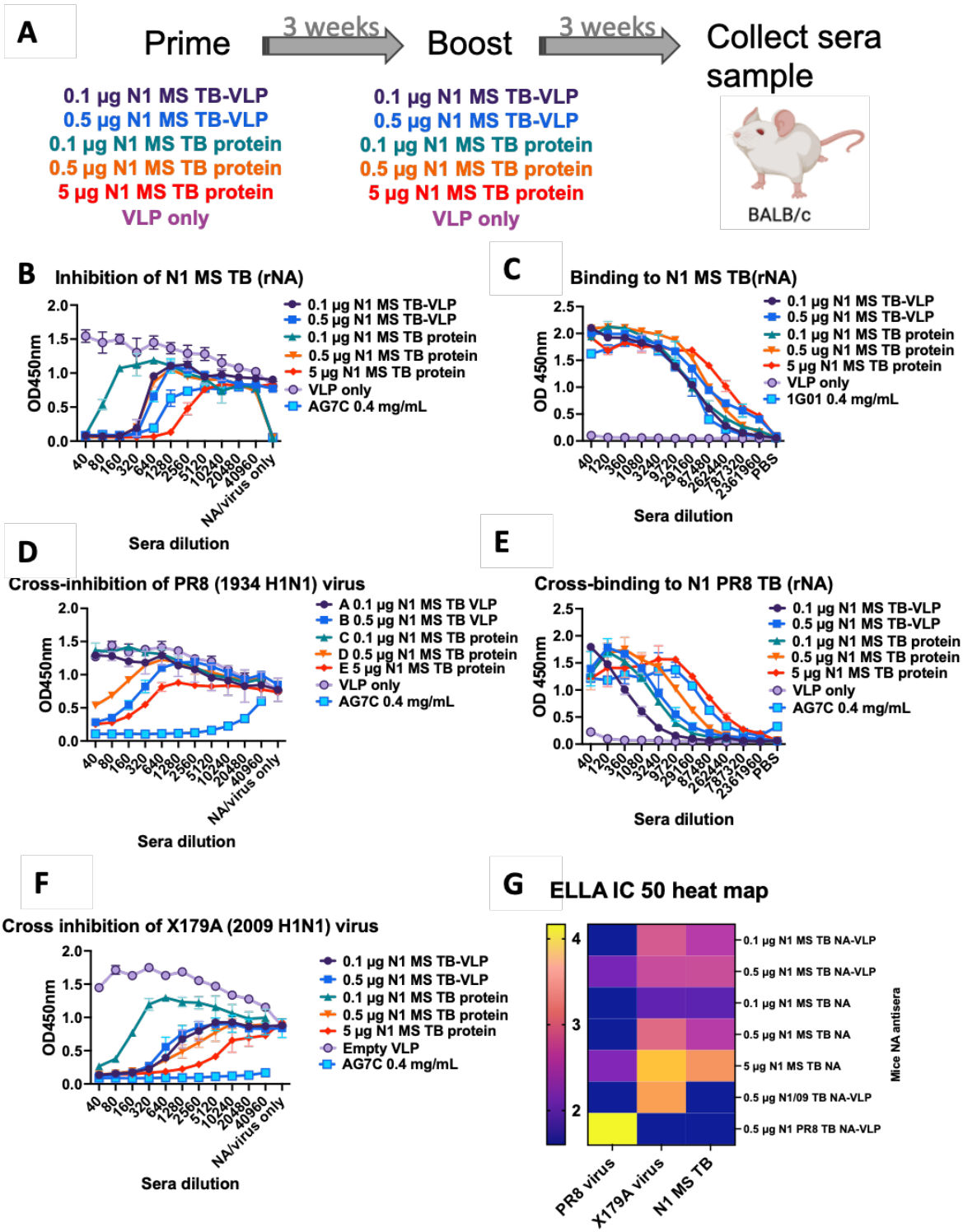

Figure 4.13 **Dose response and crossreactivity of H5N1 NA vaccine candidate towards ancient H1N1 viruses**

A) Mice were vaccinated in a prime-boost regimen with NA-VLPs or NAs as presented. B, C) 3 weeks post the boost, sera were collected and antibody inhibition against N1 MS TB was assessed via ELLA assay. Sera binding to N1 MS TB infected MDCK-SIAT1 cells pre-challenge was assessed by ELISA. At the low dose of 0.1 µg the association with VLP enhances the NAI antibody titres in ELLA by ~4x, but the 0.5 µg dose induced equivalent level of NAI antibody.

D,E) Cross-inhibition to PR8 virus was tested by ELLA. Cross-binding to N1 PR8 TB was assessed by ELISA.
F) Cross-inhibition to X179A virus was tested by ELLA.
G) Data represented as a heat map of log IC_{50} values next to a list of different N1 NAs.

4.6 Multivalent NA-VLP immunogenicity

The concept of a "Universal Vaccine" aims to offer enduring protection against multiple influenza virus strains and subtypes, addressing both seasonal outbreaks and potential pandemics (Erbelding et al., 2018). Our VLP platform offers a versatile method for developing mixed multivalent NA-VLP vaccines, which holds promise for advancing the understanding of multivalent vaccine immunity outcomes.

This approach could incorporate multiple NA antigens into VLPs, potentially enhancing the breadth and potency of immune responses against distinct influenza strains. Such multivalent NA-VLP vaccines could contribute significantly to the development of broadly protective influenza vaccines,

We performed a pilot study to test the immunogenicity of NA-VLPs admixture to obtain more information about multivalent NA immunity. C57BL/6 mice (n=3) were vaccinated with 0.5 µg of NA, 0.5 µg of NA-VLP, or a mix of 7 NA-VLPs (0.4 µg of N1 MS TB-VLP, N1 PR8 TB-VLP, N2/20 TB-VLP, N2 X31 TB-VLP, N6/16 TB-VLP, N8/20 TetDminus-VLP, and, N9/13 TB-VLP (2.8 µg NA in total), referred to as Mix7) in a prime and boost regimen (Fig. 4.14A). Following vaccination with Mix7, the antibody binding levels to each individual recombinant NA were found to be relatively lower compared to those induced by the homologous NA vaccine, as measured by ELISA. (Fig. 4.14). Eb Glycan Cap is a spike protein from Eloba virus, used as negative control in this experiment. While Figure 4.14B reveals modest background binding of Eb Glycan Cap (only 30-fold lower than specific NA groups), this phenomenon was unique to the N1 MS TB group and absent in all other experimental conditions. The observed binding pattern suggests potential low-affinity cross-reactivity. Also, the absence of detectable inhibition confirms this interaction is probably biologically irrelevant.

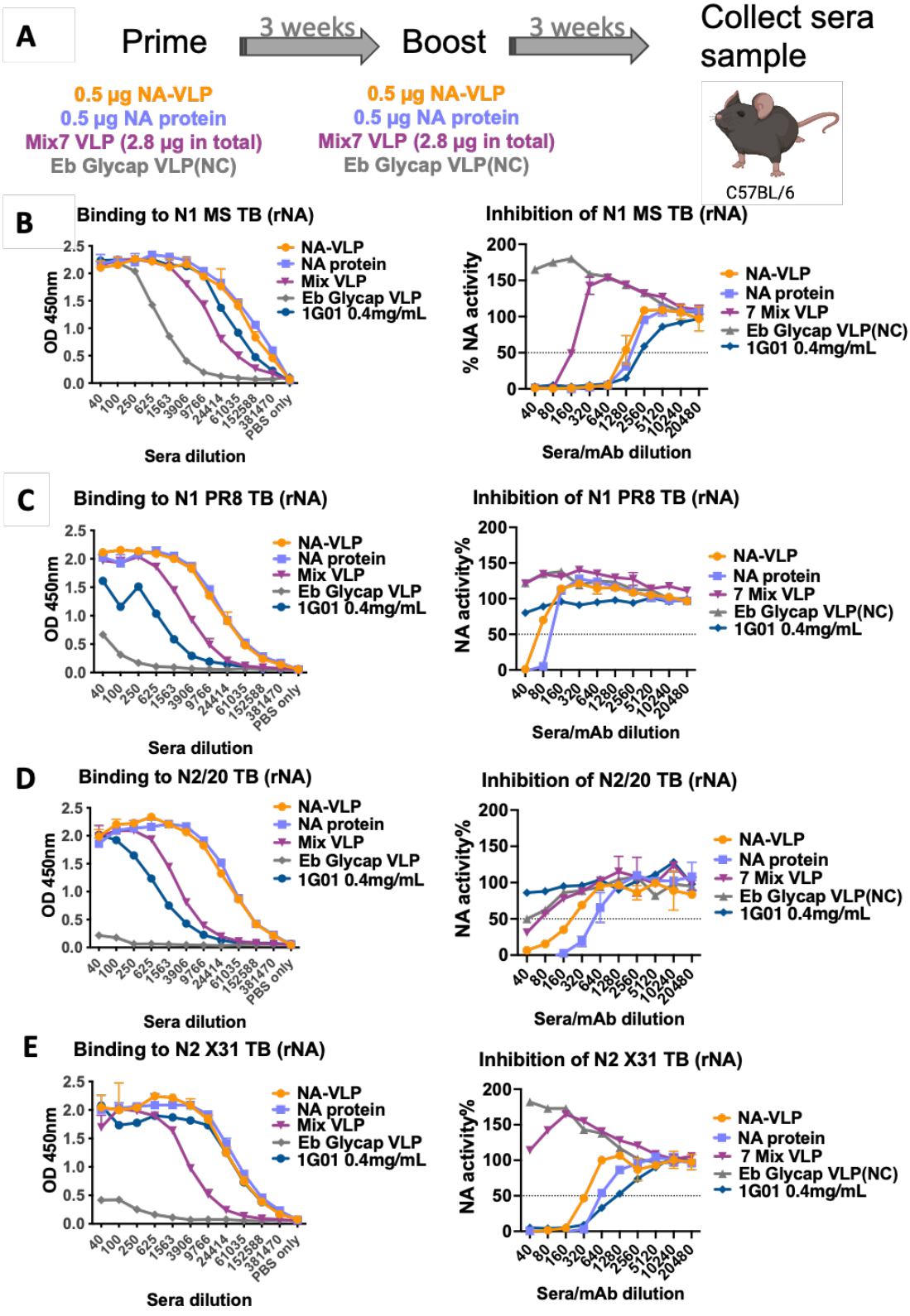
A
Prime
3 weeks
Boost
3 weeks
Collect sera sample
0.5 μg NA-VLP
0.5 μg NA protein
Mix7 VLP (2.8 μg in total)
Eb Glycap VLP(NC)
0.5 μg NA-VLP
0.5 μg NA protein
Mix7 VLP (2.8 μg in total)
Eb Glycap VLP(NC)
C57BL/6
B
Binding to N1 MS TB (rNA)
OD 450nm
Sera dilution
NA-VLP
NA protein
Mix VLP
Eb Glycap VLP
1G01 0.4mg/mL
Inhibition of N1 MS TB (rNA)
% NA activity
Sera/mAb dilution
NA-VLP
NA protein
7 Mix VLP
Eb Glycap VLP(NC)
1G01 0.4mg/mL
C
Binding to N1 PR8 TB (rNA)
Inhibition of N1 PR8 TB (rNA)
NA activity%
D
Binding to N2/20 TB (rNA)
Inhibition of N2/20 TB (rNA)
E
Binding to N2 X31 TB (rNA)
Inhibition of N2 X31 TB (rNA)

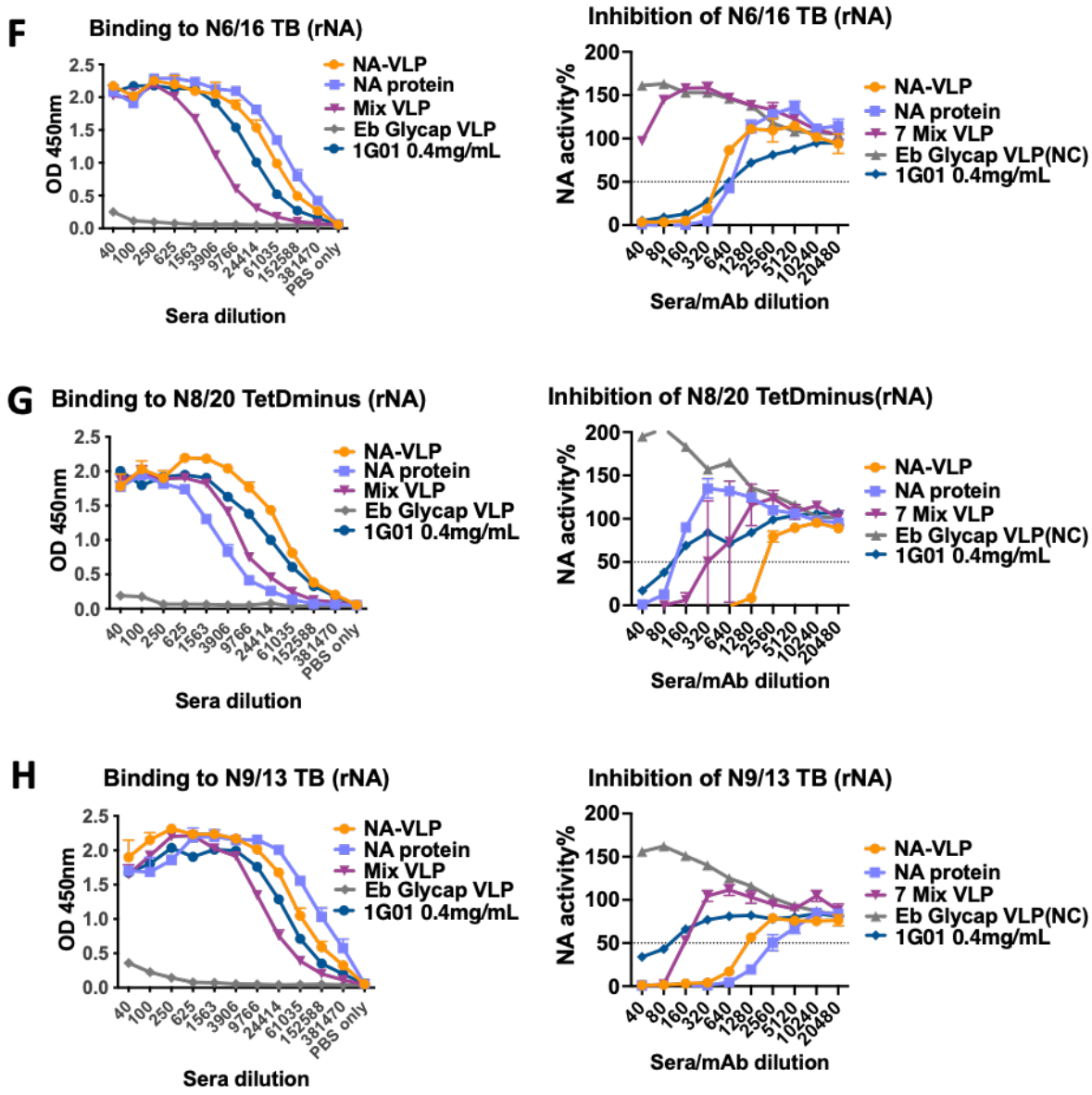

Figure 4.14 **Antibody Response by Mix of 7 NA-VLPs**
A) Mice were vaccinated in a prime-boost regimen (IM, adjuvanted with AddaVax) with Mix7 NA-VLP, NA-VLPs or NAs as presented. Mix7 contained 0.4 µg of N1 MS TB-VLP, N1 PR8 TB-VLP, N2/20 TB-VLP, N2 X31 TB-VLP, N6/16 TB-VLP, N8/20 TetDminus-VLP, and, N9/13 TB-VLP (2.8 µg NA in total).
B-H) Three weeks post the boost, sera were collected and antibody inhibition against NA was assessed via ELLA assay. Sera binding was assessed by ELISA.

However, when assessing NA inhibition (NAI) titres against each strain of NA using ELLA, the inhibition titres developed by Mix7 were generally lower compared to individual NA-VLP (Fig. 4.14 B-H). Importantly, the mixed vaccine (Mix 7) didn't produce good protection against any of the flu strains we tested - N1 PR8, N2 X31, or N6/16 (see Fig. 4.14 C, E, F). This shows that while the single NA and NA-VLP vaccines worked well in terms of generating NAI antibodies, the mixture failed to induce detectable titres for certain strains.

Mix7 included two recombinant NA from the N1 and N2 subtypes, which are antigenically distant from each other. Interestingly, the inclusion of these two NA within the same subtype

did not significantly promote inhibition antibodies against each other (Fig. 4.14 D, E). Even when mixed with 7 different NA-VLPs, the elicited inhibition antibodies appeared to be largely independent and strain-specific.

NA and NA-VLP induced similar level of NA-inhibiting antibodies at 0.5 ug doses, for most of the neuraminidases, except for N8 TetDminus (Fig. 4.14 G). In the case of N8 TetDminus, NA-VLP is more potent in terms of ELLA NA inhibiting antibodies compared to free protein vaccine. The reason could be that the N8 TetDminus is a mixture of monomer, dimers and tetramers. Coupling of these forms on VLP, may have enhanced the immune response.

These findings suggest that while the Mix7 approach incorporating multiple NA-VLPs can induce antibodies against each included subtype, the resulting inhibition antibodies tend to be specific to the individual strains rather than broadly cross-reactive within the same subtype. However, the antibody level is about 2-4 fold lower compared to individual NA or NA-VLP. In our previous results, a lower dose of 0.1 μg monovalent NA-VLP induced similar NAI antibody level compared to the 0.5 μg NA-VLP (Fig. 4.10, 4.13), however the Mix7 vaccine seem to have induced low immunogenicity. Due to the stock issue, the NA amount was not strictly contolled as the individual group used 0.5 μg of NA or NA-VLP while the Mix7 tested 0.4 μg of each NA-VLP. A further repeat with controlled NA amount might be needed to confirm this result.

Multivalent vaccination with NA-VLPs induced NAI IgG titres against all included NA subtypes. However, it did not show a significant advantage in enhancing levels of cross-inhibiting antibodies. Furthermore, a comparison of individual ELLA inhibition titres revealed that Mix1 was less effective in generating NA-inhibiting antibodies.

These findings indicated that while multivalent NA-VLP vaccination effectively stimulated immune responses against multiple NA antigens, enhancing the production of broadly cross-reactive inhibition antibodies remains uncertain. This suggested a need for further optimization in designing multivalent influenza vaccines to achieve broader protection, highlighting the challenge in achieving broad cross-reactivity across diverse influenza strains with multivalent NA-VLP vaccines.

4.7 Discussion

In our efforts to establish a definitive correlation between NA inhibition (NAI) titres measured by ELLA and protective efficacy in mice models, no clear-cut correlation has been identified so far.

For matched challenges, where mice were exposed to the same subtype of influenza virus used in vaccination, higher NAI titres generally correlated with higher statistical protection efficacy. Nevertheless, this relationship did not hold universally when examining individual mice.

Conversely, when mice were challenged with viruses within the same subtype but not identical to those used in vaccination, higher cross-inhibition titres were associated with a higher likelihood of survival.

These observations suggest that while higher NAI titres tend to indicate greater protection at a population level, individual variability and other factors may influence the protective efficacy of NA-VLP vaccination against diverse influenza strains. Further research is needed to better understand and optimize the relationship between NAI titres and vaccine-induced protection across different influenza subtypes.

Based on our extensive experimentation across various virus challenge models, we have drawn several conclusions regarding the use of VLP conjugates in influenza vaccination:

Enhanced Antibody Response at Extremely Low Doses: VLP conjugation robustly enhances the antibody response, particularly at extremely low doses of NA. Even with similar total NA-binding IgG levels, NA-VLPs demonstrate a tendency to promote higher levels of NA inhibition (NAI) antibodies when compared to NA alone at low antigen levels. This capability represents a significant advantage in achieving equivalent immune responses with significantly less antigen.

Positive Effects of Structural Integrity and VLP Conjugation: Structural integrity and conjugation with VLPs positively influence protective efficacy. Utilizing matched, correctly-folded NA-VLPs ensures robust protection in mice even at low antigen doses. Conversely, any compromise in structural integrity or VLP conjugation diminishes the protective efficacy observed.

These findings showed the critical importance of both structural integrity and VLP conjugation in optimizing influenza vaccine design, highlighting the potential of NA-VLPs to enhance immune responses efficiently, paving the way for developing effective vaccines against influenza and potentially other infectious diseases.

Chapter 5 Loop Grafting to Overcome the NA Expression Difficulty

In this chapter, we developed a loop grafting method, inspired by Colman and Varghese's published N2 structure (Colman et al., 1983; Varghese et al., 1983), to address the expression challenges of the recent pandemic N1 strain. Remarkably, we successfully expressed hybrid NA with designated antigenicity as well as enhanced expression and stability. Our findings demonstrate that upper surface loop grafting effectively transfers the majority of neuraminidase-inhibiting antibody epitopes, as confirmed by serum analysis in immunized mice. Mice immunized with these NA hybrids exhibited loop-specific protection against a high-dose, lethal virus challenge. The manuscript for this straightforward and effective technique is attached in Appendix 11 (Rijal et al., 2024).

5.1 NA Structure and Loop Grafting Method (Inspired by Colman and Varghese)

5.1.1 NA structure demonstration based on structural correlations

Neuraminidase (NA) is a type II homotetramer, with its complex structure being essential for its function in the viral life cycle (Air, 2012). Each subunit of NA consists of a polypeptide chain that folds into a propeller-like structure composed of six topologically identical β-sheets (Colman et al., 1983; Varghese et al., 1983) (Fig. 5.1A). Each β-sheet blade is made up of four β-strands connected by loops with a "W" topology (Fig. 5.1B). For clarity, the six β-sheet blades are labelled B1 through B6, and the four β-strands within each blade are labelled S1 through S4. The loop connecting the S4 strand of one sheet to the S1 strand of the next is referred to as L01, while the loop between the S1 and S2 strands is labelled L12.

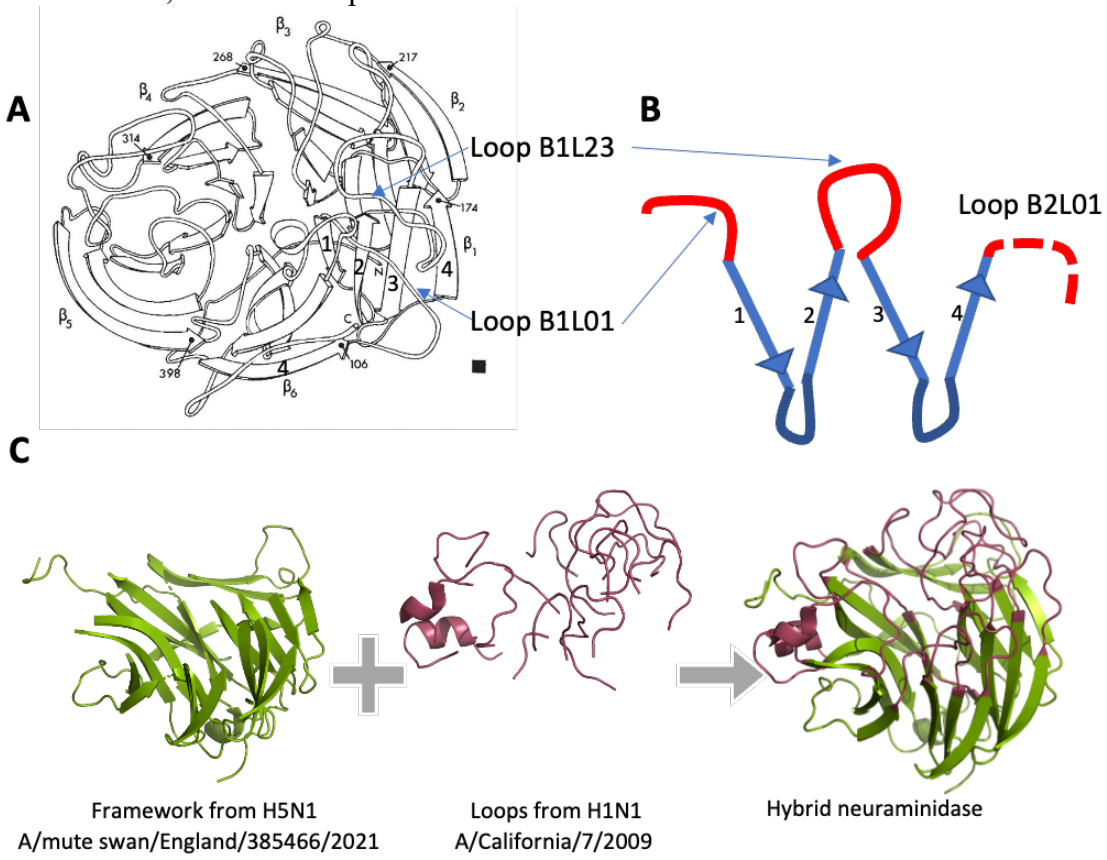

Figure 5.1 **Design of hybrid NA by the loop grafting method**
A) The crystal structure of a neuraminidase N2 monomer (Varghese et al., 1983).
B) The NA head subunit is folded into an array of six β-sheets, each composed of four β-strands connected by four loops, with a "W" topology, shown in schematic form in B. On each sheet, the loops loop L01 (between the 4th strand of the previous sheet and the 1st β −strand of the following sheet, and L23 (between the 2nd and 3rd β–strands), form the top surface of the NA monomer, surrounding the active site of the enzyme.
C) Example of loop transfer between N1 MS (A/mute swan/England/053054/2021 (H5N1)) and N1/09 (A/California/07/2009 (H1N1)). All of the L01 and L23 loops of N1 MS NA were replaced with the L01 and L23 loops from N1/09. The aim was to combine the efficient expression of the N1 MS/21 TB with the antigenicity of N1/09. Figures generated from Pymol. Sequence alignment were presented in Appendix 9.

In each β-sheet, the L01 and L23 loops form the top surface of the NA monomer, which surrounds the enzyme's active site (Colman et al., 1983; Varghese et al., 1983). Since the NA head contains six β-sheets, the top surface is primarily formed by six L01 loops and six L23 loops, with additional contributions from the C-terminal domain.

From a structural perspective, loop regions tend to exhibit greater flexibility and variability compared to β-sheets. These loops are typically more exposed and hydrophilic. In contrast, β-sheets generally display lower flexibility and variability, although their exposure and immunogenicity can vary (Koh & Kim, 2005; Salemme & Weatherford, 1981). Notably, many enzyme-inhibiting and protective antibodies bind to the upper surface loops (Colman et al., 1983; Jiang et al., 2020; Momont et al., 2023; Stadlbauer et al., 2019; Yasuhara et al., 2022).Several studies have demonstrated that most, though not all, monoclonal antibodies targeting NA select for resistant viruses with amino acid replacements within these loops. Additionally, evolutionary analyses of NAs have revealed that the majority of sequence changes over time occur at surface-exposed residues, particularly those within the L01 and L23 loops (Rijal et al., 2024).

We hypothesized that interactions between monomers within the NA tetramer significantly contribute to the stability and efficiency of recombinant tetrameric NA expression in vitro. Ellis et al. (2022) identified forty-four residues from known crystal structures that may be involved in these intermonomeric contacts in the N1 protein (Ellis et al., 2022). Of these, ten residues were located in loops L01 and L23. In their final design of the stabilized sNAp-155 N1 2009 NA, they substituted ten of these forty-four amino acids, only two of which (conserved in N1 NA) were within the surface loops B2L01 and B2L23. This suggests that the majority of intermonomer contacts are not located within the L01 and L23 surface loops.

Based on these observations, we reasoned that it might be possible to combine the antigenic features of a poorly expressed NA with the expression and stability characteristics of a highly expressed NA by grafting the L01 and L23 loops from the former onto the structural "framework" of the latter, particularly within a given NA subtype (Fig. 5.1C).

5.1.2 Loop Grafting method

Following the principle of transplanting the upper surface loops L01 and L23 from a target protein onto a scaffold protein, we pursued a loop grafting method aimed at optimizing both expression efficiency and antigenicity. Taking N1/09 loops MS TB as an example, we designed a loop grafting between the N1 MS (A/mute swan/England/053054/2021 (H5N1)) and N1/09 (A/California/07/2009 (H1N1)) neuraminidase (NA) heads (Fig. 5.1C).

The choice of these two N1 NAs for grafting was driven by their distinct but complementary properties. The N1 MS strain, derived from an H5N1 avian influenza virus, exhibits robust expression characteristics that are highly desirable for chimeric protein production. Conversely, the N1/09 strain, associated with the 2009 H1N1 pandemic, has been well characterised as an immunogenicantigen but exhibited poor yield in our previous expressed constructs (Appendix 2). By grafting the L01 and L23 loops from N1/09 onto the N1 MS framework, we aimed to create a hybrid NA that maintains high expression levels while displaying key antigenic epitopes from the pandemic strain.

The specific sequences of the L01 and L23 loops used in this grafting process are detailed in Appendix 8A. The initial design was informed by the structural insights provided by Colman and Varghese in 1983, who first identified the importance of these loops in the context of N2 neuraminidase. Their work laid the foundation for understanding how surface loops contribute to the functional and antigenic properties of the NA enzyme.

In addition to this primary design, we also developed a parallel loop grafting construct, which is documented in Appendix 8B.

The final construct, which was ultimately selected for expression studies as presented in Appendix8, was the result of a collaborative effort between Pramila and Alain. They meticulously co-designed the construct, leveraging the N2 numbering system to ensure accurate alignment and integration of the grafted loops. Similar strategy was expanded to N1/19 loops MS TB for a better expression as well.

5.2 Overcoming the expression difficulty of Seasonal N1 by loop-transfer method

5.2.1 Yield improvement by loop-transfer method

As detailed above, we engineered two hybrid proteins: N1/09 loops MS TB and N1/19 loops MS TB. These constructs were designed by incorporating the upper surface loops L01 and L23 from the poorly expressing N1/09 TB and N1/19 TB strains into the highly expressive N1 MS TB backbone.

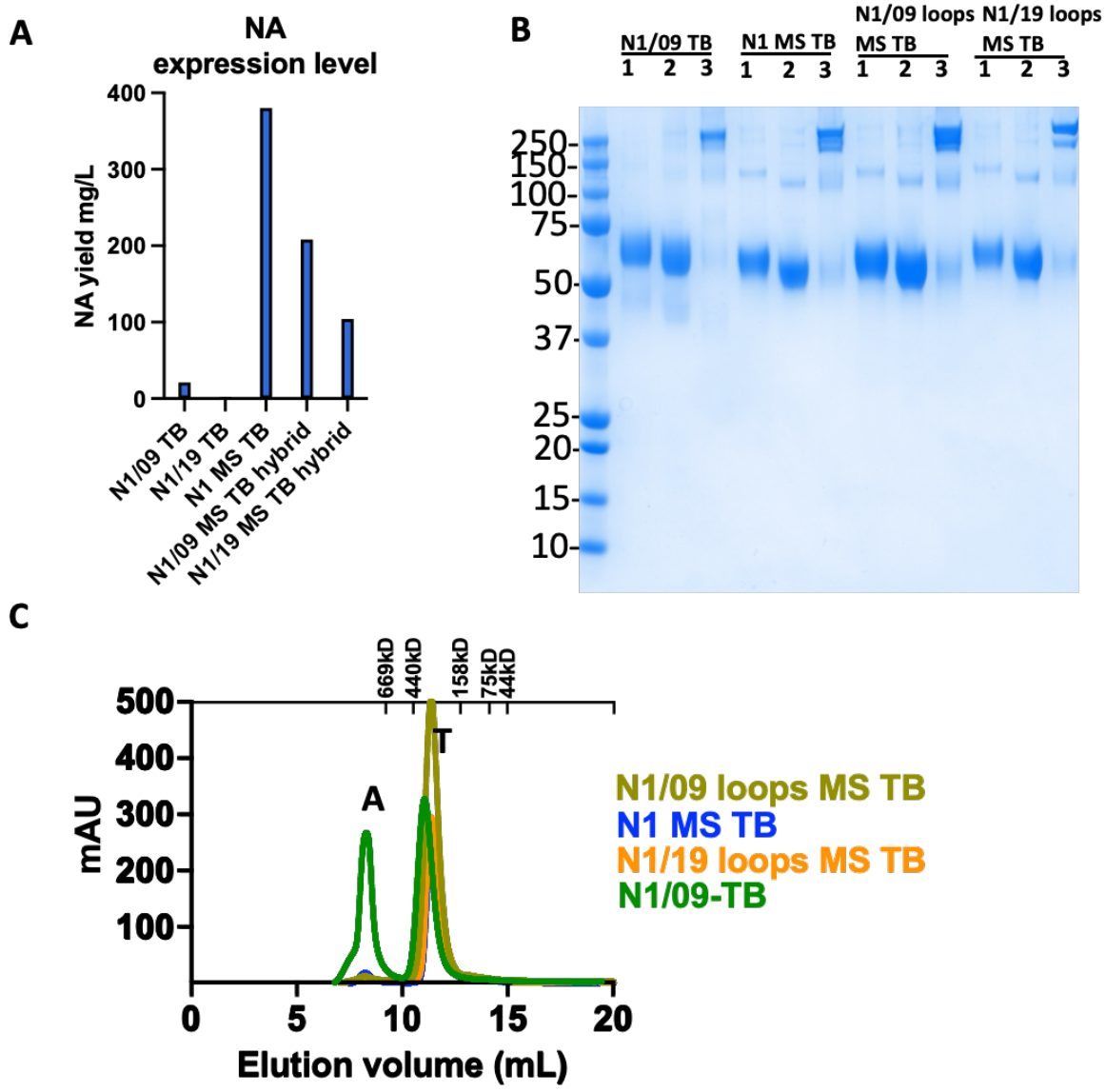

Figure 5.2 **Hybrid N1 NA expressed as tetramers with reduced aggregation**
A) Hybrid NAs successfully expressed with transferred L01 and L23 loops. The expression level of the hybrid neuraminidases increased compared to the loop donors.
B) Two micrograms of neuraminidases were loaded on SDS-PAGE (4-12% Bolt Bis-Tris) before Coomassie staining. Lane #1: non-reduced, #2: reduced, #3: BS3-crosslinked protein without reducing agent. TB= tetrabrachion linked. Presence of band above 200 kDa for BS3 cross-linked NA proteins (Lane 3) denotes the formation of cross-linked tetramers. C) Size exclusion chromatography (Superdex® 200 Increase 10/300 GL) confirmed the tetrameric form of N1/09 MS TB hybrid and N1/19 MS TB hybrid proteins. An aggregate peak (A) and

a tetramer peak (B) are marked. Minimal aggregation was seen in N1 MS TB and the two hybrid NAs. (Y-axis indicates absorbance at 280 nm shown as milli Absorbance Units).

The results of this engineering effort are illustrated in Fig. 5.2A, which shows a marked improvement in expression levels for both hybrid constructs. Specifically, the N1/09 loops MS TB hybrid achieved an expression level of 208 mg/L, while the N1/19 loops MS TB hybrid reached 104 mg/L. Although these yields were lower than that of the N1 MS TB alone, they represented a significant improvement over the original N1/09 TB and N1/19 TB proteins. Moreover, the fact that both hybrids were able to form stable tetramers, as confirmed by the BS-3 linked SDS-PAGE presented in Fig. 5.2B, indicated that the loop grafting strategy did not compromise the structural integrity of the proteins.

In terms of aggregation behaviour, the hybrid N1/09 loops MS TB construct demonstrated reduced aggregation compared to the original N1/09 TB protein (Fig. 5.2C). This improvement brought the aggregation profile of N1/09 loops MS TB closer to that of the N1 MS TB backbone, suggesting that the grafting of loops from N1/09 onto the N1 MS framework not only improved expression but also retained structural stability from the backbone construct.

In addition to these intra-subtype grafting experiments, we also explored the possibility of loop grafting between different NA subtypes. Specifically, we attempted to graft loops from the N1 subtype onto the N6 subtype, using N6/16 TB. Unfortunately, the expression of this chimeric N6/16-based construct was not successful, indicating that the compatibility between loops and the structural framework may be more subtype-specific than initially anticipated.

5.2.2 Immunogenicity and enzymatic activity maintained after loop-transfer

As illustrated in Figure 5.3A, both hybrid proteins, N1/09 loops MS TB and N1/19 loops MS TB, exhibited substantial enzymatic activity. While slightly lower than that of the parent N1 MS TB, their activity was significantly higher than that of the original N1/09 TB. This was consistent with the enzymatic activity measured by MUNANA assay (Figure 5.3B). The strong performance in these assays suggests that the hybrid proteins are mostly correctly folded, retaining the catalytic properties essential for NA activity.

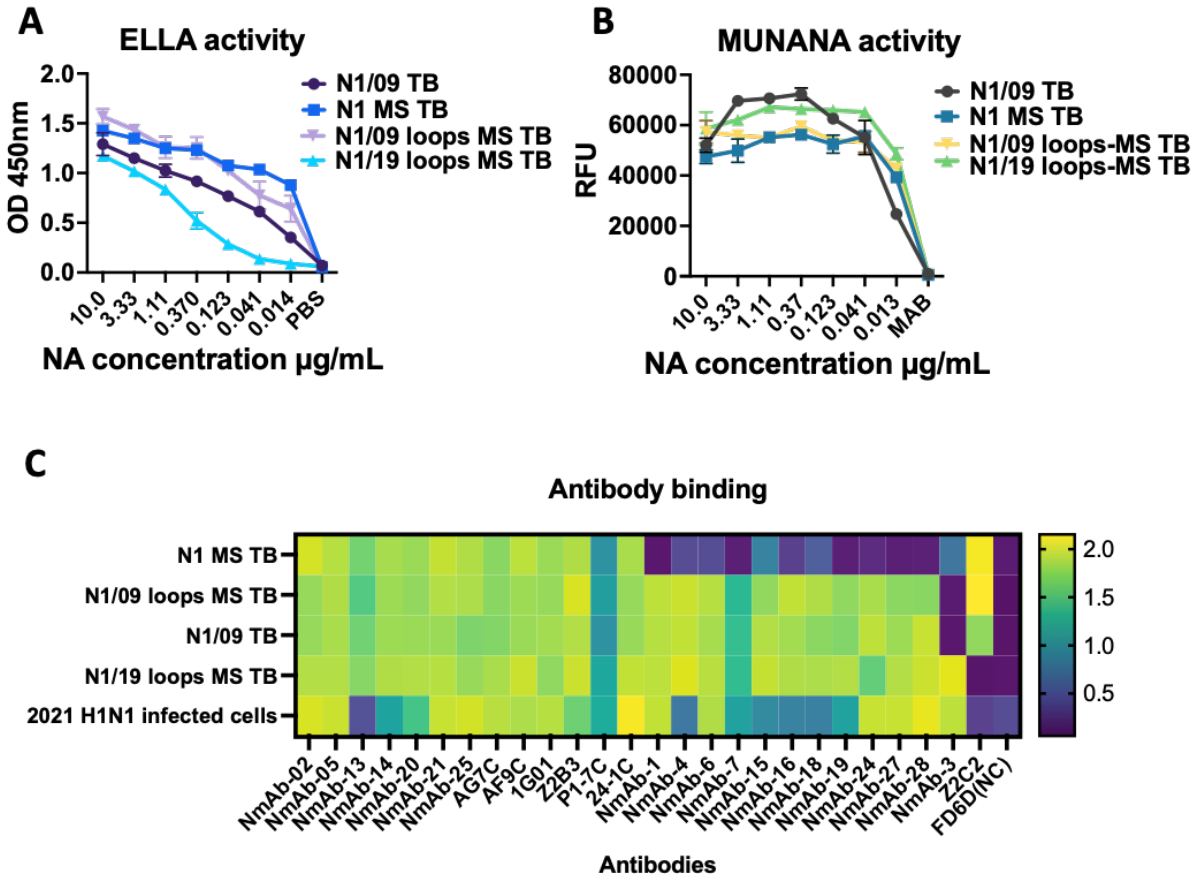

Figure 5.3 **Enzyme activity is retained and loop specific epitopes are conserved on hybrid NAs**

A, B) Comparisons of enzyme activity of purified tetrameric hybrid NAs, loop donor NA and loop recipient NA by ELLA and MUNANA assays.

B) Epitope conservation between the loop donor and the resulting hybrid neuraminidase, as detected with a set of N1 specific human monoclonal antibodies. The antibodies are grouped to show the set of 13 fully cross reactive mAbs and 12 mAbs specific for post 2009 NAs that cross react on the hybrid N1 proteins. Cells infected with 2021 virus (closely related to 2019) were used as a positive control particularly for Mab NmAb-3, which was specific for the 2019 NA Loops.

To further assess the structural and antigenic integrity of the grafted loops, we employed a monoclonal antibody (mAb) panel derived from influenza-infected patients or volunteers vaccinated with the inactivated seasonal influenza vaccine (QIV). This evaluation aimed to determine the epitope transfer following loop grafting. The single-point binding results, depicted in Fig. 5.3 C, provide critical insights into the antigenic properties of the hybrid proteins.

The mAb panel comprised five broadly reactive antibodies known for their binding to conserved epitopes within the L01 and L23 loops: 1G01 (Stadlbauer et al., 2019), Z2B3 (Jiang et al., 2020), AG7C, and AF9C (Rijal et al., 2020). These antibodies were selected based on crystal structures that indicate their interaction with the L01 and L23 loops, regions that were central to our loop grafting strategy. Additionally, the panel included 22 N1-specific monoclonal antibodies, whose detailed characteristics are provided in Appendix 9.

The binding assays revealed that of the 26 antibodies tested, 13 cross-reactive antibodies bound to all recombinant N1 NA variants, reflecting the conserved nature of certain epitopes across the N1 subtype. 11 antibodies exhibited specific binding to the grafted loops in N1/09 and N1/19, demonstrating successful epitope transfer through loop grafting as well as the antigenicity difference between the loop donor and the backbone provider. Among these, one antibody (CU5A) exclusively bound to the N1/19 loops, highlighting unique recognition of N1/19 loops. Another antibody, Z2C2, showed cross-reactivity between N1/09 and N1 MS but did not bind to N1/19, revealed an epitope loss in recent N1 pandemic strain. We also performed a binding titration of the whole mAb panel against the listed recombinant NA or viruses, as listed in Appendix 9.

The data collectively substantiate our hypothesis that the majority of B cell epitopes on the upper surface of NA can be effectively transferred using our loop grafting method. This approach not only preserved the functional integrity of the enzyme but also maintained the antigenic characteristics necessary for vaccine development and other therapeutic applications.

5.2.3 Loop-transfer NA protected mice in 2009 H1N1(X179A) challenge model

We have previously shown that recombinant NA presented on a mi3 particle is strongly immunogenic at doses as low as 0.1 µg ((Rahikainen et al., 2021), Fig. 4.10), in contrast to the 10-100 fold higher doses of free NA protein often described in the literature (Giurgea et al., 2020). Additionally, findings from Chapter 4 demonstrated that the protective effect could be further enhanced by mi3 particle coupling. Considering the advantage in both antibody titres and protective effect, we further tested the successfully expressed hybrid N1 NAs with mi3 conjugation.

Similar to previous results, N1/09 loops MS TB and N1/19 loops MS TB were conjugated at various NA: VLP ratios. The final ratio selected for the tetrameric NA to mi3 was 2.6 µg NA to 8 µg mi3 (Fig. 5.4A). All selected conjugations formed a clear NA-VLP band in SDS-PAGE (Fig. 5.4B). Both enzymatic activity and antibody binding were retained after conjugation (Fig. 5.4C, D).

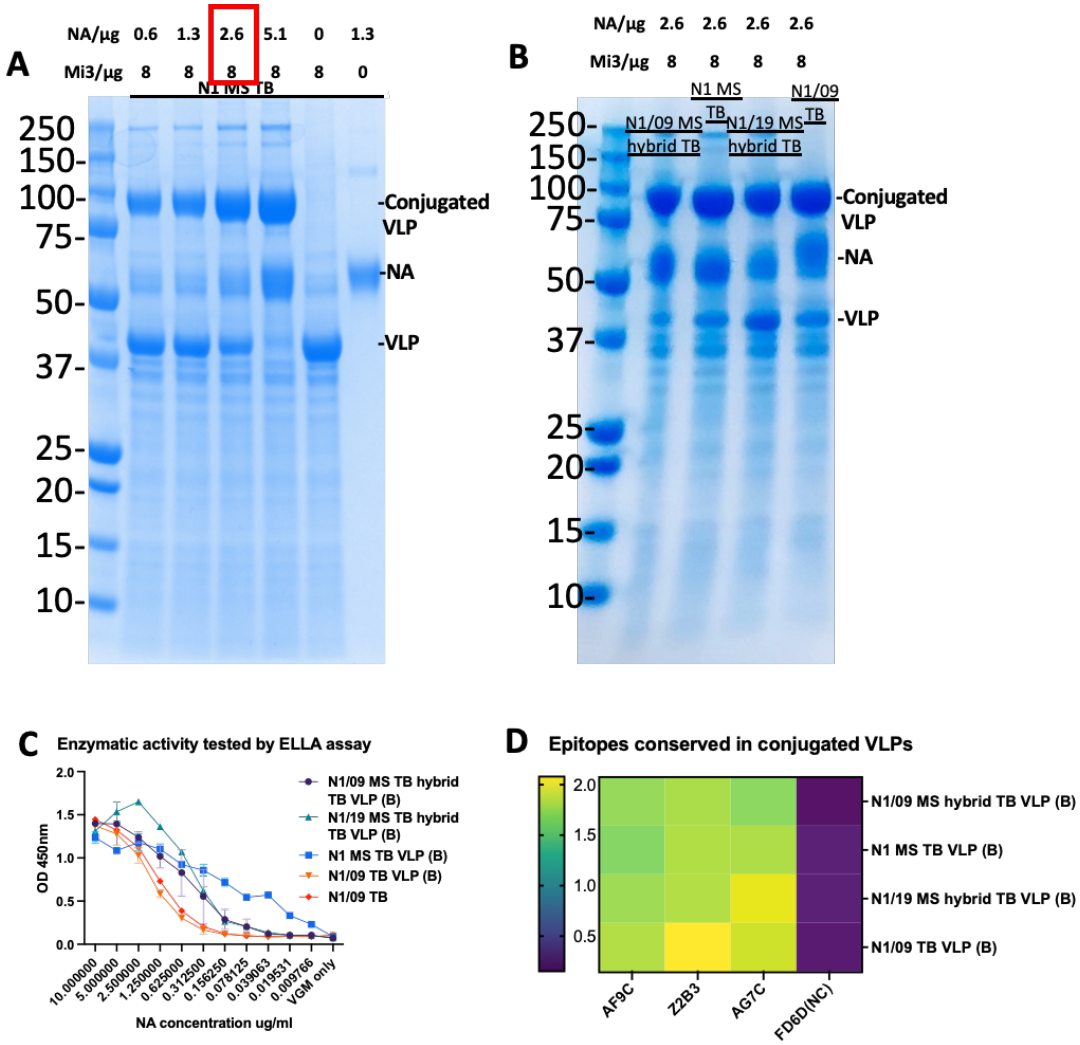

Figure 5.4 **Conjugation of the hybrid NA and SpyCather003-mi3 particles**
A) Different conjugation ratios of NA and VLP were tested in Tris Buffered Saline (TBS) buffer (with extra 90mM Ca2+ and 50mM Mg2+ added to TBS). The final conjugation ratio was chosen considering the conjugated band intensity and the level of free antigen. B) N1/09 TB, N1 MS TB, N1/09 MS hybrid TB, and N1/19 MS hybrid TB were conjugated at the same ratio. Clear conjugation bands were observed.

C) Enzymatic activity of NA was retained after conjugation. Constructs marked with '(B)' denote VLP scafolds produced in Bacillus expression systems.
D) Antigen integrity was checked after conjugation by binding of three fully characterized loop specific cross reactive antibodies AF9C, Z2B3, and AG7C in ELISA. AF9C and Z2B3 have overlapping footprints and bind into the active site, AG7C binds to one side of the active site (reviewed in Table 1.6).

A

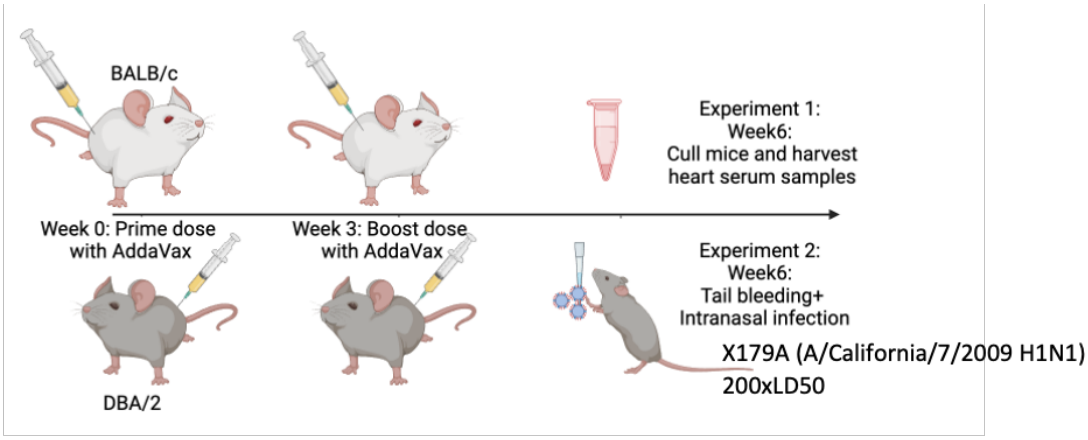
BALB/c
Week 0: Prime dose with AddaVax
Week 3: Boost dose with AddaVax
Experiment 1: Week6: Cull mice and harvest heart serum samples
Experiment 2: Week6: Tail bleeding+ Intranasal infection
X179A (A/California/7/2009 H1N1) 200xLD50
DBA/2

B

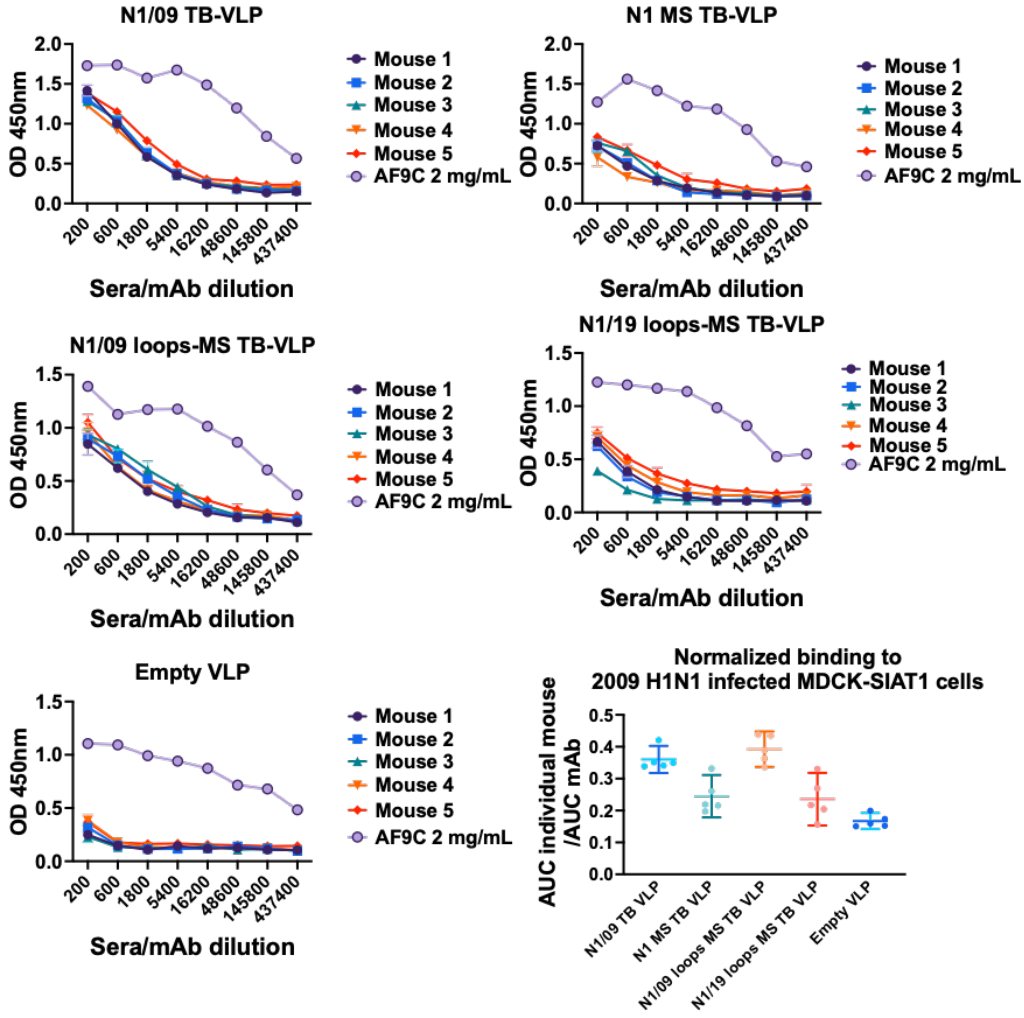
N1/09 TB-VLP
N1 MS TB-VLP
N1/09 loops-MS TB-VLP
N1/19 loops-MS TB-VLP
Empty VLP
OD 450nm
Sera/mAb dilution
200
600
1800
5400
16200
48600
145800
437400
Mouse 1
Mouse 2
Mouse 3
Mouse 4
Mouse 5
AF9C 2 mg/mL
Normalized binding to 2009 H1N1 infected MDCK-SIAT1 cells
AUC individual mouse /AUC mAb
N1/09 TB VLP
N1 MS TB VLP
N1/09 loops MS TB VLP
N1/19 loops MS TB VLP
Empty VLP

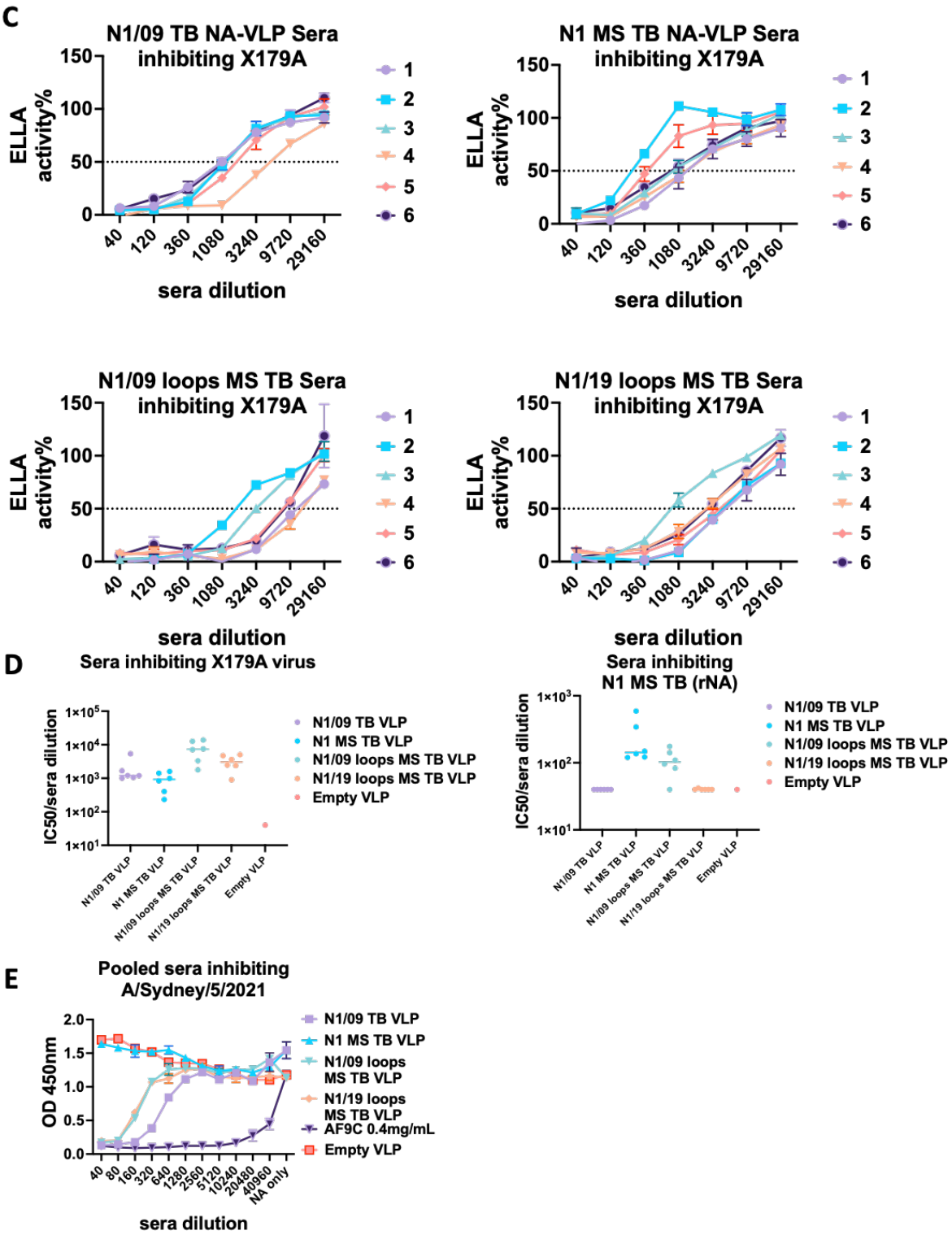

Figure 5.5 **Seroconversion of DBA/2 and BALB/c mice immunised with hybrid NA-VLP vaccines derived from 2009 H1N1 and 2021 H5N1**

A) Experimental protocol: two doses of NA-VLP were injected intramuscularly to groups of six DBA/2 mice at 3-week interval in 5 sets. Each dose contains 0.5 µg equivalent NA in 25 µL mixed with 25 µL AddaVax adjuvant. Animals immunised with N1/09 TB VLP, N1 MS TB VLP, N1/09 loops-MS TB VLP, N1/19 loops-MS TB VLP, and empty VLP were compared. BALB/c mice were culled after three weeks in Experiment 1 for analysis of sera. DBA/2 mice

were challenged three weeks post the second dose with 200 LD_{50} X179A intranasally after tail bleeding in Experiment 2. They were monitored for 14 days after challenge for weight loss.
B) Data obtained with serum samples from Experiment 2. Within each group individual mice sera were tested for binding to 2009 H1N1 NA by ELISA using X179A (A/California/7/2009) virus-infected MDCK-SIAT1 cells. AUC (Area under curve) was calculated with a log scale X axis and presented exponentialized on a log scale after calculation. Normalization was done by comparing the individual AUC and control mAb AUC,
C) Serum samples collected from Experiment 1. Within each group, inhibition of X179A (A/California/7/2009) NA in ELLA assay was tested with individual samples after two immunisation doses.
D) Serum samples collected from Expriement 1 were tested for NA inhibition in ELLA assay against X179A and N1 MS TB. IC50 was calculated.
D) Pooled sera from Experiment 2 were tested by ELLA assay for inhibition of NA on H1N1 A/Sydney/5/2021 virus particles.
Antisera from N1 MS TB VLP (2021 H5N1) immunized mice inhibited NA on A/California/7/2009 but failed to inhibit NA on the drifted A/Sydney/5/2021 – see text for discussion.

We tested seroconversion and protection in DBA/2 and BALB/c mouse models, as summarized in Fig. 5.5A. Two doses of NA-VLP were administered intramuscularly to DBA/2 and BALB/c mice at a 3-week interval. Each dose contained 0.5 µg equivalent neuraminidase, with 6 mice per group. The groups received 25 µl of N1/09 TB VLP, N1 MS TB VLP, N1/09 loops-MS TB VLP, N1/19 loops MS TB VLP, or empty VLP, along with 25 µL of AddaVax. For the BALB/c strain, we vaccinated the mice with two doses and collected sera for analysis, marked as Experiment 1. For the DBA/2 strain, we followed the same vaccination procedure and then challenged the mice with a lethal dose of 200 LD_{50} of X-179A virus, followed by a 14-day observation period, marked as Experiment 2.

As shown in Fig. 5.5B, individual mouse sera binding to 2009 H1N1 NA was tested by ELISA using X179A (A/California/7/2009) virus-infected MDCK-SIAT1 cells (mice sera from Experiment 2). AF9C was used as a mAb control. Normalized binding was calculated as the AUC of the tested sample divided by the AUC of AF9C. For specific binding to N1/2009, sera from the N1/09 TB VLP and N1/09 loops MS TB groups showed similar levels, significantly higher than those from the N1 MS TB VLP and N1/19 loops MS TB VLP groups. This confirmed our hypothesis that, in addition to cross-binding within the same subtype, the loop grafting method can significantly increase specific antibody levels.

The inhibitory activity against X179A virus was evaluated using individual serum samples collected after two immunization doses (Fig. 5.5C), with corresponding IC50 values being summarized in Fig. 5.5D. Parallel ELLA assays were performed with N1 MS TB, and cross-inhibitory activity between N1 MS TB sera and X179A virus was confirmed (Fig. 5.5D). Notably, while the majority of ELLA inhibition was found to be mediated by the upsurface loop, the protein framework was also observed to contribute to a minor portion of ELLA-reactive epitopes. The observed cross-inhibition between N1 MS TB sera and X179A virus (Fig. 5.5D) implies shared epitopes, while the NAI antibodies transferred with the hybrid design predominantly located in the upsurface loop but partially dependent on the protein framework.

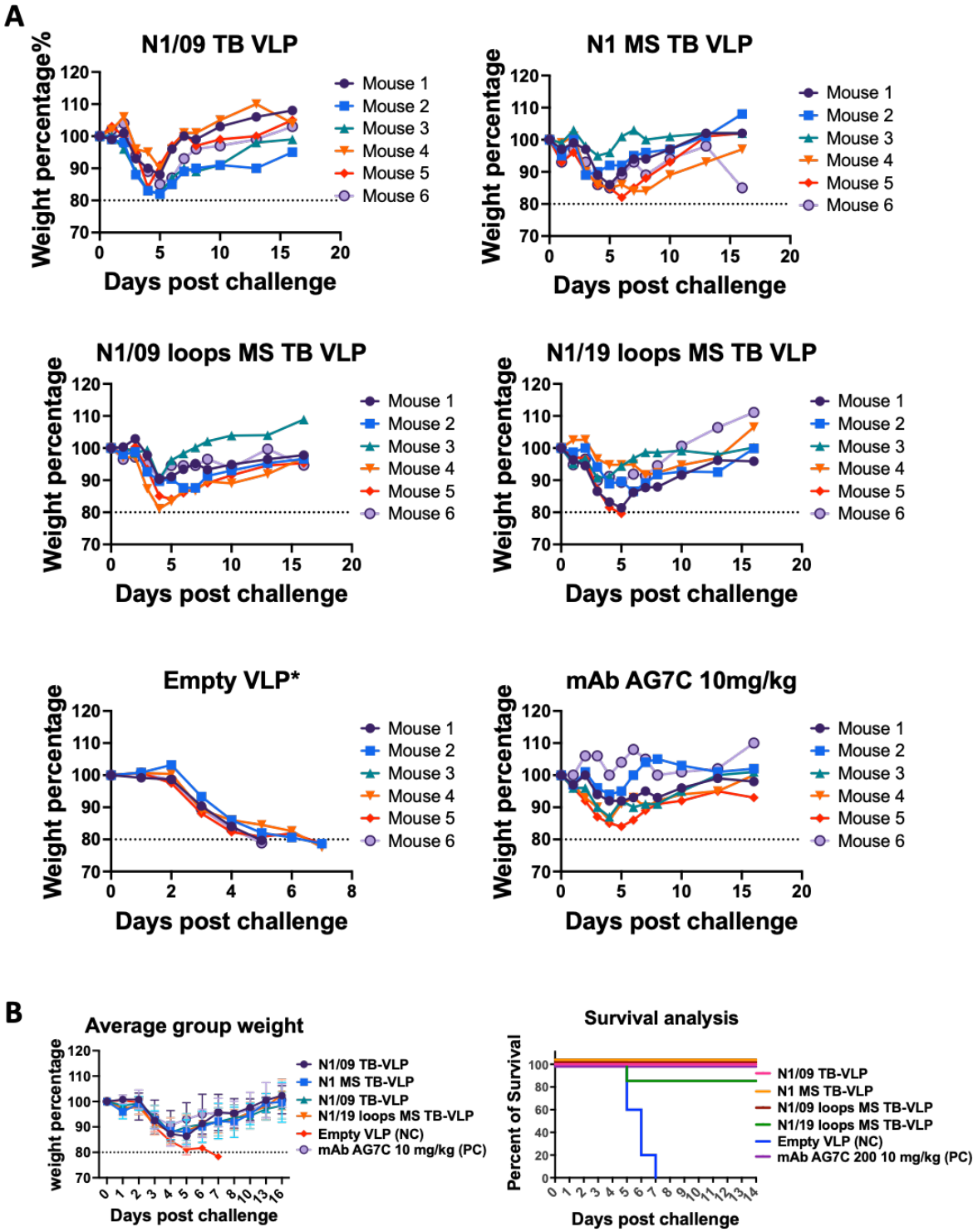

Figure 5.6 **Protection of DBA/2 mice from lethal X179A (2009 H1N1) challenge after immunisation with various loop grafted NAs**

A) Experimental protocol demonstrated in Figure 5.5 A Experiment 2: two doses of NA-VLP were injected intramuscularly to DBA/2 mice at 3-week interval in 5 sets. Mice were challenged with 200 LD_{50} X179A intranasally after tail bleeding and monitored for 14 days. *In the empty VLP group, one of the mice died after tail bleeding for unknown reasons, only 5 mice were recorded for weight change in this group.

B) Summary weight changes and survival analysis were plotted.

In Fig. 5.6, we present the individual mice weight change curves (Fig. 5.6A), along with the group averages (Fig. 5.6B) and survival analysis (Fig. 5.6C). All N1 groups survived the lethal dose X179A challenge, although with significant weight loss, including the more distantly related N1 MS TB group. This result confirmed the cross-protection within the same subtype, consistent with previous findings that the 2009 N1 could provide at least partial protection in mice and ferrets against avian H5N1 challenge (Easterbrook et al., 2012; Rockman et al., 2013; Sandbulte et al., 2009). This is also in line with well-characterized human mAbs that broadly cross-inhibit within the N1 subtype ((Rijal et al., 2020); reviewed in (Rajendran et al., 2021; Zhang & Ross, 2024).

While broad cross-reactivity of antisera within the N1 subtype has been reported ((Easterbrook et al., 2012; Rockman et al., 2013; Sandbulte et al., 2007), reviewed in (Giurgea et al., 2020), the protection effect within N1 subtype is not absolute (Wu et al., 2013). We noted that the Cambridge strain of H1N1 A/PR/8/1934 and N1 MS differ by 18 residues in the L01 and L23 loops, we observed that sera generated by N1 MS and N1 PR8 showed low level cross-reactivity against each other (Fig. 4.14). To further explore the relationship between loops and protection, we exchanged the L01 and L23 loops between N1 PR8 TB and N1 MS TB.

5.3 Loop-transfer between N1 MS and N1 PR8 NA

5.3.1 Successful expression of 2 loop-transfer N1 NAs

The successful expression of N1/09 loops MS TB and N1/19 loops MS TB provided strong evidence supporting the feasibility and practicality of the loop grafting method. However, an important question remained unanswered: can protective immunity be effectively transferred by merely transplanting the upper surface loops of NA? To address this critical question, we selected the N1 PR8 TB and N1 MS TB proteins as our loop grafting targets.

The upper loop sequences of N1 PR8 TB and N1 MS TB differ by 18 amino acids, and both tetrameric N1 variants have been shown to express with satisfactory yields, as detailed in Appendix 2. Building on this, we applied the same loop grafting principles to create two new hybrid constructs: N1 MS loops PR8 TB and N1 PR8 loops MS TB.

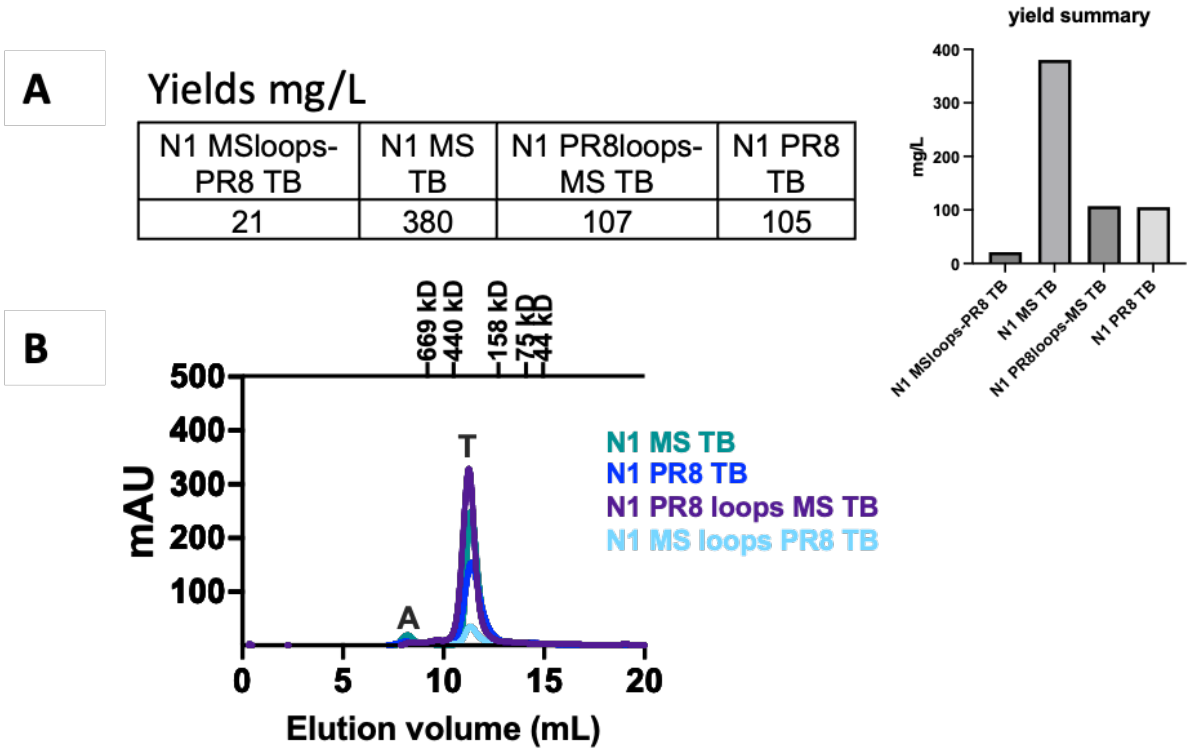

Figure 5.7 **Expression and purification of hybrid neuraminidases in which the L01 and L23 loops of 1934 H1N1 NA and 2021 H5N1 were exchanged**
A) Hybrid NAs successfully expressed with transferred L01 and L23 loops between N1 MS TB and N1 PR8 TB. The level of expression is shown for each combination.
B) Size exclusion chromatography (**Superdex® 200** Increase 10/300 **GL**) confirmed the tetrameric form of N1 PR8 loops MS TB hybrid and N1 MS loops PR8 TB hybrid proteins. An aggregate peak (A) and a tetramer peak (T) are marked. Low aggregation levels were observed in all the hybrid and parental recombinant neuraminidases. (Y-axis indicates absorbance at 280nm, peak difference due to loading amount of the protein).

The expression of these hybrid NAs was successful, though with slightly compromised yields compared to the original proteins. Specifically, the N1 MS loops PR8 TB expressed at 21 mg/L,

and N1 PR8 loops MS TB at 107 mg/L (as illustrated in Fig. 5.7 A & B). Despite the reduction in yield, the production levels were still sufficient for further characterization and analysis.

When subjected to SEC, all four proteins—N1 PR8 TB, N1 MS TB, N1 MS loops PR8 TB, and N1 PR8 loops MS TB—displayed a minor aggregation peak alongside a major tetramer peak (Fig. 3.4). This chromatographic profile is indicative of proper tetramer formation, suggesting that the recombinant proteins retained their structural integrity following loop grafting.

5.3.2 Characterisation of N1 MS loops PR8 TB and N1 PR8 loops MS TB

Similar to N1 loop grafting experiments, the newly engineered constructs, N1 MS loops PR8 TB and N1 PR8 loops MS TB, demonstrated high level enzymatic activity, as confirmed by the ELLA and the MUNANA assays (Figure 5.8 A&B). These findings indicate that the structural integrity and functionality of the enzymes were maintained post-grafting.

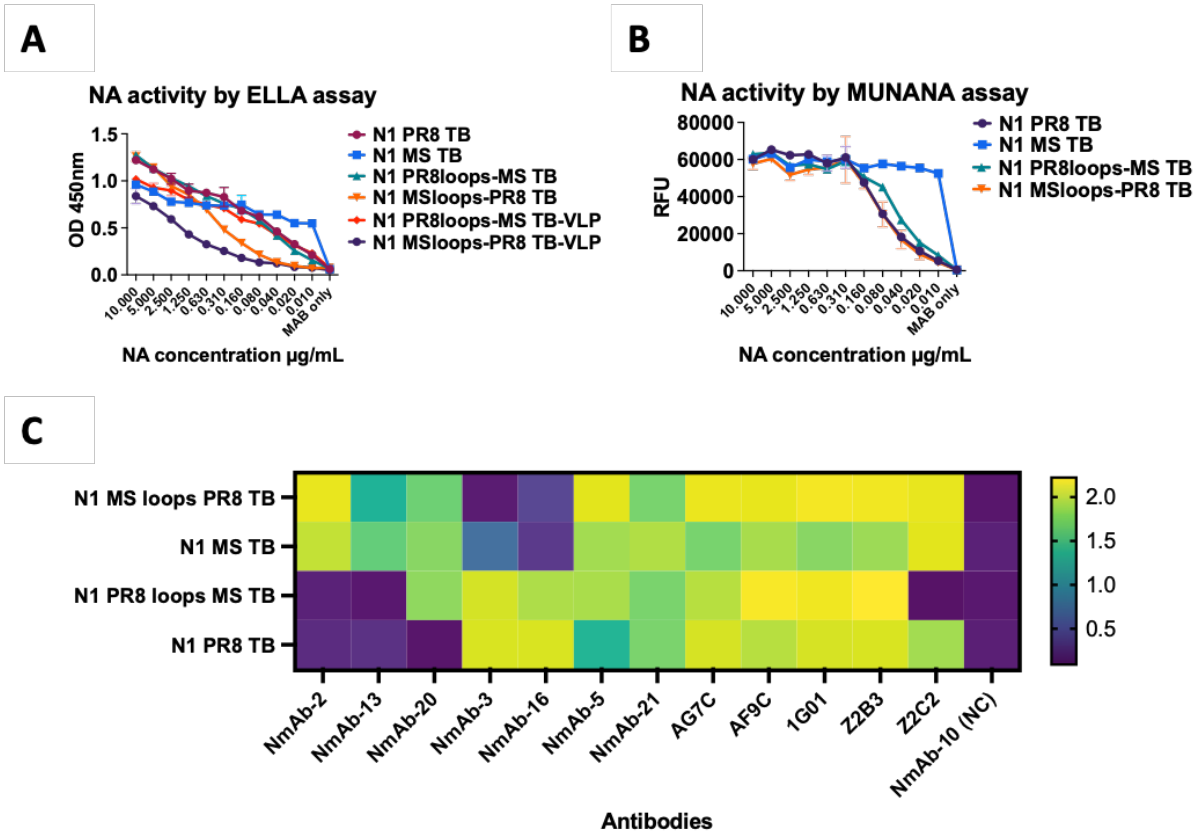

Figure 5.8 **Enzyme activity was retained and most loop specific epitopes were conserved on the hybrid NAs**
A, B) Enzymatic comparisons of purified tetramers of hybrid NAs, loop donor NA and loop recipient NA by ELLA (large substrate) and MUNANA (small substrate).
C) Epitope conservation between the loop donor and the hybrid neuraminidases, as detected with a set of N1 specific human monoclonal antibodies. The heat map was plotted according to ELISA of single point binding at 10 µg/mL mAb concentration. The N1 PR8 loops-MS hybrid retained binding by 8 of 9 MAbs that bound N1 PR8 TB. Binding by Z2C2 was lost, and binding by NmAb-20 was gained. Ten of ten antibodies that bound N1 MS TB bound the N1 MS loops-PR8 TB NA.

To assess the efficacy of epitope transfer through loop grafting, we conducted a detailed antibody binding study using a panel of 18 monoclonal antibodies. This panel was selected to comprehensively evaluate the antigenic properties of the hybrid NAs.

Among the 12 antibodies evaluated, 50% (6/12) demonstrated cross-binding to all four NA proteins, confirming the conservation of broad antigenic features across constructs. Three monoclonal antibodies (NmAb-2, NmAb-3, and NmAb-13) showed binding specificity

strictly dependent on MS and PR loops, validating successful epitope transfer from N1 MS loops.

Notably, antibody CD6 - previously characterized as a framework-binding protein - maintained its exclusive specificity for the N1 MS TB framework in this loop-grafting system. These findings both reinforce the role of framework-dependent epitope recognition and highlight its significance for rational vaccine design.

At the same time, three antibodies (Z2C2, NmAb-20, and NmAb-15) emerged as an outliers, showing an unexpected gain or loss of epitope recognition following the loop grafting process. This observation suggests that certain epitopes may be sensitive to structural changes introduced by grafting, which warrants further investigation.

We also performed a binding titration of the whole mAb panel against the listed recombinant NA or viruses, as listed in Appendix 9.

Consistent with earlier findings, the identification of 10 broadly reactive antibodies that bind across all four NA proteins reaffirms the broad immunity against NA. On the other hand, the detection of 3 loop-specific antibodies and one framework-dependent antibody highlights the nuanced effects of loop grafting on epitope presentation.

Overall, these results strengthen the validity of our loop grafting approach while also revealing the complexities of epitope transfer and the potential for unexpected outcomes in antigenicity.

5.3.3 Sera NA inhibition effect mostly transferred with NA loops in mice model

To ensure sufficient sera for all inhibition and cross-inhibition tests, we designed two separate experiments to gather comprehensive serological and protection data. As illustrated in Fig. 5.9A, two doses of NA-VLP were administered intramuscularly to mice at three-week intervals, with each dose containing 0.5 μg of neuraminidase. Each group consisted of six mice, which received 25 μL of N1 PR8 TB-VLP, N1 MS TB-VLP, N1 PR8 loops MS TB-VLP, N1 MS loops PR8 TB-VLP, or empty VLP, along with 25 μL of AddaVax. In Experiment 1, BALB/c mice were sacrificed three weeks post-injection for serological analysis, while in Experiment 2, mice were challenged with 1000 LD_{50} PR8 virus intranasally after tail bleeding and monitored for 14 days.

All seroconversion data presented in Fig. 5.9 were generated from sera collected in Experiment 1. Among the mice injected with N1 MS TB, 4 out of 6 showed no detectable inhibition titres, indicating a lower level of cross-inhibition between N1 MS TB and N1 PR8 compared to N1 MS TB and N1/09 TB. The IC50 values calculated from Fig. 5.9B are summarized in Fig. 5.9C. The results indicate that the majority of inhibition antibodies, as measured by ELLA, were successfully transferred through upper surface L01 and L23 loop grafting. N1 MS loops PR8 TB displayed slightly higher ELLA titres compared to the N1 MS TB backbone, suggesting the presence of some framework-dependent ELLA inhibition antibodies. A similar trend was observed in the N1 MS TB inhibition summary, where the majority of ELLA inhibition titres were loop-specific and successfully transferred through loop grafting.

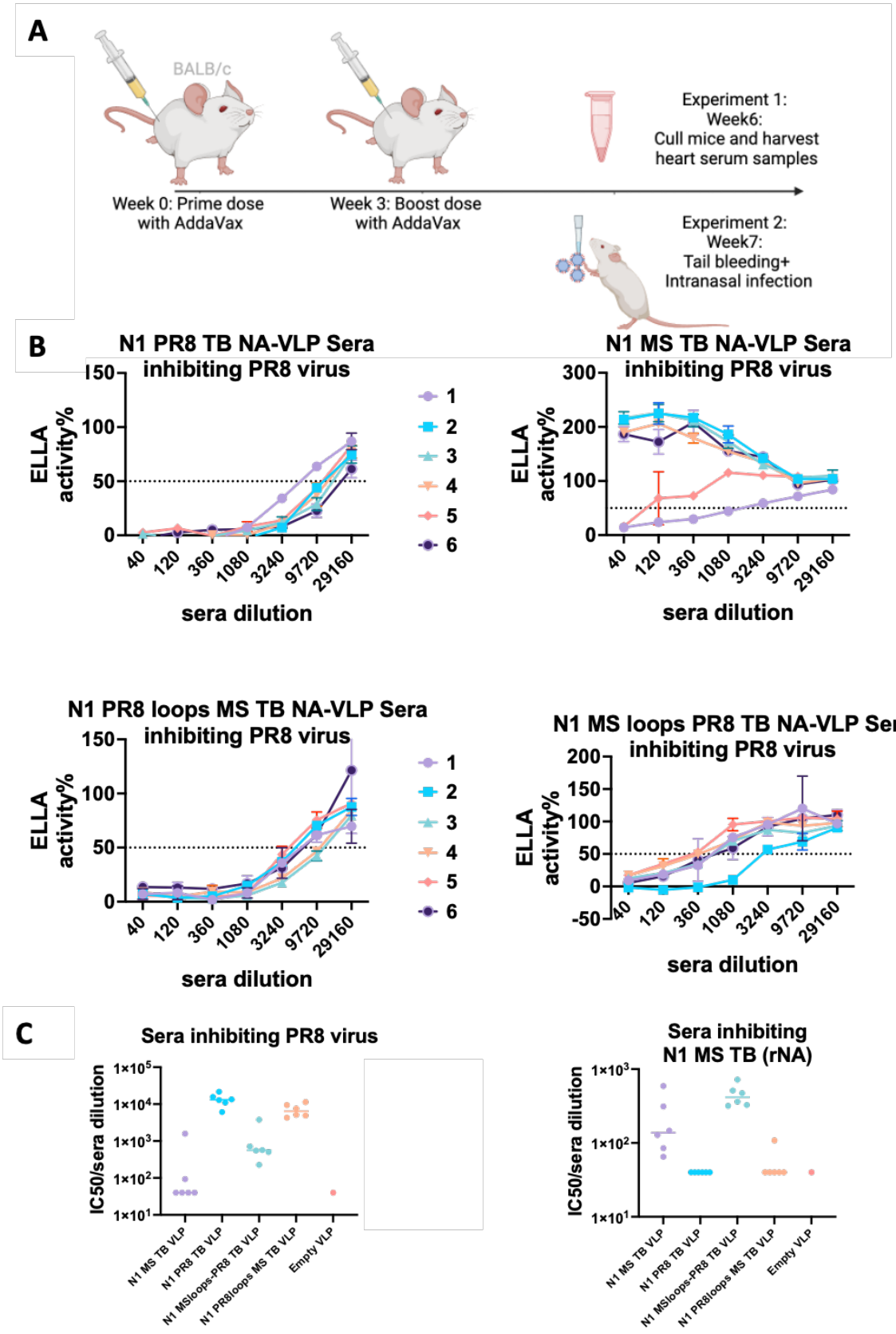
A
BALB/c
Week 0: Prime dose with AddaVax
Week 3: Boost dose with AddaVax
Experiment 1: Week6: Cull mice and harvest heart serum samples
Experiment 2: Week7: Tail bleeding+ Intranasal infection
B
N1 PR8 TB NA-VLP Sera inhibiting PR8 virus
N1 MS TB NA-VLP Sera inhibiting PR8 virus
N1 PR8 loops MS TB NA-VLP Sera inhibiting PR8 virus
N1 MS loops PR8 TB NA-VLP Sera inhibiting PR8 virus
ELLA activity%
sera dilution
40
120
360
1080
3240
9720
29160
1
2
3
4
5
6
C
Sera inhibiting PR8 virus
Sera inhibiting N1 MS TB (rNA)
IC50/sera dilution
N1 MS TB VLP
N1 PR8 TB VLP
N1 MSloops-PR8 TB VLP
N1 PR8loops MS TB VLP
Empty VLP

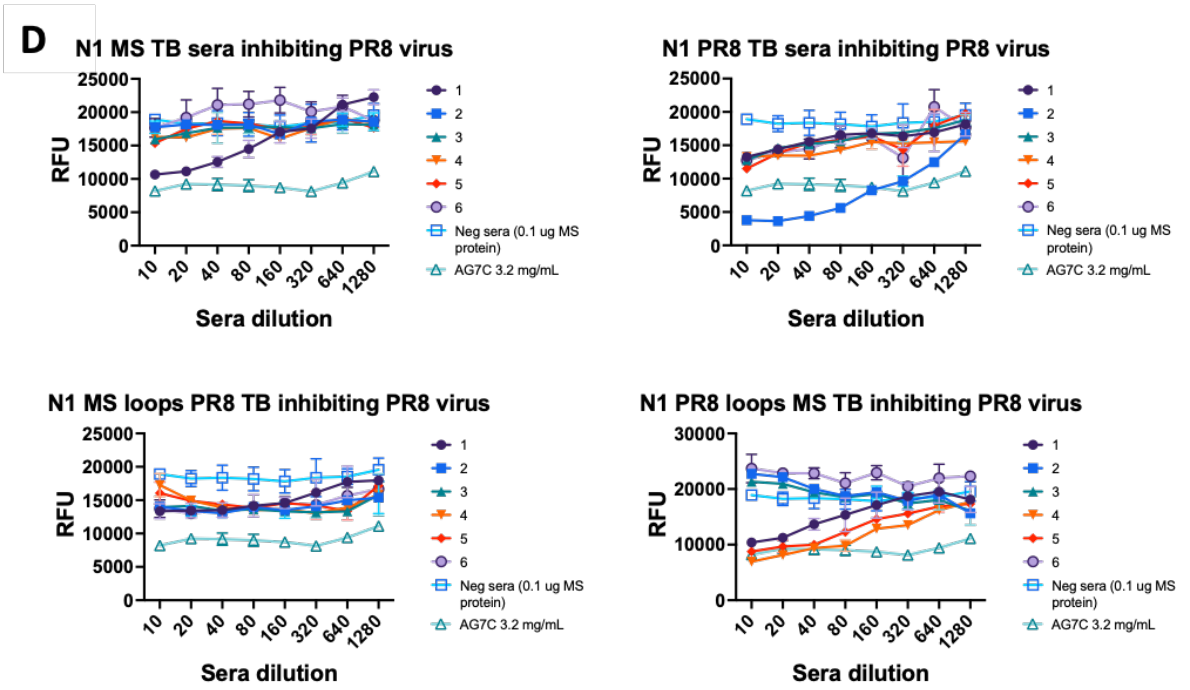

Figure 5.9 **Seroconversion of BALB/c mice immunised with hybrid NA-VLP vaccines derived from 1934 H1N1 and 2021 H5N1**

A) Experimental protocol: two doses of NA-VLP were injected intramuscularly to mice at 3-week interval in 5 groups. Each dose contains 0.5 µg equivalent neuraminidase. Each group contains 6 mice. 25 µL of N1 PR8 TB-VLP, N1 MS TB-VLP, N1 PR8 loops MS TB-VLP, N1 MS loops PR8 TB-VLP, and empty VLP together with 25 µL of AddaVax was administrated in each group. One set of mice were culled experimentally 3 weeks after the second dose for serology, a second set were challenged with 1000 LD_{50} PR8 intranasally after tail bleeding and monitored for 14 days.

B) Data obtained with serum samples from Experiment 1. Within each group, individual mice inhibiting PR8 virus were tested by ELLA.

C) Sera samples collected from Experiment 1. Within each group, inhibition to PR8 virus or N1 MS TB (rNA) was tested with individual boost serum sample via ELLA. ELLA IC 50 values against PR8 and N1 MS TB (rNA) were calculated and plotted. Note that the great majority of the inhibitory activity on NA matched the donor of the L01 and L23 loops.

D) Serum samples collected from Experiment 1. Inhibition of PR8 virus tested by MUNANA. Note that majority of mice do not mount a response that can inhibit the cleavage of the small substrate but with marked individual variation.

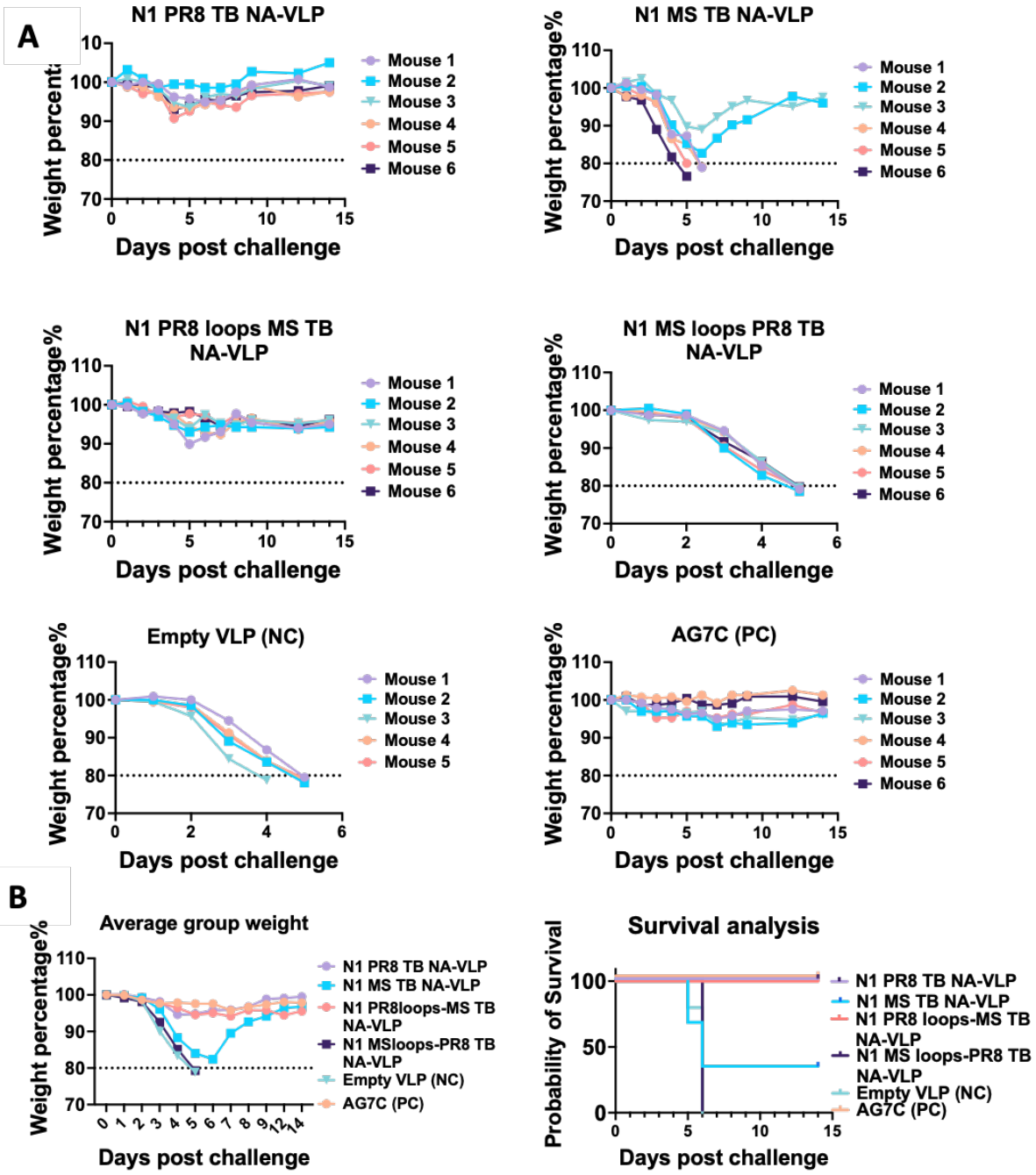

Figure 5.10 **Protection from challenge with A/PR/8/1934 of BALB/c mice immunised with hybrid NA-VLP vaccines derived from 1934 H1N1 and 2021 H5N1**
A) Experimental protocol demonstrated in Figure 5.9 A: two doses of NA-VLP were injected intramuscularly to BALB/c mice at 3-week interval in 5 sets. Mice were challenged with 1000 LD_{50} PR8 virus intranasally after tail bleeding and monitored for 14 days.
B) Summary weight changes and survival analysis were plotted.

In parallel with the serological tests, we challenged BALB/c mice with 1000 LD_{50} PR8 virus in Experiment 2 (Fig. 5.10). All mice in the N1 PR8 TB-VLP and N1 PR8 loops MS TB-VLP groups survived the challenge with negligible weight loss, comparable to the AG7C control group. In contrast, only 2 out of 6 mice in the N1 MS TB-VLP group survived, experiencing about 20% weight loss. None of the mice in the N1 MS loops PR8 TB or empty VLP groups survived. Consistent with the serological results, these findings confirm that protection can be effectively transferred through upper surface loop grafting.

5.4 Discussion and Implications

The successful expression of the four N1 hybrid NAs highlights both the potential and limitations of loop grafting as a strategy for enhancing the expression and stability of recombinant NA proteins. This approach proved effective within the N1 subtype, yielding hybrid proteins with significantly improved expression levels and reduced aggregation. However, the application of loop grafting between different subtypes, such as N1 and N6, requires further investigation. Understanding the structural and functional constraints that govern successful loop grafting will be crucial for refining this technique and extending its utility to a broader range of viral proteins.

In addition to addressing expression limitations, the PR8 and MS loop grafting experiments clearly demonstrated that the majority of enzyme-inhibiting antibodies can be successfully transferred via loop grafting. This also extends to the protective effects of these antibodies. However, it is important to note that not all B cell epitopes can be precisely transferred through this method, indicating some limitations in the specificity of epitope preservation.
Surface residues of viral proteins are known to exhibit higher mutation rates (Bhatt et al., 2011), leading to significant changes in circulating antigenicity over relatively short periods, such as within a decade (J. Gao et al., 2022). These rapid antigenic shifts present a considerable challenge for the development of a universal influenza vaccine. A strategy focused on the quick, up-to-date preparation of NA using the loop grafting method may offer a more practical solution. This approach leverages the advantages of broad NA immunity within a subtype while ensuring the feasibility of high-yield NA expression.

Such a method could provide a critical tool for influenza control, offering a balance between broad-spectrum protection and the adaptability needed to respond to the ever-changing landscape of influenza virus antigenicity. As we continue to refine loop grafting techniques, the potential for creating more robust and broadly protective NA-based vaccines becomes increasingly achievable, providing a viable alternative to the universal vaccine approach.

Chapter 6 N8 NA-VLP as a pandemic vaccine design

In this chapter, we expressed a diverse set of N8 sequences and extended the loop-transfer method to N8 head domains to overcome expression challenges. We conducted comprehensive characterization of the resulting constructs and performed immunization studies to contribute to future N8 pandemic preparedness efforts.

6.1 Expression of Multiple N8 NA Strains

6.1.1 N8: A Potential Threat to Public Health

H5N1 and its genetic reassortants (including H5N2, H5N5, H5N6, and H5N8) have been implicated in thousands of highly pathogenic avian influenza (HPAI) outbreaks globally in both poultry and wild birds (Harfoot & Webby, 2017; Yang et al., 2016). Among these, H5N8, alongside H5N1, has emerged as a potential pandemic threat. The outbreak in 2020 led to numerous cases in poultry and wild birds worldwide, resulting in significant mortality (Shi & Gao, 2021).

The virus has demonstrated the ability to cross species barriers, infecting mammals, including humans. This was evidenced by cases detected in Russian poultry workers (Tajudeen, 2021). Studies have shown that H5N8 can replicate in human respiratory tract tissues and bind to human-like receptors, although less efficiently than to avian receptors (Y.-I. Kim et al., 2014). Influenza's capacity for genetic reassortment with other circulating avian viruses could potentially lead to the emergence of novel strains with enhanced human infection capabilities (Tate, 2018).

Notably, human-isolated H3N8 viruses have been able to transmit among ferrets after single round expansion in vitro (Gu et al., 2024; Sun et al., 2023), causing severe pneumonia. Human populations, despite seasonal H3N2 vaccinations, remain immunologically naive to the novel H3N8 strain. Thus, in addition to focusing on H5Nx avian influenza, addressing population vulnerability to HxN8 could be another crucial strategy in preventing potential influenza pandemics.

Given the potential for N8 viruses to infect humans and the lack of preexisting immunity in the population, there is a pressing need for enhanced surveillance, research, and preparedness measures to mitigate this emerging public health threat.

6.1.2 Self-Tetramerizing N8/20 TetDminus

Unlike non-influenza neuraminidases, it is widely acknowledged that influenza neuraminidase (NA) requires tetramerization to maintain its catalytic activity (Da Silva et al., 2013; Von Grafenstein et al., 2015). The conformational transitions of the NA head are crucially influenced by its assembly state due to interface hydrogen-bonding, which contributes to the structural integrity of the binding site and maintains catalytic activity (Von Grafenstein et al., 2015).

For viral neuraminidase cleaved with pronase, the tetrameric structure is preserved along with enzymatic activity (Ward et al., 1982). However, when expressed as soluble recombinant proteins, the native stalk is often replaced with artificial tetramerization domains to enhance stability and solubility (Schmidt et al., 2011; Streltsov et al., 2019). Most NAs expressed without an external tetramerization domain tend to express as monomers or dimers, resulting in impaired enzymatic activity (Da Silva et al., 2013; Deng et al., 2021; McMahon et al., 2020; Strohmeier et al., 2021).Interestingly, a deletion in the NA stalk can increase virulence in chickens, enhancing viral replication and inflammatory responses (Munier et al., 2010).

As demonstrated in Figures 3.3, 3.4D, 3.5H, and 3.6G, N8/20 TetDminus (without tetramerization domain) expressed as a tetramer with enhanced NA activity, whereas the TB-linked construct failed to express in ExpiCHO or Expi293 expression systems. These findings prompted us to examine whether this rare self-tetramerization capability represents a unique property of N8/20 or constitutes a more general characteristic of N8 strains - a determination with important implications for optimizing future N8 NA production platforms.

6.1.3 Multiple N8 strains alignment and selection for recombinant NA design

We generated a comprehensive phylogenetic tree for a selection of N8 neuraminidase (NA) sequences, as depicted in Fig. 6.1. This phylogenetic analysis allows us to understand the evolutionary relationships and divergence among the N8 strains. Within this extensive set of sequences, we identified three N8 NA sequences that correspond to published structural data: A/duck/Ukraine/1/1963 (PDB: 2HT5), A/harbor_seal/Massachusetts/2011 (PDB: 4WA3), and A/gyrfalcon/Washington/41088-6/2014 (PDB: 5HUN). These sequences were selected due to their well-documented structural characteristics, providing a solid foundation for comparative analysis of key residues for structural base engineering.

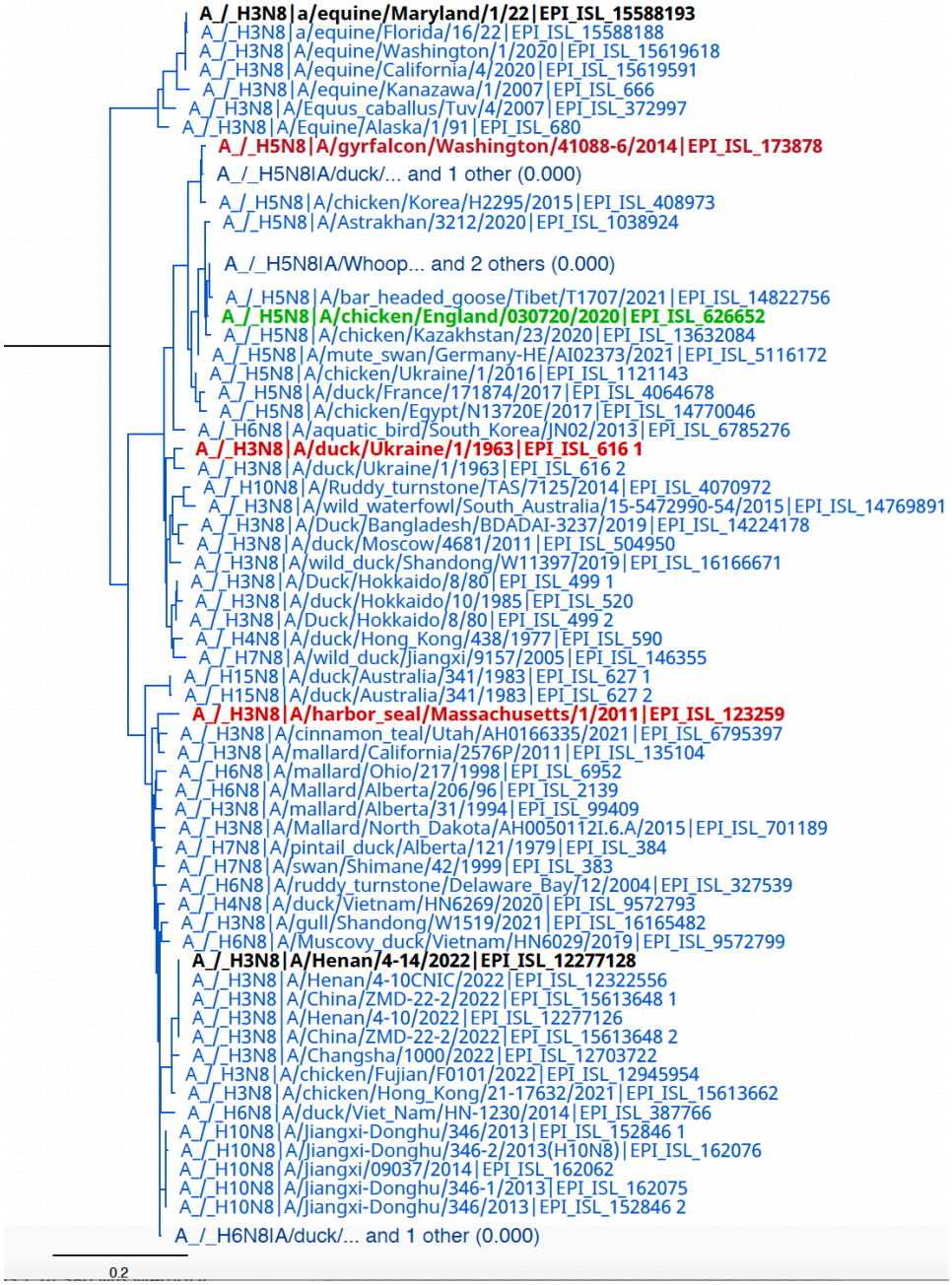

Figure 6.1 **Phylogenetic tree generated from selected N8 NA amino acid sequences**
The N8 NAs expressed were marked with colors: Green: N8/20 sequence we have expressed with VASP, TB or without tetramerization domain. Red: N8 NA with structure recorded in PDB. Black: Additional NAs to picked for comparison and analysis.

In addition to these, we included A/Henan/4-14/2022 (human-isolated strain mentioned by Sun et al. 2023) and A/equine/Maryland/1/22 from distinct branches of the phylogenetic tree to ensure a broader representation of the genetic diversity within the N8 subtype (Fig. 6.1). This selection aims to enhance our understanding of the structural and functional variations across different N8 strains, which is critical for designing effective recombinant NAs.

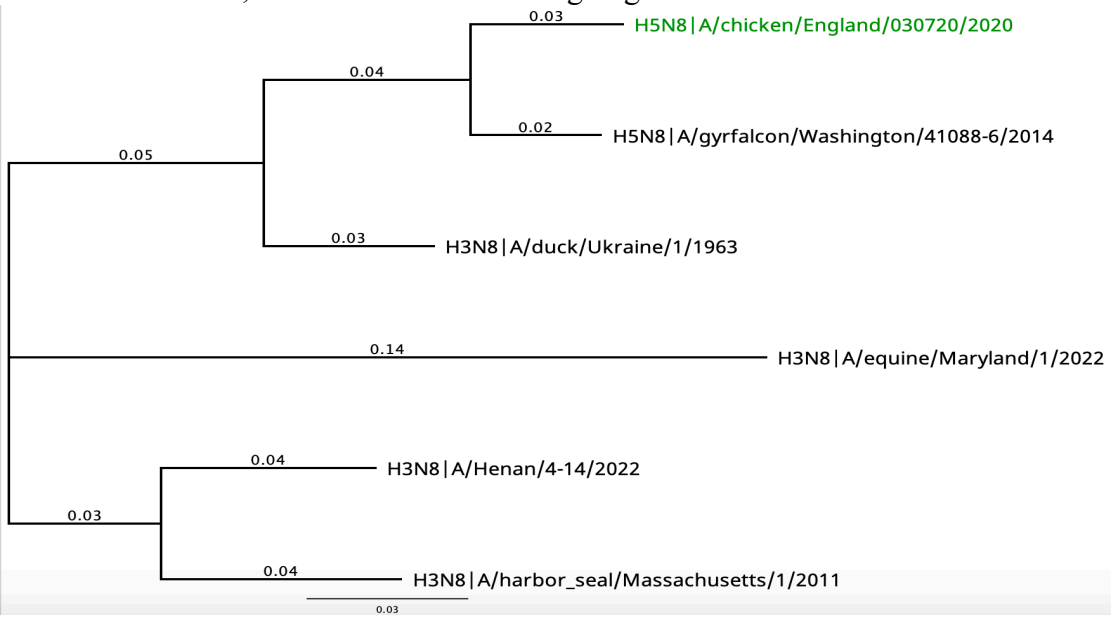

Figure 6.2 **Phylogenetic tree generated from expressed N8 NA amino acid sequences** Numbers on branches = substitutions per site

Furthermore, Fig. 6.3 shows a detailed alignment of the N8 NA sequences. In this alignment, specific loop regions have been marked according to the published structural data of the N8 NA sequence from 1963 (PDB: 2HT5). These loop regions are of particular interest because they often play critical roles in the enzyme's catalytic activity and antigenicity as we have demonstrated in Chapter 5. By comparing these regions across different N8 sequences, we can identify key structural motifs and potential sites structural engineering.

To simplify the recombinant protein names, we standardized abbreviated N8 names in Table 6.1. Instead of writing the whole influenza names, we simply marked the N8 head as sequencing time or location.

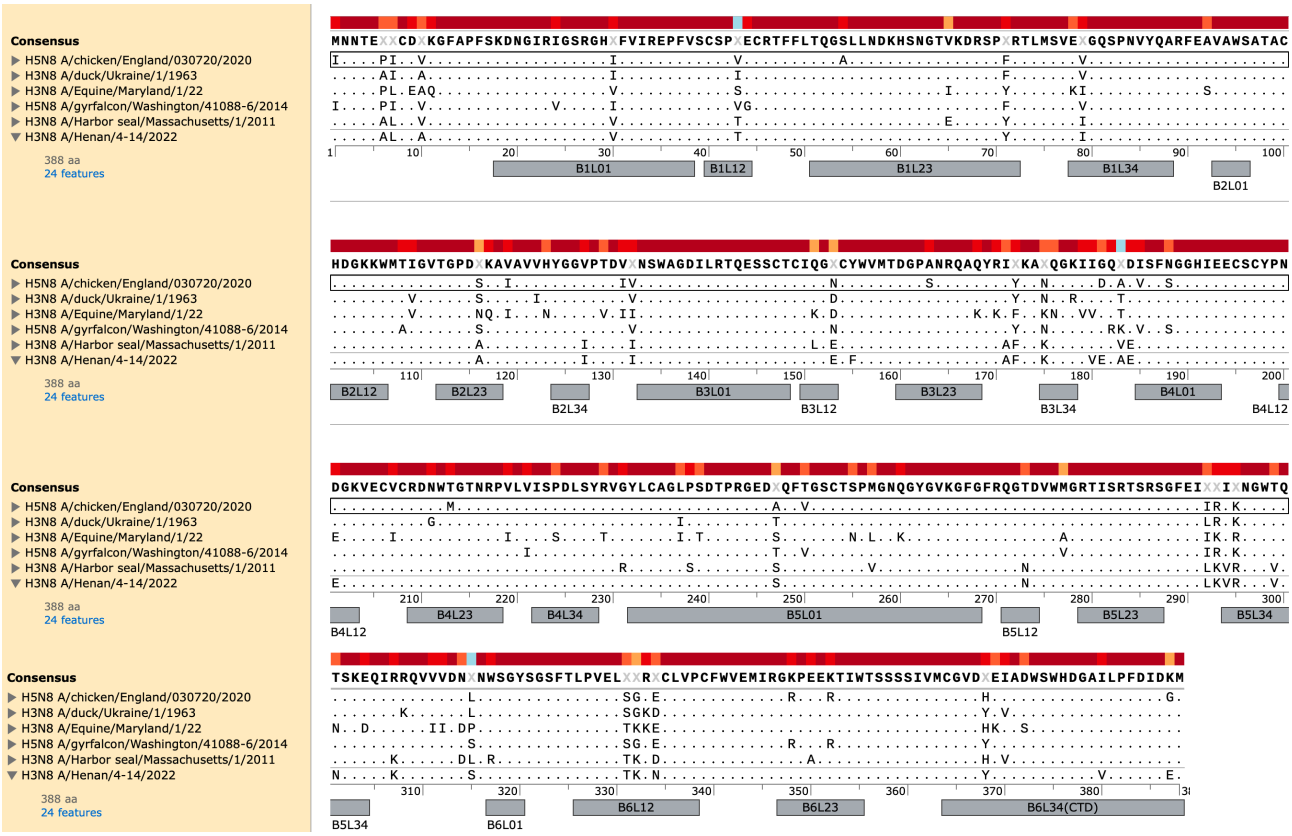

Figure 6.3 **Sequence alignment generated from selected N8 NA head amino acid sequences** Six selected sequences (aa83-470) were aligned starting from 83-INN or 83-MNN. Loop regions were marked according to the structure of NA of H3N8 A/duck/Ukraine/1/1963 (PDB: 2HT5)

6.1.4 N8 Expression and Characterization

Detailed construct designs of the chosen N8 NA sequences are listed in Appendix 1. We attempted to express the five selected N8 sequences without any tetramerization domain to investigate the self-tetramerization phenomenon observed with N8/20 TetDminus (Chapter 3, Fig.3.3, Fig.3.4). The yields of all selected N8 NA sequences are listed in Table 6.1.

Table 6.1 N8 NA head expression yields with or without TB

No.	protein name	N8 Strain	domain	mg/L
1	N8/1963 TetDminus	H3N8 A/duck/Ukraine/1/1963	None	9.4
2	N8/2011 TetDminus	H3N8 A/harbor_seal/Massachusetts/1/2011	None	No expression
3	N8/2014 TetDminus	H5N8 A/gyrfalcon/Washington/41088-6/2014	None	23
4	N8/2022 TetDminus	H3N8 A/equine/Maryland/1/22	None	No expression
5	N8 Henan TetDminus	H3N8 A/Henan/4-10/2022	None	1.1
6	N8 Henan TB	H3N8 A/Henan/4-10/2022	TB	1
7*	N8/20 TetDminus	H5N8 A/chicken/England/030720/2020	None	11-43.2
8*	N8/20 VASP	H5N8 A/chicken/England/030720/2020	VASP	0-16, precipitation
9*	N8/20 TB	H5N8 A/chicken/England/030720/2020	TB	0-1.5, precipitation

These N8 NA designs were expressed more than twice. N8/20 VASP and N8/20 TB were not expressed in some of the transfections (indicated by yield 0 mg/L).

Only three of the chosen N8 NA heads without a tetramerization domain successfully expressed, albeit at relatively low yields.. The expressed N8/1963 TetDminus, N8/2014 TetDminus, and N8 Henan TetDminus were analysed using reducing SDS-PAGE, as depicted in Fig. 6.4B in Lanes 1, 2, and 5. The 2-µg protein bands were not as clear as those of N8/20 TetDminus. With BS-3 crosslinking, the proteins were barely visible on the gel, showing only faint bands around 50 kDa. Similar to the crosslinked N1/19 TetDminus loaded SDS-PAGE (Fig. 3.3), this suggests the presence of intramolecular misfolding and some aggregation formation. This was further confirmed by size-exclusion chromatography (SEC), which showed a major aggregation peak, as depicted in Fig. 6.5C.

A

Lane	Recombinant NA
1	N8/1963 TetDminus
2	N8/2014 TetDminus
3	N8/20 TetDminus
4	N8 Henan TB
5	N8 Henan TetDminus

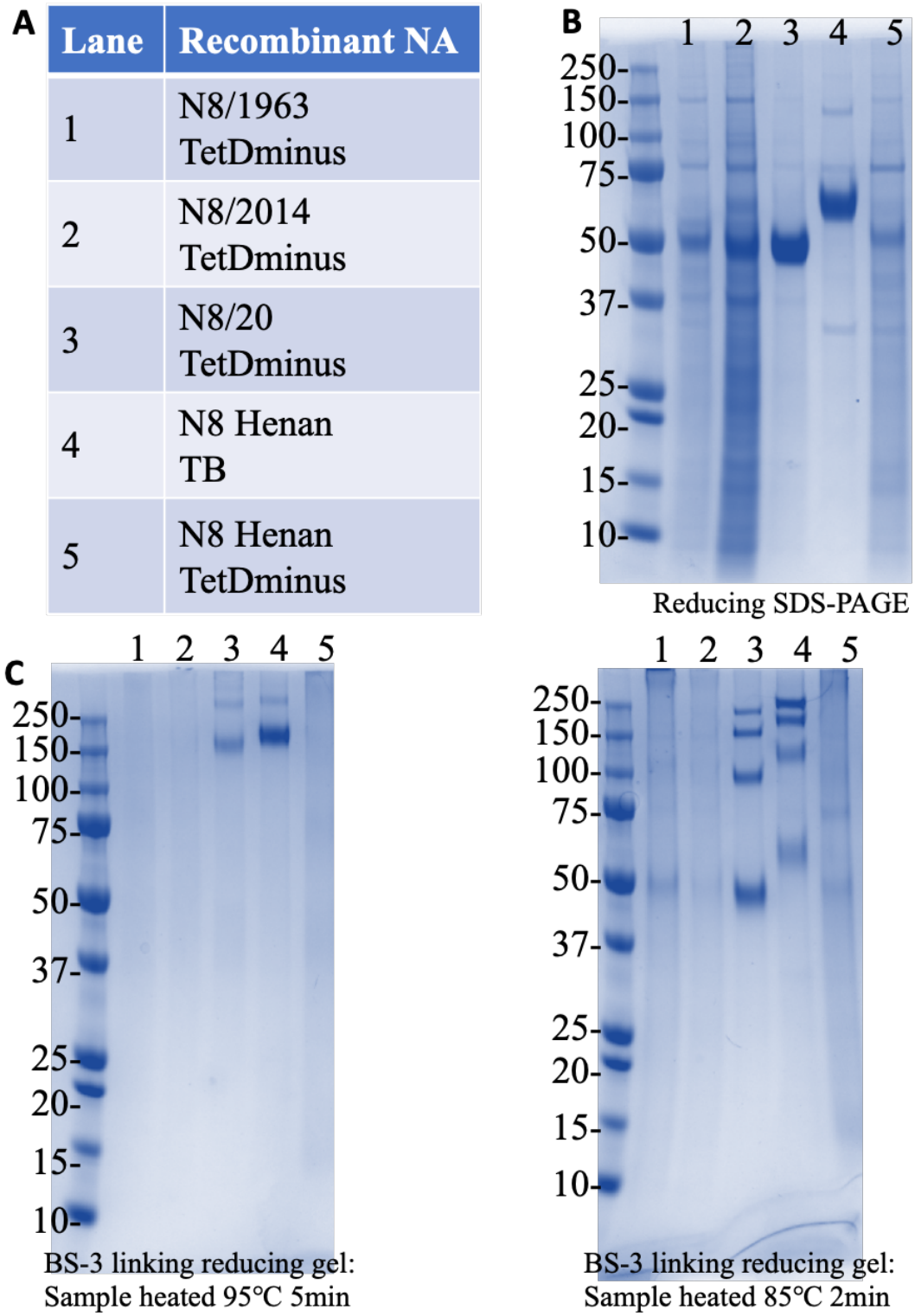

Figure 6.4 **Characterization of recombinant N8 NA by SDS-PAGE**
A) Proteins loaded in each lane were labelled.
B) Five recombinant N8 NAs were heated at 85 ℃ for 2 mins and loaded to Reducing SDS-PAGE.
C) After 30 min cross-linking with BS-3, 2 µg of the linked neuraminidase were loading to reducing SDS-PAGE. Samples were heated in two different conditions.

Similar to most NA expressed without a tetramerization domain, N8/1963 TetDminus and N8 Henan TetDminus showed impaired enzymatic activity (Fig. 6.5A, B). N8/2014 TetDminus showed moderate level enzymatic activity. However, for N8/2014 TetDminus, the aggregates made up the majority of its composition, making it difficult to confirm its tetramerization status. With the expression and characterization of the five chosen N8 NA sequences, we concluded that the self-tetramerization phenomenon was strain-specific rather than subtype-specific. This highlights the polymorphic and heterogeneous nature of NA, as well as the expression difficulties encountered with specific strains.

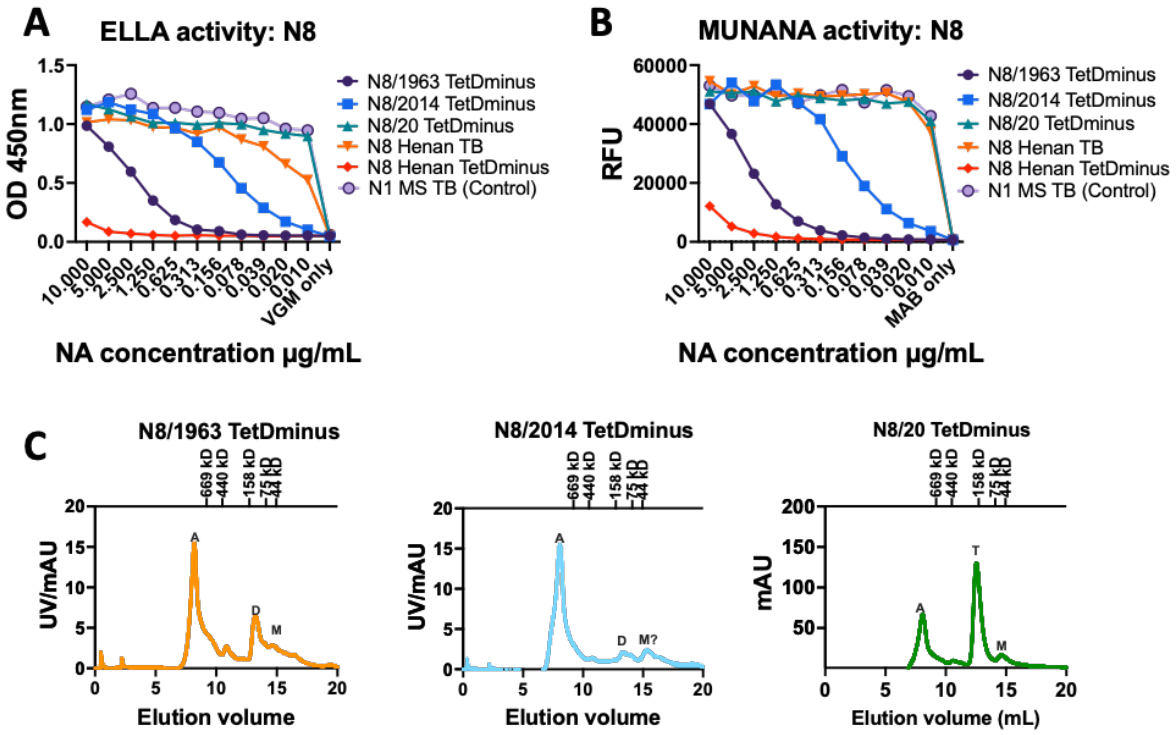

Figure 6.5 **Characterization of recombinant N8 NA**
A,B) Enzyme activity comparison via ELLA and MUNANA
C) The self-tetramerization phenomenon observed in N8/20 TetDminus is not evident in N8/1963 TetDminus and N8/2014 TetDminus.

We also attempted to express the TB-linked N8 Henan head for pandemic preparedness. Despite the low yield (1 mg/L, listed in Table 6.1), the enzymatic activity of N8 Henan TB was comparable to our exceptional N8/20 TetDminus and N1 MS TB (Fig. 6.5A, B), with a clear tetramer band shown in BS-3 crosslinked SDS-PAGE (Fig. 6.4C).

6.2 N8 NA-VLP as Vaccine Candidate

To evaluate the potential of N8 neuraminidase virus-like particles (NA-VLPs) as a vaccine candidate, we conducted an immunization study in chickens. This experiment was performed in collaboration with Munir Iqbal's research group at the Pirbright Institute.

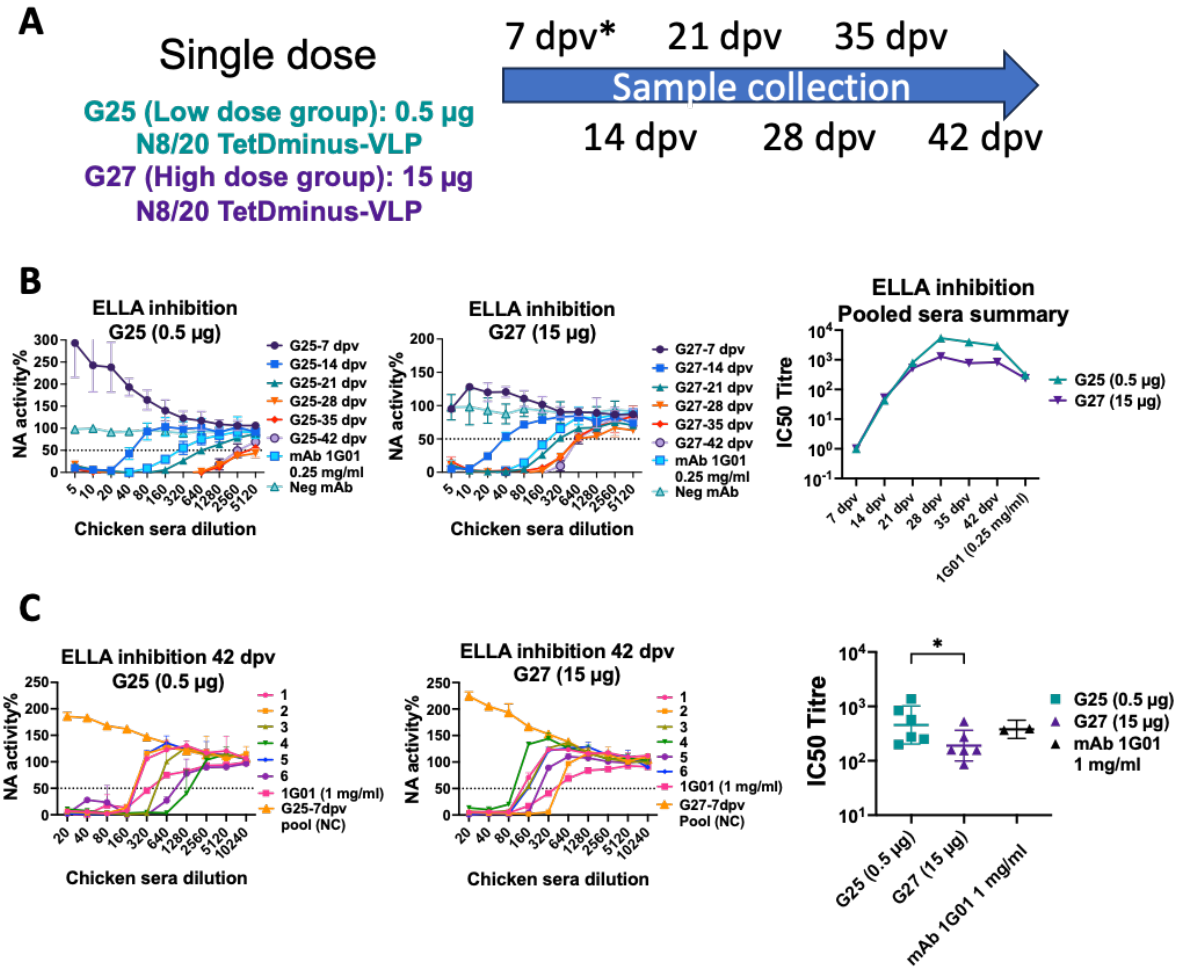

Figure 6.6 **Lower dose of N8 NA-VLP elicited higher inhibition antibody response in chicken model**
A) Chicken (n=6/group) were vaccinated with single dose NA-VLP (subcutaneous, adjuvanted with ISA71), sera samples were collected on Day 7, 14, 21, 28, 35, 42 post vaccination (dpv). Experiment was done by Munir Iqbal's group at the Pirbright Institution. Sera samples were tested for ELLA inhibition in our lab.
B) NA inhibition of the pooled sera collected at different time points were tested with ELLA. G25 vaccinated with 0.5 µg of N8/20 TetDminus VLP had consistently higher inhibition titres compare to the 15 µg group at all time points.
C) Individual ELLA inhibition titre were tested with N8/20 TetDminus recombinant NA using 42 dpv samples. IC 50 titres were plotted as Geometric mean with 95% confidence interval. Statistical significance was tested by Mann Whitney (Unpaired t-test non-parametric) test, p=0.04.

The experiment design is demonstrated in Fig 6.6A Two groups of chickens (n=6 per group, mixed sex) were vaccinated with a single dose of N8 NA-VLP. The vaccine was administered subcutaneously and adjuvanted with ISA71. The groups received either low dose 0.5 µg or high dose 15 µg of N8/20 TetDminus VLP.

Serum samples were collected at regular intervals post-vaccination: Days 7, 14, 21, 28, 35, and 42. These samples were subsequently analysed for neuraminidase inhibition using ELLA in our lab.

Initially, we assessed NA inhibition using pooled sera from each time point. Interestingly, the group vaccinated with low-dose (0.5 µg) of N8/20 TetDminus VLP consistently exhibited higher inhibition titres compared to the high-dose (15-µg) group across since day 28 post-vaccination as shown in Fig. 6.6B.

To further investigate this observation, we performed individual ELLA inhibition tests using the 42 days post-vaccination (dpv) samples (Fig 6.6C). The recombinant N8/20 TetDminus NA was used as the target antigen. IC50 titres were calculated and presented as geometric means with 95% confidence intervals. To determine the statistical significance of the observed differences between the two dosage groups, we employed the Mann-Whitney test (also known as the unpaired t-test for non-parametric data). The analysis revealed a significant difference between the groups ($p = 0.04$).

Our results demonstrate that the lower dose (0.5 µg) of N8 NA-VLP elicited significantly higher inhibition titres compared to the higher dose (15 µg). This observation is particularly noteworthy as it indicates that a 30-fold lower antigen dose was able to induce a more robust immune response.

6.3 Interface Mutations and Loop-transfer Method to Overcome N8 Expression Difficulty

6.3.1 Structurally modified N8 expression

Similar to the challenges faced with pandemic N1 expression, expressing potential pandemic N8 proved difficult. To overcome the expression difficulty, we selected N8 Henan head as the loop donor and N8/20 TetDminus as the backbone.
Inspired by the successful transition from "open-conformation" to "closed conformation" (Ellis et al., 2022) and previous observations that hybrid NA properties about structures tend to resemble the backbone NA, Pramila Rijal proposed an "interface change" approach. This involved comparing interface residues and replacing them with those from more stable structures (Appendix 6.1).

We generated two hybrid N8 Henan loops N8/20 by replacing the loops of N8/20 TetDminus and N8/20 TB with loops from N8 Henan head. Additionally, we constructed a structurally engineered N8 Henan TetDminus with interface mutations by replacing distinct interface residues between N8/20 head and N8 Henan head.

Table 6.2 compares yields of parental and structurally modified N8 NAs. Notably, N8 Henan loops N8/20 TetDminus expressed at 533 mg/L, the highest yield among our constructs. N8 Henan loops N8/20 also showed improved expression compared to its backbone. Unfortunately, the TB-linked hybrid N8 precipitated post elution. The N8 Henan TetDminus with interface mutations improved yield from 1.1 mg/L to 23.6 mg/L.

Table 6.2 N8 NA yield improvement by interface mutations and loop transfer method

No.	Recombinant protein name	N8 Strain	Tetramerization domain	Yield mg/L (highest yield was listed for multiple expressions)
1	N8 Henan TetDminus	H3N8 A/Henan/4-10/2022	None	1.1
2	N8 Henan TB	H3N8 A/Henan/4-10/2022	TB	1
3	N8/20 TetDminus	H5N8 A/chicken/England/030720/2020	None	43.2
4	N8 Henan TetDminus with interface mutations	Modified H3N8 A/Henan/4-10/2022*	None	23.6

5	**N8 Henan loops N8/20 TetDminus**	**Hybrid**	**None**	**533, precipitate in DPBS, resolve in Tris buffer (pH=8.0)**
6	**N8 Henan loops N8/20 TB**	**Hybrid**	**TB**	**70, precipitate in DPBS, fail to resolve**
7	**N8 Henan loops N1 MS TB**	**Hybrid**	**TB**	**No expression**

*Modification method was explained in Appendix 10

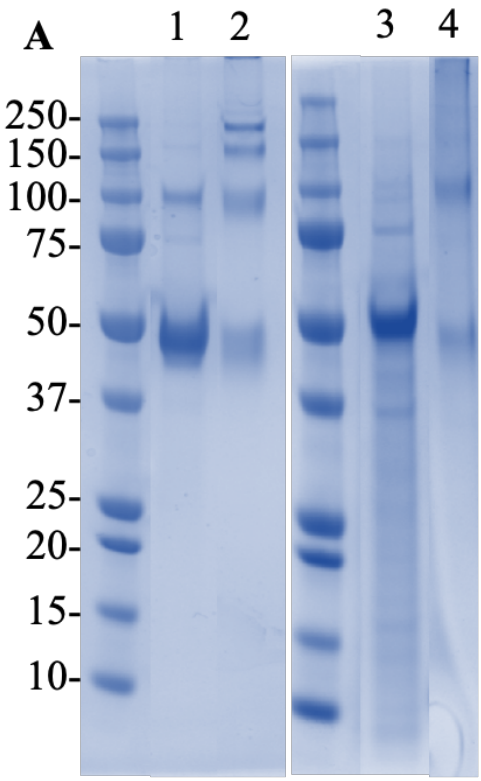

Lane	All loaded with 2 µg	Comment
	N8 Henan loops N8/20 TetDminus	
1	reducing	Heated at 85°C, 2min
2	BS-3 linked reducing	Heated at 85°C, 2min
	N8 Henan TetDminus with interface mutations	
3	reducing	Heated at 85°C, 2min
4	BS-3 linked reducing	Heated at 85°C, 2min

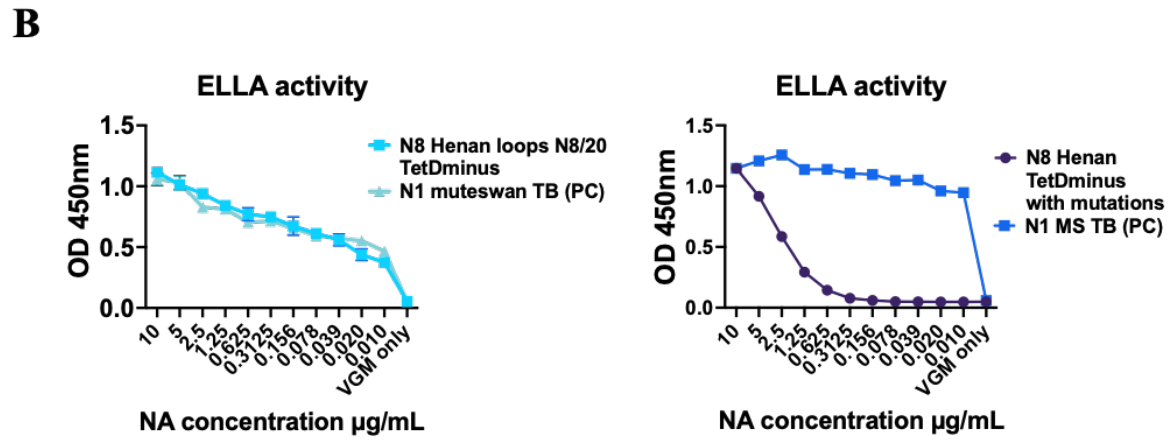

Figure 6.7 **Hybrid N8 Henan loops N8/20 TetDminus and N8 Henan TetDminus with interface mutations restored NA activity without external tetramerization domain**
A) Self-tetramerization were observed in N8 Henan loops N8/20 TetDminus. Additionally, N8 Henan TetDminus with interface mutations had the capability to form dimmers.
B) N8 Henan loops N8/20 TetDminus exhibited remarkable ELLA activity, comparable to that of N1 MS TB. Interfaces changes of N8 Henan TetDminus resulted in improved ELLA activity.

Cross-linking SDS-PAGE confirmed tetrameric N8 Henan loops N8/20 TetDminus and dimeric N8 Henan TetDminus with interface mutations (Fig 6.7A). Both engineered N8 Henan TetDminus constructs showed improved enzymatic activity compared to the original, nearly inactive N8 Henan TetDminus (Fig 6.5A). N8 Henan loops N8/20 TetDminus activity was comparable to N1 MS TB.

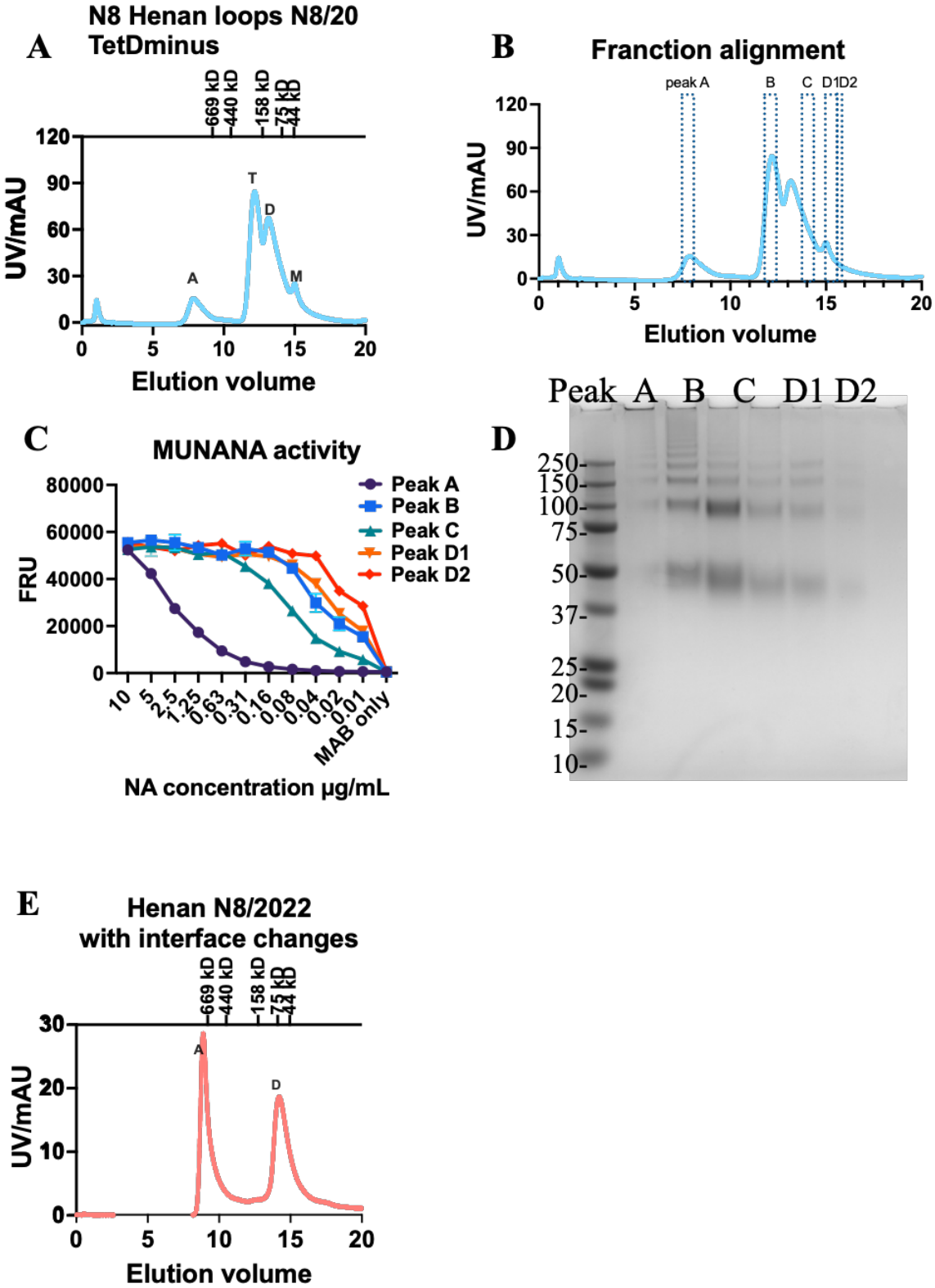

Figure 6.8 **Hybrid N8 Henan loops N8/20 TetDminus were characterize as mixture of aggregations, tetramers, dimers and monomers**

A) Mixture of aggregations, tetramers, dimers and monomers was observed with N8 Henan loops N8/20 TetDminus.

B) Fraction alignments were designated.

C) Enzymatic activity of various peaks were assessed using MUNANA

D) Fractions marked in B) were subjected to SDS-PAGE after 30 minutes of cross-linking with BS-3.
E) Mixture of aggregations and dimers was observed with N8 Henan with interface changes.

Surprisingly, N8 Henan loops N8/20 TetDminus showed a complex mixture of aggregates, tetramers, dimers, and monomers in SEC, unlike the backbone N8/20 TetDminus (Fig.6.8A). We selected five fractions from SEC elution (peaks A to D, Fig. 6.8B) for MUNANA assay and BS-3 linked gel analysis. All peaks except aggregation peak A showed high enzymatic activity (Fig. 6.8C), consistent with ELLA results (Fig. 6.7B). BS-3 cross-linking revealed monomeric, dimeric, and tetrameric bands in peaks B, C, D1, and D2, suggesting an equilibrium between these forms (Fig. 6.8D).

The interface-engineered N8 Henan TetDminus showed a combination of aggregates and dimers in SEC (Fig. 6.8E). This interface substitution successfully produced a dimeric stalkless NA, improving protein expression yield ~20-fold and with low-to-moderate level enzymatic activity.

6.3.2 Loop Transferred N8 NA-VLP in Mice Model

Following our initial findings on the efficacy of N8 NA-VLPs in chickens, we extended our research to investigate the potential of three N8 constructs in preparing for a possible N8 pandemic. This expanded study aimed to evaluate the serum response to three related N8 variants in a mouse model.

Three groups of female BALB/c mice (aged 6-8 weeks) were immunized using a prime-boost regimen. The vaccines were administered intramuscularly (IM) and adjuvanted with AddaVax. The immunization schedule involved a prime dose followed by a boost dose at a 3-week interval, as illustrated in Fig. 6.9A. The three experimental groups received 0.5 μg of the following N8 NA-VLPs: N8/20 TetDminus; N8 Henan loops N8/20 TetDminus; N8 Henan TB. Three weeks after the boost immunization, mice were humanely euthanized, and serum samples were collected for subsequent analysis.

We employed two complementary assays to evaluate the immune responses elicited by the different N8 constructs: ELLA and MUNANA assay:
Individual serum samples were tested for their inhibitory activity against three N8 variants: N8/20 TetDminus, N8 Henan loops N8/20 TetDminus, and N8 Henan TB (Fig. 6.9B). The summary results, presented as individual IC50 values, are shown in Fig. 6.9C. Sera from mice immunized with N8 Henan loops N8/20 TetDminus exhibited higher inhibition titres against N8 Henan TB compared to N8/20. This finding supports our hypothesis that the majority of ELLA inhibition-related epitopes are located on the upper surface loops of the neuraminidase protein and these antigenic sites are transferred with loop-grafting.

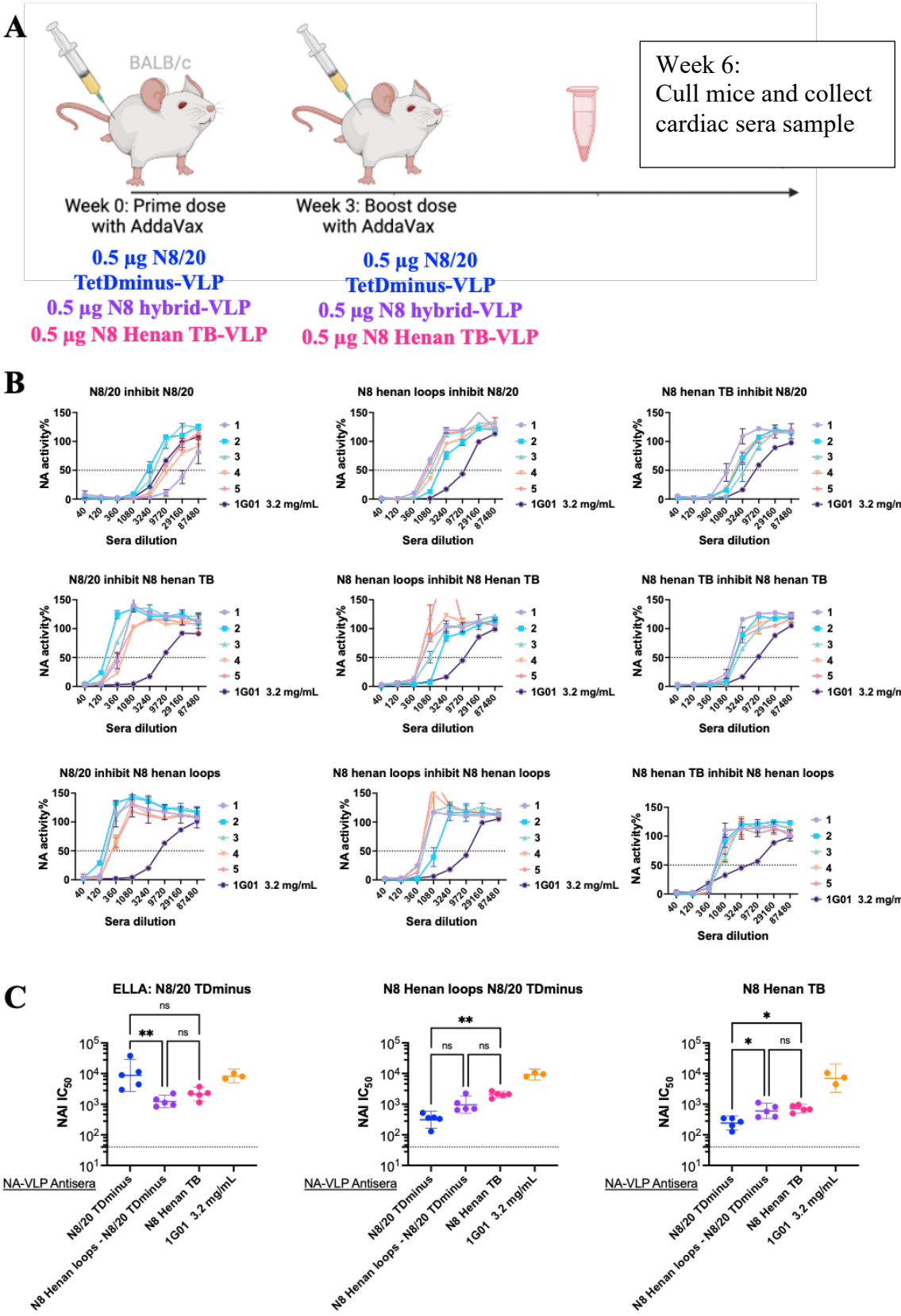

Figure 6.9 **Tetrameric N8 elicited robust antibody response in mice model**
A) BALB/c mice were vaccinated with a prime-boost regimen (IM, adjuvanted with AddaVax) with N8 NA-VLPs at 3-week interval as presented. 3 weeks post boost, mice were culled and sera samples were collected.

B) Individual serum sample inhibition to N8/20 TetDminus, N8 Henan loops N8/20 TetDminus, and N8 Henan TB was tested via ELLA.
C)Individual IC50 calculated from ELLA was represented, Statistical significance was tested by Mann Whitney (Unpaired t-test non-parametric)test, indicated by *($p < 0.05$), **($p < 0.01$), ***($p < 0.001$), ****($p < 0.0001$).

To evaluate immunogenicity of N8 NAs for pandemic preparation, we tested seroconversion of three selected recombinant N8 NAs in BALB/c mice (Fig. 6.9A). Mice (n=6/group) received two intramuscular doses of NA-VLP (0.5 µg NA equivalent/dose) or empty VLP control, each formulated with 25 µL AddaVax adjuvant, administered at 3-week intervals. Sera were collected at week 6 for analysis.

Consistent with our earlier findings, NAI titres tested with ELLA demonstrated cross-inhibitory activity against multiple recombinant N8 NAs (Fig. 6.9B), with quantitative IC50 analysis shown in Fig. 6.9C. While substantial epitope conservation was observed across N8 subtypes, inhibition profiles recapitulated the pattern seen in Fig. 5.5: the upsurface loop mediated dominant neutralizing activity, while the protein framework contributed minor but consistent ELLA-reactive epitopes. This reaffirms our previous conclusion that both structural elements participate in antibody recognition, while the majority of ELLA inhibition related epitopes can be transferred by upsurface loop-grafting.

6.4 Discussion and Implications

Our expanded studies on expression and immunization of N8 NA-VLPs have provided valuable insights into their potential as vaccine candidates.
The self-tetramerization behaviour is not generalized in all N8 groups, however, with the loop-transfer method we are able to combine the top surface loops of N8 NA of interest with self-tetramerizing N8 backbone to overcome expression challenges.
The ability to induce broadly inhibitory antibodies against N8, as demonstrated by both ELLA, is a promising indicator of their potential effectiveness in preventing N8 influenza infections. These findings support the potential of our engineered N8 constructs as vaccine candidates and contribute to N8 pandemic preparedness efforts. These N8 vaccine candidates warrants further testing in more stringent ferrets challenge model.

Chapter 7 Conclusions and Future Plans

7.1 Conclusion

Through systematic investigation of a comprehensive neuraminidase (NA) library containing most human-infective subtypes, we have elucidated key aspects of NA antigenic diversity. While current NA-focused vaccine development has prioritized N1 and N2 subtypes(Air, 2012; Creytens et al., 2021; Eichelberger & Monto, 2019) (reflecting seasonal vaccine composition), our expanded library—including N1, N2, N6, N8, and N9—revealed novel antigenic features, most notably the self-tetramerizing capability of N8/20. These findings significantly broaden our understanding of NA biology and reinforce its growing importance as a critical target for next-generation influenza vaccine design.

Our results demonstrate that NA-based vaccines can elicit protective antibody responses capable of inhibiting enzymatic activity and protecting against lethal viral challenges. Incorporating properly folded tetrameric NA onto nanoparticles further enhances this protective effect, enabling effective responses with lower antigen doses.

The loop-grafting method developed in this study presents an innovative solution to overcome protein expression limitations. Through optimized sequence engineering, we enhanced antigen yield while reducing production costs, offering significant practical benefits for vaccine manufacturing. Unlike consensus-based approaches that aim to promote conserved epitopes (Job et al., 2018), our strategy leverages existing genetic tools to rapidly generate updated recombinant NA antigens, enabling timely response to evolving influenza strains.

Despite these promising findings, several challenges remain. Further efforts are required to optimise antigen design, broaden cross-protective immunity, and ensure durable immune responses. In addition, some limitations in current assays and strategies were identified during the course of this work.

7.2 Assay and Design Limitations

ELLA Assay Limitations

Although the enzyme-linked lectin assay (ELLA) is widely used to assess neuraminidase-inhibiting antibodies in both animal models and humans, our data suggest that high ELLA titres do not always correlate with protection (Eichelberger et al., 2016; Lambré et al., 1990; Rockman et al., 2013). While our serum inhibition studies demonstrated that ELLA titers alone could not reliably distinguish protective from non-protective antigens (Appendix 7) – and even showed cases where higher titers failed to predict in vivo protection – these findings highlight fundamental limitations of current neutralization assays. ELLA effectively measures enzymatic inhibition but fails to capture other critical antibody functions, particularly Fc-mediated effector mechanisms that contribute substantially to antiviral immunity(Lu et al., 2018). This urges the need for multifactorial antibody assessment, such as specificity, affinity, isotype distribution, Fc glycosylation patterns, and functional phenotypes (ADCC, phagocytosis). Comprehensive antibody profiling may define protective correlates, enabling development of enhanced vaccines and antibody therapeutics.

Mixing of VLPs

Bivalent NA-VLP vaccines have proven to be protective in mice model as reported by (Pascha et al., 2024). Contrary to expectations, combining standard and mosaic VLPs (Mix7) did not expand cross-reactive antibody breadth. Despite individual NA-VLPs showing robust strain-specific responses, the mixture failed to induce detectable titres for certain strains. Antigenic competition may occur in mixed formulations.

And broader protection may require epitope-focused design rather than empirical mixing multivalent NA-VLP particles. A viable approach would be to strategically select and limit the NA subtypes included in the multivalent formulation. An alternative strategy could incorporate computationally optimized broadly reactive antigens (COBRAs) to enhance epitope-focused vaccine design through advanced computational methods (Ge & Ross, 2024; Zhang et al., 2024).

Limitations of the Loop-Grafting Approach

While we successfully demonstrated that grafting the upper-surface loop can transfer protective efficacy, the broader potential of the loop-grafting method remains underexplored. At present, we lack a systematic or quantitative framework to predict suitable combinations of framework donors and loop donors, or to anticipate the structural and functional properties of the resulting hybrid proteins. Further investigation, including more experimental iterations and structural analysis, will be essential to better understand and optimise this approach for wider application in antigen design.

7.3 Future Directions for Developing Improved Influenza Vaccines

NA vs. HA vs. NA+HA: Which Strategy Delivers Optimal Influenza Immunity?

The resurgence of interest in neuraminidase (NA) as a vaccine target presents a critical strategic question: should NA be pursued as a standalone immunogen or combined with hemagglutinin (HA) in influenza vaccine formulations? Emerging evidence, including our own data, suggests both approaches offer distinct advantages.

Recent studies have revealed fundamental differences in immune imprinting patterns and response kinetics between HA and NA (Lv et al., 2025). When employed as a standalone vaccine, NA elicits antibodies that primarily inhibit viral egress and reduce transmission - a mechanism that may confer more durable, 'permissive' immunity by allowing limited infection while preventing severe disease and spread (Johansson et al., 1993).

Conversely, combining HA and NA antigens could provide synergistic benefits, particularly for pandemic preparedness. The dual-target approach would simultaneously block viral entry (via HA antibodies) and limit spread (via NA inhibition), creating complementary layers of protection. This strategy may be especially valuable against emerging strains where rapid, broad protection is paramount.

Establishing a More Systematic and Comprehensive Recombinant NA Library

To better understand the diversity and cross-reactive potential of neuraminidase-based antigens, we aim to expand our current recombinant NA library to include a more systematic and representative panel of NA subtypes and strains. This broader library will allow for deeper investigation into antigenic variation, conserved epitopes, and subtype-specific immune responses, forming a stronger foundation for rational vaccine design.

Further Testing with Mixed NA-VLP Formulations

Building on our preliminary work with mixed VLP formulations, more extensive testing with various combinations of NA-VLPs, such as mosaic VLP(Cohen et al., 2021; Liu et al., 2023), carefully chosen multivalent NA-VLP (Pascha et al., 2024). These studies will explore whether optimised ratios, presentation formats, or sequential immunisation strategies can enhance the breadth and potency of the antibody response, particularly against heterologous or emerging strains.

Integrating Recombinant NA Designs with Novel Vaccine Platforms

To improve the speed and effectiveness of future pandemic responses, we intend to combine recombinant NA antigens with advanced vaccine delivery systems, such as mRNA platforms, self-assembling nanoparticles, and adjuvant-enhanced formulations. Leveraging these technologies could enhance the immunogenicity, scalability, and adaptability of NA-based vaccines, providing more efficient tools for rapid deployment during influenza outbreaks.

Appendix

Appendix 1 Recombinant Protein Design

Recombinant protein name	Signal sequence	Purification tag	Spytag	Tetramerisation domain	Original sequence
N1/09 VASP	H1	6H	Y	VASP	H1N1 A/California/7/2009
N1/09 TB	murine IgK	6H	Y	Tetrabrachion	H1N1 A/California/7/2009
N1/09 TetDminus	H1	6H	Y	None	H1N1 A/California/7/2009
N1/09 TB N222K	H1	6H	Y	Tetrabrachion	H1N1 A/California/7/2009, with N222K mutation
N1 MS TB	H7	StrepII, 6H	Y	Tetrabrachion	H5N1 A/mute swan/England/053054/2021
N1 MS TB N222K	H7	StrepII, 6H	Y	Tetrabrachion	H5N1 A/mute swan/England/053054/2021
N1 MS TetDminus	H7	StrepII, 6H	Y	None	H5N1 A/mute swan/England/053054/2021
N1 PR8 TB	H7	StrepII, 6H	Y	Tetrabrachion	H1N1 A/Puerto Rico/8/1934
N1 PR8 TetDminus	H7	StrepII, 6H	Y	None	H1N1 A/Puerto Rico/8/1934
N1/19 TB	H7	StrepII, 6H	Y	Tetrabrachion	H1N1 NYMC X-379 (A/Victoria/2570/2019)
N1/19 TetDminus	H7	StrepII, 6H	Y	None	H1N1 NYMC X-379 (A/Victoria/2570/2019)
N2 X31 TB	H7	StrepII, 6H	Y	Tetrabrachion	H3N2 A/Hong Kong/1/68
N2 X31 TetDminus	H7	StrepII, 6H	Y	None	H3N2 A/Hong Kong/1/68
N2/20 TB	H7	StrepII, 6H	Y	Tetrabrachion	H3N2 A/Cambodia/E0826360/2020
N2/20 TetDminus	H7	StrepII, 6H	Y	None	H3N2 A/Cambodia/E0826360/2020
N6/16 TB	H7	StrepII, 6H	Y	Tetrabrachion	H5N6 A/Hubei/29578/2016
N6/16 TetDminus	H7	StrepII, 6H	Y	None	H5N6 A/Hubei/29578/2016
N8/20 VASP	H7	6H	Y	VASP	H5N8 A/chicken/England/030720/2020
N8/20 TB	H7	6H	Y	Tetrabrachion	H5N8 A/chicken/England/030720/2020
N8/20 TetDminus	H7	6H	Y	None	H5N8 A/chicken/England/030720/2020
N9 Anhui TB	H7	StrepII, 6H	Y	Tetrabrachion	H7N9 A/Anhui/1/2013
N9 Anhui TetDminus	H7	StrepII, 6H	Y	None	H7N9 A/Anhui/1/2013
N2/08 ch TB	H7	StrepII, 6H	Y	Tetrabrachion	H9N2 A/chicken/Pakistan/UDL-01/2008
N8/1963 TetDminus	H7	StrepII, 6H	Y	None	H3N8 A/duck/Ukraine/1/1963
N8/2011 TetDminus	H7	StrepII, 6H	Y	None	H3N8 A/harbor_seal/Massachesetts/1/2011
N8/2014 TetDminus	H7	StrepII, 6H	Y	None	H5N8 A/gyrfalcon/Washington/41088-6/2014
N8/2022 TetDminus	H7	StrepII, 6H	Y	None	H3N8 A/equine/Maryland/1/22
N1/09 loops MS TB	H7	StrepII, 6H	Y	Tetrabrachion	Hybrid NA
N1/09 loops N6/16 TB	H7	StrepII, 6H	Y	Tetrabrachion	Hybrid NA
N1 MS loops PR8 TB	H7	StrepII, 6H	Y	Tetrabrachion	Hybrid NA
N1 PR8 loops MS TB	H7	StrepII, 6H	Y	Tetrabrachion	Hybrid NA
N1/19 loops MS TB	H7	StrepII, 6H	Y	Tetrabrachion	Hybrid NA
N8 Henan TB	H7	StrepII, 6H	Y	Tetrabrachion	H3N8 A/Henan/4-14/2022
N8 Henan TetDminus	H7	StrepII, 6H	Y	None	H3N8 A/Henan/4-14/2022

N8 Henan TetDminus with interface mutations	H7	StrepII, 6H	Y	None	Sequence modified NA
N8/2022 TetDminus with interface mutations	H7	StrepII, 6H	Y	None	Sequence modified NA
N8 Henan loops N8/20 TB	H7	StrepII, 6H	Y	Tetrabrachion	Hybrid NA
N8 Henan loops N8/20 TetDminus	H7	StrepII, 6H	Y	None	Hybrid NA
N8 Henan loops N1 MS TB	H7	StrepII, 6H	Y	Tetrabrachion	Hybrid NA

Appendix 2 Neuraminidase Expression level

Transfection date	Standardized protein name	Expression system	Yield mg/L
06/12/2023	N8 Henan loops N8/20 TetDminus	ExpiCHO	533
16/02/2022	N1 MS TB	ExpiCHO	380
19/04/2022	N1 PR8 TetDminus	ExpiCHO	362
24/11/2021	N6/16 TetDminus	Expi293	334
19/04/2022	N1 MS TetDminus	ExpiCHO	308
16/02/2022	N9 Anhui TB	ExpiCHO	242
19/04/2022	N2 X31 TetDminus	ExpiCHO	231
07/04/2022	N1/09 loops MS TB	ExpiCHO	208
24/11/2021	N2/20 TetDminus	Expi293	192.5
17/11/2021	N6/16 TetDminus	ExpiCHO	180 (protein left in SU)
16/02/2022	N2 X31 TB	ExpiCHO	142
18/04/2023	N1 MS TB	ExpiCHO	108.5
23/03/2023	N1 PR8 loops MS TB	ExpiCHO	107.5
14/11/2022	N1 MS N222K	ExpiCHO	105
16/02/2022	N1 PR8 TB	ExpiCHO	105
20/05/2022	N1/19 loops MS TB	ExpiCHO	104
31/01/2023	N2/08 ch TB	ExpiCHO	101
24/11/2021	N6/16 TB	Expi293	92
20/04/2022	N9 Anhui TetDminus	ExpiCHO	90
17/11/2021	N2/20 TB	ExpiCHO	89
18/04/2023	N1 PR8 loops MS TB	ExpiCHO	78
05/06/2022	N2 X31 TetDminus	ExpiCHO	76
11/09/2023	N8 Henan loops N8/20 TB	ExpiCHO	70
05/06/2022	N1 PR8 TetDminus	ExpiCHO	58
27/04/2021	N1/09 VASP	ExpiCHO	58
12/06/2021	N1/09 TetDminus	Expi293	54
17/11/2021	N6/16 TB	ExpiCHO	50 (protein left in SU)
21/04/2023	N1 MS TB	ExpiCHO	46.5
13/04/2022	N1/09 loops N6/16 TB	ExpiCHO	40
22/08/2022	N8/20 TetDminus	ExpiCHO	40
12/06/2021	N1/09 VASP	Expi293	36
03/08/2021	N1/09 VASP	ExpiCHO	36
12/06/2021	N8/20 TetDminus	Expi293	35
21/04/2023	N1 PR8 loops MS TB	ExpiCHO	34
14/11/2022	N1/09 TB	ExpiCHO	26
06/01/2021	N1/09 TetDminus	ExpiCHO	24
26/09/2023	N8 Henan with interface mutations	ExpiCHO	23.6
24/11/2021	N2/20 TB	Expi293	23.2
31/01/2023	N8/2014 TetDminus	ExpiCHO	23
23/03/2023	N1 MS loops PR8 TB	ExpiCHO	21.5
02/07/2021	N1/09 TetDminus	ExpiCHO	20
06/01/2021	N8/20 TetDminus	ExpiCHO	18
02/07/2021	N8/20 TetDminus	ExpiCHO	18

Transfection date	Standardized protein name	Expression system	Yield mg/L
22/08/2022	N8/20 VASP	ExpiCHO	16
12/06/2021	N1/09 TB	Expi293	15
02/07/2021	N1/09 VASP	ExpiCHO	14
03/08/2021	N8/20 VASP	ExpiCHO	12
02/10/2021	N8/20 TetDminus	Expi293	11
24/11/2021	N1/19 TetDminus	Expi293	10
06/01/2021	N8/20 VASP	ExpiCHO	10
31/01/2023	N8/1963 TetDminus	ExpiCHO	9.4
02/10/2021	N1/09 VASP	Expi293	8
02/10/2021	N1/09 TetDminus	Expi293	7
02/07/2021	N1/09 TB	ExpiCHO	6
26/07/2021	N8/20 VASP	ExpiCHO	6, after precipatation
18/9/2022	N8/20 VASP	ExpiCHO	4.4
12/06/2021	N8/20 VASP	Expi293	3.3
16/08/2021	N8/20 VASP	ExpiCHO	2, after precipatation
02/10/2021	N1/09 TB	Expi293	2
02/10/2021	N8/20 TB	Expi293	1.5
21/09/2023	N8 Henan TetDminus	ExpiCHO	1.1
21/09/2023	N8 Henan TB	ExpiCHO	1.0
02/10/2021	N8/20 VASP	Expi293	0.75
21/09/2023	N8/22 TetDminus with interface mutations	ExpiCHO	0.3
27/04/2021	N8/20 VASP	ExpiCHO	Precipitation on SEC,no yield record
26/02/2021	N1/09 VASP	Expi293	No expression
17/11/2021	N1/19 TetDminus	ExpiCHO	No expression
12/06/2021	N8/20 TB	Expi293	No expression
26/02/2021	N8/20 VASP	Expi293	No expression
02/09/2021	N8/20 VASP	Expi293	No expression
31/01/2023	N8/2011 TetDminus	ExpiCHO	No expression
31/01/2023	N8/2022 TetDminus	ExpiCHO	No expression
11/09/2023	N8 Henan loops N1 MS TB	ExpiCHO	No expression
06/01/2021	N1/09 TB	ExpiCHO	Lose track
06/01/2021	N8/20 TB	ExpiCHO	Lose track
03/11/2022	N1 MS TB N222K	ExpiCHO	Got infected
20/05/2021	N1/09 TB	ExpiCHO	Got infected
20/05/2021	N1/09 TetDminus	ExpiCHO	Got infected
20/05/2021	N8/20 TB	ExpiCHO	Got infected
20/05/2021	N8/20 TetDminus	ExpiCHO	Got infected
03/11/2022	N8/20 VASP	ExpiCHO	Got infected
17/11/2021	N2/20 TetDminus	ExpiCHO	/(SU infected after harvesting)

Appendix 3 Neuraminidase Characterization Summary

#	Protein	Virus Name	Protein Batch	Expression system	Yield mg/L	Tm1 (°C)	Tm2 (°C)	Comments on unfolding curves	Ton (°C)	Tm minus Ton (°C) Low= Uniform	Size exclusion chromatography peaks	BS-3 Cross-linking SDS-PAGE	MUNANA Activity (AUC)	ELLA Activity (AUC)	mAbs binding	Solubility score in Camsol
1	**N1/09 TetDminus**	H1N1 A/California/7/2009	02/07/2021	ExpiCHO	20	uninterpretable					Aggregate + Monomer	Aggregated	2.9E+04	0.7	Weak and partial	0.06
2	**N1/09 TB**	H1N1 A/California/7/2009	02/10/2021	Expi293		56.13		Multiple peaks	40.49	15.6	Aggregate + Tetramer	Tetramer	6.3E+05	nd	Good	-0.06
3	**N1/09 VASP**	H1N1 A/California/7/2009	02/10/2021	Expi293		46.72	80.00	Multiple peaks, no sharp peak	46.34	33.7	Mixture	Tetramer	4.9E+05	7.1	Good	0.29
4	**N1/09 TB**	H1N1 A/California/7/2009	14/11/2022	ExpiCHO	26	40.81	56.43	Two peaks, small dip + large	33.96	22.5	Aggregate + Tetramer	Mainly tetramer	5.1E+05	11.0	Good	-0.06
5	**N2/20 TB**	H3N2 A/Cambodia/E0826360/2020	24/11/2021	Expi293	23	49.42	61.71	Two sharp peaks	43.19	18.5		Four forms (mono-, di-, tri-, & tetra-mers)	5.4E+05	nd	Good	-0.01
6	**N2/20 TetDminus**	H3N2 A/Cambodia/E0826360/2020	24/11/2021	Expi293	193	54.36		Single sharp peak	47.80	6.6	Aggregate + Monomer	Monomer	1.1E+04	0.4	No	0.07
7	**N6/16 TB**	H5N6 A/Hubei/29578/2016	24/11/2021	Expi293	92	63.06		Single sharp peak	59.17	3.9		Four forms (mono-, di-, tri-, & tetra-mers)	5.5E+05	12.3	Good	0.31
8	**N6/16 TetDminus**	H5N6 A/Hubei/29578/2016	24/11/2021	Expi293	334	uninterpretable		Multiple peaks	53.99			Three forms (mono, di and tri-mers)	1.2E+05	4.0	Weak	0.41
9	**N2/20 TB**	H3N2 A/Cambodia/E0826360/2020	17/11/2021	ExpiCHO	89	61.30		Sharp two peaks, small + large	56.80	4.5	Tetramer	Four forms (mono-, di-, tri-, & tetra-mers)	5.3E+05	9.5	Good	-0.01
10	**N6/16 TB**	H5N6 A/Hubei/29578/2016	17/11/2021	ExpiCHO	50	63.06		Single sharp peak	58.94	4.1		Mainly tri- & tetra-mers	5.2E+05	13.1	Good	0.31
11	**N1 MS TB**	H1N1 A/mute swan/England/385466/2021	16/02/2022	ExpiCHO	380	69.12		Single sharp peak	62.60	6.5	Tetramer	Tetramer	5.0E+05	13.0	Good	0.01
12	**N1 PR8 TB**	H1N1 A/Puerto Rico/8/1934	16/02/2022	ExpiCHO	105	55.80		Single sharp peak	44.87	10.9	Tetramer	Tetramer	5.2E+05	15.7	Good	0.14
13	**N9/13 TB**	H7N9 A/Anhui/1/2013	16/02/2022	ExpiCHO	242	41.35	63.09	Two peaks, small dip + large	20.50	42.6		Four forms (mono-, di-, tri-, and tetra-mers)	5.4E+05	14.7	Good	0.32
14	**N2 X31 TB**	H3N2 A/Hong Kong/1/1968	16/02/2022	ExpiCHO	142	48.64	61.84	Two sharp peaks, large + large	42.93	18.9	Aggregate + Tetramer	Four forms (mono-, di-, tri-, & tetra-mers)	5.2E+05	14.4	Good	0.13
15	**N2 X31 TetDminus**	H3N2 A/Hong Kong/1/1968	19/04/2022	ExpiCHO	231	30.47	43.76	Two sharp peaks, small + large	33.54	10.2	Aggregate + Monomer	Monomer	3.6E+04	0.2	Partial	0.23
16	**N1 PR8 TetDminus**	H1N1 A/Puerto Rico/8/1934	19/04/2022	ExpiCHO	362	46.63		Single sharp peak	43.30	3.3	Aggregate + Dimer	Dimer and monomer	1.1E+04	0.1	Partial	0.24
17	**N1 MS TetDminus**	H5N1 A/mute swan/England/385466/2021	19/04/2022	ExpiCHO	308	47.15		Single sharp peak	43.05	4.1	Aggregate + Dimer	Dimer and monomer	5.6E+04	0.3	Weak and partial	0.10
18	**N9/13 TetDminus**	H7N9 A/Anhui/1/2013	20/04/2022	ExpiCHO	90	44.56		Negative sharp peak	38.42	6.1		Monomer	2.6E+03	0.6	Partial	0.43
19	**N1/09 loops - MS TB**	Hybrid	07/04/2022	ExpiCHO	208	64.42		Single sharp peak	58.05	6.4	Tetramer	Tetramer	5.6E+05	13.8	Good	0.04
20	**N1/19 loops - MS TB**	Hybrid	20/05/2022	ExpiCHO	104	72.35		Single sharp peak	66.47	5.9	Tetramer	Tetramer	6.1E+05	9.5	Good	
21	**N1 PR8 loops - MS TB**	Hybrid	23/03/2023	ExpiCHO	108	58.13		Single peak	44.52	13.6		Tetramer	5.0E+05	11.4	2/10 partial, rest good	0.009
22	**N1 MS loops - PR8 TB**	Hybrid	23/03/2023	ExpiCHO	22	64.30		Single peak	56.96	7.3		Tetramer	5.1E+05	13.3	Good	0.14
23	**N2/08 ch TB**	H9N2 A/chicken/Pakistan/UDL-01/2008	31/01/2023	ExpiCHO	101	54.52		Single peak	47.44	7.1		Tetramer	4.6E+05	9.7	Good	
24	**N8/20 VASP**	H5N8 A/chicken/England/030720/2020	12/06/2021	Expi293	10	42.70	56.88	Two peaks, small dip + large	38.30	18.6		Tetramer	5.4E+05	10.0	Good	0.13
25	**N8/20 TetDminus**	H5N8 A/chicken/England/030720/2020	12/06/2021	Expi293	25	42.94	72.79	Precipitated, inconsistent results	30.01	42.8		Monomer	5.1E+05	9.7	Good	-0.11
26	**N8/20 TetDminus**	H5N8 A/chicken/England/030720/2020	02/07/2021	ExpiCHO	18	68.54		Single peak	63.81	4.7	Aggregate + Tetramer	Four forms (mono-, di-, tri-, & tetra-mers)	6.2E+05	7.7	Good	-0.11
27	**N1/09 (N222K) TB**	H1N1 A/California/7/2009	14/11/2022	ExpiCHO	8	40.00		Single peak	36.23	3.8		Tetramer	5.0E+05	8.4	Good	-0.05
28	N1 MS (N222K) TB	H5N1 A/mute swan/England/385466/2021	14/11/2022	ExpiCHO	105	67.51		Single peak	60.51	7.0		Mainly tetramer	5.7E+05	9.2	Good	0.02

Appendix 4 Neuraminidase Characterisation SDS-PAGE and BS3 Cross-linked SDS-PAGE

Reducing SDS-PAGE

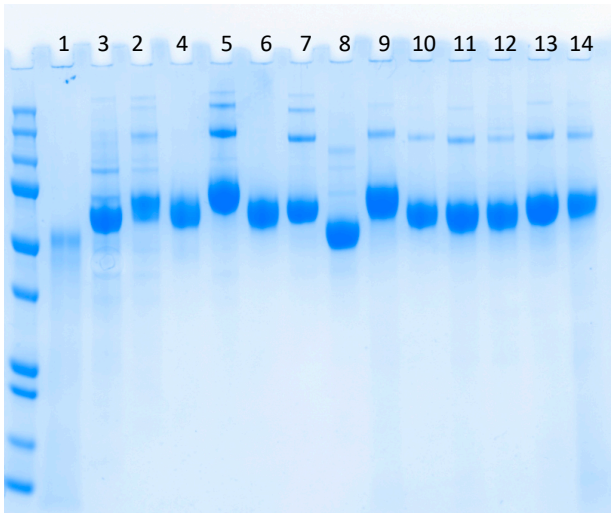

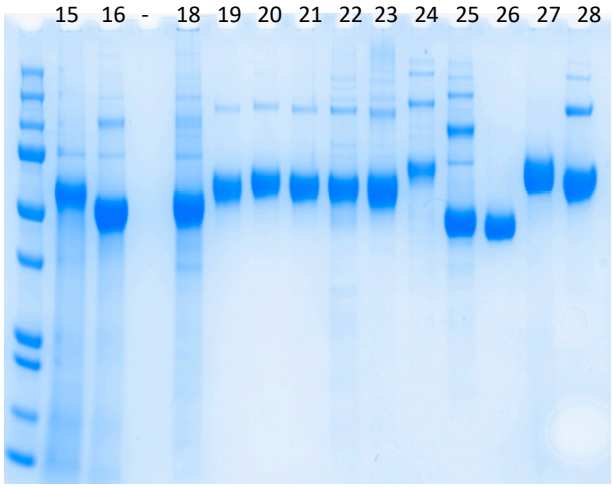

BS3 Cross-linked

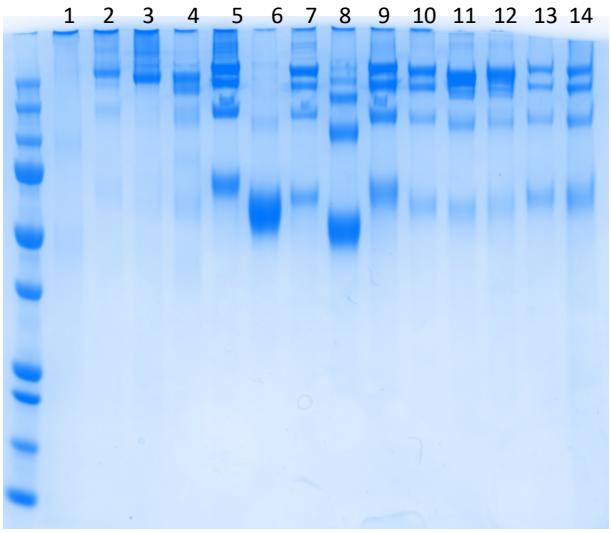

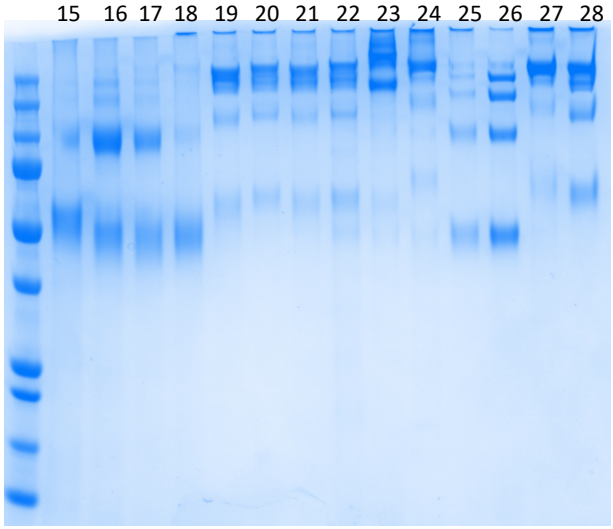

#	Protein
1	N1/09 TetDminus
2	N1/09 TB
3	N1/09 VASP
4	N1/09 TB
5	N2/20 TB
6	N2/20 TetDminus
7	N6/16 TB
8	N6/16 TetDminus
9	N2/20 TB
10	N6/16 TB
11	N1 MS TB
12	N1 PR8 TB
13	N9/13 TB
14	N2 X31 TB

15	N2 X31 TetDminus
16	N1 PR8 TetDminus
17	N1 MS TetDminus
18	N9/13 TetDminus
19	N1/09 loops - MS TB
20	N1/19 loops - MS TB
21	N1 PR8 loops - MS TB
22	N1 MS loops - PR8 TB
23	N2/08 ch TB
24	N8/20 VASP
25	N8/20 TetDminus
26	N8/20 TetDminus
27	N1/09 (N222K) TB
28	N1 MS (N222K) TB

Appendix 5 Neuraminidase Characterization Detail

1-N1/09 TetDminus
T 2/7/2021 ExpiCHO
T 6/7/2023 ExpiCHO

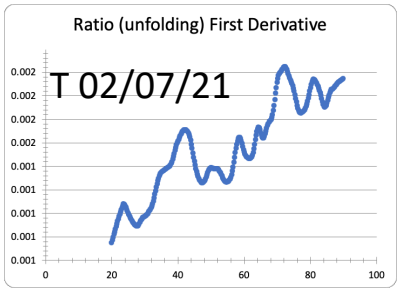

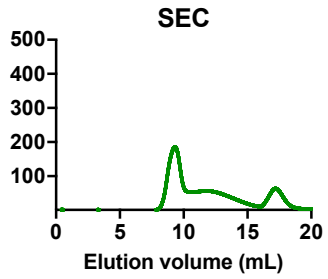

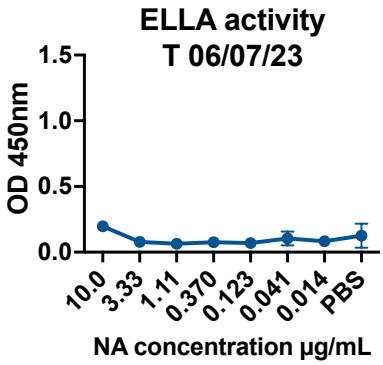

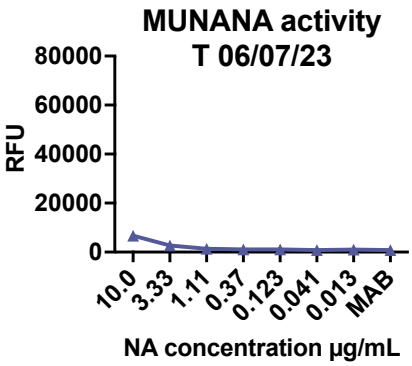

3-N1/09 VASP
T 2/10/2021 Expi293
T 21/7/2023 ExpiCHO

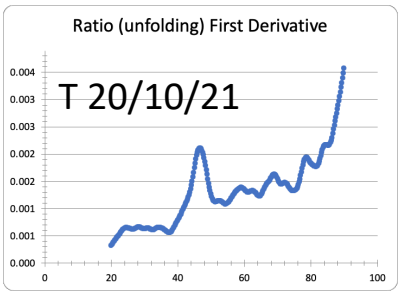

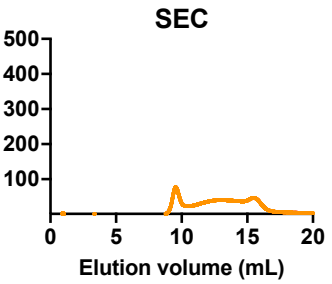

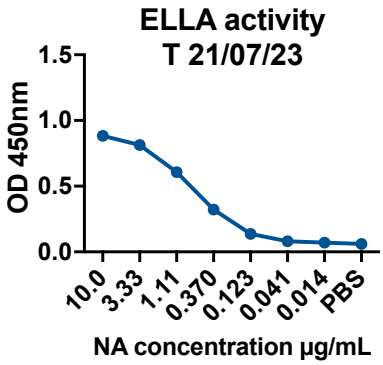

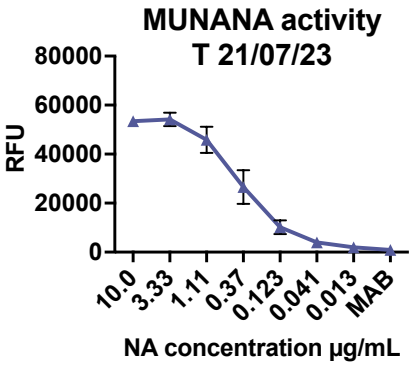

2,4-N1/09 TB
T 14/11/2022 ExpiCHO
T 21/7/2023 ExpiCHO

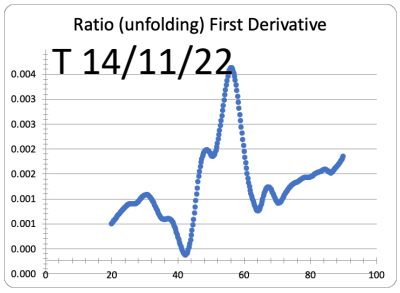

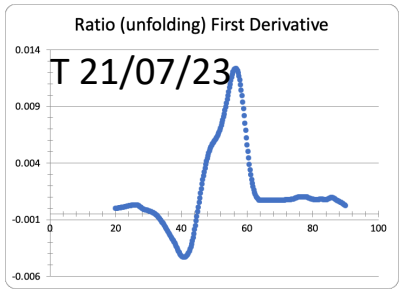

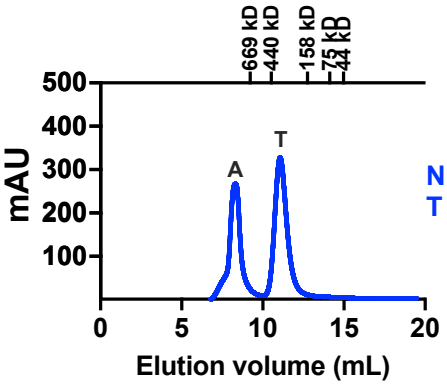

N1/09-TB NA
T 14/11/22

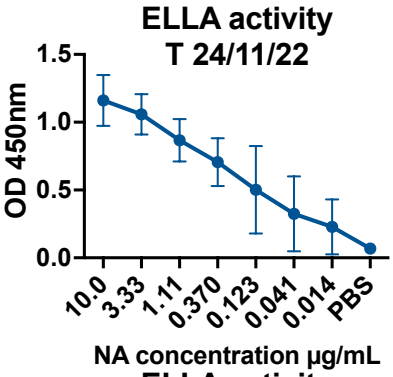

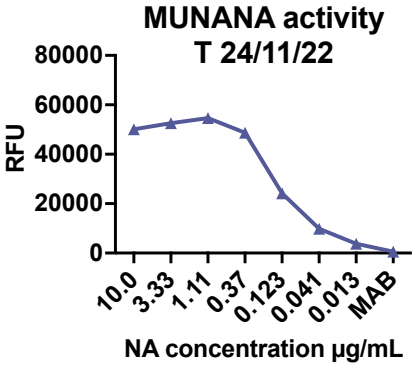

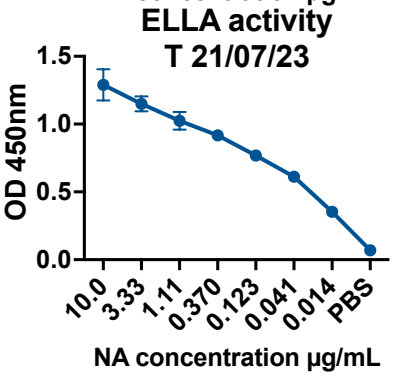

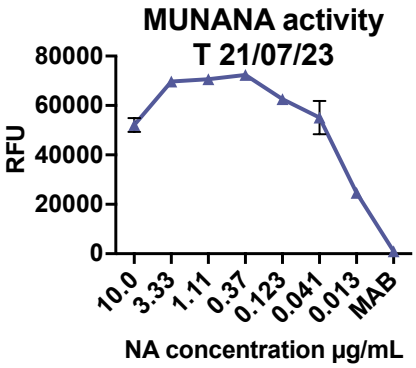

2,4-N1/09 TB
T 14/11/2022 ExpiCHO
T 21/7/2023 ExpiCHO

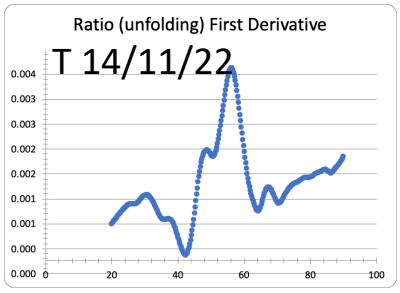

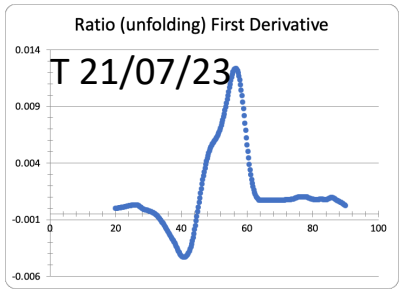

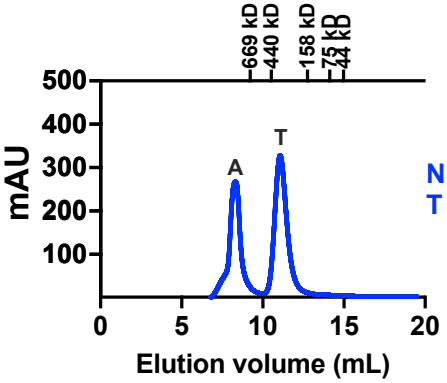

N1/09-TB NA
T 14/11/22

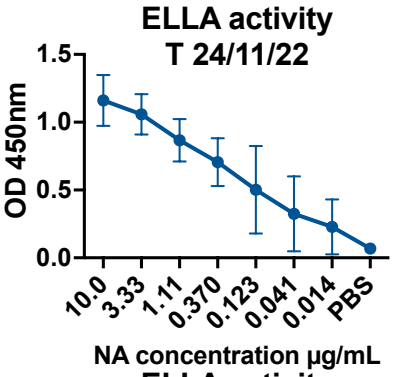

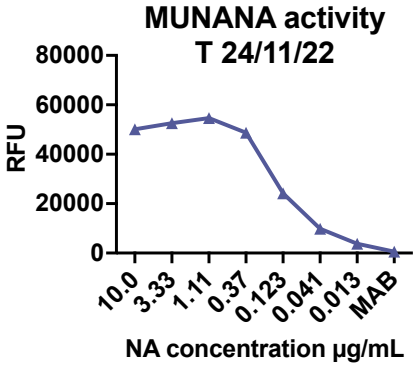

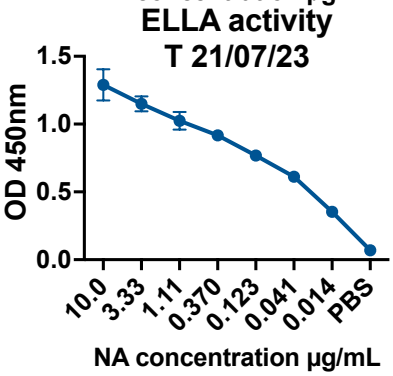

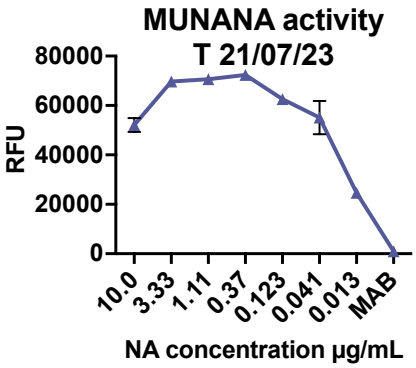

6-N2/20 TetDminus
T 24/11/21 ExpiCHO

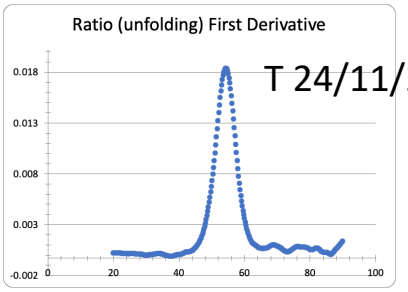

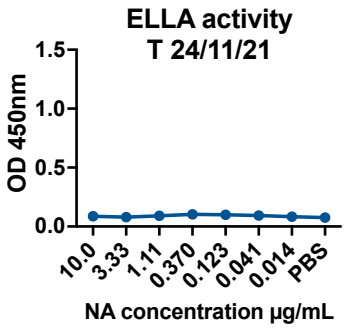

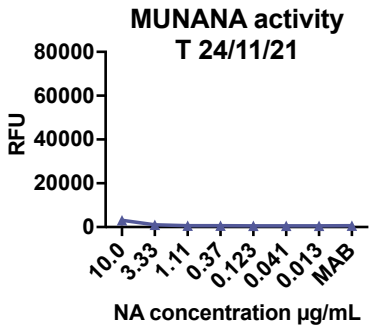

7,10-N6/16 TB
7-T 24/11/21 ExpiCHO
10-T 17/11/21 Expi293

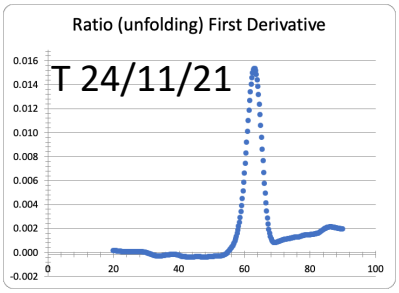

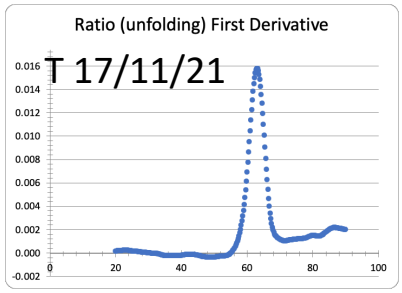

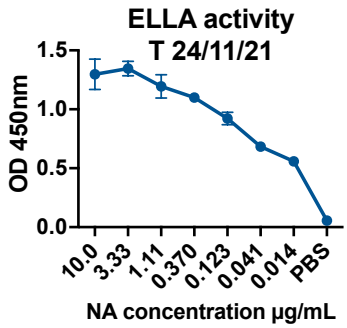

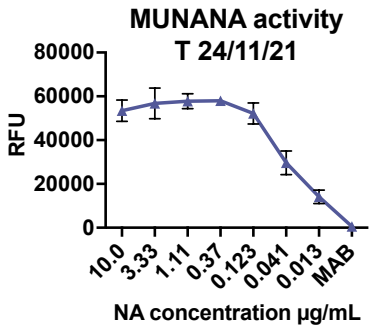

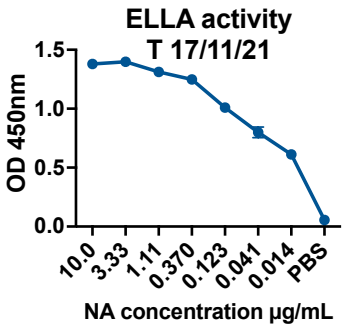

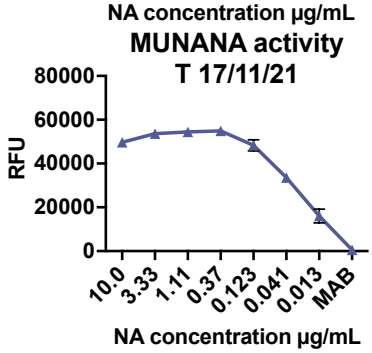

11-N1 MS TB
T 16/02/22 ExpiCHO

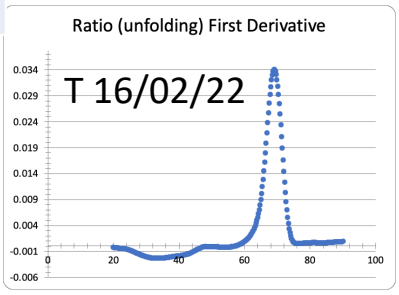

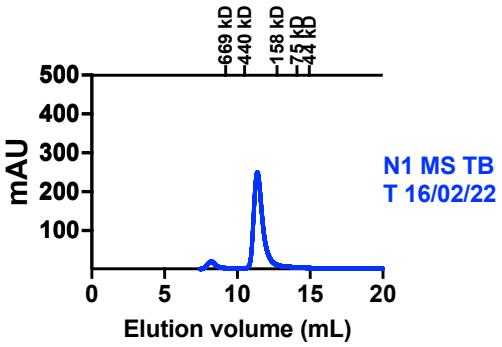

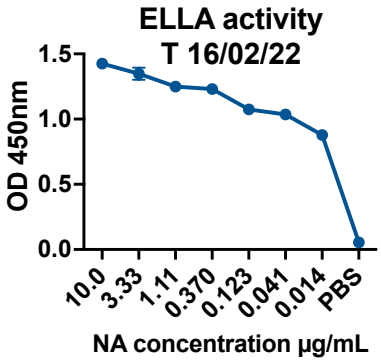

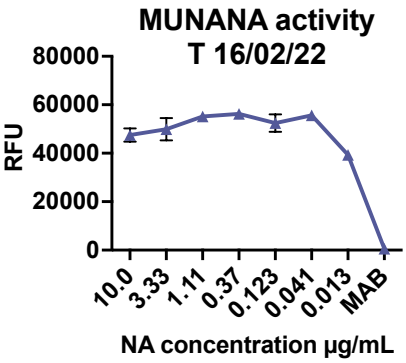

12-N1 PR8 TB
T 16/02/22 ExpiCHO

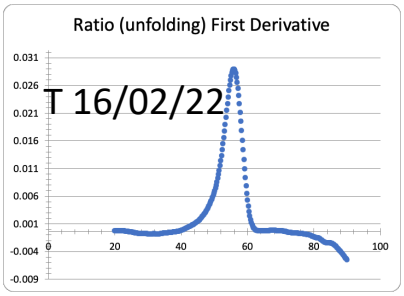

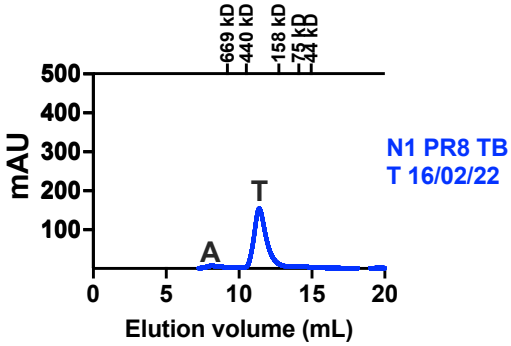

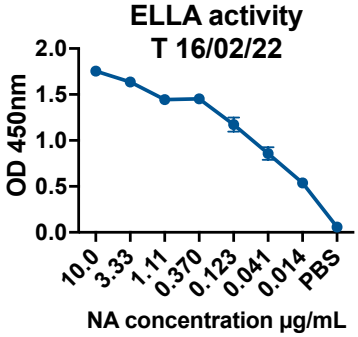

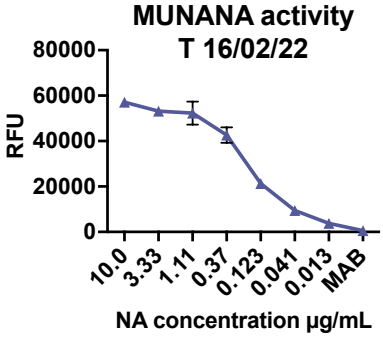

13-N9/13 TB
T 16/02/22 ExpiCHO

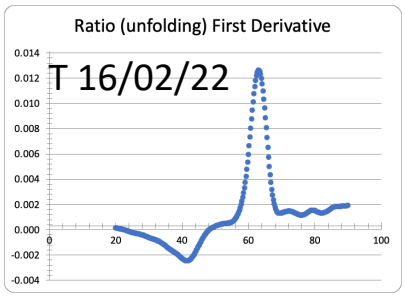

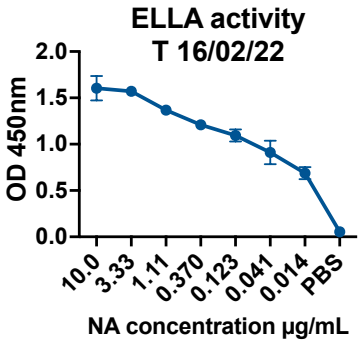

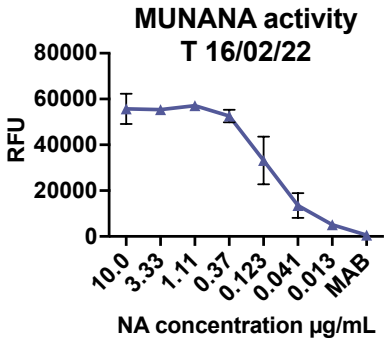

14-N2 X31 TB
T 16/02/22 ExpiCHO

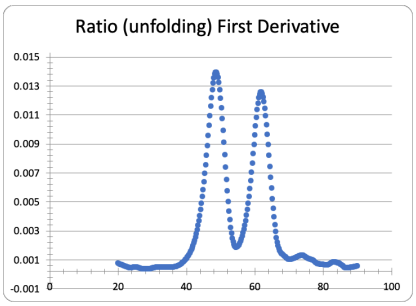

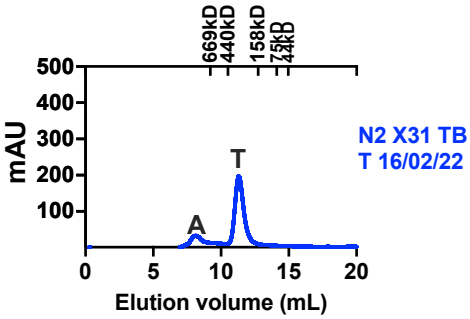

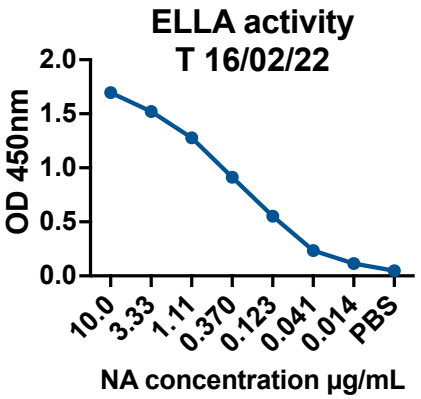

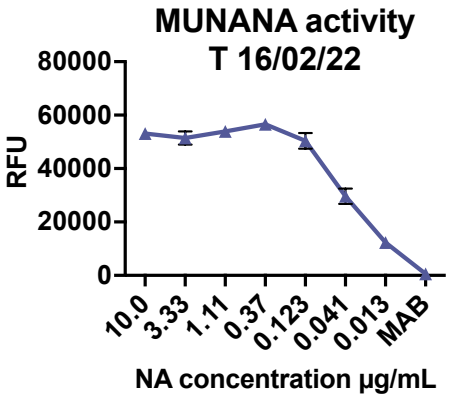

15-N2 X31 TetDminus
T 19/04/22 ExpiCHO

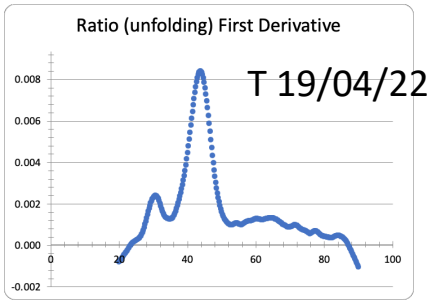

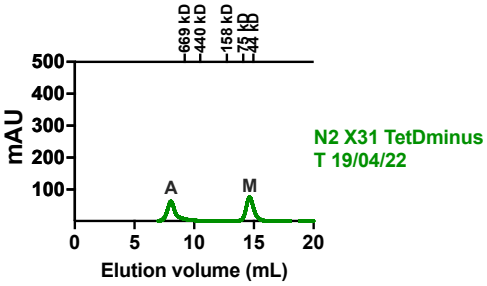

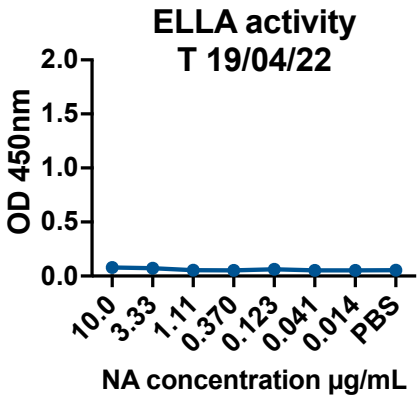

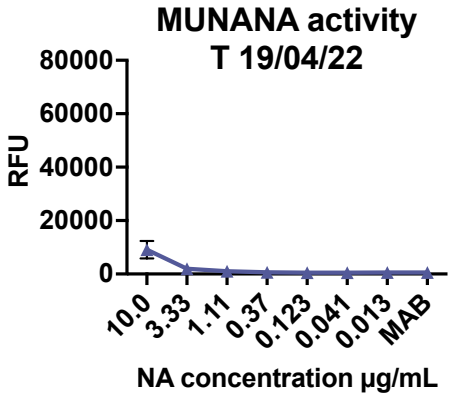

16-N1 PR8 TetDminus
T 19/04/22 ExpiCHO

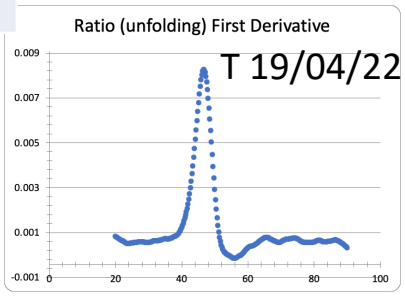

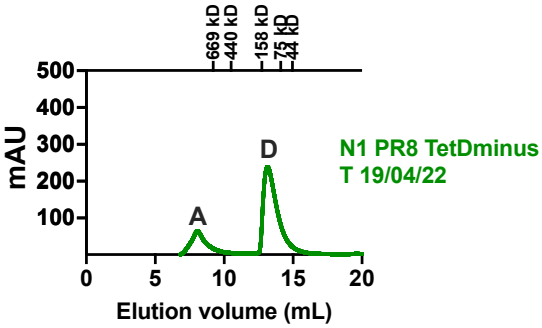

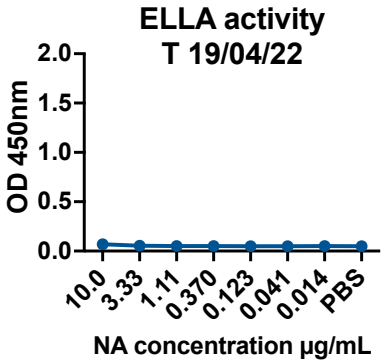

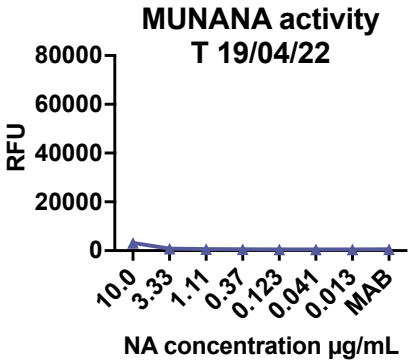

17-N1 MS TetDminus
T 19/04/22 ExpiCHO

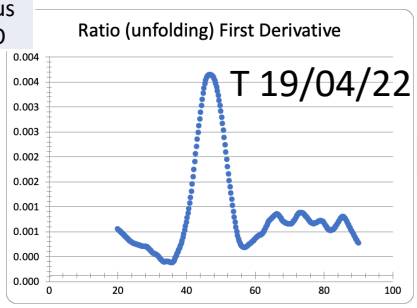

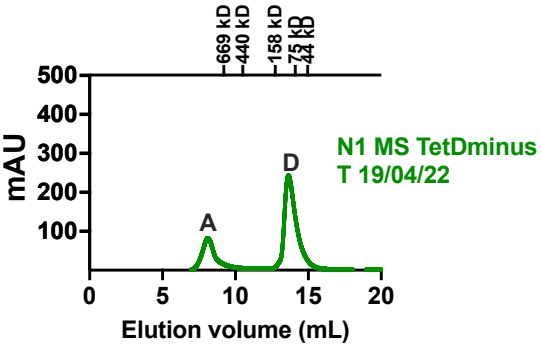

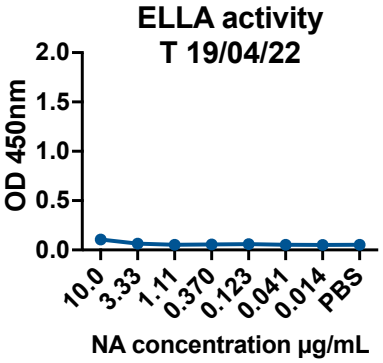

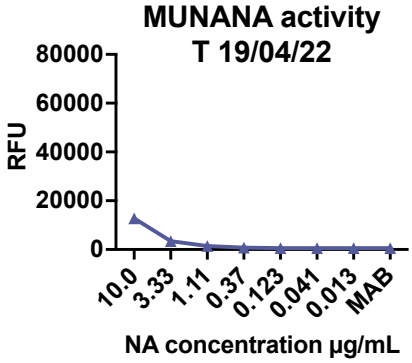

18-N9/13 TetDminus
T 19/04/22 ExpiCHO

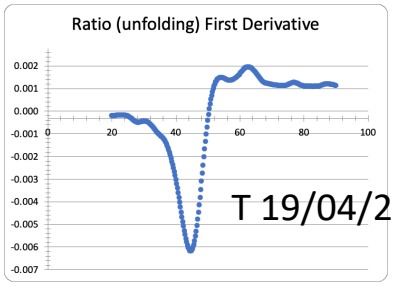

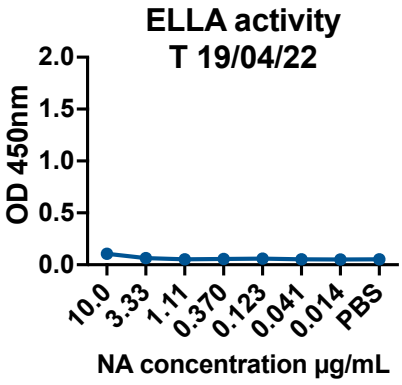

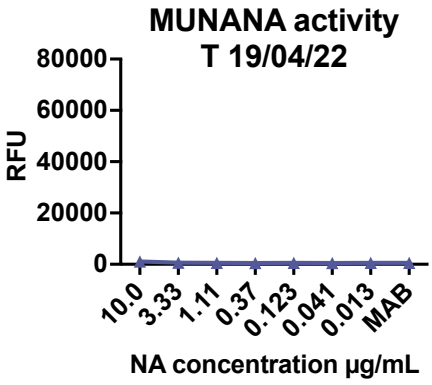

19-N1/09 loops MS TB
T 07/04/2022 ExpiCHO

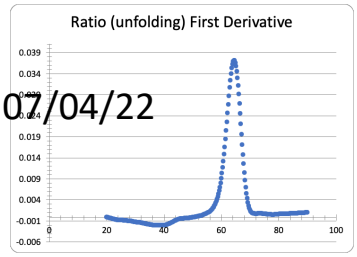

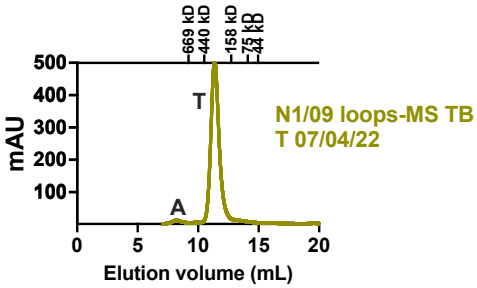

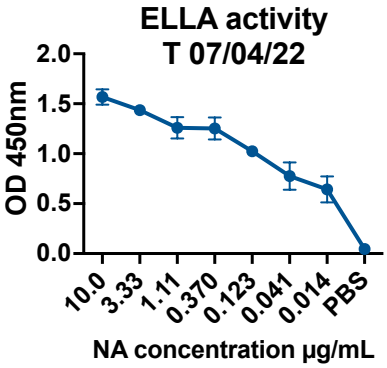

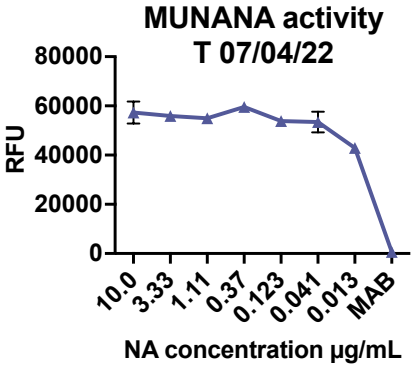

20-N1/19 loops MS TB
T 20/05/22 ExpiCHO
T 06/07/23 ExpiCHO

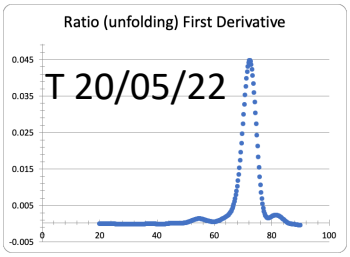

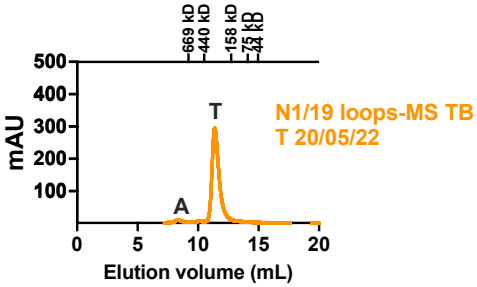

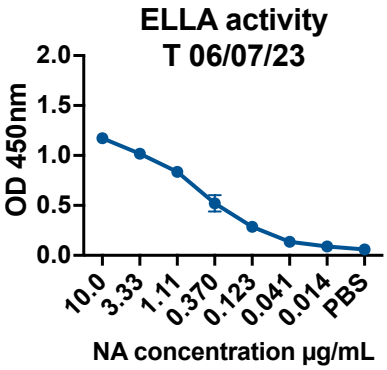

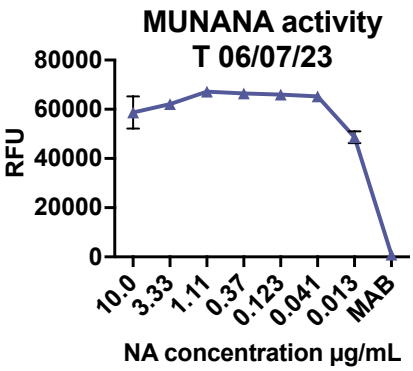

21-N1 PR8 loops MS TB T 23/03/23 ExpiCHO

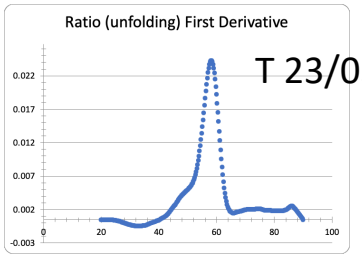

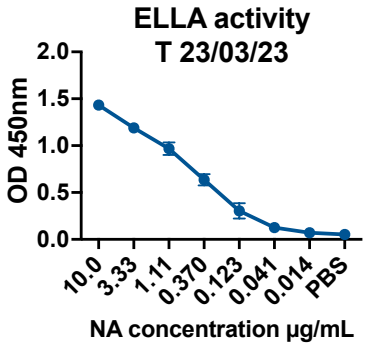

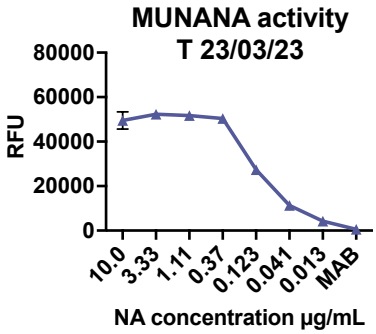

22-N1 MS loops PR8 TB T 23/03/23 ExpiCHO

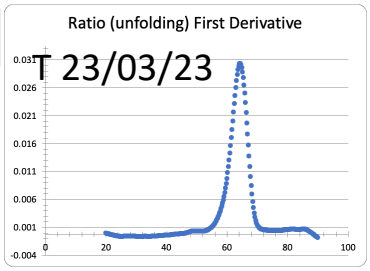

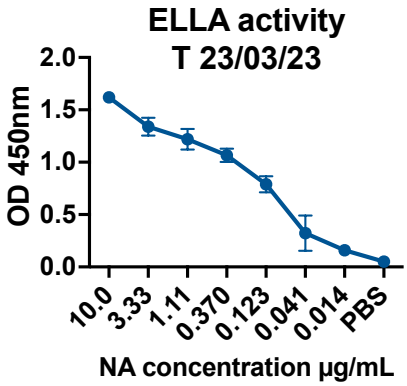

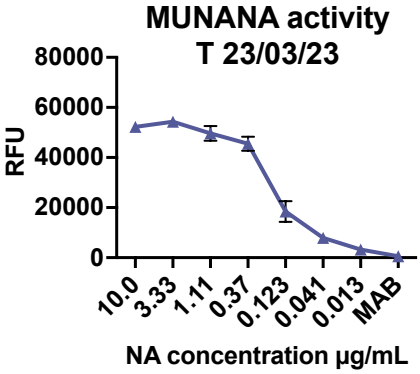

23-N2/09 ch TB
T 31/01/23 ExpiCHO

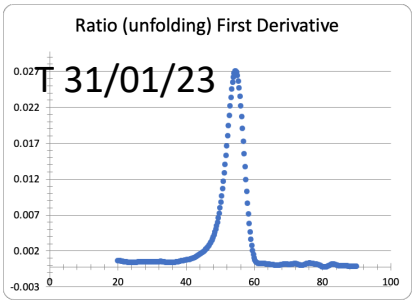

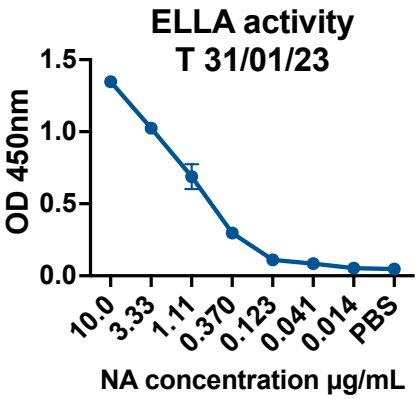

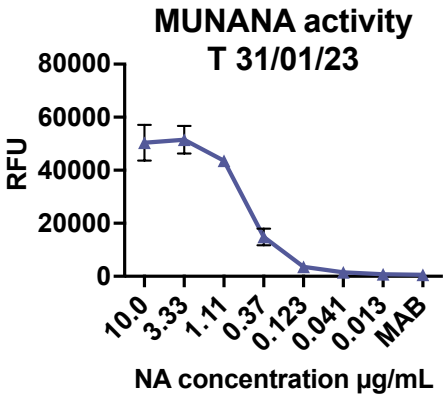

24-N8/20 VASP
T 12/06/21 Expi293

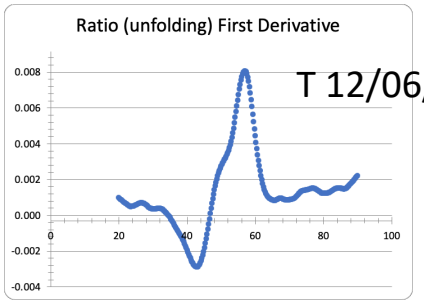

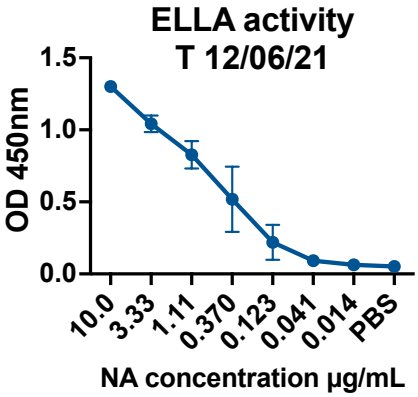

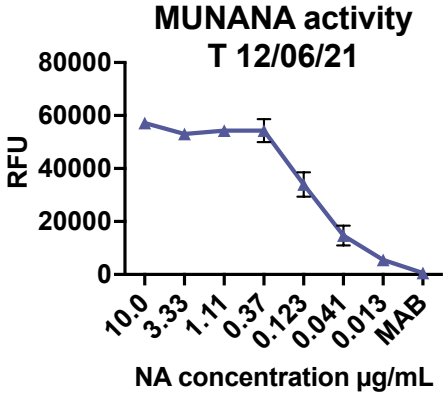

25,26-N8/20 TetDminus
25 T 12/06/21 Expi293
26 T 02/07/21 ExpiCHO

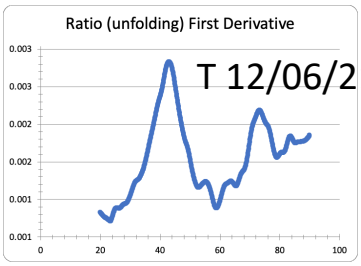

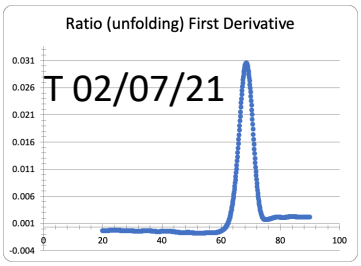

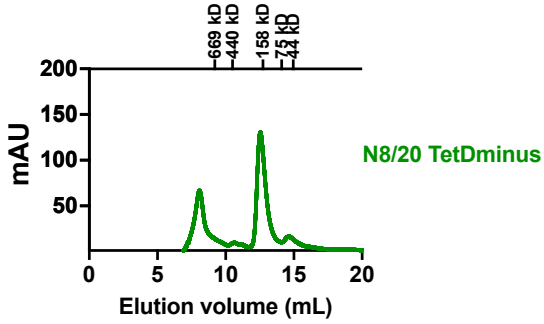

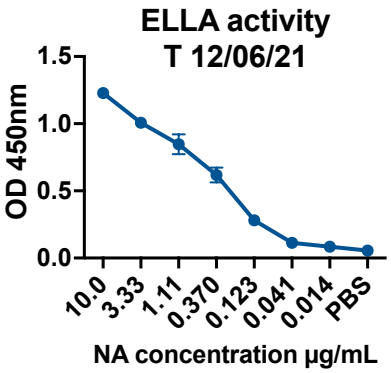

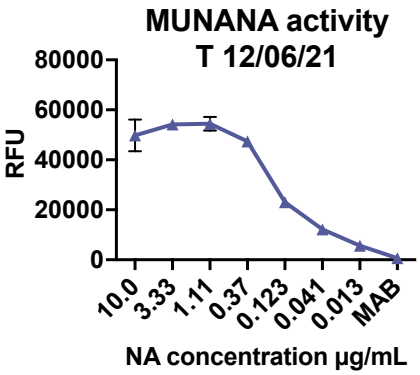

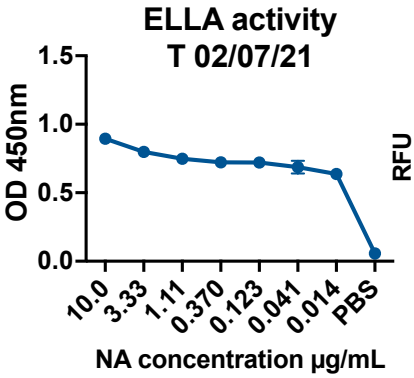

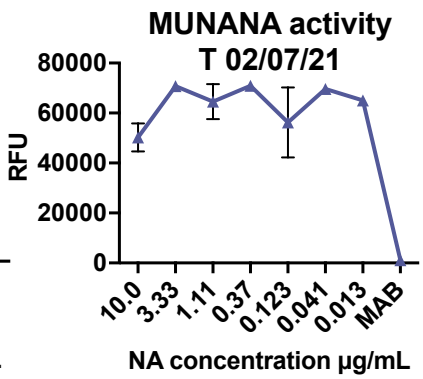

27-N1/09 TB N222K
T 14/11/22 ExpiCHO

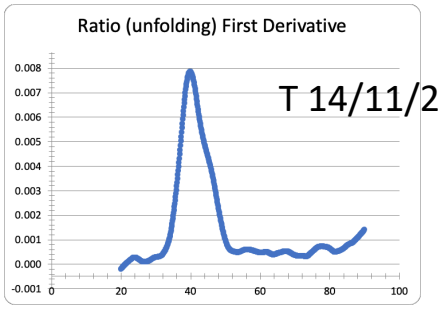

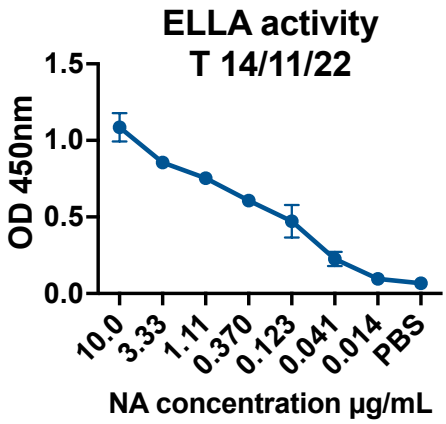

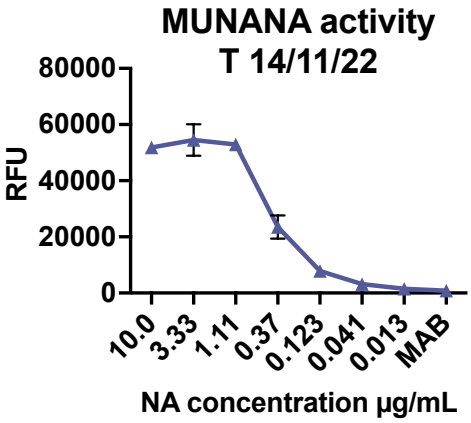

28-N1 MS TB N222K
T 14/11/22 ExpiCHO

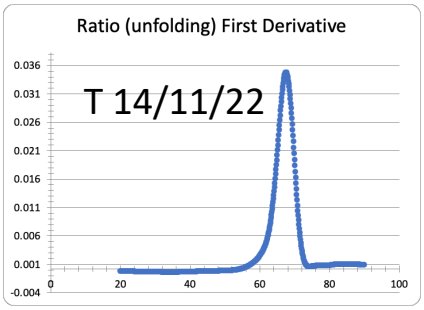

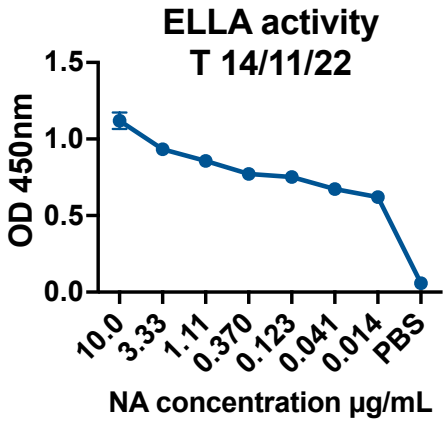

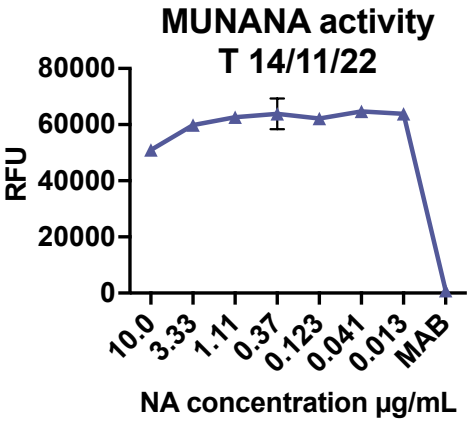

NA and NA-VLP run through SDS-PAGE before vaccination for Fig.4.3

VLPs and antigens for challenge study
- X179A model

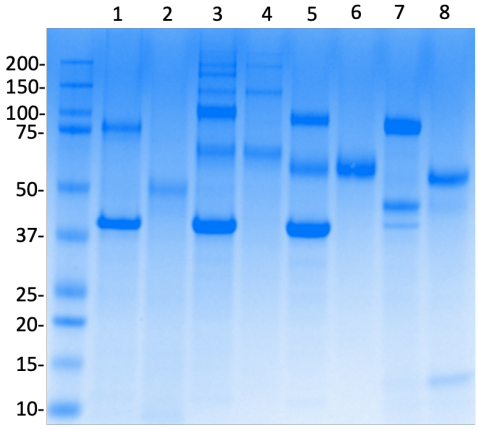

1	N1 NA monomer-VLP
2	N1 NA monomer
3	N1 NA TB in 293-VLP
4	N1 NA TB in 293
5	N1 NA TB in CHO-VLP
6	N1 NA TB in CHO
7	N1 NA VASP in CHO-VLP
8	N1 NA VASP in CHO

Loaded 2ug antigents each well,
Run at 200°C, 30min

NA and NA-VLP run through SDS-PAGE before vaccination for Fig.4.5, 4.6, 4.8, 4.9.

Mi3 particle conjugation fixed VLP(E.coli)

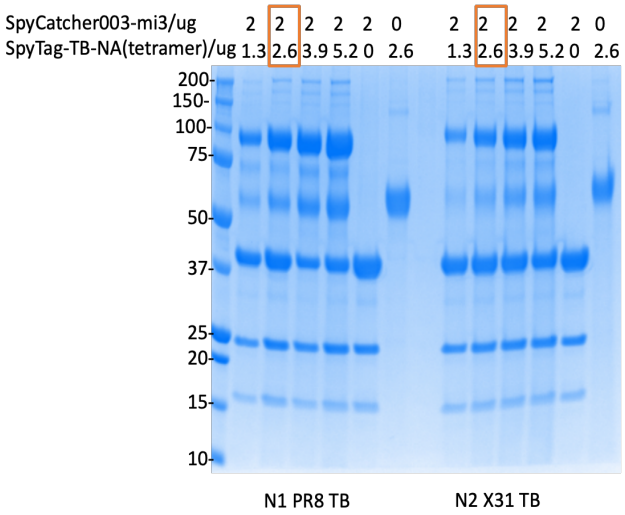

Mi3 particle 25/07/22 Batch A

thawed from -80°C and stayed at 4°C for 2 weeks

Mi3 particle conjugation fixed VLP(E.coli)

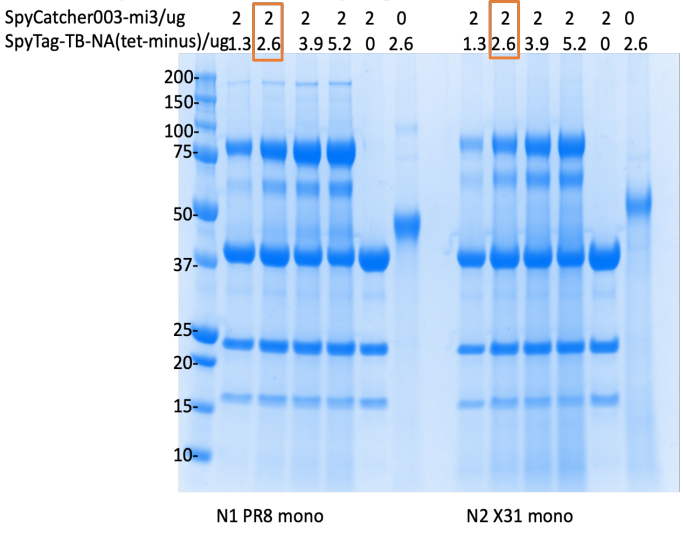

Mi3 particle 25/07/22 Batch A

thawed from -80°C and stayed at 4 for 3 weeks

Conjugation stock used
freshly thawed mi3 particles

NA and NA-VLP run through SDS-PAGE before vaccination for Fig. 4.14

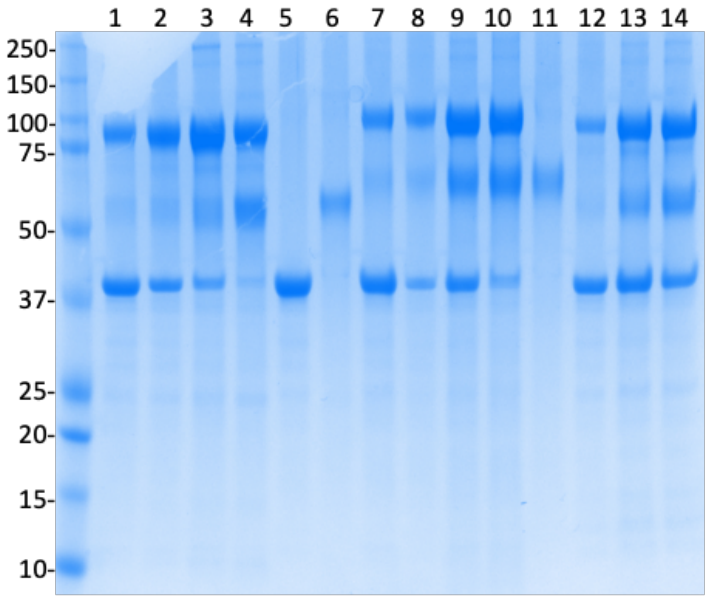

Lane	Antigen	VLP:Antigen molar ratio
1	N1 MS TB	0.1
2	N1 MS TB	0.2
3	N1 MS TB	0.3
4	N1 MS TB	0.4
5		VLP only
6	N1 MS TB	Antigen only
7	N2/20 TB	0.1
8	N2/20 TB	0.2
9	N2/20 TB	0.3
10	N2/20 TB	0.4
11	N2/20 TB	Antigen only
12	N6/16 TB	0.1
13	N6/16 TB	0.2
14	N6/16 TB	0.3

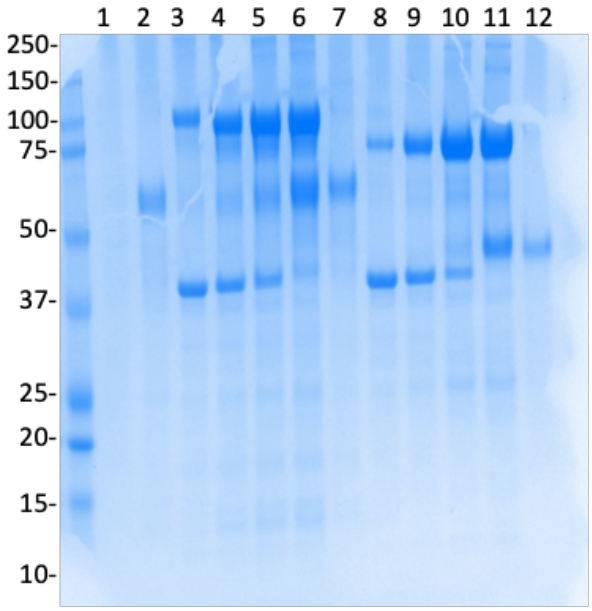

Lane	Antigen	VLP:Antigen molar ratio
1	Miss loading	
2	N6/16 TB	Antigen only
3	N9 Anhui TB	0.1
4	N9 Anhui TB	0.2
5	N9 Anhui TB	0.3
6	N9 Anhui TB	0.4
7	N9 Anhui TB	Antigen only
8	N8/20 TetDminus	0.25
9	N8/20 TetDminus	0.5
10	N8/20 TetDminus	1
11	N8/20 TetDminus	1.5
12	N8/20 TetDminus	Antigen only

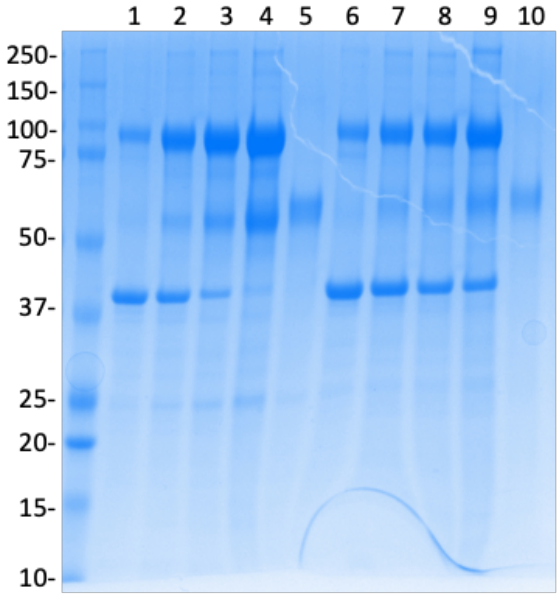

Lane	Antigen	VLP:Antigen molar ratio
1	N1 PR8 TB	0.1
2	N1 PR8 TB	0.2
3	N1 PR8 TB	0.3
4	N1 PR8 TB	0.4
5	N1 PR8 TB	Antigen only
6	N2 X31 TB	0.1
7	N2 X31 TB	0.2
8	N2 X31 TB	0.3
9	N2 X31 TB	0.4
10	N2 X31 TB	Antigen only

Put 2ug VLP for conjugation in each well,
Gel run at 150V, 50min

Appendix 7 IC 50 summary for PR8 challenge

Mice number (N1 PR8 TB	Serum IC50 titre*	Survive from challenge or not	Greatest weight reduction recorded
1	145	No	/
2	3459	Yes	18.90%
3	1143	Yes	19.70%
4	680	No	/
5	11889	No	/
6	398	No	/

Mice number (N1 PR8 TetDminus-VLP group)	Serum IC50 titre*	Survive from challenge or not	Greatest weight reduction recorded
1	7069	Yes	19.80%
2	6726	No	/
3	7666	No	/
4	17223	No	/
5	1001	No	/
6	3066	Yes	17.70%

Mice number (N1 PR8 TB-VLP group)	Serum IC50 titre*	Survive from challenge or not	Greatest weight reduction recorded
1	2676	Yes	2.90%
2	17087	Yes	3.10%
3	20293	Yes	4.80%
4	15931	Yes	3.70%
5	13113	Yes	9.10%
6	8198	Yes	1.60%

Individual mice sera comparison for N1 PR8 challenge model
*IC50 titres for obtained from pre-challenge serum ELLA analysis

Appendix 8 List of Loop annotations in Varghese et al 1983 used as a reference for creating NA hybrids.

Table 1 shows the loop regions mark discussed by Pramila and Alain with the original N2 numbering; Table 2 shows the loop regions with reference to the 2006 H5N1 crystal structure (PDB 2HTY). Residues in variable loops are highlighted in red, with the final grafted amino acid sequences corresponding to those specified in Table A.

Table A

Loops	N2 numbering	N2 NA Loops (Varghese et al 1983)	N1 numbering	mSN1 Loops	N1/09 Loops	N1/19 Loops	PR8 N1 Loops
B1L01	107-119	RLSAGGDIWVTRE	107-119	RIGSKGDVFVIRE	RIGSKGDVFVIRE	RIGSKGDVFVIRE	RIGSKGDVFVIRE
B1L23	135-156	GQGTTLDNKHSNDTVH DRIPHR	135-156	TQGALLNDKHSNGTVKDR SPYR	TQGALLNDKHSNGTIKDRS PYR	TQGALLNDKHSNGTIKDRS PYR	TQGALLNDRHSNGTVKDR SPYR
B2L01	175-177	CIA	176-178	SVA	SVA	SVA	SVA
B2L23	195-199	TGDDK	196-199	SGPD	SGPD	SGPD	SGPD
B3L01	218-227	WSQNILRTQE	219-228	WRNNILRTQE	WRNNILRTQE	WRNKILRTQE	WRKKILRTQE
B3L23	243-250	DGSASGRA	244-251	DGPSNGQA	DGPSNGQA	DGPSDGQA	DGPSDGLA
B4L01	269-277	AGSAQHVEE	269-278	LNAPNYHYEE	MNAPNYHYEE	MKAPNYHYEE	LNAPNSHYEE
B4L23	292-295	RDNW	293-296	RDNW	RDNW	RDNW	RDNW
B5L01	315-350	SYVCSGLVGDTPRNDD RSSNSNCRDPNNERGT	314-347	IGYICSGVFGDNPRPNDGT GSCSPMSSNGAYGVK	IGYICSGIFGDNPRPNDKTG SCGPVSSNGANGVK	MGYICSGVFGDNPRPNDK TGSCGPVSSNGANGVK	IGYICSGVFGDNPRPKDGT GSCGPVYVDGANGVK
B5L23	367-371	SKDLR	364-369	STSSRS	SISSRN	SISSRK	SHSSRH
B6L01	399-403	DSDNR	395-399	EITDW	GINEW	GINEW	AMTDW
B6L23	429-437	GRKQETRVW	430-437	RPKENTIW	RPKENTIW	RPEENTIW	GRPKEKTIW
Comments					12 aa changes in 5 Loops	16 aa changes in 8 Loops	18 aa changes in 8 Loops

Table B

Loops	N2 numbering	N2 loops by Varghese et al. 1983	N1 numbering	N1 numbering by Russell et al. 2006; PDB: 2HTY	N1/09 loops	N1/19 loops	N1 MS loops	N1 PR8 loops
B1L01	107-119	RLSAGGDIWVTRE	103-114	DNSVRIGSKGDV	DNSVRIGSKGDV	DNSVRIGSKGDV	DNGIRIGSKGDV	DNSIRIGSKGDV
B1L23	135-156	GQGTTLDNKHSNDT VHDRIPHR	140-156	LNDKHSNGTIKDRSP YR	LNDKHSNGTIKDRSP YR	LNDKHSNGTIKDRSP YR	LNDKHSNGTVKDRS PYR	LNDKHSNGTVKDRS PYR
B2L01	175-177	CIA	178-179	AW	AW	AW	AW	AW
B2L23	195-199	TGDDK	197-202	DPDNGA	DPDNGA	DPDSGA	DPDNGA	DPDNGA
B3L01	218-227	WSQNILRTQE	217-224	KSWRNNIL	KSWRNNIL	KSWRNKIL	KSWRNNIL	KSWRKKIL
B3L23	243-250	DGSASGRA	245-251	GPSNGQA	GPSNGQA	GPSDGQA	GPSNGQA	GPSDGLA
B4L01	269-277	AGSAQHVEE	269-279	MNNAPNYHYEEC	MNAPNYHYEEC	MKAPNYHYEEC	LNAPNYHYEEC	LNAPNYHYEEC
B4L23	292-295	RDNW	292-301	CRDNWHGSNR	CRDNWHGSNR	CRDNWHGSNR	CRDNWHGSNR	CRDNWHGSNR
B5L01	315-350	SYVCSGLVGDTPRN DDRSSNSNCRDPNN ERGT	317-349	ICSGIFGDNPRNDKT GSCGPVSSNGANGV KGF	ICSGIFGDNPRNDKT GSCGPVSSNGANGV KGF	ICSGIFGDNPRNDKT GSCGPVSSNGANGVK GF	ICSGIFGDNPRNDKT GSCGPVSSNGANGV KGF	ICSGIFGDNPRNDKT GSCGPVSSNGANGV KGF
B5L23	367-371	SKDLR	362-368	TKSSISSR	TKSSISSR	TKSSISSR	TKSSTSSR	TKSSHSSR
B6L01	399-403	DSDNR	400-402	SGY	SGY	SGY	SGY	SGY
B6L23	429-437	GRKQETRVW	430-438	RPKENTIWT	RPEENTIWT	RPKENTIWT	RPKENTIWT	RPKENTIWT

Appendix 9 Binding titration of mAbs against recombinant soluble proteins or NA expressed on the cell surface.
a) Twenty-five anti-N1 mAbs were titrated for binding against mSN1, N1/09 and N1/19 and their loop transferred hybrid variants. b) Binding titration of eighteen mAbs that bind either PR8 N1 or mSN1 on wild type sequence proteins and their loop-grafted hybrid proteins. Area under curve (AUC) was calculated and normalised against one of the strongest binders to rank the order. mAbs that showed Loops-specific binding or anomalous binding are highlighted with arrows.

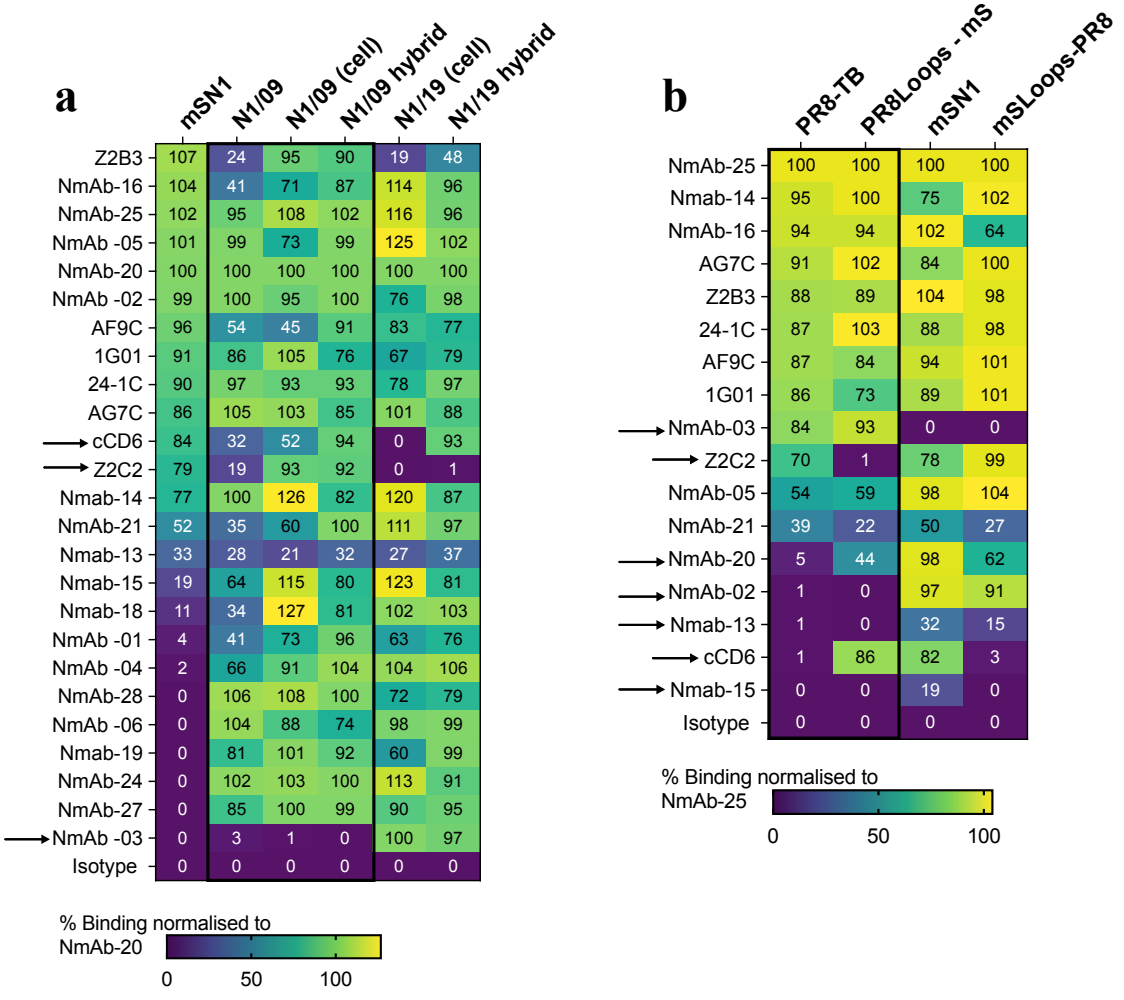

Appendix 10 Interface residues are listed according to PDB 2HT5. Residues of N8 Henan TetDminus listed as interface ones were replaced by the amino acid from N8/20 TetDminus at same position.

accession	type	label	start	end	notes	PDB numbering (2HT5)
Q07599	Interaction interfaces	Neuraminidase (self) (Q07599)	102	102	Type: Interface Range: ASN102 - ASN102 Partner: Neuraminidase Observed in 6 entries; e.g. 4gb1;	N104
Q07599	Interaction interfaces	Neuraminidase (self) (Q07599)	105	105	Type: Interface Range: ARG105 - ARG105 Partner: Neuraminidase Observed in 12 entries; e.g. 2ht8;	R107
Q07599	Interaction interfaces	Neuraminidase (self) (Q07599)	106	106	Type: Interface Range: ILE106 - ILE106 Partner: Neuraminidase Observed in 4 entries; e.g. 4mju;	I108
Q07599	Interaction interfaces	Neuraminidase (self) (Q07599)	108	108	Type: Interface Range: SER108 - SER108 Partner: Neuraminidase Observed in 9 entries; e.g. 2ht8;	S110
Q07599	Interaction interfaces	Neuraminidase (self) (Q07599)	109	109	Type: Interface Range: ARG109 - ARG109 Partner: Neuraminidase Observed in 12 entries; e.g. 2ht8;	R111
Q07599	Interaction interfaces	Neuraminidase (self) (Q07599)	111	111	Type: Interface Range: HIS111 - HIS111 Partner: Neuraminidase Observed in 12 entries; e.g. 2ht8;	H113
Q07599	Interaction interfaces	Neuraminidase (self) (Q07599)	134	134	Type: Interface Range: GLN134 - GLN134 Partner: Neuraminidase Observed in 12 entries; e.g. 2ht8;	Q136
Q07599	Interaction interfaces	Neuraminidase (self) (Q07599)	135	135	Type: Interface Range: GLY135 - GLY135 Partner: Neuraminidase Observed in 9 entries; e.g. 2ht8;	G137
Q07599	Interaction interfaces	Neuraminidase (self) (Q07599)	136	136	Type: Interface Range: SER136 - SER136 Partner: Neuraminidase Observed in 2 entries; e.g. 2ht5;	S138
Q07599	Interaction interfaces	Neuraminidase (self) (Q07599)	138	138	Type: Interface Range: LEU138 - LEU138 Partner: Neuraminidase Observed in 4 entries; e.g. 2ht8;	L140
Q07599	Interaction interfaces	Neuraminidase (self) (Q07599)	139	139	Type: Interface Range: ASN139 - ASN139 Partner: Neuraminidase Observed in 1 entry; e.g. 3o9j;	N141
Q07599	Interaction interfaces	Neuraminidase (self) (Q07599)	140	140	Type: Interface Range: ASP140 - ASP140 Partner: Neuraminidase Observed in 12 entries; e.g. 2ht8;	D142
Q07599	Interaction interfaces	Neuraminidase (self) (Q07599)	141	141	Type: Interface Range: LYS141 - LYS141 Partner: Neuraminidase Observed in 12 entries; e.g. 2ht8;	K143
Q07599	Interaction interfaces	Neuraminidase (self) (Q07599)	142	142	Type: Interface Range: HIS142 - HIS142 Partner: Neuraminidase Observed in 8 entries; e.g. 4gb1;	H144
Q07599	Interaction interfaces	Neuraminidase (self) (Q07599)	153	153	Type: Interface Range: PHE153 - PHE153 Partner: Neuraminidase Observed in 6 entries; e.g. 4gb1;	F155
Q07599	Interaction interfaces	Neuraminidase (self) (Q07599)	163	163	Type: Interface Range: GLN163 - GLN163 Partner: Neuraminidase Observed in 12 entries; e.g. 2ht8;	Q165
Q07599	Interaction interfaces	Neuraminidase (self) (Q07599)	167	167	Type: Interface Range: VAL167 - VAL167 Partner: Neuraminidase Observed in 10 entries; e.g. 2ht8;	V169
Q07599	Interaction interfaces	Neuraminidase (self) (Q07599)	168	168	Type: Interface Range: TYR168 - TYR168 Partner: Neuraminidase Observed in 5 entries; e.g. 2ht8;	Y169_A
Q07599	Interaction interfaces	Neuraminidase (self) (Q07599)	169	169	Type: Interface Range: GLN169 - GLN169 Partner: Neuraminidase Observed in 12 entries; e.g. 2ht8;	Q170
Q07599	Interaction interfaces	Neuraminidase (self) (Q07599)	170	170	Type: Interface Range: ALA170 - ALA170 Partner: Neuraminidase Observed in 12 entries; e.g. 2ht8;	A171
Q07599	Interaction interfaces	Neuraminidase (self) (Q07599)	187	187	Type: Interface Range: LYS187 - LYS187 Partner: Neuraminidase Observed in 2 entries; e.g. 2ht7;	K188
Q07599	Interaction interfaces	Neuraminidase (self) (Q07599)	194	194	Type: Interface Range: THR194 - THR194 Partner: Neuraminidase Observed in 12 entries; e.g. 2ht8;	T195
Q07599	Interaction interfaces	Neuraminidase (self) (Q07599)	212	212	Type: Interface Range: ASP212 - ASP212 Partner: Neuraminidase Observed in 1 entry; e.g. 4gb1;	D213
Q07599	Interaction interfaces	Neuraminidase (self) (Q07599)	215	215	Type: Interface Range: ASN215 - ASN215 Partner: Neuraminidase Observed in 11 entries; e.g. 3o9j;	N216
Q07599	Interaction interfaces	Neuraminidase (self) (Q07599)	260	260	Type: Interface Range: ARG260 - ARG260 Partner: Neuraminidase Observed in 9 entries; e.g. 2ht8;	R261
Q07599	Interaction interfaces	Neuraminidase (self) (Q07599)	408	408	Type: Interface Range: LEU408 - LEU408 Partner: Neuraminidase Observed in 1 entry; e.g. 2ht7;	L412
Q07599	Interaction interfaces	Neuraminidase (self) (Q07599)	411	411	Type: Interface Range: GLU411 - GLU411 Partner: Neuraminidase Observed in 1 entry; e.g. 3o9j;	E412_C
Q07599	Interaction interfaces	Neuraminidase (self) (Q07599)	413	413	Type: Interface Range: SER413 - SER413 Partner: Neuraminidase Observed in 8 entries; e.g. 2ht8;	S413
Q07599	Interaction interfaces	Neuraminidase (self) (Q07599)	414	414	Type: Interface Range: GLY414 - GLY414 Partner: Neuraminidase Observed in 2 entries; e.g. 4mjv;	G414
Q07599	Interaction interfaces	Neuraminidase (self) (Q07599)	450	450	Type: Interface Range: TYR450 - TYR450 Partner: Neuraminidase Observed in 1 entry; e.g. 4gb1;	Y451
Q07599	Interaction interfaces	Neuraminidase (self) (Q07599)	451	451	Type: Interface Range: GLU451 - GLU451 Partner: Neuraminidase Observed in 11 entries; e.g. 3o9j;	E452
Q07599	Interaction interfaces	Neuraminidase (self) (Q07599)	457	457	Type: Interface Range: TRP457 - TRP457 Partner: Neuraminidase Observed in 12 entries; e.g. 2ht8;	W458
Q07599	Interaction interfaces	Neuraminidase (self) (Q07599)	462	462	Type: Interface Range: ILE462 - ILE462 Partner: Neuraminidase Observed in 10 entries; e.g. 2ht8;	I463
Q07599	Interaction interfaces	Neuraminidase (self) (Q07599)	464	464	Type: Interface Range: PRO464 - PRO464 Partner: Neuraminidase Observed in 11 entries; e.g. 2ht8;	P465

Appendix 11 Manuscript of "Structure-Guided Loop Grafting Improves Expression and Stability of Influenza Neuraminidase for Vaccine Development"

Structure-Guided Loop Grafting Improves Expression and Stability of Influenza Neuraminidase for Vaccine Development

Pramila Rijal[1,2*], Leiyan Wei[1,2], Guido C Paesen[3], David I Stuart[1,3], Mark R Howarth[4], Kuan-Ying A Huang[5*], Thomas A Bowden[3], Alain RM Townsend[1,2*]

[1] Chinese Academy of Medical Science Oxford Institute, Nuffield Department of Medicine, University of Oxford, Oxford, UK
[2] MRC Human Immunology Unit, MRC Weatherall Institute of Molecular Medicine, John Radcliffe Hospital, University of Oxford, Oxford, UK
[3] Division of Structural Biology, Centre for Human Genetics, University of Oxford, Oxford, UK
[4] Department of Pharmacology, University of Cambridge, Tennis Court Road, Cambridge, UK
[5] Graduate Institute of Immunology and Department of Paediatrics, National Taiwan University Hospital, College of Medicine, National Taiwan University, Taipei, Taiwan

*Correspondence: Alain Townsend (alain.townsend@rdm.ox.ac.uk), Pramila Rijal (pramila.rijal@rdm.ox.ac.uk), Kuan-Ying A Huang (arthurhuang1726@ntu.edu.tw)

Abstract

Influenza neuraminidase is a crucial target for protective antibodies, yet the development of recombinant neuraminidase protein as a vaccine has been held back by instability and variable expression. We have taken a pragmatic approach to improving expression and stability of neuraminidase by grafting antigenic surface loops from low-expressing neuraminidase proteins onto the scaffold of high-expressing counterparts. The resulting hybrid proteins retained the antigenic properties of the loop donor while benefiting from the high-yield expression, stability, and tetrameric structure of the loop recipient. These hybrid proteins were recognised by a broad set of human monoclonal antibodies elicited by influenza infection or vaccination, with X-ray structures validating the accurate structural conformation of the grafted loops and the enzymatic cavity. Immunisation of mice with neuraminidase hybrids induced inhibitory antibodies to the loop donor and conferred protected against lethal influenza challenge. This pragmatic technique offers a robust solution for improving the expression and stability of influenza neuraminidase proteins for vaccine development.

References

Air, G. M. (2012). Influenza neuraminidase. *Influenza and Other Respiratory Viruses*, *6*(4), 245–256. https://doi.org/10.1111/J.1750-2659.2011.00304.X

Akkina, R. K., Richardson, J. C., Aguilera, M. C., & Yang, C. M. (1991). Heterogeneous forms of polymerase proteins exist in influenza A virus-infected cells. *Virus Research*, *19*(1), 17–30. https://doi.org/10.1016/0168-1702(91)90091-9

Baek, Y. H., Song, M.-S., Lee, E.-Y., Kim, Y., Kim, E.-H., Park, S.-J., Park, K. J., Kwon, H., Pascua, P. N. Q., Lim, G.-J., Kim, S., Yoon, S.-W., Kim, M. H., Webby, R. J., & Choi, Y.-K. (2014). Profiling and Characterization of Influenza Virus N1 Strains Potentially Resistant to Multiple Neuraminidase Inhibitors. *Journal of Virology*, *89*(1), 287. https://doi.org/10.1128/JVI.02485-14

Bessa, J., Zabel, F., Link, A., Jegerlehner, A., Hinton, H. J., Schmitz, N., Bauer, M., Kündig, T. M., Saudan, P., & Bachmann, M. F. (2012). Low-affinity B cells transport viral particles from the lung to the spleen to initiate antibody responses. *Proceedings of the National Academy of Sciences of the United States of America*, *109*(50), 20566–20571. https://doi.org/10.1073/pnas.1206970109

Bhatt, S., Holmes, E. C., & Pybus, O. G. (2011). The genomic rate of molecular adaptation of the human influenza A virus. *Molecular Biology and Evolution*, *28*(9), 2443–2451. https://doi.org/10.1093/molbev/msr044

Boonstra, S., Blijleven, J. S., Roos, W. H., Onck, P. R., van der Giessen, E., & van Oijen, A. M. (2018). Hemagglutinin-Mediated Membrane Fusion: A Biophysical Perspective. *Annual Review of Biophysics*, *47*, 153–173. https://doi.org/10.1146/annurev-biophys-070317-033018

Brenner, S., & Horne, R. W. (1959). A negative staining method for high resolution electron microscopy of viruses. *Biochimica et Biophysica Acta*, *34*, 103–110. https://doi.org/10.1016/0006-3002(59)90237-9

Bresee, J., Fitzner, J., Campbell, H., Cohen, C., Cozza, V., Jara, J., Krishnan, A., & Lee, V. (2018). Progress and Remaining Gaps in Estimating the Global Disease Burden of Influenza. *Emerging Infectious Diseases*, *24*(7), 1173–1177. https://doi.org/10.3201/eid2407.171270

Bright, R. A., Carter, D. M., Daniluk, S., Toapanta, F. R., Ahmad, A., Gavrilov, V., Massare, M., Pushko, P., Mytle, N., Rowe, T., Smith, G., & Ross, T. M. (2007). Influenza virus-like particles elicit broader immune responses than whole virion inactivated influenza virus or recombinant hemagglutinin. *Vaccine*, *25*(19), 3871–3878. https://doi.org/10.1016/j.vaccine.2007.01.106

Brouwer, P. J. M., Antanasijevic, A., Ronk, A. J., Müller-Kräuter, H., Watanabe, Y., Claireaux, M., Perrett, H. R., Bijl, T. P. L., Grobben, M., Umotoy, J. C., Schriek, A. I., Burger, J. A., Tejjani, K., Lloyd, N. M., Steijaert, T. H., van Haaren, M. M., Sliepen, K., de Taeye, S. W., van Gils, M. J., … Sanders, R. W. (2022). Lassa virus glycoprotein nanoparticles elicit neutralizing antibody responses and protection. *Cell Host & Microbe*, *30*(12), 1759-1772.e12. https://doi.org/10.1016/j.chom.2022.10.018

Bruun, T. U. J., Andersson, A. M. C., Draper, S. J., & Howarth, M. (2018). Engineering a Rugged Nanoscaffold To Enhance Plug-and-Display Vaccination. *ACS Nano*, *12*(9), 8855–8866. https://doi.org/10.1021/ACSNANO.8B02805

Bucher, D. J. (1977). Purification of neuraminidase from influenza viruses by affinity chromatography. *Biochimica Et Biophysica Acta*, *482*(2), 393–399. https://doi.org/10.1016/0005-2744(77)90253-4

Bullard, B. L., & Weaver, E. A. (2021). Strategies Targeting Hemagglutinin as a Universal Influenza Vaccine. *Vaccines*, *9*(3), 257. https://doi.org/10.3390/vaccines9030257

Burnet, F. M. (1951). Mucoproteins in relation to virus action. *Physiological Reviews*, *31*(2), 131–150. https://doi.org/10.1152/physrev.1951.31.2.131

Butler, D. (2013). Mapping the H7N9 avian flu outbreaks. *Nature*. https://doi.org/10.1038/nature.2013.12863

Cao, G., Guo, Z., Liu, J., & Liu, M. (2023). Change from low to out-of-season epidemics of influenza in China during the COVID-19 pandemic: A time series study. *Journal of Medical Virology*, *95*(6), e28888. https://doi.org/10.1002/jmv.28888

CDC. (2024, October 11). *Effectiveness Against Different Flu Viruses*. Flu Vaccines Work. https://www.cdc.gov/flu-vaccines-work/effectiveness/index.html

Chan, P. K. S. (2002). Outbreak of avian influenza A(H5N1) virus infection in Hong Kong in 1997. *Clinical Infectious Diseases: An Official Publication of the Infectious Diseases Society of America*, *34 Suppl 2*, S58-64. https://doi.org/10.1086/338820

Chen, Y. Q., Wohlbold, T. J., Zheng, N. Y., Huang, M., Huang, Y., Neu, K. E., Lee, J., Wan, H., Rojas, K. T., Kirkpatrick, E., Henry, C., Palm, A. K. E., Stamper, C. T., Lan, L. Y. L., Topham, D. J., Treanor, J., Wrammert, J., Ahmed, R., Eichelberger, M. C., … Wilson, P. C. (2018). Influenza Infection in Humans Induces Broadly Cross-Reactive and Protective Neuraminidase-Reactive Antibodies. *Cell*, *173*(2), 417-429.e10. https://doi.org/10.1016/J.CELL.2018.03.030/ATTACHMENT/85AEFD89-E726-49AC-B3E7-68A60C112A43/MMC1.PDF

Cohen, A. A., Gnanapragasam, P. N. P., Lee, Y. E., Hoffman, P. R., Ou, S., Kakutani, L. M., Keeffe, J. R., Wu, H. J., Howarth, M., West, A. P., Barnes, C. O., Nussenzweig, M. C., & Bjorkman, P. J. (2021). Mosaic nanoparticles elicit cross-reactive immune

responses to zoonotic coronaviruses in mice. *Science*, *371*(6530), 735–741. https://doi.org/10.1126/science.abf6840

Colman, P. M., Laver, W. G., Varghese, J. N., Baker, A. T., Tulloch, P. A., Air, G. M., & Webster, R. G. (1987). Three-dimensional structure of a complex of antibody with influenza virus neuraminidase. *Nature 1987 326:6111*, *326*(6111), 358–363. https://doi.org/10.1038/326358a0

Colman, P. M., Varghese, J. N., & Laver, W. G. (1983). Structure of the catalytic and antigenic sites in influenza virus neuraminidase. *Nature*, *303*(5912), 41–44. https://doi.org/10.1038/303041A0

Couch, R. B., Atmar, R. L., Franco, L. M., Quarles, J. M., Wells, J., Arden, N., Niño, D., & Belmont, J. W. (2013). Antibody correlates and predictors of immunity to naturally occurring influenza in humans and the importance of antibody to the neuraminidase. *The Journal of Infectious Diseases*, *207*(6), 974–981. https://doi.org/10.1093/infdis/jis935

Couch, R. B., Kasel, J. A., Gerin, J. L., Schulman, J. L., & Kilbourne, E. D. (1974). Induction of partial immunity to influenza by a neuraminidase-specific vaccine. *The Journal of Infectious Diseases*, *129*(4), 411–420. https://doi.org/10.1093/infdis/129.4.411

Couzens, L., Gao, J., Westgeest, K., Sandbulte, M., Lugovtsev, V., Fouchier, R., & Eichelberger, M. (2014). An optimized enzyme-linked lectin assay to measure influenza A virus neuraminidase inhibition antibody titers in human sera. *Journal of Virological Methods*, *210*, 7–14. https://doi.org/10.1016/j.jviromet.2014.09.003

Creytens, S., Pascha, M. N., Ballegeer, M., Saelens, X., & de Haan, C. A. M. (2021). Influenza Neuraminidase Characteristics and Potential as a Vaccine Target. *Frontiers in Immunology*, *12*, 786617. https://doi.org/10.3389/fimmu.2021.786617

Da Silva, D. V., Nordholm, J., Madjo, U., Pfeiffer, A., & Daniels, R. (2013). Assembly of subtype 1 influenza neuraminidase is driven by both the transmembrane and head domains. *Journal of Biological Chemistry*, *288*(1), 644–653. https://doi.org/10.1074/jbc.M112.424150

Dai, M., Guo, H., Dortmans, J. C. F. M., Dekkers, J., Nordholm, J., Daniels, R., van Kuppeveld, F. J. M., de Vries, E., & de Haan, C. A. M. (2016). Identification of Residues That Affect Oligomerization and/or Enzymatic Activity of Influenza Virus H5N1 Neuraminidase Proteins. *Journal of Virology*, *90*(20), 9457–9470. https://doi.org/10.1128/JVI.01346-16

Deng, X., Wang, Q., Liu, M., Zheng, Q., Wu, F., & Huang, J. (2021). Tetrameric Neuraminidase of Influenza A Virus Is Required to Induce Protective Antibody Responses in Mice. *Frontiers in Microbiology*, *12*. https://doi.org/10.3389/fmicb.2021.729914

Desheva, Y. A., Smolonogina, T. A., Donina, S. A., & Rudenko, L. G. (2015). Serum strain-specific or cross-reactive neuraminidase inhibiting antibodies against pandemic A/California/07/2009(H1N1) influenza in healthy volunteers. *BMC Research Notes*, *8*(1), 136. https://doi.org/10.1186/s13104-015-1086-z

Doyle, T. M., Hashem, A. M., Li, C., Van Domselaar, G., Larocque, L., Wang, J., Smith, D., Cyr, T., Farnsworth, A., He, R., Hurt, A. C., Brown, E. G., & Li, X. (2013). Universal anti-neuraminidase antibody inhibiting all influenza A subtypes. *Antiviral Research*, *100*(2), 567–574. https://doi.org/10.1016/j.antiviral.2013.09.018

Durocher, Y., & Butler, M. (2009). Expression systems for therapeutic glycoprotein production. *Current Opinion in Biotechnology*, *20*(6), 700–707. https://doi.org/10.1016/j.copbio.2009.10.008

Easterbrook, J. D., Schwartzman, L. M., Gao, J., Kash, J. C., Morens, D. M., Couzens, L., Wan, H., Eichelberger, M. C., & Taubenberger, J. K. (2012). Protection against a lethal H5N1 influenza challenge by intranasal immunization with virus-like particles containing 2009 pandemic H1N1 neuraminidase in mice. *Virology*, *432*(1), 39–44. https://doi.org/10.1016/j.virol.2012.06.003

Eichelberger, M. C., Couzens, L., Gao, Y., Levine, M., Katz, J., Wagner, R., Thompson, C. I., Höschler, K., Laurie, K., Bai, T., Engelhardt, O. G., & Wood, J. (2016). Comparability of neuraminidase inhibition antibody titers measured by enzyme-linked lectin assay (ELLA) for the analysis of influenza vaccine immunogenicity. *Vaccine*, *34*(4), 458–465. https://doi.org/10.1016/j.vaccine.2015.12.022

Eichelberger, M. C., & Monto, A. S. (2019). Neuraminidase, the Forgotten Surface Antigen, Emerges as an Influenza Vaccine Target for Broadened Protection. *The Journal of Infectious Diseases*, *219*(Supplement_1), S75–S80. https://doi.org/10.1093/infdis/jiz017

Ellis, D., Lederhofer, J., Acton, O. J., Tsybovsky, Y., Kephart, S., Yap, C., Gillespie, R. A., Creanga, A., Olshefsky, A., Stephens, T., Pettie, D., Murphy, M., Sydeman, C., Ahlrichs, M., Chan, S., Borst, A. J., Park, Y. J., Lee, K. K., Graham, B. S., … Kanekiyo, M. (2022). Structure-based design of stabilized recombinant influenza neuraminidase tetramers. *Nature Communications 2022 13:1*, *13*(1), 1–16. https://doi.org/10.1038/s41467-022-29416-z

Expi293 Expression System—UK. (n.d.). Retrieved 9 January 2025, from https://www.thermofisher.com/uk/en/home/life-science/protein-biology/protein-expression/mammalian-protein-expression/transient-mammalian-protein-expression/expi293-expression-system.html

ExpiCHO Expression System | Thermo Fisher Scientific—UK. (n.d.). Retrieved 2 December 2024, from https://www.thermofisher.com/uk/en/home/life-science/protein-biology/protein-expression/mammalian-protein-expression/transient-mammalian-protein-expression/expicho-expression-system.html?gclid=Cj0KCQiAr7C6BhDRARIsAOUKifgYpTyEl7AJEPxTz7V4nMLD57oPNKlta_9CG6kAZUifkUiYz9r5MYsaAp3fEALw_wcB&ef_id=Cj0KCQiAr7C6BhDRARIsAOUKifgYpTyEl7AJEPxTz7V4nMLD57oPNKlta_9CG6kAZUifkUiYz9r5MYsaAp3fEALw_wcB:G:s&s_kwcid=AL!3652!3!558254974742!e!!g!!expicho!13483165 64!64157103517&cid=bid_clb_pex_r01_co_cp0000_pjt0000_bid00000_0se_gaw_bt_pur_con&gad_source=1

Fereidouni, S., Starick, E., Karamendin, K., Genova, C. D., Scott, S. D., Khan, Y., Harder, T., & Kydyrmanov, A. (2023). Genetic characterization of a new candidate hemagglutinin subtype of influenza A viruses. *Emerging Microbes & Infections*, *12*(2), 2225645. https://doi.org/10.1080/22221751.2023.2225645

Fiebiger, E., Meraner, P., Weber, E., Fang, I.-F., Stingl, G., Ploegh, H., & Maurer, D. (2001). Cytokines Regulate Proteolysis in Major Histocompatibility Complex Class II–Dependent Antigen Presentation by Dendritic Cells. *The Journal of Experimental Medicine*, *193*(8), 881–892.

Field's Virology; Volume 1: Emerging Viruses, 7th Edition (Vol. 2020, Issue 13). (n.d.). Ringgold, Inc.

Fischer, W. A., Chason, K. D., Brighton, M., & Jaspers, I. (2014). Live attenuated influenza vaccine strains elicit a greater innate immune response than antigenically-matched seasonal influenza viruses during infection of human nasal epithelial cell cultures. *Vaccine*, *32*(15), 1761–1767. https://doi.org/10.1016/j.vaccine.2013.12.069

Flu vaccines for the 2024 to 2025 season. (n.d.). GOV.UK. Retrieved 28 November 2024, from https://www.gov.uk/government/publications/flu-vaccines-for-the-current-season/flu-vaccines-for-the-2023-to-2024-season

Francis, T., Salk, J. E., & Quilligan, J. J. (1947). Experience with Vaccination Against Influenza in the Spring of 1947: A Preliminary Report. *American Journal of Public Health and the Nation's Health*, *37*(8), 1013–1016. https://doi.org/10.2105/ajph.37.8.1013

Gamblin, S. J., & Skehel, J. J. (2010). Influenza Hemagglutinin and Neuraminidase Membrane Glycoproteins. *The Journal of Biological Chemistry*, *285*(37), 28403–28409. https://doi.org/10.1074/jbc.R110.129809

Gao, J., Klenow, L., Parsons, L., Malik, T., Phue, J.-N., Gao, Z., Withers, S. G., Cipollo, J., Daniels, R., & Wan, H. (2021). Design of the Recombinant Influenza Neuraminidase Antigen Is Crucial for Its Biochemical Properties and Protective Efficacy. *Journal of Virology*, *95*(24). https://doi.org/10.1128/JVI.01160-21

Gao, J., Li, X., Klenow, L., Malik, T., Wan, H., Ye, Z., & Daniels, R. (2022). Antigenic comparison of the neuraminidases from recent influenza A vaccine viruses and 2019–2020 circulating strains. *Npj Vaccines*, *7*(1), undefined-undefined. https://doi.org/10.1038/S41541-022-00500-1

Gao, Z., Robinson, K., Skowronski, D. M., De Serres, G., & Withers, S. G. (2020). Quantification of the total neuraminidase content of recent commercially-available influenza vaccines: Introducing a neuraminidase titration reagent. *Vaccine*, *38*(4), 715–718. https://doi.org/10.1016/j.vaccine.2019.11.041

Ge, P., & Ross, T. M. (2024). COBRA HA and NA vaccination elicits long-live protective immune responses against pre-pandemic H2, H5, and H7 influenza virus subtypes. *Virology*, *597*, 110119. https://doi.org/10.1016/j.virol.2024.110119

Genetics of the Influenza Virus | Learn Science at Scitable. (n.d.). Retrieved 26 September 2024, from https://www.nature.com/scitable/topicpage/genetics-of-the-influenza-virus-716/

Gilbert, P. B., Fong, Y., Juraska, M., Carpp, L. N., Monto, A. S., Martin, E. T., & Petrie, J. G. (2019). HAI and NAI titer correlates of inactivated and live attenuated influenza vaccine efficacy. *BMC Infectious Diseases*, *19*(1), 453. https://doi.org/10.1186/s12879-019-4049-5

Giurgea, L. T., Morens, D. M., Taubenberger, J. K., & Memoli, M. J. (2020). Influenza neuraminidase: A neglected protein and its potential for a better influenza vaccine. *Vaccines*, *8*(3), 1–17. https://doi.org/10.3390/vaccines8030409

Giurgea, L. T., Park, J. K., Walters, K. A., Scherler, K., Cervantes-Medina, A., Freeman, A., Rosas, L. A., Kash, J. C., Taubenberger, J. K., & Memoli, M. J. (2021). The effect of calcium and magnesium on activity, immunogenicity, and efficacy of a recombinant N1/N2 neuraminidase vaccine. *Npj Vaccines*, *6*(1), 1–7. https://doi.org/10.1038/s41541-021-00310-x

Global Influenza Strategy 2019–2030. (n.d.). Retrieved 28 November 2024, from https://www.who.int/publications/i/item/9789241515320

Gottschalk, A. (1957). Neuraminidase: The specific enzyme of influenza virus and Vibrio cholerae. *Biochimica Et Biophysica Acta*, *23*(3), 645–646. https://doi.org/10.1016/0006-3002(57)90389-x

Gu, C., Fan, S., Dahn, R., Babujee, L., Chiba, S., Guan, L., Maemura, T., Pattinson, D., Neumann, G., & Kawaoka, Y. (2024). Characterization of a human H3N8 influenza virus. *eBioMedicine*, *101*. https://doi.org/10.1016/j.ebiom.2024.105034

Guo, J., Zhou, A., Sun, X., Sha, W., Ai, K., Pan, G., Zhou, C., Zhou, H., Cong, H., & He, S. (2019). Immunogenicity of a Virus-Like-Particle Vaccine Containing Multiple

Antigenic Epitopes of Toxoplasma gondii Against Acute and Chronic Toxoplasmosis in Mice. *Frontiers in Immunology*, *10*. https://doi.org/10.3389/fimmu.2019.00592

Harfoot, R., & Webby, R. J. (2017). H5 influenza, a global update. *Journal of Microbiology (Seoul, Korea)*, *55*(3), 196–203. https://doi.org/10.1007/s12275-017-7062-7

He, R., Yang, X., Liu, C., Chen, X., Wang, L., Xiao, M., Ye, J., Wu, Y., & Ye, L. (2018). Efficient control of chronic LCMV infection by a CD4 T cell epitope-based heterologous prime-boost vaccination in a murine model. *Cellular and Molecular Immunology*, *15*(9), 815–826. https://doi.org/10.1038/cmi.2017.3

Hirst, G. K. (1941). THE AGGLUTINATION OF RED CELLS BY ALLANTOIC FLUID OF CHICK EMBRYOS INFECTED WITH INFLUENZA VIRUS. *Science (New York, N.Y.)*, *94*(2427), 22–23. https://doi.org/10.1126/science.94.2427.22

Hirst, G. K. (1942). THE QUANTITATIVE DETERMINATION OF INFLUENZA VIRUS AND ANTIBODIES BY MEANS OF RED CELL AGGLUTINATION. *The Journal of Experimental Medicine*, *75*(1), 49–64. https://doi.org/10.1084/jem.75.1.49

History of flu (influenza): Outbreaks and vaccine timeline. (n.d.). Retrieved 28 November 2024, from https://www.mayoclinic.org/diseases-conditions/history-disease-outbreaks-vaccine-timeline/flu

History of influenza vaccination. (n.d.). Retrieved 28 November 2024, from https://www.who.int/news-room/spotlight/history-of-vaccination/history-of-influenza-vaccination

Horne, R. W., Waterson, A. P., Wildy, P., & Farnham, A. E. (1960). The structure and composition of the myxoviruses: I. Electron microscope studies of the structure of myxovirus particles by negative staining techniques. *Virology*, *11*(1), 79–98. https://doi.org/10.1016/0042-6822(60)90056-8

Hsia, Y., Bale, J. B., Gonen, S., Shi, D., Sheffler, W., Fong, K. K., Nattermann, U., Xu, C., Huang, P. S., Ravichandran, R., Yi, S., Davis, T. N., Gonen, T., King, N. P., & Baker, D. (2016). Design of a hyperstable 60-subunit protein icosahedron. *Nature 2016 535:7610*, *535*(7610), 136–139. https://doi.org/10.1038/nature18010

Hu, Z., Lu, S.-H., Lowrie, D. B., & Fan, X.-Y. (2022). Research Advances for Virus-vectored Tuberculosis Vaccines and Latest Findings on Tuberculosis Vaccine Development. *Frontiers in Immunology*, *13*. https://doi.org/10.3389/fimmu.2022.895020

Huang, P., Xu, Y., Ni, H., Zhong, J., Zhang, X., Tan, S., Wu, D., Qiu, B., Guan, D., Wen, M., Yan, J., & Zhang, Y. (2011). Linear B-cell epitope mapping of neuraminidases of the 2009 A H1N1 viruses based on immunoinformatics. *Vaccine*, *29*(6), 1278–1282. https://doi.org/10.1016/j.vaccine.2010.11.080

Influenza: A(H5N1). (n.d.). Retrieved 2 December 2024, from https://www.who.int/news-room/questions-and-answers/item/influenza-h5n1

Iuliano, A. D., Roguski, K. M., Chang, H. H., Muscatello, D. J., Palekar, R., Tempia, S., Cohen, C., Gran, J. M., Schanzer, D., Cowling, B. J., Wu, P., Kyncl, J., Ang, L. W., Park, M., Redlberger-Fritz, M., Yu, H., Espenhain, L., Krishnan, A., Emukule, G., … Global Seasonal Influenza-associated Mortality Collaborator Network. (2018). Estimates of global seasonal influenza-associated respiratory mortality: A modelling study. *Lancet (London, England)*, *391*(10127), 1285–1300. https://doi.org/10.1016/S0140-6736(17)33293-2

Jiang, H., Peng, W., Qi, J., Chai, Y., Song, H., Bi, Y., Rijal, P., Wang, H., Oladejo, B. O., Liu, J., Shi, Y., Gao, G. F., Townsend, A. R., & Wu, Y. (2020). Structure-based modification of an anti-neuraminidase human antibody restores protection efficacy against the drifted influenza virus. *mBio*, *11*(5), 1–14. https://doi.org/10.1128/mBio.02315-20

Job, E. R., Ysenbaert, T., Smet, A., Christopoulou, I., Strugnell, T., Oloo, E. O., Oomen, R. P., Kleanthous, H., Vogel, T. U., & Saelens, X. (2018). Broadened immunity against influenza by vaccination with computationally designed influenza virus N1 neuraminidase constructs. *NPJ Vaccines*, *3*(1), 55–55. https://doi.org/10.1038/s41541-018-0093-1

Johansson, B. E., Grajower, B., & Kilbourne, E. D. (1993). Infection-permissive immunization with influenza virus neuraminidase prevents weight loss in infected mice. *Vaccine*, *11*(10), 1037–1039. https://doi.org/10.1016/0264-410X(93)90130-P

Johansson, B. E., Matthews, J. T., & Kilbourne, E. D. (1998). Supplementation of conventional influenza A vaccine with purified viral neuraminidase results in a balanced and broadened immune response. *Vaccine*, *16*(9), 1009–1015. https://doi.org/10.1016/S0264-410X(97)00279-X

Johansson, B. E., Moran, T. M., & Kilbourne, E. D. (1987). Antigen-presenting B cells and helper T cells cooperatively mediate intravirionic antigenic competition between influenza A virus surface glycoproteins. *Proceedings of the National Academy of Sciences of the United States of America*, *84*(19), 6869–6873. https://doi.org/10.1073/pnas.84.19.6869

Kawai, A., Yamamoto, Y., Nogimori, T., Takeshita, K., Yamamoto, T., & Yoshioka, Y. (2021). The Potential of Neuraminidase as an Antigen for Nasal Vaccines To Increase Cross-Protection against Influenza Viruses. *Journal of Virology*, *95*(20), e0118021. https://doi.org/10.1128/JVI.01180-21

Keeble, A. H., & Howarth, M. (2020). Power to the protein: Enhancing and combining activities using the Spy toolbox. *Chemical Science*, *11*(28), 7281–7291. https://doi.org/10.1039/d0sc01878c

Keene, J.-A., & Forman, J. (1982). Helper activity is required for the in vivo generation of cytotoxic T lymphocytes. *The Journal of Experimental Medicine*, *155*(3), 768–782.

Khanna, M., Kumar, B., Gupta, N., Kumar, P., Gupta, A., Vijayan, V. K., & Kaur, H. (2009). Pandemic swine influenza virus (H1N1): A threatening evolution. *Indian Journal of Microbiology*, *49*(4), 365–369. https://doi.org/10.1007/s12088-009-0064-3

Kilbourne, E. D. (1976). Comparative efficacy of neuraminidase-specific and conventional influenza virus vaccines in induction of antibody to neuraminidase in humans. *The Journal of Infectious Diseases*, *134*(4), 384–394. https://doi.org/10.1093/infdis/134.4.384

Kilbourne, E. D. (2006). Influenza Pandemics of the 20th Century. *Emerging Infectious Diseases*, *12*(1), 9–14. https://doi.org/10.3201/eid1201.051254

Kilbourne, E. D., Couch, R. B., Kasel, J. A., Keitel, W. A., Cate, T. R., Quarles, J. H., Grajower, B., Pokorny, B. A., & Johansson, B. E. (1995). Purified influenza A virus N2 neuraminidase vaccine is immunogenic and non-toxic in humans. *Vaccine*, *13*(18), 1799–1803. https://doi.org/10.1016/0264-410x(95)00127-m

Kilbourne, E. D., Laver, W. G., Schulman, J. L., & Webster, R. G. (1968). Antiviral activity of antiserum specific for an influenza virus neuraminidase. *Journal of Virology*, *2*(4), 281–288. https://doi.org/10.1128/JVI.2.4.281-288.1968

Kim, Y.-I., Pascua, P. N. Q., Kwon, H.-I., Lim, G.-J., Kim, E.-H., Yoon, S.-W., Park, S.-J., Kim, S. M., Choi, E.-J., Si, Y.-J., Lee, O.-J., Shim, W.-S., Kim, S.-W., Mo, I.-P., Bae, Y., Lim, Y. T., Sung, M. H., Kim, C.-J., Webby, R. J., … Choi, Y. K. (2014). Pathobiological features of a novel, highly pathogenic avian influenza A(H5N8) virus. *Emerging Microbes & Infections*, *3*(1), 1–13. https://doi.org/10.1038/emi.2014.75

Kim, Y.-J., Ko, E.-J., Kim, M.-C., Lee, Y.-N., Kim, K.-H., Jung, Y.-J., & Kang, S.-M. (2017). Roles of antibodies to Influenza A virus hemagglutinin, neuraminidase, and M2e in conferring cross protection. *Biochemical and Biophysical Research Communications*, *493*(1), 393–398. https://doi.org/10.1016/j.bbrc.2017.09.011

Koh, E., & Kim, T. (2005). Minimal surface as a model of beta-sheets. *Proteins*, *61*(3), 559–569. https://doi.org/10.1002/prot.20636

Kühnel, K., Jarchau, T., Wolf, E., Schlichting, I., Walter, U., Wittinghofer, A., & Strelkov, S. V. (2004). The VASP tetramerization domain is a right-handed coiled coil based on a 15-residue repeat. *Proceedings of the National Academy of Sciences*, *101*(49), 17027–17032. https://doi.org/10.1073/pnas.0403069101

Kunert, R., & Reinhart, D. (2016). Advances in recombinant antibody manufacturing. *Applied Microbiology and Biotechnology*, *100*(8), 3451–3461. https://doi.org/10.1007/s00253-016-7388-9

Lambré, C. R., Terzidis, H., Greffard, A., & Webster, R. G. (1990). Measurement of anti-influenza neuraminidase antibody using a peroxidase-linked lectin and microtitre plates coated with natural substrates. *Journal of Immunological Methods*, *135*(1–2), 49–57. https://doi.org/10.1016/0022-1759(90)90255-t

Lambré, C. R., Terzidis, H., Greffard, A., & Webster, R. G. (1991). An enzyme-linked lectin assay for sialidase. *Clinica Chimica Acta*, *198*(3), 183–193. https://doi.org/10.1016/0009-8981(91)90352-D

Laver, W. G. (1978). Crystallization and peptide maps of neuraminidase 'heads' from H2N2 and H3N2 influenza virus strains. *Virology*, *86*(1), 78–87. https://doi.org/10.1016/0042-6822(78)90009-0

Laver, W. G., & Kilbourne, E. D. (1966). Identification in a recombinant influenza virus of structural proteins derived from both parents. *Virology*, *30*(3), 493–501. https://doi.org/10.1016/0042-6822(66)90125-5

Laver, W. G., & Valentine, R. C. (1969). Morphology of the isolated hemagglutinin and neuraminidase subunits of influenza virus. *Virology*, *38*(1), 105–119. https://doi.org/10.1016/0042-6822(69)90132-9

Laver, W. G., & Webster, R. G. (1966). The structure of influenza viruses: IV. chemical studies of the host antigen. *Virology*, *30*(1), 104–115. https://doi.org/10.1016/S0042-6822(66)81014-0

Link, A., Zabel, F., Schnetzler, Y., Titz, A., Brombacher, F., & Bachmann, M. F. (2012). Innate immunity mediates follicular transport of particulate but not soluble protein antigen. *Journal of Immunology (Baltimore, Md.: 1950)*, *188*(8), 3724–3733. https://doi.org/10.4049/jimmunol.1103312

Liu, X., Zhao, T., Wang, L., Yang, Z., Luo, C., Li, M., Luo, H., Sun, C., Yan, H., & Shu, Y. (2023). A mosaic influenza virus-like particles vaccine provides broad humoral and cellular immune responses against influenza A viruses. *Npj Vaccines*, *8*(1), 1–14. https://doi.org/10.1038/s41541-023-00728-5

Lopez, C. E., Zacharias, Z. R., Ross, K. A., Narasimhan, B., Waldschmidt, T. J., & Legge, K. L. (2024). Polyanhydride nanovaccine against H3N2 influenza A virus generates mucosal resident and systemic immunity promoting protection. *Npj Vaccines*, *9*(1), 1–14. https://doi.org/10.1038/s41541-024-00883-3

Lowen, A. C. (2017). Constraints, Drivers, and Implications of Influenza A Virus Reassortment. *Annual Review of Virology*, *4*(1), 105–121. https://doi.org/10.1146/annurev-virology-101416-041726

Loyola, P. K. R., Campos-Rodríguez, R., Bello, M., Rojas-Hernández, S., Zimic, M., Quiliano, M., Briz, V., Muñoz-Fernández, M. A., Tolentino-López, L., & Correa-Basurto, J. (2013). Theoretical analysis of the neuraminidase epitope of the Mexican A H1N1 influenza strain, and experimental studies on its interaction with rabbit and human hosts. *Immunologic Research*, *56*(1), 44–60. https://doi.org/10.1007/s12026-013-8385-z

Lu, L. L., Suscovich, T. J., Fortune, S. M., & Alter, G. (2018). Beyond binding: Antibody effector functions in infectious diseases. *Nature Reviews Immunology*, *18*(1), 46–61. https://doi.org/10.1038/nri.2017.106

Lv, H., Teo, Q. W., Lee, C.-C. D., Liang, W., Choi, D., Mao, K. J., Ardagh, M. R., Gopal, A. B., Mehta, A., Szlembarski, M., Bruzzone, R., Wilson, I. A., Wu, N. C., & Mok, C. K. P. (2025). Differential antigenic imprinting effects between influenza H1N1 hemagglutinin and neuraminidase in a mouse model. *Journal of Virology*, *99*(1), e0169524. https://doi.org/10.1128/jvi.01695-24

Malby, R. L., Tulip, W. R., Harley, V. R., McKimm-Breschkin, J. L., Laver, W. G., Webster, R. G., & Colman, P. M. (1994). The structure of a complex between the NC10 antibody and influenza virus neuraminidase and comparison with the overlapping binding site of the NC41 antibody. *Structure*, *2*(8), 733–746. https://doi.org/10.1016/S0969-2126(00)00074-5

Manolova, V., Flace, A., Bauer, M., Schwarz, K., Saudan, P., & Bachmann, M. F. (2008). Nanoparticles target distinct dendritic cell populations according to their size. *European Journal of Immunology*, *38*(5), 1404–1413. https://doi.org/10.1002/eji.200737984

Marcandalli, J., Fiala, B., Ols, S., Perotti, M., de van der Schueren, W., Snijder, J., Hodge, E., Benhaim, M., Ravichandran, R., Carter, L., Sheffler, W., Brunner, L., Lawrenz, M.,

Dubois, P., Lanzavecchia, A., Sallusto, F., Lee, K. K., Veesler, D., Correnti, C. E., … King, N. P. (2019). Induction of Potent Neutralizing Antibody Responses by a Designed Protein Nanoparticle Vaccine for Respiratory Syncytial Virus. *Cell*, *176*(6), 1420-1431.e17. https://doi.org/10.1016/j.cell.2019.01.046

Matrosovich, M., Matrosovich, T., Carr, J., Roberts, N. A., & Klenk, H.-D. (2003). Overexpression of the alpha-2,6-sialyltransferase in MDCK cells increases influenza virus sensitivity to neuraminidase inhibitors. *Journal of Virology*, *77*(15), 8418–8425. https://doi.org/10.1128/jvi.77.15.8418-8425.2003

McAuley, J. L., Gilbertson, B. P., Trifkovic, S., Brown, L. E., & McKimm-Breschkin, J. L. (2019). Influenza Virus Neuraminidase Structure and Functions. *Frontiers in Microbiology*, *10*, 39. https://doi.org/10.3389/fmicb.2019.00039

McMahon, M., Strohmeier, S., Rajendran, M., Capuano, C., Ellebedy, A. H., Wilson, P. C., & Krammer, F. (2020). Correctly folded—But not necessarily functional—Influenza virus neuraminidase is required to induce protective antibody responses in mice. *Vaccine*, *38*(45), 7129–7137. https://doi.org/10.1016/J.VACCINE.2020.08.067

Momont, C., Dang, H. V., Zatta, F., Hauser, K., Wang, C., di Iulio, J., Minola, A., Czudnochowski, N., De Marco, A., Branch, K., Donermeyer, D., Vyas, S., Chen, A., Ferri, E., Guarino, B., Powell, A. E., Spreafico, R., Yim, S. S., Balce, D. R., … Pizzuto, M. S. (2023). A pan-influenza antibody inhibiting neuraminidase via receptor mimicry. *Nature*, *618*(7965), Article 7965. https://doi.org/10.1038/s41586-023-06136-y

Monto, A. S., Petrie, J. G., Cross, R. T., Johnson, E., Liu, M., Zhong, W., Levine, M., Katz, J. M., & Ohmit, S. E. (2015). Antibody to Influenza Virus Neuraminidase: An Independent Correlate of Protection. *The Journal of Infectious Diseases*, *212*(8), 1191–1199. https://doi.org/10.1093/INFDIS/JIV195

Moulès, V., Terrier, O., Yver, M., Riteau, B., Moriscot, C., Ferraris, O., Julien, T., Giudice, E., Rolland, J.-P., Erny, A., Bouscambert-Duchamp, M., Frobert, E., Rosa-Calatrava, M., Pu Lin, Y., Hay, A., Thomas, D., Schoehn, G., & Lina, B. (2011). Importance of viral genomic composition in modulating glycoprotein content on the surface of influenza virus particles. *Virology*, *414*(1), 51–62. https://doi.org/10.1016/j.virol.2011.03.011

Munier, S., Larcher, T., Cormier-Aline, F., Soubieux, D., Su, B., Guigand, L., Labrosse, B., Cherel, Y., Quéré, P., Marc, D., & Naffakh, N. (2010). A Genetically Engineered Waterfowl Influenza Virus with a Deletion in the Stalk of the Neuraminidase Has Increased Virulence for Chickens. *Journal of Virology*, *84*(2), 940–952. https://doi.org/10.1128/JVI.01581-09

Myers, M. L., Gallagher, J. R., Kim, A. J., Payne, W. H., Maldonado-Puga, S., Assimakopoulos, H., Bock, K. W., Torian, U., Moore, I. N., & Harris, A. K. (2023). Commercial influenza vaccines vary in HA-complex structure and in induction of cross-reactive HA antibodies. *Nature Communications*, *14*(1), 1763. https://doi.org/10.1038/s41467-023-37162-z

Nachbagauer, R., & Palese, P. (2020). Is a Universal Influenza Virus Vaccine Possible? *Annual Review of Medicine*, *71*(Volume 71, 2020), 315–327. https://doi.org/10.1146/annurev-med-120617-041310

Nagashima, K. A., & Mousa, J. J. (2021). Next-Generation Influenza HA Immunogens and Adjuvants in Pursuit of a Broadly Protective Vaccine. *Viruses*, *13*(4), 546. https://doi.org/10.3390/v13040546

Natali, A., Panizzi, P. F., Chezzi, C., & Oxford, J. S. (1984). Human sera possess a limited antibody repertoire to influenza neuraminidase antigenic variants selected in vitro.

Epidemiology & Infection, *92*(2), 243–250. https://doi.org/10.1017/S0022172400064263

Nooraei, S., Bahrulolum, H., Hoseini, Z. S., Katalani, C., Hajizade, A., Easton, A. J., & Ahmadian, G. (2021). Virus-like particles: Preparation, immunogenicity and their roles as nanovaccines and drug nanocarriers. *Journal of Nanobiotechnology*, *19*(1), 59. https://doi.org/10.1186/s12951-021-00806-7

Ortiz de Lejarazu, R., & Tamames, S. (2015). [Influenza vaccination. Effectiveness of current vaccines and future challenges]. *Enfermedades Infecciosas Y Microbiologia Clinica*, *33*(7), 480–490. https://doi.org/10.1016/j.eimc.2015.06.011

Parker, D. C. (1993). T cell-dependent B cell activation. *Annual Review of Immunology*, *11*, 331–360. https://doi.org/10.1146/annurev.iy.11.040193.001555

Pascha, M. N., Ballegeer, M., Roelofs, M. C., Meuris, L., Albulescu, I. C., van Kuppeveld, F. J. M., Hurdiss, D. L., Bosch, B. J., Zeev-Ben-Mordehai, T., Saelens, X., & de Haan, C. a. M. (2024). Nanoparticle display of neuraminidase elicits enhanced antibody responses and protection against influenza A virus challenge. *Npj Vaccines*, *9*(1), 1–14. https://doi.org/10.1038/s41541-024-00891-3

Pica, N., Iyer, A., Ramos, I., Bouvier, N. M., Fernandez-Sesma, A., Garcia-Sastre, A., Lowen, A. C., Palese, P., & Steel, J. (2011). The DBA.2 mouse is susceptible to disease following infection with a broad, but limited, range of influenza A and B viruses. *Journal of Virology*, *85*(23), 12825–12829. https://doi.org/10.1128/JVI.05930-11

Pica, N., & Palese, P. (2013). Toward a universal influenza virus vaccine: Prospects and challenges. *Annual Review of Medicine*, *64*, 189–202. https://doi.org/10.1146/annurev-med-120611-145115

Portela Catani, J. P., Ysenbaert, T., Smet, A., Vuylsteke, M., Vogel, T. U., & Saelens, X. (2023). Anti-neuraminidase and anti-hemagglutinin immune serum can confer inter-lineage cross protection against recent influenza B. *PloS One*, *18*(1), e0280825. https://doi.org/10.1371/journal.pone.0280825

Prevato, M., Ferlenghi, I., Bonci, A., Uematsu, Y., Anselmi, G., Giusti, F., Bertholet, S., Legay, F., Telford, J. L., Settembre, E. C., Maione, D., & Cozzi, R. (2015). Expression and characterization of recombinant, tetrameric and enzymatically active influenza neuraminidase for the setup of an enzyme-linked lectin-based assay. *PLoS ONE*, *10*(8), 1–18. https://doi.org/10.1371/journal.pone.0135474

Pushko, P., & Tretyakova, I. (2020). Influenza Virus Like Particles (VLPs): Opportunities for H7N9 Vaccine Development. *Viruses*, *12*(5), 518. https://doi.org/10.3390/v12050518

Rahikainen, R., Rijal, P., Tan, T. K., Wu, H. J., Andersson, A. M. C., Barrett, J. R., Bowden, T. A., Draper, S. J., Townsend, A. R., & Howarth, M. (2021). Overcoming Symmetry Mismatch in Vaccine Nanoassembly through Spontaneous Amidation. *Angewandte Chemie - International Edition*, *60*(1), 321–330. https://doi.org/10.1002/anie.202009663

Rajendran, M., Krammer, F., & McMahon, M. (2021). The Human Antibody Response to the Influenza Virus Neuraminidase Following Infection or Vaccination. *Vaccines*, *9*(8), 846. https://doi.org/10.3390/vaccines9080846

Richardson, J. C., & Akkina, R. K. (1991). NS2 protein of influenza virus is found in purified virus and phosphorylated in infected cells. *Archives of Virology*, *116*(1–4), 69–80. https://doi.org/10.1007/BF01319232

Rijal, P., Wang, B. B., Tan, T. K., Schimanski, L., Janesch, P., Dong, T., McCauley, J. W., Daniels, R. S., Townsend, A. R., & Huang, K.-Y. A. (2020). Broadly Inhibiting Antineuraminidase Monoclonal Antibodies Induced by Trivalent Influenza Vaccine

and H7N9 Infection in Humans. *Journal of Virology*, *94*(4), 1–17. https://doi.org/10.1128/jvi.01182-19

Rijal, P., Wei, L., Paesen, G. C., Stuart, D. I., Howarth, M. R., Huang, K.-Y. A., Bowden, T. A., & Townsend, A. R. (2024). *Structure-Guided Loop Grafting Improves Expression and Stability of Influenza Neuraminidase for Vaccine Development* (p. 2024.10.11.617814). bioRxiv. https://doi.org/10.1101/2024.10.11.617814

Rockman, S., Brown, L. E., Barr, I. G., Gilbertson, B., Lowther, S., Kachurin, A., Kachurina, O., Klippel, J., Bodle, J., Pearse, M., & Middleton, D. (2013). Neuraminidase-Inhibiting Antibody Is a Correlate of Cross-Protection against Lethal H5N1 Influenza Virus in Ferrets Immunized with Seasonal Influenza Vaccine. *Journal of Virology*, *87*(6), 3053–3061. https://doi.org/10.1128/JVI.02434-12

Ross, T. M. (2019). Universal Influenza Vaccine Approaches Using Full-Length or Head-Only Hemagglutinin Proteins. *The Journal of Infectious Diseases*, *219*(Supplement_1), S57–S61. https://doi.org/10.1093/infdis/jiz004

Rumfelt, K. E., Lauring, A. S., Martin, E. T., Monto, A., & Petrie, J. (2023). 302. Investigating NAI Titer as a Neutralizing IAV Correlate of Protection. *Open Forum Infectious Diseases*, *10*(Supplement_2), ofad500.374. https://doi.org/10.1093/ofid/ofad500.374

Sahasrabudhe, A., Lawrence, L., Epa, V. C., Varghese, J. N., Colman, P. M., & McKimm-Breschkin, J. L. (1998). Substrate, Inhibitor, or Antibody Stabilizes the Glu 119 Gly Mutant Influenza Virus Neuraminidase. *Virology*, *247*(1), 14–21. https://doi.org/10.1006/viro.1998.9222

Sakai, T., Nishimura, S. I., Naito, T., & Saito, M. (2017). Influenza A virus hemagglutinin and neuraminidase act as novel motile machinery. *Scientific Reports*, *7*(1), 45043. https://doi.org/10.1038/srep45043

Salemme, F. R., & Weatherford, D. W. (1981). Conformational and geometrical properties of beta-sheets in proteins. II. Antiparallel and mixed beta-sheets. *Journal of Molecular Biology*, *146*(1), 119–141. https://doi.org/10.1016/0022-2836(81)90369-7

Sandbulte, M. R., Gao, J., Straight, T. M., & Eichelberger, M. C. (2009). A miniaturized assay for influenza neuraminidase-inhibiting antibodies utilizing reverse genetics-derived antigens. *Influenza and Other Respiratory Viruses*, *3*(5), 233–240. https://doi.org/10.1111/j.1750-2659.2009.00094.x

Sandbulte, M. R., Jimenez, G. S., Boon, A. C. M., Smith, L. R., Treanor, J. J., & Webby, R. J. (2007). Cross-Reactive Neuraminidase Antibodies Afford Partial Protection against H5N1 in Mice and Are Present in Unexposed Humans. *PLOS Medicine*, *4*(2), e59. https://doi.org/10.1371/journal.pmed.0040059

Schmidt, P. M., Attwood, R. M., Mohr, P. G., Barrett, S. A., & McKimm-Breschkin, J. L. (2011). A generic system for the expression and purification of soluble and stable influenza neuraminidase. *PLoS ONE*, *6*(2). https://doi.org/10.1371/journal.pone.0016284

Schulman, J. L., & Kilbourne, E. D. (1969). Independent variation in nature of hemagglutinin and neuraminidase antigens of influenza virus: Distinctiveness of hemagglutinin antigen of Hong Kong-68 virus. *Proceedings of the National Academy of Sciences of the United States of America*, *63*(2), 326–333. https://doi.org/10.1073/pnas.63.2.326

Sebastian, S., & Lambe, T. (2018). Clinical Advances in Viral-Vectored Influenza Vaccines. *Vaccines*, *6*(2), 29. https://doi.org/10.3390/vaccines6020029

Serradell, M. C., Rupil, L. L., Martino, R. A., Prucca, C. G., Carranza, P. G., Saura, A., Fernández, E. A., Gargantini, P. R., Tenaglia, A. H., Petiti, J. P., Tonelli, R. R., Reinoso-Vizcaino, N., Echenique, J., Berod, L., Piaggio, E., Bellier, B., Sparwasser, T., Klatzmann, D., & Luján, H. D. (2019). Efficient oral vaccination by

bioengineering virus-like particles with protozoan surface proteins. *Nature Communications*, *10*(1), 361. https://doi.org/10.1038/s41467-018-08265-9

Shao, W., Li, X., Goraya, M. U., Wang, S., & Chen, J.-L. (2017). Evolution of Influenza A Virus by Mutation and Re-Assortment. *International Journal of Molecular Sciences*, *18*(8), 1650. https://doi.org/10.3390/ijms18081650

Shi, W., & Gao, G. F. (2021). Emerging H5N8 avian influenza viruses. *Science*, *372*(6544), 784–786. https://doi.org/10.1126/science.abg6302

Shtyrya, Y. A., Mochalova, L. V., & Bovin, N. V. (2009). Influenza Virus Neuraminidase: Structure and Function. *Acta Naturae*, *1*(2), 26.

Smith, W., Andrewes, C. H., & Laidlaw, P. P. (1933). A VIRUS OBTAINED FROM INFLUENZA PATIENTS. *The Lancet*, *222*(5732), 66–68. https://doi.org/10.1016/S0140-6736(00)78541-2

Stadlbauer, D., Zhu, X., McMahon, M., Turner, J. S., Wohlbold, T. J., Schmitz, A. J., Strohmeier, S., Yu, W., Nachbagauer, R., Mudd, P. A., Wilson, I. A., Ellebedy, A. H., & Krammer, F. (2019). Broadly protective human antibodies that target the active site of influenza virus neuraminidase. *Science (New York, N.Y.)*, *366*(6464), 499–504. https://doi.org/10.1126/science.aay0678

Steel, J., & Lowen, A. C. (2014). Influenza A virus reassortment. *Current Topics in Microbiology and Immunology*, *385*, 377–401. https://doi.org/10.1007/82_2014_395

Stetefeld, J., Jenny, M., Schulthess, T., Landwehr, R., Engel, J., & Kammerer, R. A. (2000). Crystal structure of a naturally occurring parallel right-handed coiled coil tetramer. *Nature Structural Biology*, *7*(9), 772–776. https://doi.org/10.1038/79006

Streltsov, V. A., Schmidta, P. M., & Breschkina, J. L. M. K. (2019). Structure of an Influenza A virus N9 neuraminidase with a tetrabrachion-domain stalk. *Acta Crystallographica.*

Section F, Structural Biology Communications, *75*(Pt 2), 89–97. https://doi.org/10.1107/S2053230X18017892

Strohmeier, S., Carreño, J. M., Brito, R. N., & Krammer, F. (2021). Introduction of Cysteines in the Stalk Domain of Recombinant Influenza Virus N1 Neuraminidase Enhances Protein Stability and Immunogenicity in Mice. *Vaccines*, *9*(4), 404. https://doi.org/10.3390/vaccines9040404

Sun, H., Li, H., Tong, Q., Han, Q., Liu, J., Yu, H., Song, H., Qi, J., Li, J., Yang, J., Lan, R., Deng, G., Chang, H., Qu, Y., Pu, J., Sun, Y., Lan, Y., Wang, D., Shi, Y., … Liu, J. (2023). Airborne transmission of human-isolated avian H3N8 influenza virus between ferrets. *Cell*, *0*(0). https://doi.org/10.1016/j.cell.2023.08.011

Syomin, B. V., & Ilyin, Y. V. (2019). Virus-Like Particles as an Instrument of Vaccine Production. *Molecular Biology*, *53*(3), 323–334. https://doi.org/10.1134/S0026893319030154

Tajudeen, Y. A. (2021). Emerging Strain (H5N8) of Highly Pathogenic Avian Influenza Virus: An Impending Pandemic Threat. *Journal of Infectious Diseases and Epidemiology*, *7*(7), 217. https://doi.org/10.23937/2474-3658/1510217

Tan, T. K., Rijal, P., Rahikainen, R., Keeble, A. H., Schimanski, L., Hussain, S., Harvey, R., Hayes, J. W. P., Edwards, J. C., McLean, R. K., Martini, V., Pedrera, M., Thakur, N., Conceicao, C., Dietrich, I., Shelton, H., Ludi, A., Wilsden, G., Browning, C., … Townsend, A. R. (2021). A COVID-19 vaccine candidate using SpyCatcher multimerization of the SARS-CoV-2 spike protein receptor-binding domain induces potent neutralising antibody responses. *Nature Communications 2021 12:1*, *12*(1), 1–16. https://doi.org/10.1038/s41467-020-20654-7

Tate, M. D. (2018). Highly pathogenic avian H5N8 influenza viruses: Should we be concerned? *Virulence*, *9*(1), 20–21. https://doi.org/10.1080/21505594.2017.1386832

Threats, I. of M. (US) F. on M., Knobler, S. L., Mack, A., Mahmoud, A., & Lemon, S. M. (2005). The Story of Influenza. In *The Threat of Pandemic Influenza: Are We Ready? Workshop Summary*. National Academies Press (US). https://www.ncbi.nlm.nih.gov/books/NBK22148/

Tulip, W. R., Varghese, J. N., Laver, W. G., Webster, R. G., & Colman, P. M. (1992). Refined crystal structure of the influenza virus N9 neuraminidase-NC41 Fab complex. *Journal of Molecular Biology*, *227*(1), 122–148. https://doi.org/10.1016/0022-2836(92)90687-f

Tulip, W. R., Varghese, J. N., Webster, R. G., Laver, W. G., & Colman, P. M. (1992). Crystal structures of two mutant neuraminidase-antibody complexes with amino acid substitutions in the interface. *Journal of Molecular Biology*, *227*(1), 149–159. https://doi.org/10.1016/0022-2836(92)90688-G

Urbaniak, K., & Markowska-Daniel, I. (2014). In vivo reassortment of influenza viruses. *Acta Biochimica Polonica*, *61*(3), 427–431.

van der Woude, R., Turner, H. L., Tomris, I., Bouwman, K. M., Ward, A. B., & de Vries, R. P. (2020). Drivers of recombinant soluble influenza A virus hemagglutinin and neuraminidase expression in mammalian cells. *Protein Science*, *29*(9), 1975–1982. https://doi.org/10.1002/pro.3918

Varghese, J. N., Laver, W. G., & Colman, P. M. (1983). Structure of the influenza virus glycoprotein antigen neuraminidase at 2.9 A resolution. *Nature*, *303*(5912), 35–40. https://doi.org/10.1038/303035A0

Veneziano, R., Moyer, T. J., Stone, M. B., Wamhoff, E.-C., Read, B. J., Mukherjee, S., Shepherd, T. R., Das, J., Schief, W. R., Irvine, D. J., & Bathe, M. (2020). Role of nanoscale antigen organization on B-cell activation probed using DNA origami. *Nature Nanotechnology*, *15*(8), 716–723. https://doi.org/10.1038/s41565-020-0719-0

Von Grafenstein, S., Wallnoefer, H. G., Kirchmair, J., Fuchs, J. E., Huber, R. G., Schmidtke, M., Sauerbrei, A., Rollinger, J. M., & Liedl, K. R. (2015). Interface dynamics explain assembly dependency of influenza neuraminidase catalytic activity. *Journal of Biomolecular Structure & Dynamics*, *33*(1), 104–120. https://doi.org/10.1080/07391102.2013.855142

Walls, A. C., Fiala, B., Schäfer, A., Wrenn, S., Pham, M. N., Murphy, M., Tse, L. V., Shehata, L., O'Connor, M. A., Chen, C., Navarro, M. J., Miranda, M. C., Pettie, D., Ravichandran, R., Kraft, J. C., Ogohara, C., Palser, A., Chalk, S., Lee, E.-C., … King, N. P. (2020). Elicitation of Potent Neutralizing Antibody Responses by Designed Protein Nanoparticle Vaccines for SARS-CoV-2. *Cell*, *183*(5), 1367-1382.e17. https://doi.org/10.1016/j.cell.2020.10.043

Wan, H., Gao, J., Xu, K., Chen, H., Couzens, L. K., Rivers, K. H., Easterbrook, J. D., Yang, K., Zhong, L., Rajabi, M., Ye, J., Sultana, I., Wan, X.-F., Liu, X., Perez, D. R., Taubenberger, J. K., & Eichelberger, M. C. (2013). Molecular basis for broad neuraminidase immunity: Conserved epitopes in seasonal and pandemic H1N1 as well as H5N1 influenza viruses. *Journal of Virology*, *87*(16), 9290–9300. https://doi.org/10.1128/JVI.01203-13

Wan, H., Sultana, I., Couzens, L. K., Mindaye, S., & Eichelberger, M. C. (2017). Assessment of influenza A neuraminidase (subtype N1) potency by ELISA. *Journal of Virological Methods*, *244*, 23–28. https://doi.org/10.1016/j.jviromet.2017.02.015

Wan, H., Yang, H., Shore, D. A., Garten, R. J., Couzens, L., Gao, J., Jiang, L., Carney, P. J., Villanueva, J., Stevens, J., & Eichelberger, M. C. (2015). Structural characterization of a protective epitope spanning A(H1N1)pdm09 influenza virus neuraminidase monomers. *Nature Communications*, *6*. https://doi.org/10.1038/ncomms7114

Ward, C. W., Elleman, T. C., & Azad, A. A. (1982). Amino acid sequence of the Pronase-released heads of neuraminidase subtype N2 from the Asian strain A/Tokyo/3/67 of influenza virus. *Biochemical Journal*, *207*(1), 91–95.

Webster, R. G., Air, G. M., Metzger, D. W., Colman, P. M., Varghese, J. N., Baker, A. T., & Laver, W. G. (1987). Antigenic structure and variation in an influenza virus N9 neuraminidase. *Journal of Virology*, *61*(9), 2910–2916. https://doi.org/10.1128/jvi.61.9.2910-2916.1987

Westgeest, K. B., de Graaf, M., Fourment, M., Bestebroer, T. M., van Beek, R., Spronken, M. I. J., de Jong, J. C., Rimmelzwaan, G. F., Russell, C. A., Osterhaus, A. D. M. E., Smith, G. J. D., Smith, D. J., & Fouchier, R. A. M. (2012). Genetic evolution of the neuraminidase of influenza A (H3N2) viruses from 1968 to 2009 and its correspondence to haemagglutinin evolution. *The Journal of General Virology*, *93*(Pt 9), 1996–2007. https://doi.org/10.1099/vir.0.043059-0

Williams, T. L., Pirkle, J. L., & Barr, J. R. (2012). Simultaneous quantification of hemagglutinin and neuraminidase of influenza virus using isotope dilution mass spectrometry. *Vaccine*, *30*(14), 2475–2482. https://doi.org/10.1016/j.vaccine.2011.12.056

Wohlbold, T. J., & Krammer, F. (2014). In the shadow of hemagglutinin: A growing interest in influenza viral neuraminidase and its role as a vaccine antigen. *Viruses*, *6*(6), 2465–2494. https://doi.org/10.3390/v6062465

Wohlbold, T. J., Nachbagauer, R., Xu, H., Tan, G. S., Hirsh, A., Brokstad, K. A., Cox, R. J., Palese, P., & Krammer, F. (2015). Vaccination with Adjuvanted Recombinant Neuraminidase Induces Broad Heterologous, but Not Heterosubtypic, Cross-Protection against Influenza Virus Infection in Mice. *mBio*, *6*(2), 10.1128/mbio.02556-14. https://doi.org/10.1128/mbio.02556-14

Wu, Y., Qin, G., Gao, F., Liu, Y., Vavricka, C. J., Qi, J., Jiang, H., Yu, K., & Gao, G. F. (2013). Induced opening of influenza virus neuraminidase N2 150-loop suggests an important role in inhibitor binding. *Scientific Reports*, *3*. https://doi.org/10.1038/SREP01551

Yang, H., Carney, P. J., Mishin, V. P., Guo, Z., Chang, J. C., Wentworth, D. E., Gubareva, L. V., & Stevens, J. (2016). Molecular Characterizations of Surface Proteins Hemagglutinin and Neuraminidase from Recent H5Nx Avian Influenza Viruses. *Journal of Virology*, *90*(12), 5770–5784. https://doi.org/10.1128/JVI.00180-16

Yasuhara, A., Yamayoshi, S., Kiso, M., Sakai-Tagawa, Y., Okuda, M., & Kawaoka, Y. (2022). A broadly protective human monoclonal antibody targeting the sialidase activity of influenza A and B virus neuraminidases. *Nature Communications*, *13*(1), 6602. https://doi.org/10.1038/s41467-022-34521-0

Zhang, X., & Ross, T. M. (2024). Anti-neuraminidase immunity in the combat against influenza. *Expert Review of Vaccines*. https://www.tandfonline.com/doi/abs/10.1080/14760584.2024.2343689

Zhang, X., Skarlupka, A. L., Shi, H., & Ross, T. M. (2024). COBRA N2 NA vaccines induce protective immune responses against influenza viral infection. *Human Vaccines & Immunotherapeutics*, *20*(1), 2403175. https://doi.org/10.1080/21645515.2024.2403175